Szkoła Główna Gospodarstwa Wiejskiego
w Warszawie
Instytut Medycyny Weterynaryjnej

lek. wet. Kamil Paweł Górski

Ocena kliniczna i radiologiczna zmian zwyrodnieniowych okolicy krawędzi wyrostków zębodołowych kości siekaczowej i żuchwy w populacji koni w centralnej Polsce

Clinical and radiological assessment of degenerative changes around the edges of the alveolar processes of the incisive bone and mandible in the horse population in central Poland

Rozprawa doktorska
Doctoral thesis

Praca wykonana pod kierunkiem:
Promotor: Profesor dr hab. Izabela Polkowska
Promotor pomocniczy: Dr Andrzej Bereznowski
Katedra Chorób Dużych Zwierząt i Klinika
Instytut Medycyny Weterynaryjnej
Szkoła Główna Gospodarstwa Wiejskiego w Warszawie

Warszawa, 2024

Moim nauczycielom

Oświadczenie promotora pracy

Oświadczam, że niniejsza praca została przygotowana pod moim kierunkiem i stwierdzam, że spełnia ona warunki do przedstawienia jej w postępowaniu o nadanie tytułu naukowego.

Data. 6.06.2024 r. Podpis promotora pracy. Jacek Policiński

Oświadczenie autora pracy

Świadom odpowiedzialności prawnej oświadczam, że niniejsza praca doktorska została napisana przeze mnie samodzielnie i nie zawiera treści uzyskanych w sposób niezgodny z obowiązującymi przepisami.

Oświadczam również, że przedstawiona praca nie była wcześniej przedmiotem procedur związanych z uzyskaniem tytułu naukowego w wyższej uczelni.

Oświadczam ponadto, że niniejsza wersja pracy jest identyczna z załączoną wersją elektroniczną.

Data. 6 VI 2024 r. Podpis autora pracy. Kamil Górski

Streszczenie

Wady zgryzu i choroby zębów siecznych stanowią około 31% wszystkich zaburzeń w obrębie zębów u koni. Jednym z nich jest syndrom EOTRH (Equine Odontoclastic Tooth Resorption and Hipercementosis), którego nazwa jest ściśle związana z procesami patologicznymi – resorpcją tkanek zęba i nieuregulowanym odkładaniem się cementu. W przebiegu tego syndromu dochodzi do uszkodzenia zęba, któremu towarzyszy ból. Objawy kliniczne syndromu EOTRH pojawiają się u koni w wieku powyżej 15–go roku życia, natomiast radiologiczne nawet u 10–letnich koni. Niniejsze badanie miało na celu określenie częstości i rodzaju zaburzeń w obrębie zębów w populacji koni w Polsce, w tym występowania syndromu EOTRH, a następnie określenie przydatności protokołów analizy tekstury obrazu z wykorzystaniem macierzy poziomu szarości i miar entropii oraz skalowanego liczenia pikseli w ocenie radiogramów zębów siecznych w przebiegu tego syndromu EOTRH. W pierwszej części pracy opisano wyniki szczegółowego badania jamy ustnej 206 koni, z uwzględnieniem występowania najważniejszych wad zgryzu i chorób zębów. W drugiej części pracy, oceniano radiogramy okolicy krawędzi wyrostków zębodołowych kości siekaczowej 80 koni z wykorzystaniem trzech protokołów oceny ilościowej obrazów. Radiogramy klasyfikowano według stopnia zaawansowania syndromu EOTRH (0–3), a następnie poddano wstępnemu przetwarzaniu obrazu oraz ocenie ilościowej obrazów z wykorzystaniem protokołów analizy tekstury obrazu opartych na macierzach poziomu szarości i miarach entropii oraz protokołu skalowanego liczenia pikseli. W grupie 206 koni zaburzenia w obrębie zębów siecznych występowały u 31% koni. Częściej stwierdzano wady zgryzu, niż choroby zębów siecznych, a najczęstszą patologią była nieprawidłowa krzywizna i obecność kamienia nazębnego. Objawy kliniczne syndromu EOTRH ze strony zębów siecznych stwierdzono u 3,11% koni w wieku powyżej 15 lat. Analiza tekstury obrazów radiologicznych koni z tym syndromem wykazała przydatność oceny cech macierzy współwystępowania poziomu szarości (GLCM) i macierzy długości biegu poziomu szarości (GLRLM) w rozróżnieniu radiogramów zębów siecznych dotkniętych EOTRH o różnym stopniu zaawansowania. Również dwuwymiarowa dystrybucja entropii (DistEn2D) oraz protokół skalowanego liczenia pikseli oparty na wykorzystaniu wzorca gęstości umożliwiły identyfikację radiologicznych objawów syndromu związanych z zaawansowaniem choroby. Na podstawie uzyskanych wyników można stwierdzić, że zaburzenia dotyczące zębów siecznych stanowią istotną część chorób jamy ustnej koni, a wprowadzenie nowych metod przetwarzania i analizy radiogramów okolicy krawędzi wyrostków zębodołowych kości siekaczowej może przyczynić się do wczesnego rozpoznania zaburzeń w obrębie zębów siecznych, w tym syndromu EOTRH, a co za tym idzie postępu w dziedzinie stomatologii koni.

Słowa kluczowe: stomatologia koni, zęby sieczne, EOTRH, radiografia, analiza tekstury, entropia

Summary

Malocclusions and incisor teeth diseases constitute approximately 31% of all dental disorders in horses. One notable disorder is EOTRH (Equine Odontoclastic Tooth Resorption and Hypercementosis) syndrome. EOTRH can be described by the underlying pathological processes that occur within this syndrome–resorption of dental tissue and irregular cement deposition. The progression of EOTRH syndrome leads to tooth damage and pain. Clinical symptoms typically manifest after the age of 15, while radiological signs can be observed in horses as young as 10 years old. This study aimed to investigate the frequency and types of dental disorders found in the horse population in Poland, with a specific focus on the occurrence of EOTRH syndrome. Additionally, the study aimed to assess the utility of image texture analysis protocols, incorporating grayscale level matrices, entropy measures, and scaled–pixel–counting in evaluating incisor radiographs throughout the progression of EOTRH syndrome. In the first part of the study, the oral cavities of 206 horses were meticulously examined, taking into account significant malocclusions and dental diseases. The second part involved the evaluation of radiographs of the edges of the alveolar processes of the incisive bone of 80 horses using three quantitative image analysis protocols. The radiographs were categorized based on the severity of EOTRH syndrome and assigned to one of four grade–related EOTRH groups (0–3). Subsequently, the radiographs were subjected to initial image preprocessing and quantitative analysis using image texture analysis protocols based on grayscale level matrices and entropy measures, along with a scaled–pixel–counting protocol. Among the group of 206 horses, dental disorders involving the incisors were identified in 31% of cases, with malocclusions being more common than incisor pathologies. The most prevalent dental condition recorded was the improper curvature of the incisors and the presence of dental calculus. Clinical symptoms of EOTRH syndrome were found in 3,11% of horses over the age of 15. Texture analysis of radiographic images of horses manifesting EOTRH syndrome demonstrated the utility of assessing Gray Level Co-occurrence Matrix (GLCM) and Gray Level Run Length Matrix (GLRLM) features in distinguishing radiographs of EOTRH-affected incisors at different stages of advancement. Two-dimensional entropy distribution (DistEn2D) and a scaled–pixel–counting protocol based on a density standard also facilitated the identification of radiological signs associated with the progression of EOTRH syndrome. In conclusion, incisor disorders are a significant aspect of oral cavity diseases in horses. The implementation of new methods for processing and analyzing radiographs of edge of the alveolar processes of the incisive bone can contribute to the early diagnosis of incisor disorders, including EOTRH syndrome, thereby advancing the field of equine dentistry.

Key words: equine dentistry, incisor teeth, EOTRH, radiography, texture analysis, entropy

Spis treści

1. Wykaz artykułów naukowych wchodzących w skład rozprawy doktorskiej

Badania zostały szczegółowo przedstawione w zbiorze powiązanych tematycznie artykułów naukowych opublikowanych w czasopismach z listy Ministerstwa Nauki i Szkolnictwa Wyższego (MNiSW):

1. **Górski, K.**; Stefanik, E.; Turek, B.; Bereznowski, A.; Czopowicz, M.; Polkowska, I.; Domino, M. Malocclusions and Dental Diseases in Privately Owned Horses in the Mazovia Region of Poland. Animals **2022a**, 12, 3120. DOI: 10.3390/ani12223120 (Punkty $MNiSW_{2022}$ = 100, IF_{2022} = 2,752).
2. **Górski, K.**; Tremaine, H.; Obrochta, B.; Buczkowska, R.; Turek, B.; Bereznowski, A.; Rakowska, A.; Polkowska, I. EOTRH syndrome in polish half–bred horses–two clinical cases. Journal of Equine Veterinary Science **2021**, 101, 103428. DOI: 10.1016/j.jevs.2021.103428 (Punkty $MNiSW_{2021}$ = 70, IF_{2021} = 2,31).
3. **Górski, K.**; Borowska, M.; Stefanik, E.; Polkowska, I.; Turek, B.; Bereznowski, A.; Domino, M. Selection of Filtering and Image Texture Analysis in the Radiographic Images Processing of Horses' Incisor Teeth Affected by the EOTRH Syndrome. Sensors **2022b**, 22, 2920. DOI: 10.3390/s22082920 (Punkty $MNiSW_{2022}$ = 100, IF_{2022} = 3,847).
4. **Górski, K.**; Borowska, M.; Stefanik, E.; Polkowska, I.; Turek, B.; Bereznowski, A.; Domino, M. Application of Two–Dimensional Entropy Measures to Detect the Radiographic Signs of Tooth Resorption and Hypercementosis in an Equine Model. Biomedicines **2022c**, 10, 2914. DOI: 10.3390/biomedicines10112914 (Punkty $MNiSW_{2022}$ = 100, IF_{2022} = 4,757).
5. **Górski, K.**; Borowska, M.; Turek, B.; Pawlikowki, M.; Jankowski, K.; Bereznowski, A.; Polkowska, I.; Domino, M. An application of the density standard and scaled–pixel–counting protocol to assess the radiodensity of equine incisor teeth affected by resorption and hypercementosis: preliminary advancement in standard in field dental radiography. BMC Veterinary Research **2023**, 19, 116. DOI: 10.1186/s12917–023–03675–4 (Punkty $MNiSW_{2023}$ = 140, IF_{2022} = 2,600)

Sumaryczny IF wynosi 16,266.

Sumaryczna punktacja Ministerstwa Nauki i Szkolnictwa Wyższego wynosi: 510.

2. Wykaz skrótów

AREAs	(regions of interest representing S1–S10) – obszary zainteresowania reprezentujące S1 – S10
bwt	(by the weight) – według wagi
CBCT	(cone–beam computed tomography) – tomografia komputerowa wiązki stożkowej
CT	(computed tomography) – tomografia komputerowa
DispEn2D	(two–dimensional dispersion entropy) – dwuwymiarowa entropia rozrzutu
DistEn2D	(two–dimensional distribution entropy) – dwuwymiarowa entropia rozkładu
EOTRH	(Equine Odontoclastic Tooth Resorption and Hypercementosis) – Odontoklastyczna Resorpcja i Hipercementoza Zęba u Koni
EOTRH 0	(degree 0 – healthy) – stopień 0 – zdrowy
EOTRH 1	(degree 1 – mild EOTRH) – stopień 1 – łagodny syndrom EOTRH
EOTRH 2	(degree 2 – moderate EOTRH) – stopień 2 – zaawansowany syndrom EOTRH
EOTRH 3	(degree 3 – severe EOTRH) – stopień 3 – ciężki syndrom EOTRH
ETR	(excessive transverse ridges) – nadmiernie wykształcone krawędzie poprzeczne
FBCT	(fan–beam computed tomography) – tomografia komputerowa wiązki wachlarzowej
FOS	(first order statistics) – statystyki pierwszego rzędu
FuzzEn2D	(two–dimensional fuzzy entropy) – dwuwymiarowa entropia rozmyta
GLCM	(gray level co–occurrence matrix) – macierz współwystąpień odcieni szarości
GLDM	(gray level dependence matrix) – macierz współzależności odcieni szarości
GLRLM	(gray level run length matrix) – macierz długości ciągów odcieni szarości
GLSZM	(gray level size zone matrix) – macierz wielkości obszarów poziomu szarości
hr MRI	(high resolution–magnetic resonance imaging) – rezonans magnetyczny o wysokiej rozdzielczości
hr pQCT	(high–resolution peripheral quantitative computed tomography) – obwodowa, ilościowa tomografia komputerowa o wysokiej rozdzielczości
HU	(Hounsfield units) – jednostki Hounsfielda
i.m	(intramuscular) – iniekcja domięśniowa
i.v	(intravenous) – iniekcja dożylna
MDCT	(multi–detector computed tomography) – wielodetektorowa tomografia komputerowa
MIMICS	(materialises interactive medical image control system) – materializujący interaktywny system kontroli obrazu medycznego

MRI	(magnetic resonance imaging) – obrazowanie metodą rezonansu magnetycznego
NGTDM	(neighbouring gray tone difference matrix) – macierz sąsiednich różnic odcieni szarości
nHU	(normalized Hounsfield unit) – znormalizowana jednostka Hounsfielda
NP	(number of pixels) – liczba pikseli
nPB	(normalized pixel brightness) – znormalizowana jasność pikseli
NPV	(negative predictive value) – wartość predykcyjna ujemna
PB	(pixel brightness) – jasność pikseli
PermEn2D	(two–dimensional permutation entropy) – dwuwymiarowa entropia permutacyjna
PPID	(pituitary pars intermedia dysfunction) – dysfunkcja części pośredniej przysadki mózgowej
PPV	(positive predictive value) – wartość predykcyjna dodatnia
PWB	(polish warmblood) – polski koń sportowy
r	(the Pearson correlation coefficient) – współczynnik korelacji Pearsona
RDT	(retained deciduous teeth) – przetrwałe zęby mleczne
ROI	(region of interest) – obszar zainteresowania
S1–S10	(ten steps of the density standard) – dziesięciostopniowa standaryzacja gęstości
SampEn2D	(two–dimensional sample entropy) – dwuwymiarowa entropia próbki
SD	(standard deviation) – odchylenie standardowe
Se	(sensitivity) – czułość
SEM	(scanning electron microscope) – skaningowy mikroskop elektronowy
Sp	(specificity) – swoistość

3. Wstęp

Powszechnie przyjmuje się, że choroby jamy ustnej i ich następstwa stanowią poważny problem zdrowotny u koni na całym świecie (Kirkland i wsp., 1994). Zarówno rutynowe (Brigham i wsp., 2000; Walker i wsp., 2012; Vemming i wsp., 2015), jak i pośmiertne (Anthony i wsp., 2010; Gere i Dixon, 2010) badania jamy ustnej wykazały, że najczęściej rozpoznawaną nieprawidłowością w jej obrębie są choroby zębów. Jak wskazali Salem i wsp. (2017) większość badań dotyczących rodzaju i częstości występowania chorób zębów koni opiera się na przypadkach klinicznych hospitalizowanych koni lub autopsjach głów koni pobranych z rzeźni (Baker, 1979; Brigham i wsp., 2000; du Toit i wsp., 2008; du Toit i wsp., 2009; Gere i Dixon, 2010). Według badań przeprowadzonych na 500 czaszkach koni wyizolowanych ze zwłok, u 80% badanych koni wykazano wyraźne zaburzenia w obrębie zębów (Baxter, 2013). W podobnym badaniu anatomopatologicznym 50 czaszek, stwierdzono, że zaburzenia w obrębie zębów występują u 74% badanych koni (Brigham i wsp., 2000).

W Ameryce Północnej choroby zębów należą do pięciu najczęściej stwierdzanych problemów zdrowotnych u dorosłych koni (Traub–Dargatz i wsp., 1991) i dotykają 79% lokalnej populacji koni (Anthony i wsp., 2010). 42% ankietowanych właścicieli koni w Anglii podało, że ich koń cierpiał z powodu problemów stomatologicznych (Ireland i wsp., 2012). W Szkocji stwierdzono badaniami, że 87% miejscowej populacji koni cierpi na choroby zębów (Dixon i wsp., 2000). W Australii spośród 400 koni skierowanych do klinik z powodu problemów stomatologicznych, 87% z nich miało pierwotne schorzenie w obrębie zębów policzkowych, 13% poważne zaburzenie wynikające ze znacznego zużycia zębów, a 11% nie wykazywało objawów klinicznych chorób zębów (Chinkangsadarn i wsp., 2015). Aż w 94% spośród 400 głów koni przebadanych w australijskiej rzeźni stwierdzono występowanie co najmniej jednej choroby zębów lub wady zgryzu (Chinkangsadarn i wsp., 2015). Podobne badanie przeprowadzone w kanadyjskiej rzeźni na 556 głowach koni wykazało, że u 70% z nich występował co najmniej jeden rodzaj nieprawidłowości w obrębie zębów policzkowych (Traub–Dargatz i wsp., 1991).

Choroby zębów są na ogół źródłem bólu (Rehrl i wsp., 2018; Pehkonen i wsp., 2019), a zatem w dużym stopniu wpływają zarówno na jakość życia koni (McGowan i Ireland, 2016), jak i na sposób ich użytkowania (Foster, 2013; Björnsdóttir i wsp., 2014). Konsekwencje chorób zębów, takie jak ból, dyskomfort i zmiany w pobieraniu paszy, mają negatywny wpływ na dobrostan koni i są częścią protokołu systemu oceny monitorowania dobrostanu koni (Wageningen, 2012). W odniesieniu do użytkowania konia, obecność zębów wilczych i haków na zębach przedtrzonowych może kolidować z wędzidłem, wpływając na reakcję związaną z napięciem wodzy, a w konsekwencji na prowadzenie konia. Obecność wilczych zębów

i związane z nimi problemy z właściwym działaniem wędzidła, są wskazaniem do usunięcia wilczych zębów jak najwcześniej, najlepiej u młodego konia, aby ograniczyć problemy w jego użytkowaniu. Podobnie, w przypadku stwierdzenia obecności haków, zwłaszcza w drugich zębach przedtrzonowych szczęki lub żuchwy, należy je skorygować, aby uniknąć dyskomfortu związanego z użyciem wędziła (Foster, 2013). U koni pociągowych i rekreacyjnych często występuje nadmierne starcie lub złamanie krawędzi mezjalnej drugich zębów przedtrzonowych oraz kłów żuchwy (Cook, 2011; Björnsdóttir i wsp., 2014). W tym przypadku, podobnie jak w przypadku zdiagnozowania wielu innych chorób zębów, wymagane jest specjalistyczne leczenie i często niezbędne jest zrobienie przerwy w treningach oraz użytkowaniu konia. Ponadto w przypadku nasilenia się objawów lub wystąpienia powikłań leczenie przedłuża się, a jego koszty są znacznie wyższe (Gergeleit i Bienert–Zeit, 2020). Tak więc, zarówno bezpośrednie straty finansowe właściciela, jak i zakłócenie planu treningowego konia sprawiają, że choroby zębów są ważnym problemem w branży jeździeckiej. Salem i wsp. (2017) podkreślili integralną rolę badań terenowych w określaniu częstości występowania chorób jamy ustnej i zębów oraz zauważyli, że uzyskane dane przyczyniają się do poszerzenia wiedzy lekarzy weterynarii i właścicieli na temat wpływu chorób zębów na zdrowie i dobrostan koni (Salem i wsp., 2017).

3.1. Wady zgryzu i choroby zębów u koni

Do wad zgryzu zębów siecznych u koni zalicza się przodozgryz, tyłozgryz, przetrwały ząb mleczny, ząb dodatkowy (polidontię), oligodontię, nieprawidłową krzywiznę, diastemę, oraz obecność haków (Ryc. 1). Najczęstsze choroby zębów siecznych to obecność nadliczbowego zęba, ruchomy ząb, złamanie, próchnica, obecność kamienia nazębnego oraz Odontoklastyczna Resorpcja i Hipercementoza Zęba u Koni (Equine Odontoclastic Tooth Resorption and Hypercementosis, EOTRH) (Ryc. 1).

Wady zgryzu	Lewa szczęka	Prawa szczęka	Prawa żuchwa	Lewa żuchwa	**Choroby zębów**
Przodozgryz Tyłozgryz Przetrwały ząb mleczny Ząb dodatkowy Oligodontia Nieprawidłowa krzywizna Diastema Haki	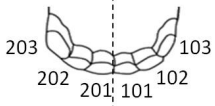		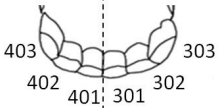		Ząb nadliczbowy Ruchomy ząb Złamanie Próchnica Kamień nazębny EOTRH

Ryc. 1. Klasyfikacja wad zgryzu i chorób zębów siecznych (101, 102, 103, 201, 202, 203, 301, 302, 303, 401, 402 i 403 wg zmodyfikowanej skali Triadana) u koni.

Przodozgryzem (Ryc. 2A) określa się stan, w którym powierzchnia żująca zębów siecznych żuchwy leży rostralnie w stosunku do powierzchni żującej zębów siecznych szczęki, z zachowaniem częściowego kontaktu (Rodrigues i wsp., 2013). Odwrotnie jest w przypadku

tyłozgryzu (Ryc. 2B), w którym powierzchnie żujące zębów siecznych szczęki leżą rostralnie w stosunku do powierzchni żującej zębów siecznych żuchwy, z zachowaniem częściowego kontaktu (Rodrigues i wsp., 2013). Wady te najczęściej skutkują niedopasowaniem powierzchni żującej zębów policzkowych i jako konsekwencja, pojawieniem się na nich haków.

W obrębie siekaczy (Ryc. 2C), a także zębów przedtrzonowych (Ryc. 5I), spotkać można przetrwały ząb mleczny. Jest to zaburzenie polegające na obecności zęba mlecznego lub jego fragmentu, pozostającego w jamie ustnej po terminie jego fizjologicznej utraty (Simhofer i wsp., 2008).

Obecność zęba dodatkowego (*dens suplementarius*), stwierdza się m.in. w obrębie siekaczy. Zaburzenie to jest określane jako obecność większej liczby zębów w stosunku do prawidłowej formuły zębowej, przy czym ma on prawidłową budowę (Górski i wsp., 2020) i może występować w obrębie zębów siecznych (Ryc. 2D) jak i zębów policzkowych (Ryc. 5H). Ząb dodatkowy rozwija się najczęściej w wyniku nieprawidłowego różnicowania zawiązków zębów podczas rozwoju płodu, przy czym uraz zewnętrzny dotyczący zawiązków zębowych może również pełnić rolę czynnika inicjującego (Rodrigues i wsp., 2013).

Zupełnie odwrotną formą jest oligodontia, gdzie zmniejszeniu ulega liczba zębów w stosunku do prawidłowej formuły zębowej. Może mieć ona charakter wrodzony i rozwijać się w wyniku nieprawidłowego różnicowania blaszki zębowej i zawiązków zębowych, jak również może wystąpić w okresie życia postnatalnego konia i rozwinąć się wskutek urazu, wraz z wiekiem zwierzęcia lub wtórnie do innych wad zgryzu (Dixon i wsp., 1999a; Rodrigues i wsp., 2013). Oligodontia może dotyczyć wszystkich zębów, lecz najczęściej spotykana jest w obrębie zębów siecznych (Ryc. 2E) i zębów policzkowych (Ryc. 5G).

Powszechną wadą zgryzu w obrębie zębów siecznych jest nieprawidłowa krzywizna ich powierzchni żującej. Charakteryzuje się ona obecnością nieprawidłowej linii biegnącej między powierzchnią żującą zębów siecznych szczęki i żuchwy. Linia ta powinna być linią prostą; każde jej odchylenie, czy to dobrzuszne, dogrzbietowe, skośne czy też nieregularne, stanowi nieprawidłowość (Rodrigues i wsp., 2013). Wyróżniamy więc krzywiznę dobrzuszną (Ryc. 2Fa), dogrzbietową (Ryc. 2Fb), skośną (Ryc. 2Fc) i nieregularną (Ryc. 2Fd).

Diastemę najczęściej spotyka się w obrębie zębów przedtrzonowych i trzonowych żuchwy (Ryc. 5F), rzadziej zębów siecznych (Ryc. 2G). Określa się ją jako wykrywalna nieprawidłowa przestrzeń międzyzębowa (interproksymalna), między dwoma sąsiednimi zębami, często z uwięźnięciem w niej pokarmu, co może być przyczyną zapalenia przyzębia (Dixon i wsp. 1999b; Carmalt, 2003; du Toit i Dixon, 2012). W przypadku zębów przedtrzonowych i trzonowych diastemy występują między powierzchnią dystalną i mezjalną sąsiednich zębów.

W przypadku zębów siecznych diastema występuje między krawędzią boczną a przyśrodkową sąsiednich zębów.

Haki, jako kolejna wada zgryzu to obecność nadmiernie wyrośniętych fragmentów korony klinicznej zęba (Klugh, 2010). Haki najczęściej występują w zębach 06 lub 11 (Ryc. 5J) i często mają związek z niedopasowaniem ich powierzchni żującej (przodozgryzem lub tyłozgryzem). Haki u koni w wieku 9–11 lat pojawia się na krawędzi językowej skrajnych zębów siecznych szczęki (Ryc. 2H) w wyniku zmiany ukątowania zębów siecznych i utraty styku powierzchni żującej (Dixon i Dacre, 2005).

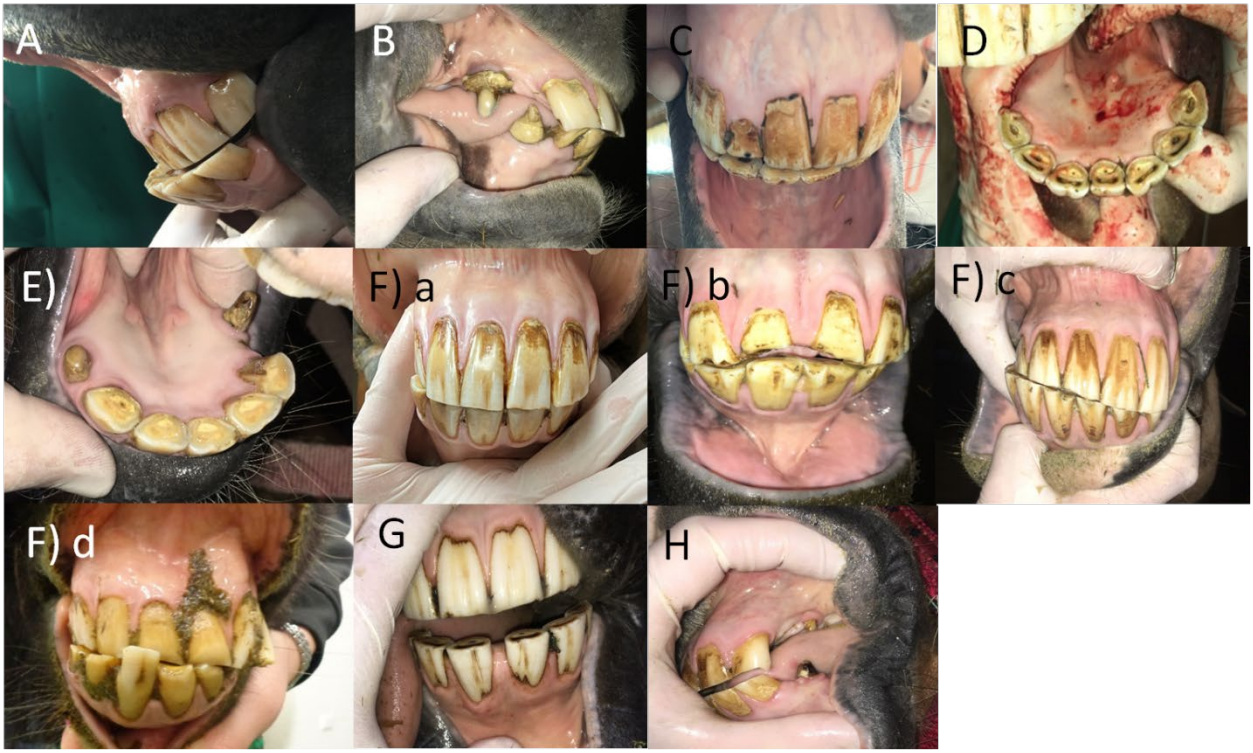

Ryc. 2. Wady zgryzu zębów siecznych u koni: A) przodozgryz; B) tyłozgryz; C) przetrwały ząb mleczny; D) ząb dodatkowy; E) oligodontia; F) nieprawidłowa krzywizna powierzchni żującej: a) krzywizna dobrzuszna, b) krzywizna dogrzbietowa, c) krzywizna skośna, d) krzywizna nieregularna; G) diastema; H) haki (Foto. K. Górski).

Formą polidontii, zaliczaną do chorób zębów jest ząb nadliczbowy (*dens supernumerarius*). Ząb nadliczbowy charakteryzuje się obecnością większej liczby zębów w stosunku do prawidłowej formuły zębowej lecz występujący ząb/zęby jest/są nieprawidłowej budowy (Górski i wsp., 2020), np. zęby sieczne (Ryc. 3A).

Częstym skutkiem występowania diastem jest nadmierna ruchomość zęba, określana jako ruchomy ząb, spowodowany najczęściej uszkodzeniem lub zanikiem więzadeł zębodołowych (Gieche, 2010). Nadmierna ruchomość często dotyczy zębów siecznych (Ryc. 3B) lub policzkowych (Ryc. 6A).

Złamanie zęba to najczęściej jego pourazowe uszkodzenie, dotykające części lub wszystkich jego fragmentów (korona kliniczna, korona rezerwowa, korzeń) (Ramzan, 2009). W przypadku zębów siecznych (Ryc. 3C) i kłów (Ryc. 11A) najczęściej spotyka się złamanie w obrębie korony klinicznej. W przypadku zębów wilczych złamanie występuje najczęściej po próbie ekstrakcji (Ryc. 9A). Złamanie zębów policzkowych szczęki w przeważającej liczbie przypadków przebiega w linii strzałkowej, natomiast zębów policzkowych żuchwy poprzecznie (Ryc. 6B).

Do chorób zębów zaliczamy także próchnicę. Istotą choroby jest zniszczenie zwapniałych tkanek zęba w wyniku demineralizacji i zakażenia bakteryjnego (ubytek i ciemne przebarwienie) cementu z rozszerzeniem zmian na szkliwo i zębinę lub bez takiego rozszerzenia (du Toit i Dixon, 2012). Próchnica najczęściej lokalizuje się w obrębie lejka/ów zęba policzkowego szczęki (Ryc. 6C), rzadziej zęba siecznego i nazywana jest próchnicą lejka/ów. Próchnicę obwodową, która może występować na wszystkich powierzchniach zęba z wyjątkiem powierzchni żującej najczęściej spotkać można w obrębie zębów siecznych (Ryc. 3D) i zębów policzkowych żuchwy.

Często spotykane jest także nadmierne nagromadzenie kamienia nazębnego, do którego dochodzi w wyniku mineralizacji płytki bakteryjnej zębów. Najbardziej predysponowane są kły żuchwy, na których kamień gromadzi się w obrębie ich korony klinicznej, często całkowicie ją pokrywając (Ryc. 11B). Na zębach siecznych kamień nazębny gromadzi się głównie na ich powierzchni wargowej (Ryc. 3E). W przypadku przedtrzonowców i trzonowców (Ryc. 6D) najczęściej gromadzi się on na powierzchni policzkowej zęba/ów (Klugh, 2010).

Coraz częściej, szczególnie w obrębie zębów siecznych rozpoznawany jest Syndrom Odontoklastycznej Resorpcji i Hipercementozy Zęba u Koni (Ryc. 3F) – (syndrom EOTRH, Equine Odontoclastic Tooth Resorption and Hypercementosis Syndrome). Dokładne omówienie Syndromu EOTRH znajduje się w rozdziale 3.2.

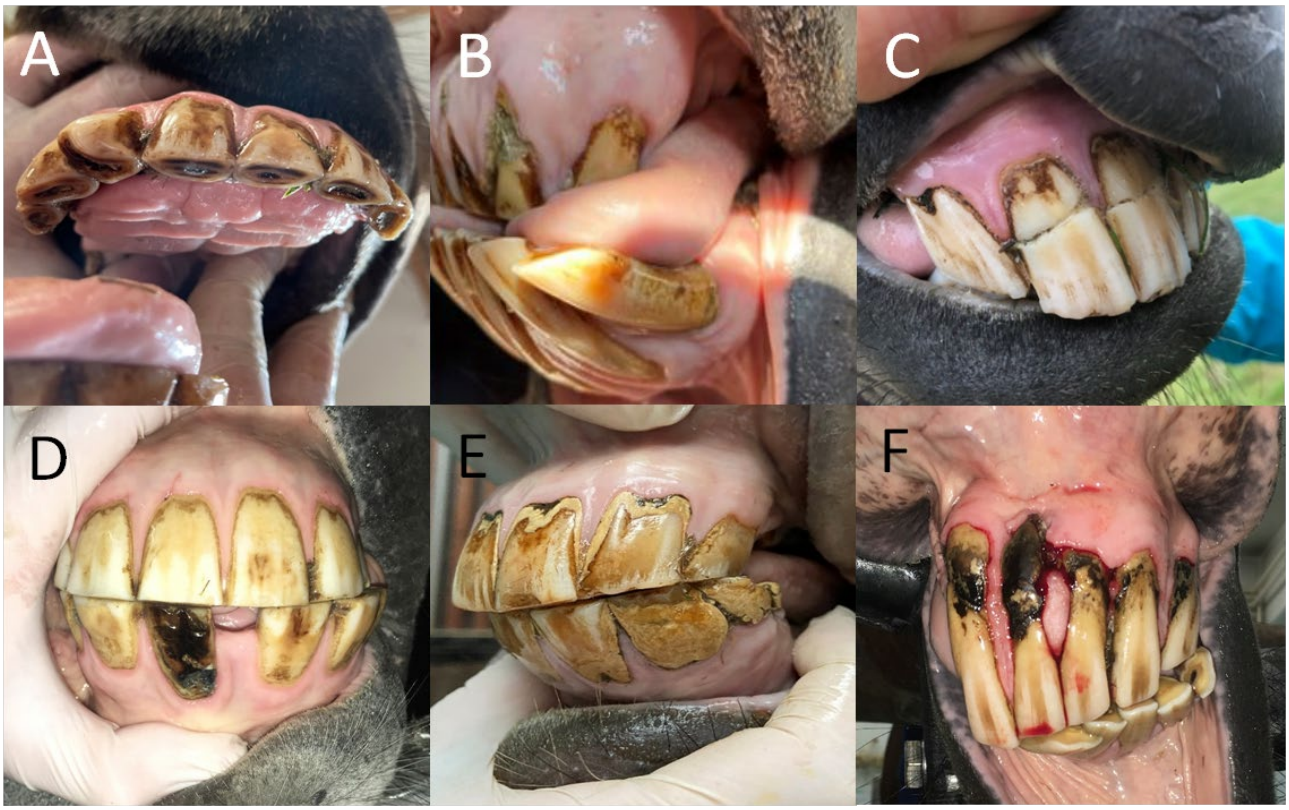

Ryc. 3. Choroby zębów siecznych u koni: A) ząb nadliczbowy; B) ruchomy ząb; C) załamanie zęba siecznego; D) próchnica; E) kamień nazębny: F) EOTRH syndrom (Foto. K. Górski).

Do wad zgryzu zębów przedtrzonowych i trzonowych zalicza się ostre krawędzie zębów, nadmiernie wysunięty zęby, zgryz falisty, zgryz schodkowy, ząb przemieszczony, diastema, oligodontia, ząb dodatkowy, przetrwały ząb mleczny, haki i nadmiernie wystające krawędzie poprzeczne (ETR) (Ryc. 4). Najczęstsze choroby zębów przedtrzonowych i trzonowych to obecność ruchomego zęba, złamanie, próchnica, obecność kamienia nazębnego (Ryc. 4).

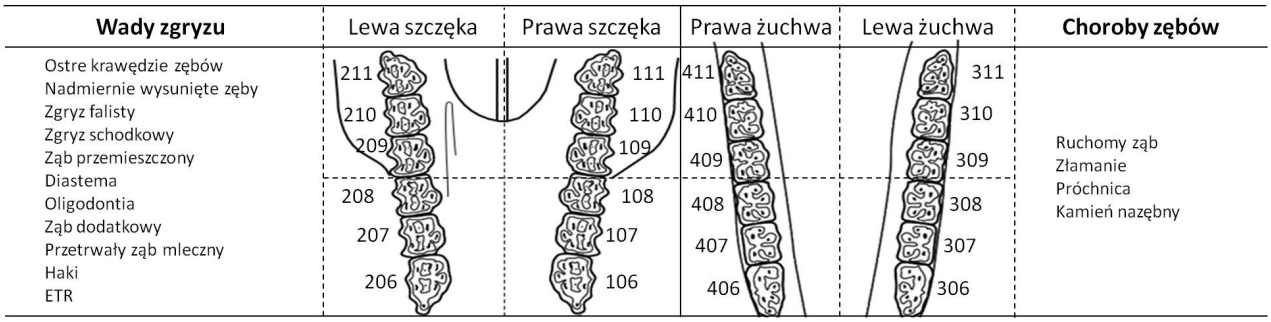

Ryc. 4. Klasyfikacja wad zgryzu i chorób zębów przedtrzonowych (106, 107, 108, 206, 207, 208, 306, 307, 308, 406, 407 i 408) i trzonowych (109, 110, 111, 209, 210, 211, 309, 310, 311, 409, 410 i 411 wg zmodyfikowanej skali Triadana) u koni.

Najbardziej powszechną wadą zgryzu u koni jest występowanie ostrych krawędzi zębów policzkowych (Ryc. 5A), a dokładnie obecność wystających fałdów szkliwa na policzkowych krawędziach zębów policzkowych szczęki i językowych krawędziach zębów policzkowych żuchwy, które powstają w wyniku anizognatyzmu i specyficznego sposobu żucia u koni (du Toit i Dixon, 2012). Ich obecność powoduje mechaniczne drażnienie błony śluzowej policzków i/lub języka, co skutkuje pojawieniem się nadżerek, wrzodów lub w skrajnych przypadkach ran błony śluzowej.

Obecność nadmiernie wystających krawędzi poprzecznych (Ryc. 5K), o wysokości co najmniej 3 mm, na powierzchni żującej zęba policzkowego określane są jako nadmiernie wystające krawędzie poprzeczne – (ETR, Exaggerated Transverse Ridges) (Klugh, 2010). Ich występowanie może prowadzić do powstania diastemy i rozwoju chorób przyzębia z powodu nadmiernego wtłaczania fragmentów pożywienia, podczas procesu żucia w przestrzenie międzyzębowe w przeciwległych łukach zębowych (Chinkangsadarn i wsp., 2015).

Zgryz falisty (Ryc. 5C) jest koleją powszechną wadą zgryzu zębów policzkowych, polegający na obecność nierównej lub pofałdowanej powierzchni żującej w obrębie jednego łuku zębowego lub obecność więcej niż jednego zęba z nadmiernie wysuniętą koroną kliniczną w obrębie jednego łuku zębowego (Dixon i Dacre, 2005; Klugh, 2010).

Dość często spotyka się także nadmiernie wysunięty ząb policzkowy (Ryc. 5B). Jest to stan, w którym ząb nie ulega prawidłowemu starciu o ząb przeciwstawny i wysuwa się nadmiernie ponad linię powierzchni trącej sąsiednich zębów. Do nadmiernego wysunięcia zęba dochodzi najczęściej wskutek złamania korony klinicznej, nadmiernego zużycia lub zupełnej utraty zęba przeciwstawnego. Nadmierne wysunięcie dotyczy najczęściej pojedynczego zęba (Dixon i wsp., 1999b; du Toit i Dixon, 2012).

Zgryz schodkowy (Ryc. 5D) jest bardziej nasiloną wadą zgryzu, spowodowany obecnością więcej niż jednego nadmiernie wysuniętego zęba, zwykle przy utracie przeciwstawnych zębów policzkowych (Dixon i wsp., 2000).

Ząb przemieszczony (Ryc. 5E) to rzadko spotykana wada, będąca skutkiem zmiany fizjologicznego położenia zęba w obrębie łuku zębowego. Najczęściej dochodzi do przemieszczenia zęba policzkowego w kierunku policzkowym lub doogonowym (Dixon i Dacre, 2005; Ramzan, 2009).

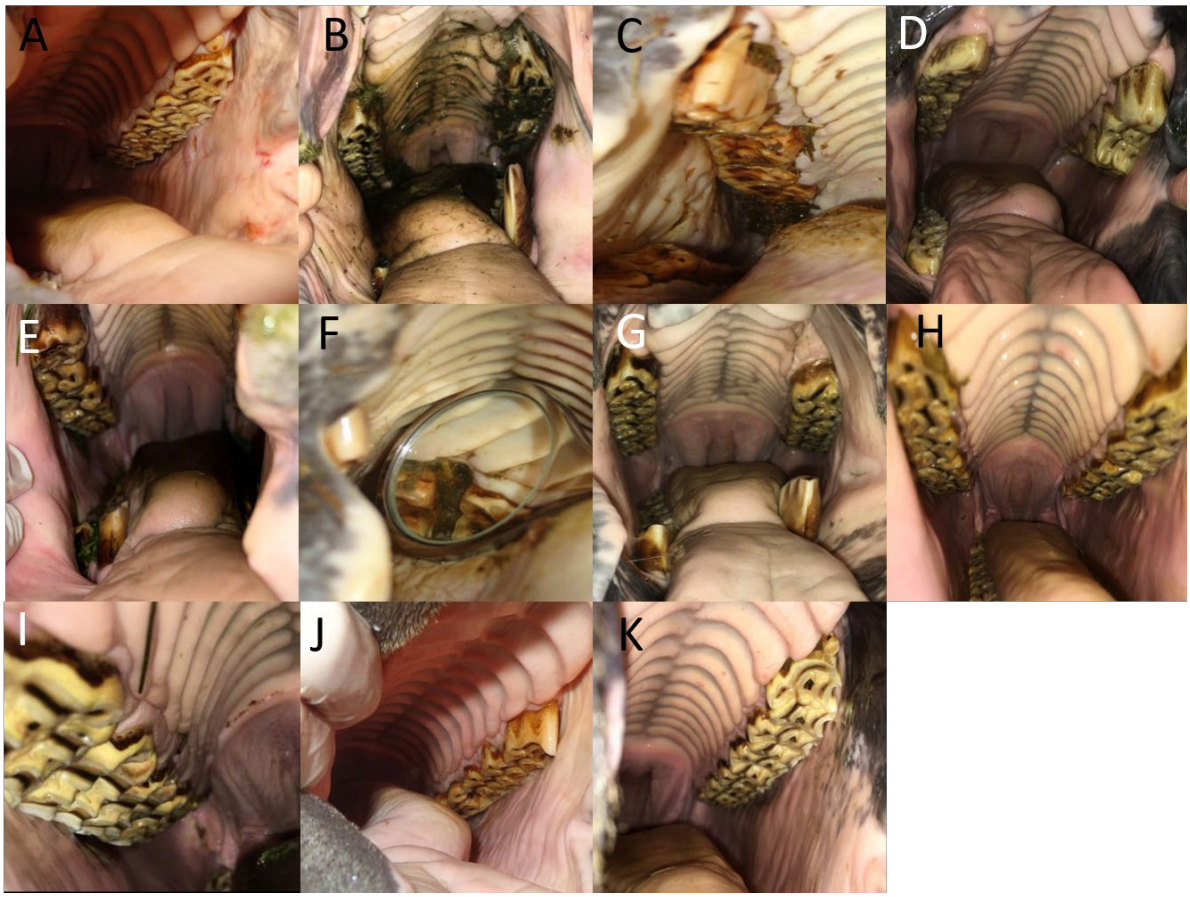

Ryc. 5. Wady zgryzu zębów przedtrzonowych i trzonowych u koni : A) ostre krawędzie zębów policzkowych; B) nadmiernie wysunięty ząb policzkowy; C) zgryz falisty; D) zgryz schodkowy; E) ząb przemieszczony; F) diastema; G) oligodontia; H) ząb dodatkowy; I) przetrwały ząb mleczny; J) haki; K) ETR (Foto. K. Górski).

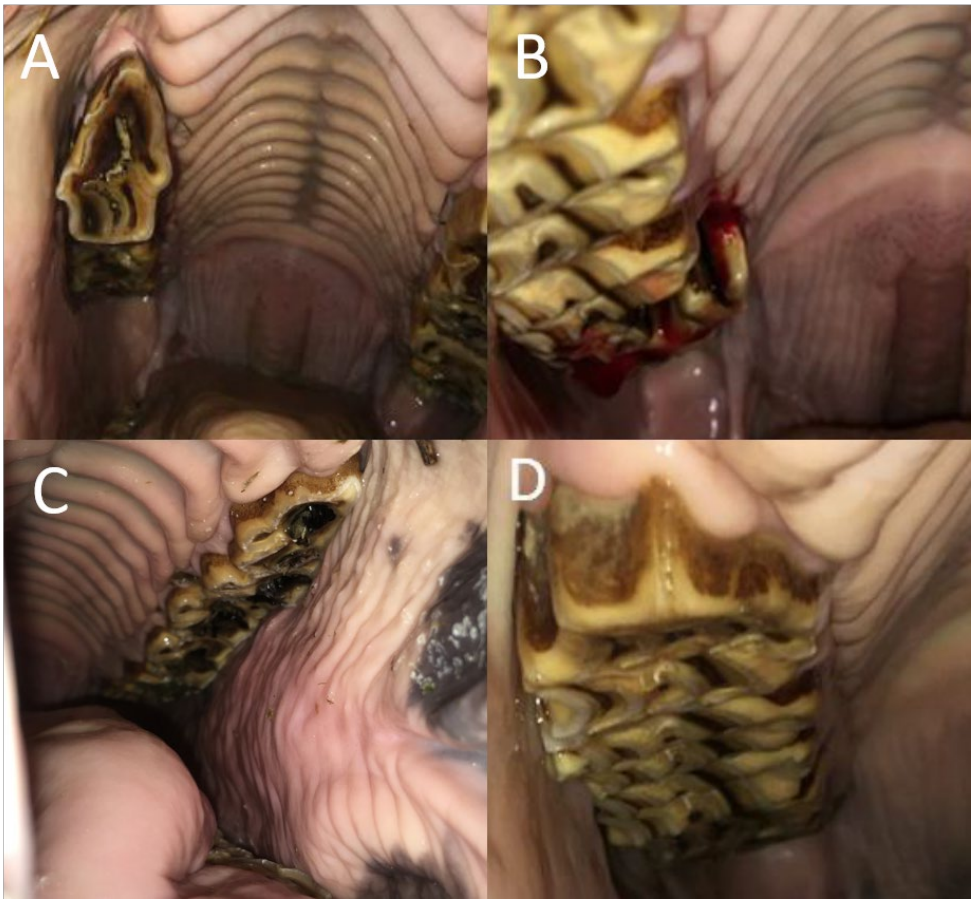

Ryc. 6. Choroby zębów przedtrzonowych i trzonowych u koni: A) ruchomy ząb; B) złamanie zęba; C) próchnica; D) kamień nazębny (Foto. K. Górski).

Do wad zgryzu zębów wilczych i kłów zaliczamy odpowiednio ślepy ząb wilczy oraz niewyrznięty kieł (Ryc. 7). Najczęstsze choroby zębów wilczych i kłów to złamanie i obecność kamienia nazębnego. (Ryc. 7).

Wady zgryzu	Lewa szczęka	Prawa szczęka	Prawa żuchwa	Lewa żuchwa	**Choroby zębów**
Ślepy ząb wilczy	205	105	405	305	Złamanie
Niewyrznięty kieł	204	104	404	304	Złamanie Kamień nazębny

Ryc. 7 Klasyfikacja wad zgryzu i chorób zębów wilczych (105, 205, 305 i 405) i kłów (104, 204, 304 i 404 wg zmodyfikowanej skali Triadana) u koni.

Ślepy ząb wilczy (Ryc. 8A) spotykany jest najczęściej w szczęce. W wyniku zaburzenia procesu wyrzynania jego korona znajduje się pod dziąsłem. Jest on najczęściej przesunięty donosowo w stosunku do drugiego zęba przedtrzonowego (Broman, 2021). Skutkiem zaburzenia procesu wyrzynania, może być także niewyrznięty kieł (Ryc. 10A). Zaburzenie to dotyczy samców, występują głównie w szczęce i spotykane jest u koni w wieku powyżej 6 lat, czyli powyżej wieku granicznego dla wyrzynania się kłów (Dixon i wsp., 1999a).

Ryc. 8. Wady zgryzu zębów wilczych u koni: A) ślepy ząb wilczy (Foto. K. Górski).

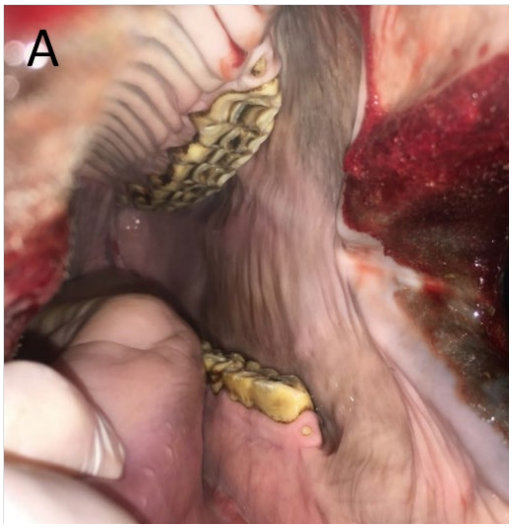

Ryc. 9. Choroby zębów wilczych u koni: A) złamanie zęba wilczego (Foto. K. Górski).

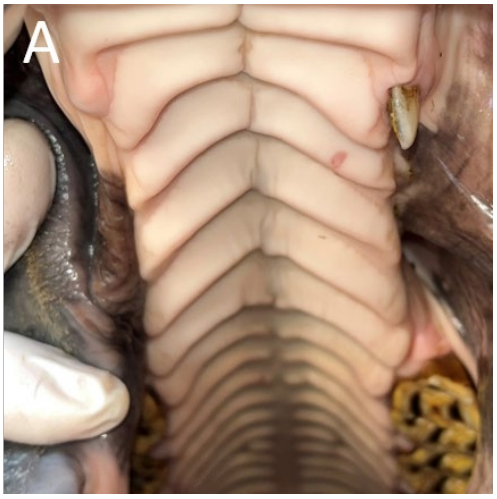

Ryc. 10. Wady zgryzu kłów u koni: A) niewyrznięty kieł (Foto. K. Górski).

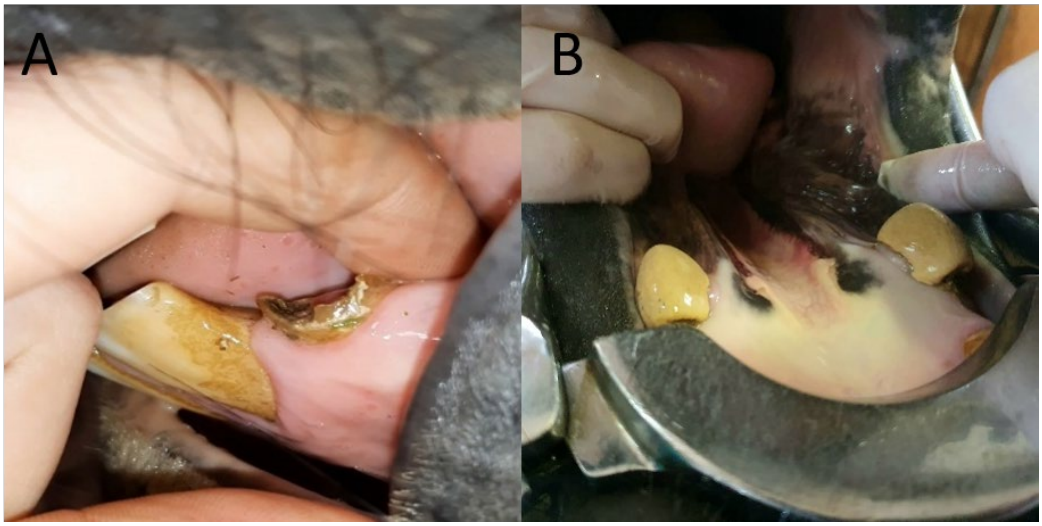

Ryc. 11. Choroby kłów u koni: A) złamanie kła; B) kamień nazębny (Foto. K. Górski).

3.2. Syndrom Odontoklastycznej Resorpcji i Hipercementozy Zęba u Koni

Syndrom Odontoklastycznej Resorpcji i Hipercementozy Zęba u Koni jest polskim tłumaczeniem Syndromu EOTRH – ang. Equine Odontoclastic Tooth Resorption and Hipercementosis. Objawy kliniczne syndromu EOTRH po raz pierwszy opisał w 2004 roku David O. Klugh, jako rzadkie i niezidentyfikowane zaburzenie w obrębie siekaczy u koni (Klugh, 2004). Nazwę syndromu EOTRH zaproponowali w 2008 r. Staszyk i wsp., jako odzwierciedlenie dwóch procesów patologicznych – resorpcji tkanek zęba i nadmiernym odkładaniem się cementu (Moore i wsp., 2016; Baratt, 2016). Przypadki patologii w obrębie siekaczy związane z resorpcją zęba i bulwiastym powiększeniem zawartości zębodołu opisywano również w kolejnych latach (Staszyk i wsp., 2008; Hole i Staszyk, 2018). Stwierdzono również,

że problem ten jest często związany ze współistniejącymi chorobami przyzębia (Gregory i wsp., 2006; Baratt, 2007; Staszyk i wsp., 2008; Rawlinson i Earley, 2013; du Toit i Rucker, 2013; Sykora i wsp., 2014; Hole i Staszyk, 2018).

Występowanie syndromu EOTRH opisano na całym świecie, w tym w Europie, Stanach Zjednoczonych i Australii (Staszyk i wsp., 2008, Staszyk, 2010; Lee, 2010; Sykora i wsp., 2014; Smedley i wsp., 2015). Syndrom EOTRH dotyka głównie siekaczy (Staszyk, 2010; Pearson i wsp.,2013; Rawlinson i Carmalt, 2014), chociaż opisywano także przypadki dotyczące kłów, przedtrzonowców oraz trzonowców (Barrett i Easley, 2013; Luedke i wsp., 2017; Hole i Staszyk, 2018). Chorują głównie konie w wieku powyżej piętnastego roku życia (Hole i Staszyk, 2018), choć najnowsze badania potwierdzają występowanie formy łagodnej syndromu EOTRH nawet u koni dziesięcioletnich (Rehrl i wsp., 2018). Niektóre badania sugerują również, że płeć i rasa mogą wpływać na rozwój syndromu EOTRH (Smedley i wsp., 2015; Rahmani i wsp., 2019). Kilka doniesień sugeruje, że najczęściej dotyczy on wałachów (Smedley i wsp., 2015; Lorello i wsp., 2016; Rahmani i wsp., 2019). Niektórzy autorzy sugerują, że konie ras sportowych i pełnej krwi angielskiej mogą być bardziej podatne na jej wystąpienie (Pearson i wsp., 2013), jednak nie zostało to w pełni potwierdzone (Rehrl i wsp., 2018).

3.2.1. Etiologia i patogeneza syndromu EOTRH

Przyczyna syndromu EOTRH nie została w pełni poznana, choć wymienia się kilka teorii, mogących mieć wpływ na jego powstawanie i rozwój (Hole i Staszyk, 2018). Jedną z nich jest podłoże immunologiczne, analogiczne do patogenezy MIRR (Multiple Idiopathic Root Resorption) u ludzi oraz FORL (Feline Odontoclastic Resorptive Lesions) u kotów (Staszyk i wsp., 2008; Staszyk, 2010; Moore i wsp., 2016; Baratt, 2016; Hole i Staszyk, 2018). W obu przypadkach, podobnie do EOTRH typowa jest nieznanej przyczyny resorpcja tkanek zęba (Hole i Staszyk, 2018). Resorpcja dotyczy wszystkich struktur zęba, tj. cementu, szkliwa, zębiny oraz sporadycznie jamy miazgi (Moore i wsp., 2016). Syndrom EOTRH ma głównie charakter proliferacyjny, a dominującą cechą jest hipercementoza (Hole i Staszyk, 2018). W ciężkich przypadkach syndromu może występować bulwiaste powiększenie zawartości zębodołu oraz nawet kilkukrotne powiększenie wielkości korony rezerwowej w porównaniu do prawidłowego zęba (Staszyk i wsp., 2008; Moore i wsp., 2016). Takiemu obrazowi klinicznemu przypisuje się udział bakterii *Treponema spp.* i *Tannerella spp.*, które izolowano z jamy ustnej chorych koni, a które są brane pod uwagę jako jeden z czynników etiologicznych syndromu EOTRH (Sykora i wsp., 2014; Lorello i wsp., 2016; Moore i wsp., 2016; Hole i Staszyk, 2018; Kennedy i Dixon, 2018). Wśród czynników predysponujących do rozwoju tego syndromu

wymienia się: martwicę niedokrwienną korzenia i korony rezerwowej zęba, dietę niedoborową, czynniki ogólnoustrojowe, tj. hiperwitaminozę A, fluorozę, hipokalcemię, nadczynność przytarczyc, dysfunkcję części pośredniej przysadki (PPID – pituitary pars intermedia dysfunction), zespół metaboliczny oraz ciężkie zapalenie przyzębia. Niektórzy autorzy wskazują na podłoże genetyczne lub idiopatyczne syndromu EOTRH, a także podłoże jatrogenne związane z błędną korekcją zębów siecznych i kłów (Staszyk i wsp., 2008; Pearson i wsp., 2013; Hole i Staszyk, 2018; Rehrl i wsp., 2018).

Według badań Staszyka i wsp. (2008) czynnikiem inicjującym wystąpienie tego syndromu i najbardziej prawdopodobną przyczyną procesów patologicznych jest nadmierny nacisk wywierany na powierzchnię zgryzu podczas procesu żucia (Pearson i wsp., 2013; Hole i Staszyk, 2018). Szczególnie istotne jest to u starszych koni, u których sukcesywnie dochodzi do zmniejszenia się ilości więzadeł zębodołowych w stosunku do powierzchni żującej, przy czym siły wywierane na te struktury są takie same jak u koni młodych. Nadmierne mechaniczne obciążania więzadeł zębodołowych powodują ogniskową martwicę i uwalnianie cytokin, co prowadzi do napływu i aktywacji odontoklastów. Następnie komórki te powodują resorpcję tkanek zęba. Proces ten zapoczątkowuje reakcję naprawczą, polegającą na odkładaniu się cementu przez cementoblasty (Hole i Staszyk, 2018). Ta hipoteza pozostaje w sprzeczności w stosunku do kłów, które nie biorą udziału w procesie żucia, przez co nie podlegają nadmiernym naciskom i odkształceniom. Jednak przeprowadzone symulacje naprężeń i odkształceń zębów siecznych wykazały przenoszenie nadmiernych sił wywieranych przez fragmenty kości szczęki i żuchwy okolicy brzegu bezzębnego również na więzadła zębodołowe kłów. Jednak siły te były zdecydowanie mniejsze niż w przypadku zębów siecznych (Hole i Staszyk, 2018). Również badania histopatologiczne konsekwentnie wskazują, że jedną z przyczyn syndromu EOTRH mogą być biomechaniczne naprężenia i odkształcenia oraz wtórne zakażenie drobnoustrojami (Sykora i wsp., 2014; Hole i Staszyk, 2018).

3.2.2. Diagnostyka syndromu EOTRH

Rozpoznanie syndromu EOTRH stawiane jest na podstawie objawów klinicznych oraz zmian w obrazie radiologicznym zmienionych zębów (Hole i Staszyk, 2018). Objawy radiologiczne tego syndromu pojawiają się wcześniej niż objawy kliniczne (Barrett i Easley, 2013; Moore i wsp., 2016; Pearce, 2020). Należy zwrócić uwagę, że u 88% koni nie wykazujących wyraźnych objawów klinicznych stwierdzono radiologiczne objawy resorpcji zębów siecznych, a u 20% koni stwierdzono również radiologiczne objawy hipercementozy (Rehrl i wsp., 2018).

Badanie jamy ustnej może być trudne do przeprowadzenia, ponieważ manipulacje oraz ucisk dotkniętych chorobą zębów wywołują silną reakcję bólową (Rawlinson i Carmalt, 2014). Należy zachować szczególną ostrożność podczas zakładania rozwieracza jamy ustnej, ze względu na ryzyko niebezpiecznego zachowania konia nawet po użyciu wysokich dawek środka sedacyjnego (Rawlinson i Carmalt, 2014).

Badanie radiologiczne jest niezbędne do postawienia ostatecznego rozpoznania, a także kluczowe w ocenie stopnia zaawansowania syndromu EOTRH, szczególnie w jej początkowym stadium, w którym większość zmian dotyczy warstwy poddziąsłowej (Hole i Staszyk, 2018; Rehrl i wsp., 2018). Badanie radiologiczne pomaga także w ustaleniu planu leczenia w tym podjęcia decyzji o ewentualnej ekstrakcji dotkniętych zębów (Rawlinson i Carmalt, 2014). Radiogramy obrazują również stan okolicznych tkanek miękkich i twardych, pomagają w ustaleniu zakresu zmian oraz pokazują ułożenie zębów, które jest niezwykle pomocne w przypadku konieczności wykonania późniejszej ekstrakcji (Rawlinson i Carmalt, 2014).

Przed wykonaniem zdjęć rentgenowskiego zaleca się farmakologicznie uspokojenie konia. Do zobrazowania stanu siekaczy konieczne jest wykonanie zdjęcia rentgenowskiego w projekcji wewnątrzustnej grzbietowo–dobrzusznej dla zębów szczęki i brzuszno–dogrzbietowej dla zębów żuchwy (Barrett i Easley, 2013; Lorello i wsp., 2016). W części przypadków pomocne jest wykonanie dodatkowych projekcji skośnych. Warto zauważyć, że projekcja boczna nie daje zadowalającego efektu diagnostycznego (Rawlinson i Carmalt, 2014). W celu wykonania zdjęcia rentgenowskiego w projekcji grzbietowo–dobrzusznej i brzuszno–dogrzbietowej, kasetę umieszcza się w jamie ustnej konia, najbardziej doogonowo jak to jest możliwe. Kąt nachylenia wiązki promienia względem kasety powinien wynosić 45^{o} dla zębów siecznych szczęki oraz 80^{o} dla zębów siecznych żuchwy (Rawlinson i Earley, 2013; Rawlinson i Carmalt, 2014; Sykora i wsp., 2014; Hole i Staszyk, 2018; Rehrl i wsp., 2018). Pomocne może być również użycie rozwieracza klinowego, który zapobiega potencjalnemu uszkodzeniu kasety (Barrett i Easley, 2013) oraz podpórki pod głowę, która ułatwia jej ustabilizowanie.

3.2.3. Kierunek rozwoju diagnostyki syndromu EOTRH

Większość dotychczasowych badań skupia się na opisie etiologii, patogenezy i przebiegu syndromu EOTRH, natomiast problem wynikający z trudności diagnostycznych, szczególnie we wczesnym stadium, pozostaje nierozwiązany. Zwłaszcza we wczesnych stadiach, rozpoznanie syndromu EOTRH wymaga uwidocznienia wyrostków zębodołowych, w obrębie których objawy radiologiczne są najsilniej wyrażone (Staszyk i wsp., 2008; Rehrl i wsp., 2018). Warto zauważyć, że naprzemienne występowanie objawów radiologicznych resorpcji i hipercementozy zębów

siecznych tworzy mozaikę struktury zęba, którą można rozróżnić wizualnie (Henry i wsp., 2016; Rehrl i wsp., 2018). Proces resorpcji zęba obejmuje cement, szkliwo, zębinę, a niekiedy jamę miazgi (Staszyk i wsp., 2008), a zmiany te widoczne są na radiogramach jako utrata gęstości tkanki zębowej. Zjawisko resorpcji dotyczy też kości wyrostka zębodołowego. Zaobserwować można także poszerzenie przestrzeni więzadłowej, co jest widoczne jako liniowe przejaśnienie między zębem a krawędzią wyrostka zębodołowego (Henry i wsp., 2016). Hipercementoza objawia się jako bulwiaste zacienienie i powiększenie okolicy wierzchołka korzenia zęba (Baratt, 2013; Smedley i wsp., 2015). Dlatego w niniejszej pracy postawiłem hipotezę, że objawy radiologiczne syndromu EOTRH można ocenić ilościowo za pomocą analizy tekstury obrazu, a następnie wykorzystać uzyskane wyniki liczbowe do oceny stopnia zaawansowania syndromu. Weryfikację hipotezy zaproponowałem w oparciu o opisane poniżej protokoły cyfrowego przetwarzania obrazu.

Szybki postęp diagnostyki obrazowej w stomatologii koni (Manso–Díaz i wsp., 2015; Baratt, 2020) umożliwia uzyskanie obrazów cyfrowych o wysokiej rozdzielczości (Dakin i wsp., 2014; Górski i wsp., 2022b; Górski i wsp., 2022c; ; Górski i wsp., 2023). Takie radiogramy można poddać cyfrowemu przetwarzaniu obrazu, które jest coraz częściej wykorzystywane do dostarczania ważnych diagnostycznie danych (van der Stelt, 2005). Głównym celem cyfrowego przetwarzania obrazu jest wdrożenie automatyzacji wykrywania wczesnych objawów radiologicznych, które mogą zostać przeoczone podczas oceny wizualnej. W tym celu stosuje się wspomagane komputerowo algorytmy wykrywania różnic w obrazach radiologicznych (Tan i wsp., 2013; Vidal i wsp., 2021).

Wstępny etap cyfrowego przetwarzania obrazu obejmuje filtrację obrazu w celu zredukowanie szumów. Proces filtrowania poprawia jasność, kontrast i/lub rozgraniczenie obszarów o różnej jasności pikseli (Górski i wsp., 2022b; Górski i wsp., 2022c). Następnie obrazy poddawane są segmentacji, w celu wyznaczenia obszaru podlegającego ocenie ilościowej. Tak przygotowany obraz może zostać poddany analizie tekstury w wyznaczonym obszarze (Maillard, 2003; Mohanaiah i wsp., 2013; Wazarkar i Keshavamurthy, 2018). Analiza tekstury umożliwia opis obrazu za pomocą zestawu cech ilościowych, takich jak cechy oparte na histogramie intensywności pikseli i macierzach poziomu szarości. Metody analizy tekstury obrazu reprezentują siedem głównych klas: podejścia statystyczne, strukturalne, oparte na transformacji obrazu, oparte na modelach, oparte na wykresach, oparte na uczeniu się i oparte na entropii (Floyd, 1991; van Griethuysen i wsp., 2017). W niniejszej pracy dwa wybrane podejścia – podejście statystyczne oraz to oparte na entropii – zostały wykorzystane co oceny cech ilościowych obrazów radiologicznych wyrostków zębodołowych kości siekaczowej koni w przebiegu syndromu EOTRH.

Statystyki opisowe pierwszego i drugiego rzędu są z powodzeniem wykorzystywane w medycynie ludzkiej do ekstrakcji cech tekstury obrazów pozyskanych w badaniach ultrasonograficznych (Sohail i wsp., 2011), termograficznych (Abdel–Nasser i wsp., 2019), rezonansu magnetycznego (Zhang i wsp., 2019; Bębas i wsp., 2021), tomografii komputerowej (Raja i wsp., 2012) oraz radiologicznych (Girejko i wsp., 2018; Sangeetha i wsp., 2021). W medycynie koni statystyki opisowe zostały zastosowane ostatnio w analizie tekstury obrazów termograficznych (Maśko i wsp., 2021; Domino i wsp. 2022a; Domino i wsp. 2022b). Ponieważ metody filtrowania i ekstrakcji cech mogą wpływać na ilościowe cechy obrazu (Humeau–Heurtier, 2019), w niniejszej pracy porównano dziewięć algorytmów filtrowania i sześć metod ekstrakcji cech tekstury obrazu. Miary entropii są stosunkowo nowymi metodami kwantyfikacji nieregularności i złożoności obrazów (Humeau–Heurtier, 2019), z powodzeniem wdrożonymi do opisu obrazów biomedycznych (Da Silva wsp., 2018) w wielu zastosowaniach klinicznych w medycynie ludzkiej (Zarychta, 2019). W medycynie koni miary entropii zostały z powodzeniem zastosowane do analizy tekstury obrazów termograficznych (Domino i wsp., 2022c; Borowska i wsp., 2022).

Obydwa podejścia pozwalają na wprowadzenie cyfrowego przetwarzania obrazu i oceny ilościowej objawów radiograficznych syndromu EOTRH do stomatologii koni. Jednak największym postępem w stomatologii koni będzie wykorzystanie zautomatyzowanych algorytmów sztucznej inteligencji (Tan i wsp., 2013; Nagarajan i wsp., 2014), które będą ułatwiać wczesne rozpoznawanie syndromu EOTRH oraz określać jego stopnia zaawansowania.

4. Cel pracy

Celem pracy było:

1. Określenie rodzajów oraz częstości występowania wybranych wad zgryzu i chorób zębów u koni, zwłaszcza syndromu EOTRH na terenie województwa mazowieckiego (Górski i wsp., 2022a);
2. Analiza skuteczności wybranej metody leczenia ciężkiej postaci syndromu EORTH (Górski i wsp., 2021);
3. Określenie przydatności i skuteczności oceny ilościowej objawów radiologicznych syndromu EOTRH z wykorzystaniem:
    a. protokołów analizy tekstury obrazu opartych na macierzach poziomu szarości (Górski i wsp., 2022b);
    b. protokołów analizy tekstury obrazu opartych na miarach entropii (Górski i wsp., 2022c);
    c. protokołu skalowanego liczenia pikseli (Górski i wsp., 2023).

5. Materiały i metody

5.1. Badane zwierzęta

W pierwszej części pracy zbadano 206 koni, będących w rękach właścicieli prywatnych (114 wałachów, 78 klaczy, 14 ogierów), których średnia wieku wynosiła ± SD: 16,9 ± 7,0 lat. Konie zostały zgłoszone przez właścicieli do lekarza weterynarii na coroczne rutynowe badanie stomatologiczne. Badanie to było klinicznym badaniem weterynaryjnym, wobec którego nie stosuje się Ustawy z dnia 15 stycznia 2015 r. o ochronie zwierząt wykorzystywanych do celów naukowych lub edukacyjnych i nie wymagało zgody komisji etycznej. W badanej grupie zwierząt określano częstość występowania wad zgryzu i chorób zębów w odniesieniu do trzech zmiennych: wieku, płci i rasy. Konie podzielono na cztery grupy wiekowe: (i) 0–5 lat (n = 20; 9 wałachów, 6 ogierów, 5 klaczy), (ii) 6–10 lat (n = 75; 45 wałachów, 4 ogiery), 26 klaczy), (iii) 11–15 lat (n = 57; 30 wałachów, 3 ogiery, 24 klacze) oraz (iv) > 15 lat (n = 54; 30 wałachów, 1 ogier, 23 klacze). Następnie konie grupowano zależnie od płci na: samce (n = 128; 114 wałachów, 14 ogierów) i samice (n = 78; 78 klaczy). Konie podzielono również na trzy podgrupy zależne od rasy: (i) polskie konie sportowe (n = 109; 69 wałachów, 4 ogiery, 36 klaczy), (ii) kuce (n = 40; 22 wałachów, 3 ogiery, 15 klaczy) oraz (iii) „inne" (n = 57; 23 wałachy, 7 ogierów, 27 klaczy) zgodnie z klasyfikacją szczegółowo opisaną w publikacji Górski i wsp., 2022a. Przypadki kliniczne dwóch koni z w/w grupy opisano szczegółowo w publikacji Górski i wsp., 2021.

Druga część badań została przeprowadzona na 80 koniach będących własnością prywatną (średnia wieku ± SD: 16,9 ± 7,0 lat; 37 wałachów, i 43 klaczy). Konie zostały zgłoszone przez właścicieli do lekarza weterynarii na coroczne rutynowe badanie stomatologiczne. Badania zostały przeprowadzone za zgodą II Lokalnej Komisji Etycznej ds. Badań na Zwierzętach w Warszawie (zgoda nr WAW2/091/2020 z dnia 29 lipca 2020 r.). W badanej grupie określano cechy obrazów radiologicznych w odniesieniu do stopnia nasilenia syndromu EOTRH. Badaną grupę scharakteryzowano szczegółowo w publikacjach Górski i wsp., 2022b, 2022c, 2023.

5.2. Badanie kliniczne i radiologiczne

W pierwszej części badań konie (n = 206) poddano badaniu stomatologicznemu obejmującemu podstawowe badanie kliniczne (Radostits i wsp., 2006) i szczegółowe badanie jamy ustnej (Salem i wsp., 2017). Dwa konie z tej grupy zostały poddane dodatkowemu badaniu radiologicznemu oraz wdrożono u nich leczenie (Górski i wsp., 2021). W drugiej części badań konie (n = 80) poddano badaniu stomatologicznemu obejmującemu podstawowe badanie kliniczne (Radostits i wsp., 2006), szczegółowe badanie jamy ustnej (Quinn i wsp., 2005; Salem i wsp., 2017) oraz badanie dodatkowe w postaci badania radiologicznego (Rehrl i wsp., 2018).

Podstawowe badanie kliniczne przeprowadzono według standardowego protokołu (Radostits i wsp., 2006), który obejmowało pomiar temperatury wewnętrznej ciała, liczby tętna, częstotliwości oddechów, ocenę błon śluzowych i czasu kapilarnego oraz węzłów chłonnych podżuchwowych. Na podstawie wyników badania klinicznego, u żadnego z badanych koni nie stwierdzono przeciwwskazań klinicznych do sedacji. Sedację przeprowadzono przez podanie dożylne chlorowodorku detomidyny (Domosedan; Orion Corporation, Espoo, Finlandia) w dawce 0,01 mg/kg m.c. chlorowodorku ksylazyny (Xylapan; Vetoquinol Biowet Sp. z o.o., Gorzów Wielkopolski, Polska) w dawce 0,4 mg/kg m.c. lub obydwu łącznie. W niezbędnych przypadkach podano dożylnie dodatkowo dawkę winianu butorfanolu (Torbugesic; Zoetis Polska Sp. z o.o., Warszawa, Polska) w dawce 0,01 mg/kg m.c.). Uspokojone konie poddano szczegółowemu badaniu jamy ustnej według standardowego protokołu (Quinn i wsp., 2005; Salem i wsp., 2017). Badanie obejmowało oglądanie oraz omacywanie zębów i zostało przeprowadzone z wykorzystaniem narządzi stomatologicznych (Ryc. 12), których wykorzystanie opisano w publikacji Górski i wsp., 2022a.

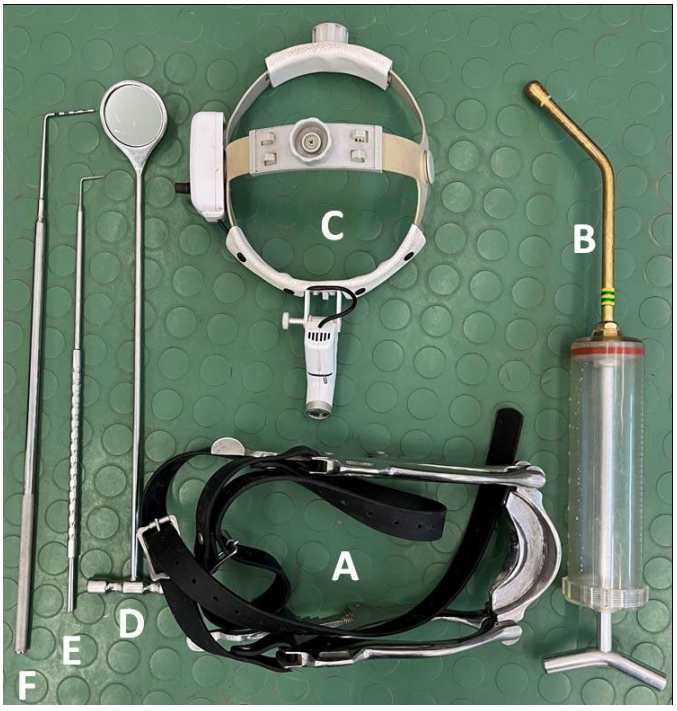

Ryc. 12. Narzędzia stomatologiczne wykorzystywane w badaniu szczegółowym jamy ustnej koni. Rozwieracz Haussmanna (A); strzykawka 400 ml (B); punktowe źródło światła (C); lusterko stomatologiczne (D); hak stomatologiczny i (E) zgłębnik periodontologiczny (Foto. K. Górski).

Wynik szczegółowego badania jamy ustnej, w tym objawy ze strony zębów, przestrzeni międzyzębowych, dziąseł oraz błony śluzowej policzków i języka wskazujące na obecność wad zgryzu i chorób zębów, zapisano na jednolitej Karcie Badania Jamy Ustnej Konia (Ryc. 13).

W terenowej praktyce weterynaryjnej, szczegółowe badanie stomatologiczne obejmuje oglądanie i badanie palpacyjne zębów. Zapisanie wyników badania z wykorzystaniem jednolitej Karty Badania Jamy Ustnej Konia (Ryc. 13) ułatwia kategoryzację objawów i monitorowanie wad zgryzu i chorób zębów nawet u dużej liczby pacjentów. W formularzu tym stosowana jest nomenklatura dentystyczna koni, ujednolicona zgodnie ze zmodyfikowanym systemem Triadana (Floyd, 1991). Prawy łuk zębowy szczęki oznaczony jest jako „1", a lewy jako „2". Lewy łuk zębowy żuchwy oznaczony jest jako „3", a prawy jako „4". Zęby są numerowane kolejno, zaczynając od centralnego zęba siecznego danego łuku („01"), przesuwając się dystalnie i używając kolejnych cyfr ciągu liczbowego, aż do ostatniego zęba trzonowego („11"). Przykładowo centralny (pierwszy) siekacz szczęki prawej oznaczony jest numerem 101, a ostatni ząb trzonowy żuchwy lewej oznaczony jest numerem 311.

KARTA BADANIA JAMY USTNEJ KONIA

DATA	KOŃ	WIEK	PŁEĆ	RASA
MAŚĆ	UŻYTKOWOŚĆ	OSTATNIE BADANIE		
WŁAŚCICIEL		HISTORIA		
ADRES			TEL	

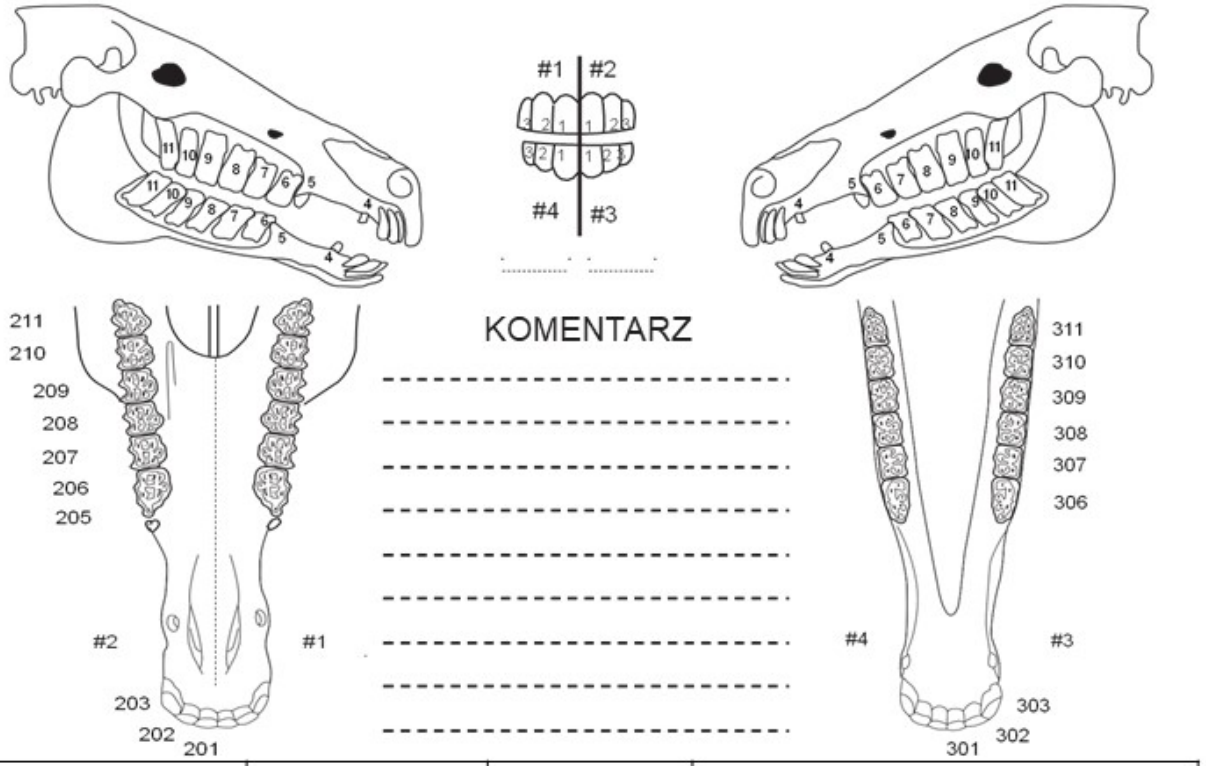

SIEKACZE	KŁY	ZĘBY WILCZE	PRZEDTRZONOWCE / TRZONOWCE
▫ W normie ▫ Przodozgryz ▫ Tyłozgryz ▫ Krzywizna dobrzuszna ▫ Krzywizna dogrzbietowa ▫ Krzywizna skośna ▫ Krzywizna nieregularna ▫ Złamanie ▫ Ząb nadliczbowy ▫ Brak zęba ▫ Kamień nazębny ▫ Zapalenie przyzębia ▫ Inne	▫ W normie ▫ Brak ▫ Skrócony ▫ Zaokrąglony ▫ Kamień nazębny ▫ Złamanie ▫ Ślepy ▫ Zapalenie przyzębia ▫ Inne	▫ Obecne ▫ Brak ▫ Ślepy ▫ Złamanie ▫ Ekstrakcja ▫ Inne	▫ W normie ▫ Ostre krawędzie zębów policzkowych ▫ Zgryz falisty ▫ Zgryz schodkowaty ▫ Zgryz nożycowaty ▫ Haki ▫ ETR ▫ Nadżerki / Wrzody ▫ Zapalenie przyzębia ▫ Ząb mleczny ▫ Fragment zęba mlecznego ▫ Pochyły ▫ Ruchomy ▫ Nadmiernie wysunięty ▫ Nadliczbowy ▫ Brak zęba ▫ Złamanie ▫ Inne Stopień 1 2 3 4

Sedacja: ..... Zalecane ponowne badanie: .....

Ryc. 13. Jednolita Karta Badania Jamy Ustnej Konia. Nazewnictwo wg zmodyfikowanej skali Triadana obejmuje: siekacze (101, 102, 103, 201, 202, 203, 301, 302, 303, 401, 402 i 403); kły (104, 204, 304 i 404); zęby wilcze (105, 205, 305 i 405); przedtrzonowce (106, 107, 108, 206, 207, 208, 306, 307, 308, 406, 407 i 408); trzonowce (109, 110, 111, 209, 210, 211, 309, 310, 311, 409, 410 i 411). ETR – nadmiernie wykształcone krawędzie poprzeczne zębów policzkowych.

Badanie dodatkowe w postaci badania radiologicznego okolicy krawędzi wyrostków zębodołowych kości siekaczowej przeprowadzono zgodnie ze standardowym protokołem (Rehrl i wsp., 2018). Obrazy rentgenowskie uzyskano poprzez zastosowanie techniki kąta dwusiecznego w projekcji wewnątrzustnej, grzbietowo–brzusznej, która wymagała wprowadzenia zabezpieczonej przed pogryzieniem kasety radiologicznej do otwartej jamy ustnej konia (Barrett i Easley, 2013; Henry i wsp., 2016; Górski i wsp., 2021). Zastosowano następujące nastawy lampy rentgenowskiej: 2,5 mAs; 65 kV (Orange 9020HF, Ecoray Co., Ltd.; 3F, Urbanlight B/D, 630, Eonju–ro, Gangnam–gu, Seul, Korea). Oległość lampy do kasety radiologicznej (Saturn 8000, Vievorks Co., Ltd., 41–3, Burim–ro, 170beon–gil, Dongan–gu, Anyang–si, Gyeonggi–do, 14055 Korea) wynosiła 80 cm. Zdjęcia rentgenowskie zapisano na komputerze przenośnym (HP Inc UK Ltd., Earley West, 300 Thames Valley Park Drive, Wielka Brytania) przy użyciu oprogramowania DxWorks (Vievorks Co., Ltd., 41–3, Burim–ro, 170beon–gil, Dongan–gu, Anyang–si, Gyeonggi–do, 14055 Korea) w formacie jpg. Przebieg badania radiologicznego opisano w publikacjach Górski i wsp., 2021; Górski i wsp., 2022b; Górski i wsp., 2022c; Górski i wsp., 2023).

5.3. Ocena obrazów radiologicznych

5.3.1. Klasyczna ocena radiologiczna

Klasyczna ocena radiologiczna radiogramów okolicy krawędzi wyrostków zębodołowych kości siekaczowej obejmowała ocenę wizualną specyficznych objawów radiologicznych typowych dla syndromu EOTRH. Ocena została przeprowadzona zgodnie z wytycznymi radiologicznego systemu klasyfikacji zmian w obrębie zębów siecznych koni zaproponowanego przez Hüls'a i wsp. (2012) z poźniejszą modyfikacją Rehrl i wsp. (2018) (Tabela 1). System ten obejmował ocenę kształtu, struktury powierzchni, konturu zębów siecznych, jak również konturu, gęstość cienia i przebiegu linii będącej odwzorowaniem przestrzeni przyzębia.

Stan każdego zęba siecznego szczęki oceniano indywidualnie i klasyfikowano do jednej z czterech grup w zależności od stopnia nasilenia zmian: normalny (0), łagodny (1), umiarkowany (2) i ciężki (3) (Ryc. 14). Radiogramy oceniano zgodnie z klasyfikacją wprowadzoną przez Hüls'a i wsp. (2012) z późniejszą modyfikacją Rehrl i wsp. (2018). Kryteria radiologiczne obejmowały ocenę kształtu, konturów, wysycenia cienia i przebiegu linii, będącej odwzorowaniem przestrzeni przyzębia.

Tabela 1.Radiologiczny system klasyfikacji zmian w obrębie siekaczy wg Hüls i wsp.

Obraz	Stopień	Zakres zmian radiologicznych
Ciężki	3	Utrata kształtu zęba / część zębodołowa zęba jest szersza niż korona kliniczna / złamanie zęba; powierzchnia zębodołowa zęba nieregularna / szorstka.
Umiarkowany	2	Kształt zęba w dużej mierze zachowany / część zębodołowa zęba nie jest szersza niż korona kliniczna / wyraźnie stępiony wierzchołek korzenia zęba; powierzchnia zębodołowa zęba nieregularna / szorstka.
Łagodny	1	Zachowany kształt zęba / lekko stępiony wierzchołek korzenia zęba / powierzchnia zębodołowa zęba nieregularna / szorstka.
Normalny	0	Brak uchwytnych zmian radiologicznych.

Ryc. 14. Obraz radiologiczny czterech stopni nasilenia syndromu EOTRH. (A) normalny (0), (B) łagodny (1), (C) umiarkowany (2) i (D) ciężki (3) (Foto. K. Górski).

Na podstawie uzyskanych wyników 105 zębów siecznych zakwalifikowano do grupy normalnej (EOTRH 0), 195 do łagodnej (EOTRH 1), 111 do umiarkowanej (EOTRH 2 i 61 do ciężkiej (EOTRH 3). Łącznie poddano ocenie 472 siekaczy z 480 obrazowanych zębów. Z badania wykluczono 8 siekaczy z powodu ich złamania (Górski i wsp., 2022a).

5.3.2 Ocena radiologiczna z wykorzystaniem macierzy poziomu szarości

Etapy przetwarzania obrazu radiograficznego do analizy tekstury z wykorzystaniem macierzy poziomu szarości obejmowały (1) pozyskanie obrazu, (2) segmentację obrazu poprzez naniesienie masek (obszarów zainteresowania – regions of interest (ROIs)), (3) filtrowanie obrazów oraz (4) ekstrakcję cech tekstury obrazu z wykorzystaniem macierzy poziomu szarości (Ryc. 15).

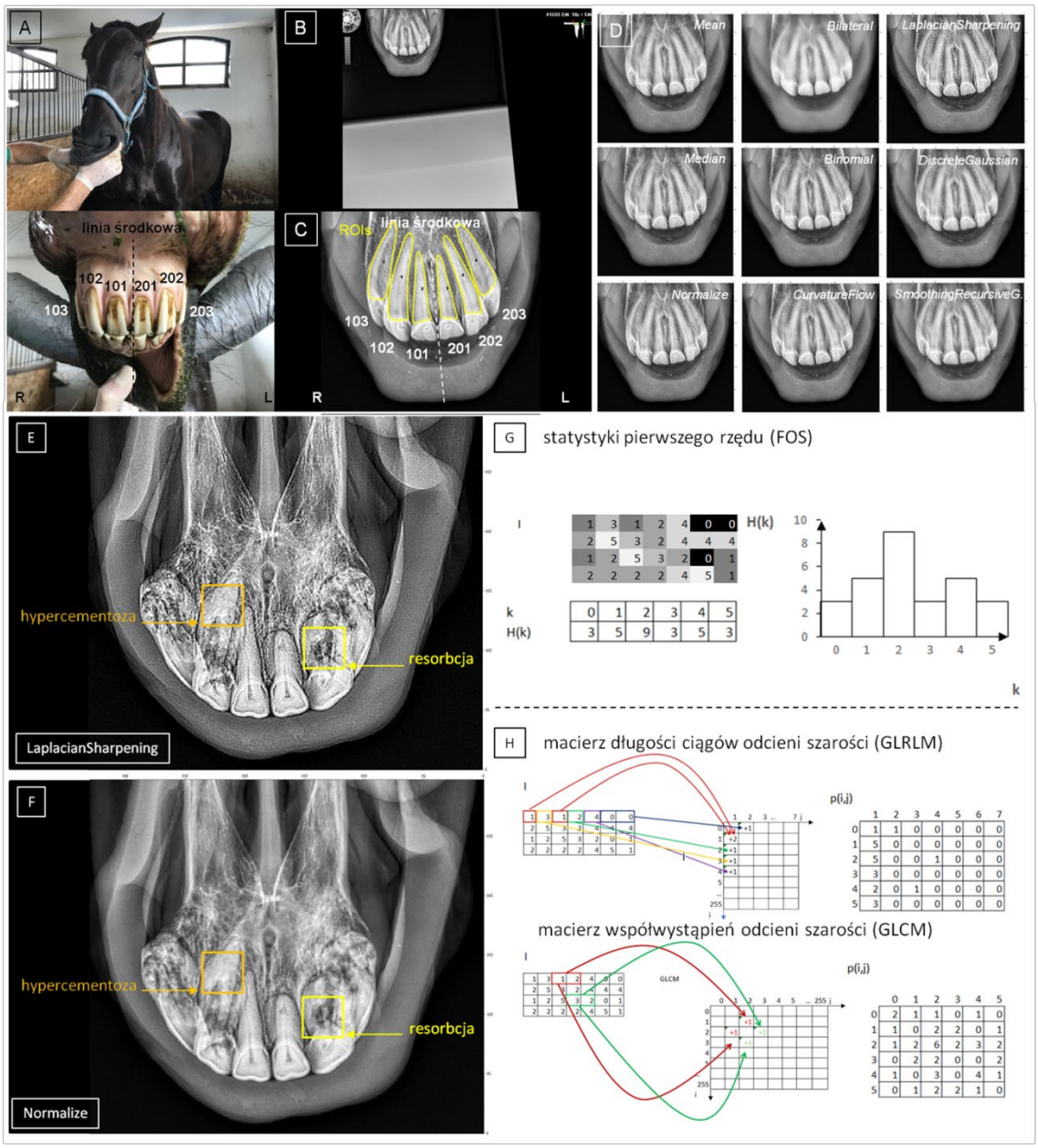

Ryc. 15. Etapy analizy tekstury obrazu radiograficznego zębów siecznych szczęki koni z wykorzystaniem macierzy poziomu szarości. (A,B) pozyskanie obrazu, (C) segmentacja obrazu, (D-F) filtrowanie obrazu, (G,H) ekstrakcja cech tekstury obrazu (Foto. K. Górski).

Do identyfikacji poszczególnych zębów siecznych zastosowano zmodyfikowany system Triadana (Floyd, 1991). Prawy łuk zębowy szczęki oznaczono cyfrą 1, a lewy cyfrą 2. Poszczególne zęby sieczne ponumerowano kolejno, zaczynając od centralnego zęba siecznego szczęki prawej, przypisując mu cyfrę 01, a każdy kolejny ząb, przemieszczając się w kierunku dystalnym miał wyższą cyfrę. Tak więc zęby sieczne 103, 102, 101, 201, 202 i 203 zostały opisane oddzielnie (Ryc. 15A).

Na obrazie zębów siecznych szczęki ROI obrysowano ręcznie. Każdy ROI obejmował największy możliwy obszar korony klinicznej, korony rezerwowej i korzenia zęba. Każdy ROI

był otoczony czterema liniami reprezentującymi: powierzchnię żującą zęba siecznego, jego powierzchnię przyśrodkową, powierzchnię wierzchołka korzenia zęba oraz powierzchnię boczną. ROIs były indywidualnie dopasowane do poszczególnych zębów i nie obejmowały warg, błon śluzowych i kości wyrostków zębodołowych kości siekaczowej jak pokazano w Ryc. 15C. W ten sposób opisano sześć zębów siecznych szczęki każdego konia. ROI zostały opisane przy użyciu oprogramowania ImageJ w wersji 1.46r (Wayne Rasband, National Institutes of Mental Health, Bethesda, MD, USA) i zapisane jako pliki .png.

Analiza tekstury obrazu, w tym etapy filtrowania i ekstrakcji cech, zastosowano do ROIs oznaczonych przez maski podczas segmentacji obrazu. Każdy ROI rozpatrywano oddzielnie. Filtrowanie obrazów wejściowego przeprowadzono przy użyciu dziewięciu algorytmów filtrowania: Mean, Median, Normalize, Bilateral, Binomial, Curvature Flow, Laplacian Sharpening, Discrete Gaussian i Smoothing Recursive Gaussian w pakiecie SimpleITK w środowisku Python (Ryc. 15D-F).

Ekstrakcję cech tekstury obrazu z przefiltrowanych obrazów wyjściowych przeprowadzono przy użyciu sześciu podejść analitycznych: statystyki pierwszego rzędu (FOS), macierz współwystąpień odcieni szarości (GLCM), macierz sąsiednich różnic odcieni szarości (NGTDM), macierz współzależności odcieni szarości (GLDM), macierz długości ciągów odcieni szarości (GLRLM) i macierz wielkości obszarów poziomu szarości (GLSZM). Cechy tekstury obliczono niezależnie dla poszczególnych przefiltrowanych obrazów wyjściowych przy użyciu pakietu PyRadiomics w środowisku Python (Ryc. 15G,H). Protokół oceny radiologicznej z wykorzystaniem macierzy poziomu szarości opisano szczegółowo w publikacji Górski i wsp., 2022b.

5.3.2 Ocena radiologiczna z wykorzystaniem miar entropii

Etapy przetwarzania obrazu radiograficznego do analizy tekstury z wykorzystaniem miar entropii obejmowały (1) pozyskanie obrazu, (2) segmentację obrazu poprzez naniesienie masek, (3) filtrowanie obrazów oraz (4) ekstrakcję cech tekstury obrazu z wykorzystaniem miar entropii (Ryc. 16).

Do badania wybrano centralne siekacze szczęki. W nazewnictwie użyto zmodyfikowanego systemu Triadana (Floyd, 1991), a badane zęby sieczne zostały ponumerowane jako 101 (pierwszy – centralny ząb sieczny szczęki prawej) i 201 (pierwszy – centralny ząb sieczny szczęki lewej) (Ryc. 16A).

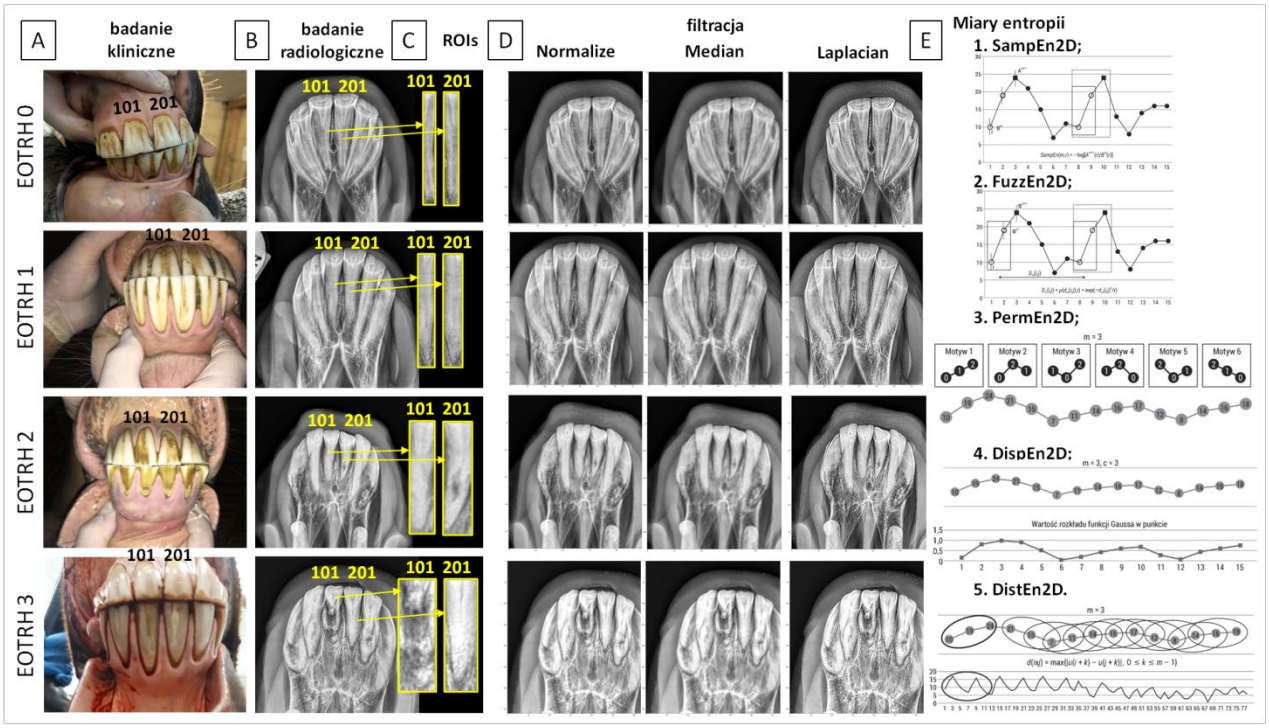

Ryc. 16. Etapy analizy tekstury obrazu radiograficznego zębów siecznych szczęki koni z wykorzystaniem miar entropii. (A,B) pozyskanie obrazu, (C) segmentacja obrazu, (D) filtrowanie obrazu, (E) ekstrakcja cech tekstury obrazu (Foto. K. Górski).

Na obrazie centralnych zębów siecznych szczęki ROIs o kształcie prostokątów naniesiono ręcznie. Każdy ROI obejmuje największy możliwy obszar korony klinicznej, korony rezerwowej i korzenia zęba. ROIs były indywidualnie dopasowane do poszczególnych zębów i nie obejmowały warg, błon śluzowych i kości wyrostków zębodołowych kości siekaczowej jak pokazano w (Ryc. 16C). ROI zostały opisane przy użyciu oprogramowania ImageJ w wersji 1.46r (Wayne Rasband, National Institutes of Mental Health, Bethesda, MD, USA) i zapisane jako pliki .png.

Analiza tekstury obrazu, w tym etapy filtrowania i ekstrakcji cech, zastosowano do ROIs oznaczonych przez maski podczas segmentacji obrazu. Każdy ROI rozpatrywano oddzielnie. Filtrowanie obrazów wejściowego przeprowadzono przy użyciu trzech algorytmów filtrowania: Median, Normalize i Laplacian Sharpening w pakiecie SimpleITK w środowisku Python (Ryc. 16D).

Ekstrakcję cech tekstury obrazu z przefiltrowanych obrazów wyjściowych przeprowadzono przy użyciu pięciu miar entropii: dwuwymiarowej entropii próbki (SampEn2D), dwuwymiarowej entropii rozmytej (FuzzEn2D), dwuwymiarowej entropii permutacyjnej (PermEn2D), dwuwymiarowej entropii rozrzutu (DispEn2D) i dwuwymiarowej entropii rozkładu (DistEn2D) (Borowska, 2023). Cechy tekstury obliczono niezależnie dla poszczególnych przefiltrowanych obrazów wyjściowych za pomocą EntopyHub w środowisku Python (Ryc. 16E). Protokół oceny radiologicznej z wykorzystaniem miar entropii opisano szczegółowo w publikacji Górski i wsp., 2022c.

5.3.4 Ocena radiologiczna z wykorzystaniem protokołu skalowanego liczenia pikseli

Etapy przetwarzania obrazu radiograficznego do skalowanego liczenia pikseli z wykorzystaniem wzorca gęstości obejmowały (1) pozyskanie obrazu, (2) segmentację obrazu poprzez naniesienie masek na zęby sieczne (ROIs) oraz kolejne stopnie (S1-S10) standardu gęstości (AREAs), (3) filtrowanie obrazów oraz (4) ekstrakcję cech tekstury obrazu z wykorzystaniem miar entropii (Ryc. 17).

Do badania wykorzystano sześć zębów siecznych szczęki. W nazewnictwie użyto zmodyfikowanego systemu Triadana (Floyd, 1991). Poszczególne zęby sieczne ponumerowano kolejno, zaczynając od centralnego siekacza szczęki prawej, przypisując mu cyfrę 01, a każdy kolejny ząb, przemieszczając się w kierunku dystalnym miał wyższą cyfrę. Tak więc zęby sieczne 103, 102, 101, 201, 202 i 203 zostały opisane oddzielnie (Ryc. 17A-C).

Na obrazie zębów siecznych szczęki ROI obrysowano ręcznie. Każdy ROI obejmował największy możliwy obszar korony klinicznej, korony rezerwowej i korzenia zęba. Każdy ROI był otoczony czterema liniami reprezentującymi: powierzchnię żującą, powierzchnię przyśrodkową, powierzchnię wierzchołka korzenia oraz powierzchnię boczną zęba siecznego. ROIs były indywidualnie dopasowane do poszczególnych zębów i nie obejmowały warg, błon śluzowych i wyrostków zębodołowych kości siekaczowej jak pokazano w Ryc. 17C. W ten sposób opisano sześć zębów siecznych szczęki każdego konia. ROIs zostały opisane przy użyciu oprogramowania ImageJ w wersji 1.46r (Wayne Rasband, National Institutes of Mental Health, Bethesda, MD, USA) i zapisane jako pliki .png. Na każdym radiogramie opatrzono ręcznie adnotacjami dziesięć prostokątnych obszarów zainteresowania reprezentujących dziesięć stopni (S1–S10) standardu gęstości (AREA). AREAs zostały opisane przy użyciu oprogramowania ImageJ w wersji 1.46r (Wayne Rasband, National Institutes of Mental Health, Bethesda, MD, USA) i zapisane jako pliki .png (Ryc. 17D).

Następnie na każdym radiogramie wyodrębniono jasność pikseli (PB) dla każdego AREA reprezentującego dziesięć stopni (S1–S10) wzorca gęstości. Każdy AREA zwrócił wartości PB w przedziale < 0; 255 > i wyznaczyłem zakresy PB dla S1–S10. Zakresy < PB S1; PB S10 > zliczano w postaci liczby pikseli (NP) dla każdego obszaru ROI reprezentującego każdy ząb sieczny. W ten sposób określono ilościowo stopień absorbcji wiązki promieni rentgenowskich dla każdego zęba siecznego w postaci zestawu danych liczbowych (NP) składającego się z dziesięciu wartości (< NP1; NP10 >). Algorytm zaimplementowano w środowisku Python (Ryc. 17E). Dla każdego ROI obliczono liczbę pikseli (NP) z każdego zakresu. (Górski i wsp., 2023).

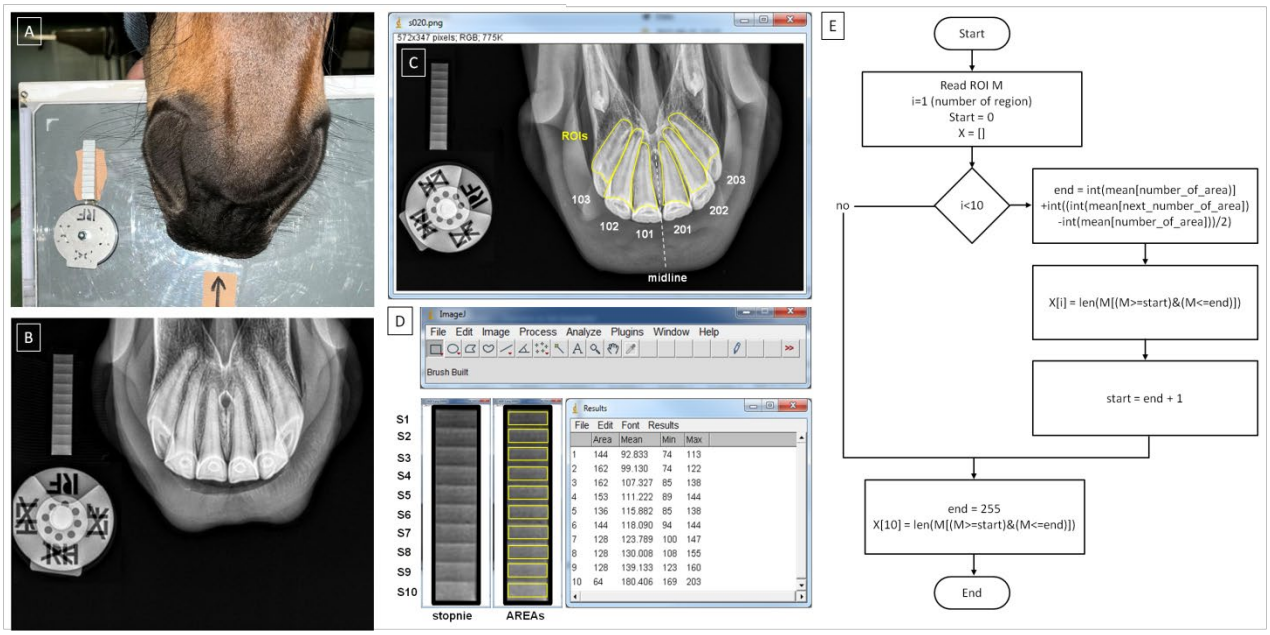

Ryc. 17. Etapy analizy tekstury obrazu radiograficznego zębów siecznych szczęki koni z wykorzystaniem wzorca gęstości i protokołu skalowanego liczenia pikseli. (A,B) pozyskanie obrazu, (C) segmentacja obrazu, (D) segmentacja stopni wzorca gęstości, (E) ekstrakcja cech jasności pikseli i skalowane liczenie pikseli (Foto. K. Górski).

5.4. Analiza statystyczna

Analizę statystyczną przeprowadzono przy użyciu oprogramowania GraphPad Prism6 (GraphPad Software Inc., San Diego, CA, USA).

Częstość występowania wad zgryzu i chorób zębów określono dla całej populacji badanych koni oraz dla poszczególnych podgrup reprezentujących wiek, płeć i rasę za pomocą testu chi– kwadrat. Wartości liczbowe w postaci procentowego udziału wad zgryzu i chorób zębów zwracano względem całkowitej liczby zębów oraz liczby zmienionych zębów. Różnice uznawano za istotne dla $p < 0,05$. Rozkład częstości występowania wad zgryzu i chorób zębów zestawiono w postaci serii danych liczbowych. Rozkład danych testowano za pomocą testu Shapiro-Wilka. Wobec rozkładu niezgodnego z rozkładem normalnym serie danych porównywano za pomocą testu Kruskala–Wallisa dla zębów siecznych, przedtrzonowych i trzonowych oraz testu Manna-Whitneya dla kłów. Różnice uznawano za istotne dla $p < 0,05$. Szczegółowy opis przeprowadzonej analizy danych przedstawiono w publikacji (Górski i wsp., 2022a).

Wartości cech tekstury obrazu w postaci parametrów macierzy poziomów szarości i miar entropii, jak również liczbę pikseli zwróconą przez protokół skalowanego liczenia pikseli zestawiono w postaci bazy danych dla każdego stopnia zaawansowania syndromu EOTRH. Każdą cechę i serie danych testowano niezależnie w kierunku zgodności rozkładu danych

z rozkładem normalnym za pomocą testu Shapiro-Wilka. Wartości cech porównywano pomiędzy stopniami zaawansowania syndromu EOTRH. Serie danych o rozkładzie zgodnym z rozkładem normalnym porównywano przy użyciu jednokierunkowej analizy wariancji popartej testem wielokrotnych powtórzeń Tukey'a. Serie danych z których co najmniej jedna prezentowała rozkład niezgodny z rozkładem normalny porównywano z wykorzystaniem testu Kruskala–Wallisa popartego testem wielokrotnych porównań Dunna. Różnice uznawano za istotne dla $p < 0,05$.

Wartości cech tekstury obrazu w postaci parametrów macierzy poziomów szarości i miar entropii, jak również liczbę pikseli zwróconą przez protokół skalowanego liczenia pikseli wykorzystano następnie do grupowania zębów do grup reprezentujących kolejne stopnie zaawansowania syndromu EOTRH. Czułość (Se), swoistość (Sp), wartość predykcyjną dodatnią (PPV) i wartość predykcyjną ujemną (NPV) obliczano za pomocą standardowych wzorów.

Szczegółowy opis przeprowadzonej analizy danych, w tym wykorzystanie dodatkowych testów i porównań dla poszczególnych serii danych, przedstawiono w poszczególnych publikacjach (Górski i wsp., 2022b; Górski i wsp., 2022c; Górski i wsp., 2023).

6. Wyniki i dyskusja

W wielu przypadkach badanie wizualne jamy ustnej u koni pozwala już na wczesnym etapie na rozpoznanie zaburzeń stomatologicznych i rozpoczęcie leczenia (Limone, 2022). W pierwszej części niniejszej pracy przedstawiono wyniki badania wizualnego i palpacyjnego jamy ustnej 206 koni, u których oceniono łącznie 7912 zębów. W badaniu tym wykazano znaczne rozpowszechnienie zaburzeń w obrębie zębów w populacji badanych koni, co uzasadniło istotność podjęcia szczegółowych badań nad usprawnieniem diagnostyki radiologicznej wybranej wady zgryzu.

W przypadku niektórych zaburzeń, takich jak złamania zębów (Greet, 1999; Dixon i Dacre, 2005; Dacre i wsp., 2007), zakażenie zębów (Greet, 1999; Dixon i Dacre, 2005), przebudowa i liza kości wyrostka zębodołowego (Greet, 1999; Easley, 2002; Dixon i Dacre, 2005) oraz syndrom EOTRH (Henry i wsp., 2016; Rehrl i wsp. 2018), niezbędne jest wykonanie badania radiologicznego. W przypadku oceny wizualnej radiogramów wczesne objawy radiologiczne wymienionych zaburzeń, w tym syndromu EOTRH mogą zostać przeoczone. Późne objawy radiologiczne, odpowiadające ciężkiej hipercementozie i resorpcji zębów są w 3 stopniu zaawansowania syndromu EOTRH stosunkowo dobrze rozróżnialne wizualnie od 0 stopnia zaawansowania EOTRH, a więc zębów zdrowych (Henry i wsp., 2016; Rehrl i wsp. 2018). Natomiast odróżnienie 1 i 2 stopnia zaawansowania tego syndromu niejednokrotnie stanowi wyzwanie kliniczne. Dlatego też, wykorzystanie cyfrowego przetwarzania obrazów radiologicznych oraz automatyzacja tego procesu byłoby niezwykle przydatne w stomatologii koni, szczególnie w wykrywaniu wczesnych objawów radiologicznych syndromu EOTRH (Górski i wsp., 2023).

W prezentowanych badaniach z powodzeniem zastosowano analizę tekstury obrazu z wykorzystaniem macierzy poziomu szarości (Górski i wsp., 2022b), analizę tekstury obrazu z wykorzystaniem dwuwymiarowych miar entropii (Górski i wsp., 2022c) oraz protokół skalowanego liczenia pikseli opartych na wykorzystaniu wzorca gęstości (Górski i wsp., 2023) do oceny ilościowej objawów radiologicznych syndromu EOTRH. Należy zwrócić uwagę, że metody usprawnienia wczesnego wykrywania objawów radiologicznych chorób koni, w tym chorób zębów, stanowią ważny kierunek najnowszych badań w diagnostyce obrazowej koni i wpisują się w aktualny kierunek rozwoju klinicznej medycyny weterynaryjnej (Weller i wsp., 2001; Henninger i wsp., 2003; Pearce, 2020; Pauwels i wsp., 2021; Górski i wsp., 2022b; Górski i wsp., 2022c; Górski i wsp., 2023, Albers i wsp., 2023; Nagy i wsp., 2023; Steel i wsp., 2023). Tym samym można stwierdzić, że niniejsza praca przyczynia się do rozwoju dyscypliny weterynaria w dziedzinie nauk rolniczych.

6.1. Występowanie wad zgryzu i chorób zębów u koni

Ponieważ populacje koni różnią się w poszczególnych krajach i regionach, specyficzna charakterystyka występowania zaburzeń uzębienia może być pomocna dla lokalnych lekarzy weterynarii zajmujących się końmi.

W niniejszym badaniu uwzględniono łącznie 7912 zębów w tym 2444 zębów siecznych, 2462 zębów przedtrzonowych i 2471 zębów trzonowych, przy czym oligodoncję stwierdzono w przypadku 28 zębów siecznych, 10 zębów przedtrzonowych i 3 zębów trzonowych. Ponadto w przypadku 2 zębów trzonowych stwierdzono ząb dodatkowy. Obecność kłów stwierdzono jedynie u samców, w łącznej liczbie 512 kłów, a zęby wilcze u 16 koni w łącznej liczbie 23 zębów wilczych (Tabela 2). Co najmniej jedną wadę zgryzu stwierdzono w 2336 zębach siecznych spośród łącznie 191 koni, co oznacza, że tylko u 9 koni nie stwierdzono wad zgryzu. Wady zgryzu kłów stwierdzono w 2 zębach u 2 różnych koni, zatem 126 samców i wszystkie samice były wolne od tego zaburzenia. Wada zgryzu zębów wilczych występowała w 6 zębach 4 koni, w tym u 2 koni obustronnie. Tylko u 1 konia nie stwierdzono wad zgryzu zębów przedtrzonowych, przy czym u każdego z pozostałych 205 koni wykryto co najmniej jedną wadę zgryzu zębów przedtrzonowych, łącznie w 2450 zębach. Podobnie tylko u 1 konia nie stwierdzono wad zgryzu zębów trzonowych, podczas gdy u 205 koni stwierdzono wady zgryzu łącznie w 2459 zębach trzonowych. Co najmniej jedna wada zgryzu dotyczyła 7253 zębów, co stanowi ponad 91,7% wszystkich zbadanych zębów (Tabela 2).

Tabela 2. Częstość występowania wad zgryzu i chorób zębów w grupie badanych koni.

Zęby	**Liczba zębów**	**Wady zgryzu**	**Choroby**
Sieczne	2444 (30,9)	2336 (29,5; 32,2)	89 (1,1; 34,8)
Kły	512 (6,5)	2 (0,03; 0,03)	88 (1,1; 34,4)
Wilcze	23 (0,3)	6 (0,1; 0,1)	2 (0,03; 0,8)
Przedtrzonowe	2462 (31,1)	2450 (31,0; 33,8)	27 (0,3; 10,5)
Trzonowe	2471 (31,2)	2459 (31,1; 33,9)	50 (0,6; 19,5)
Łącznie	7912	7253 (91,7; 100,0)	256 (3,2; 100,0)
Test chi-kwadrat		$p < 0,0001$	$p < 0,0001$

Dane przedstawiono jako n (% wszystkich koni i % koni w stosunku do liczby zębów dotkniętych wadą / chorobą). Różnice uznano za istotne, dla $p < 0,05$.

Choroby stwierdzono w 89 zębach siecznych u 17 koni, natomiast u 189 koni ich nie stwierdzono W 88 kłach u 44 koni występowały choroby, zatem u 84 samców i u wszystkich samic nie stwierdzono chorób kłów. Choroby zębów wilczych stwierdzono jedynie w przypadku 2 zębów. Choroby zębów przedtrzonowych i trzonowych dotyczyły 27 i 50 zębów odpowiednio u 20 i 33 koni, zatem 186 i 173 konie były wolne od chorób tych zębów. Ogółem stwierdzono co najmniej jedną chorobę w 256 zębach, co stanowi zaledwie 3,2% wszystkich zbadanych zębów (Tabela 2). Zatem częstość występowania wad zgryzu była wyższa niż chorób zębów

w przypadku zębów siecznych, wilczych, przedtrzonowych i trzonowych, ale nie kłów. Wady zgryzu najczęściej dotyczyły zębów siecznych (32,2%), przedtrzonowców (33,8%) i trzonowców (33,9%), natomiast choroby zębów występowały najczęściej w obrębie zębów siecznych (34,8%) i kłów (34,4%) (Tabela 2). Spośród wad zgryzu zębów siecznych, nieprawidłowa krzywizna powierzchni żującej występowała częściej niż inne wady zgryzu. Natomiast spośród chorób zębów siecznych, najczęściej obserwowano obecność kamienia nazębnego. Rozkład częstotliwości występowania poszczególnych wad zgryzu i chorób pozostałych zębów omówiono szczegółowo w publikacji Górski i wsp. (2022a).

W niniejszych badaniach 32,2% i 34,8% badanych koni wykazywało odpowiednio wady zgryzu i choroby w okolicy zębów siecznych. W poprzednich badaniach przeprowadzonych w Polsce wykazano obecność zaburzeń w obrębie zębów siecznych u 53% badanych koni (Siwińska i wsp. 2017), a ogólnie zaburzenia dotyczące co najmniej jednego zęba u 95% badanych koni. Wynik ten jest zbliżony do występowania zaburzeń w obrębie zębów w Australii (94%) (Chinkangsadarn i wsp., 2015) i Szkocji (87%) (Dixon i wsp., 2000), i wyższe niż występowania zaburzeń w obrębie zębów w USA (80%) (Baxter, 2013), Wielkiej Brytanii (79%) (Brigham i wsp., 2000) oraz północno-zachodniej Anglii i północnej Walii (42%) (Ireland i wsp., 2012). Warto zauważyć, że cytowani autorzy (Brigham i wsp., 2000; Baxter 2013; Ireland i wsp., 2012; Dixon i wsp. 2000; Chinkangsadarn i wsp., 2015; Siwińska i wsp., 2017) nie różnicowali problemów stomatologicznych na wady zgryzu i choroby zębów, dlatego wyniki obecnego badania wskazujący na większą częstotliwość występowania wad zgryzu niż chorób zębów jest trudny do porównania. Jednak uzyskane wyniki wskazują na potrzebę okresowego badania stomatologicznego koni, ponieważ w wielu przypadkach wady zgryzu można skorygować prostymi zabiegami, co może zapobiec rozwojowi bardziej zaawansowanych zaburzeń, w tym chorób zębów i przyzębia (Omura i wsp., 2015). Jeśli chodzi o rodzaj i umiejscowienie wad zgryzu, w obrębie zębów siecznych najczęściej stwierdzano nieprawidłową krzywiznę. W przypadku zębów siecznych linia tworzona przez powierzchnie żujące zębów siecznych szczęki i żuchwy powinna leżeć w płaszczyźnie poziomej, a każde jej odchylenie, czy to dobrzuszne, dogrzbietowe, skośne czy nieregularne, stanowi nieprawidłowość (Rodrigues i wsp., 2013). W prezentowanych badaniach krzywiznę dobrzuszną stwierdzono u 157 koni, krzywiznę nieregularną i skośną odpowiednio u 21 i 10 koni, a krzywizny dogrzbietowej nie zaobserwowano. Krzywiznę zębów można uznać za zaburzenie nabyte, związane z wiekiem, prawdopodobnie wtórne do zaburzeń występujących w zębach policzkowych (du Toit wsp., 2009; Rodrigues i wsp., 2013). Jednak niezależnie od jej charakterystyki, zaleca się stopniową korekcję każdej nieprawidłowej krzywizny zębów w celu przywrócenia prawidłowego kształtu zębów siecznych i profilaktyki nieprawidłowości w obrębie powierzchni żującej zębów policzkowych

(Dixon i Dacre, 2005, Rodrigues i wsp., 2013). Ze względu na rozkład poszczególnych chorób zębów, w obrębie zębów siecznych najczęściej stwierdzano kamień nazębny. Kamień nazębny, a w zasadzie jego nagromadzenie, powstaje w wyniku mineralizacji flory bakteryjnej płytki nazębnej (Klugh, 2010). Kły i zęby sieczne żuchwy są najczęściej predysponowane do odkładania się kamienia nazębnego (Klugh, 2010), co jest zgodne z prezentowanymi wynikami.

Biorąc pod uwagę wiek koni, w grupie koni do 5 roku życia stwierdzono co najmniej 1 wadę zgryzu w 143 zębach siekaczy u 12 koni. Natomiast w obrębie zębów siecznych nie stwierdzono objawów klinicznych chorób zębów. W grupie koni w wieku od 6 do 10 lat stwierdzono co najmniej jedną wadę zgryzu we wszystkich zębach siecznych, czyli w 900 zębach u 75 koni, a choroby zębów stwierdzono w przypadku 5 zębów siecznych u 4 koni. W grupie koni w wieku od 11 do 15 lat, spośród wszystkich zębów siecznych tylko jeden ząb nie wykazywał cech wad zgryzu, a choroby zębów stwierdzono w przypadku 17 siekaczy u 6 koni. W najstarszej grupie koni, czyli powyżej 15 roku życia, wady zgryzu stwierdzono w przypadku 610 zębów u 53 koni, a choroby zębów w przypadku 67 siekaczy u 7 koni (Tabela 3). Wady zgryzu dotyczyły najczęściej zębów siecznych, przedtrzonowych i trzonowych we wszystkich badanych grupach wiekowych i mieściły się w przedziale od 22,9% do 38,4% wszystkich zmienionych zębów. Natomiast choroby zębów najczęściej dotyczyły kłów u koni w wieku 6–10 lat (65,1%) i 11–15 lat (45,3%), oraz zębów siecznych w najstarszej grupie koni (48,9%) (Tabela 3). Występowanie syndromu EOTRH stwierdzono w 0,21% zębów siecznych koni w wieku 11–15 lat oraz w 3,11% zębów siecznych koni w wieku powyżej 15 lat. Częstość występowania wad zgryzu i chorób zębów pozostałych zębów w odniesieniu do wieku koni omówiono szczegółowo w publikacji Górski i wsp. (2022a).

Warto zauważyć, że niektóre wrodzone wady zgryzu, takie jak przodozgryz i tyłozgryz, które łatwo diagnozuje się u źrebiąt, można wcześnie skorygować (Easley, 1998; Omura i wsp., 2015), zapobiegając pogłębianiu się wady i rozwojowi dalszych zaburzeń uzębienia. Wymienione wady predysponują do zaburzeń ułożenia i stykania się zębów policzkowych, co może skutkować powstawaniem haków zębów szczęki lub żuchwy (Foster, 2013). Obserwacja ta jest zgodna z uzyskanymi wynikami zgodnie z którymi w najmłodszej grupie wiekowej nie stwierdzono chorób zębów.

Tabela 3. Częstość występowania wad zgryzu i chorób zębów w grupie badanych koni w odniesieniu do wieku koni (grupa 0–5 lat, n = 20, grupa 6–10 lat, n = 75; grupa 11–15 lat, n = 57; grupa > 15 lat, n = 54).

Wiek	Zęby	Liczba zębów	Wady zgryzu	Choroby
0–5 lat	Sieczne	239 (3,0)	143 (1,8; 22,9)	0 (0; 0)
	Kły	60 (0,8)	0 (0; 0)	0 (0; 0)
	Wilcze	5 (0,1)	2 (0,03; 0,3)	1 (0,01; 100,0)
	Przedtrzonowe	240 (3,0)	240 (3,0; 38,4)	0 (0; 0)
	Trzonowe	240 (3,0)	240 (3,0; 38,4)	0 (0; 0)
Łącznie		784 (9,9)	625 (7,9)	1 (0,01)
Test chi-kwadrat			p < 0,0001;	p < 0,0001
6–10 lat	Sieczne	900 (11,4)	900 (11,4; 33,3)	5 (0,1; 11,6)
	Kły	196 (2,5)	1 (0,01; 0,04)	28 (0,35; 65,1)
	Wilcze	12 (0,2)	4 (0,1; 0,1)	1 (0,01; 2,3)
	Przedtrzonowe	899 (11,4)	899 (11,4; 33,2)	4 (0,05; 9,3)
	Trzonowe	900 (11,4)	900 (11,4; 33,3)	5 (0,1; 11,6)
Łącznie		2907 (36,7)	2704 (34,2)	43 (0,5)
Test chi-kwadrat			p < 0,0001;	p < 0,0001
11–15 lat	Sieczne	684 (8,6)	683 (8,6; 33,3)	17 (0,2; 22,7)
	Kły	132 (1,7)	1 (0,01; 0,05)	34 (0,4; 45,3)
	Wilcze	1 (0,01)	0 (0; 0)	0 (0; 0)
	Przedtrzonowe	684 (8,6)	684 (8,6; 33,3)	10 (0,1; 13,3)
	Trzonowe	685 (8,7)	685 (8,7; 33,4)	14 (0,2; 18,7)
Łącznie		2185 (26,7)	2053 (25,9)	75 (0,9)
Test chi-kwadrat			p < 0,0001;	p < 0,0001
>15 lat	Sieczne	622 (7,9)	610 (7,7; 32,6)	67 (0,9; 48,9)
	Kły	124 (1,6)	0 (0; 0)	26 (0,3; 19,0)
	Wilcze	5 (0,1)	0 (0; 0)	0 (0; 0)
	Przedtrzonowe	639 (8,1)	627 (7,9; 33,5)	13 (0,2; 9,5)
	Trzonowe	646 (8,2)	634 (8,0; 33,9)	31 (0,4; 22,6)
Łącznie		2036 (25,7)	1871 (23,6)	137 (1,7)
Test chi-kwadrat			p < 0,0001;	p < 0,0001
Łącznie		7912	7253 (91,7)	256 (3,2)

Dane przedstawiono jako n (% wszystkich koni i % koni w stosunku do liczby zębów dotkniętych wadą / chorobą). Różnice uznano za istotne, dla p < 0,05.

Warto jednak zauważyć, że częstość występowania chorób zębów, a nie wad zgryzu, wzrastała wraz z wiekiem. Biorąc pod uwagę, że niektóre zaburzenia zębów, zwłaszcza choroby zębów, są powszechne u koni starszych, edukowanie właścicieli starych koni i zalecanie profilaktycznych zabiegów dentystycznych w tej grupy wiekowej może być kluczem do minimalizacji negatywnego wpływu chorób zębów na stan zdrowia i kondycję koni starszych (du Toit i wsp., 2011). W przypadku zębów siecznych, syndrom EOTRH i kamień nazębny nie występował u koni poniżej 5 roku życia, występował z większą częstością u koni powyżej 15 roku życia. Obecne obserwacje są zgodne z wcześniejszymi badaniami dotyczącymi predylekcji wieku w występowaniu zarówno wad zgryzu (Staszyk i wsp., 2008), jak i chorób zębów (Klugh, 2010).

Ryzyko wystąpienia EOTRH związane z wiekiem zostało potwierdzone w wielu badaniach (Rehrl i wsp., 2018; Hole i Staszyk, 2018).

Biorąc pod uwagę płeć koni, co najmniej jedną wadę zgryzu stwierdzono w 1449 zębach siecznych u 122 samców, oraz 887 zębach siecznych u 75 samic. Choroby zębów siecznych zaobserwowano w przypadku 45 zębów siecznych u 11 samców, oraz 44 zębów siecznych u 6 klaczy. Wady zgryzu dotyczyły przede wszystkim zębów siecznych, zarówno u samców (32,2%) jak i samic (32,3%), natomiast choroby zębów najczęściej dotyczyły kłów u samców (50,6%) i zębów siecznych u samic (53,7%) (Tabela 4).

Tabela 4. Częstość występowania wad zgryzu i chorób zębów w grupie badanych koni w odniesieniu do płci koni (grupa samców, n = 128; grupa samic, n = 78).

Płeć	**Zęby**	**Liczba zębów**	**Wady zgryzu**	**Choroby**
Samce	Sieczne	1521 (19,2)	1449 (18,3; 32,2)	45 (0,6; 25,9)
	Kły	512 (6,5)	2 (0,03; 0,04)	88 (1,1; 50,6)
	Wilcze	14 (0,2)	6 (0,1; 0,1)	1 (0,01; 0,6)
	Przedtrzonowe	1533 (19,4)	1521 (19,2; 33,8)	16 (0,2; 9,2)
	Trzonowe	1537 (19,4)	1525 (19,3; 33,9)	24 (0,3; 13,8)
Łącznie		5117 (64,7)	4503 (56,9)	174 (2,2)
Test chi-kwadrat			$p < 0,0001$;	$p < 0,0001$
Samice	Sieczne	923 (11,7)	887 (11,2; 32,3)	44 (0,6; 53,7)
	Kły	0 (0)	0 (0; 0)	0 (0; 0)
	Wilcze	9 (0,1)	0 (0; 0)	1 (0,01; 1,2)
	Przedtrzonowe	929 (11,7)	929 (11,7; 33,8)	11 (0,1; 13,4)
	Trzonowe	934 (11,8)	934 (11,8; 34,0)	26 (0,3; 31,7)
Łącznie		2795 (35,3)	2750 (34,8)	82 (1,0)
Test chi-kwadrat			$p < 0,0001$;	$p < 0,0001$
Łącznie		7912	7253 (91,7)	256 (3,2)

Dane przedstawiono jako n (% wszystkich koni i % koni w stosunku do liczby zębów dotkniętych wadą / chorobą). Różnice uznano za istotne, dla $p < 0,05$.

W odniesieniu do płci, nie stwierdzono zębów nadliczbowych zarówno u samców, jak i u samic, natomiast tylko w grupie samic nie zaobserwowano diastem. W grupie samców najczęściej występującą chorobą był kamień nazębny, natomiast w grupie samic nie stwierdzono różnic w rozkładzie częstotliwości występowania chorób zębów. Nie stwierdzono różnic w występowaniu syndromu EOTRH pomiędzy grupą samic i samców. Częstość występowania wad zgryzu i chorób zębów pozostałych zębów w odniesieniu do płci koni omówiono szczegółowo w publikacji Górski i wsp. (2022a).

Biorąc pod uwagę rasę koni, wśród polskich koni sportowych stwierdzono co najmniej jedną wadę zgryzu w obrębie 1270 zębów siecznych u 108 koni, zatem tylko u 1 konia tej rasy nie stwierdzono wady zgryzu zębów siecznych. W grupie kucy stwierdzono co najmniej jedną wadę zgryzu we wszystkich zębach siecznych. Natomiast w grupie koni innych ras stwierdzono co najmniej jedną wadę zgryzu w 600 zębów siecznych u 50 koni, a u 7 koni nie stwierdzono wad

zgryzu zębów siecznych. Chorobę zębów siecznych stwierdzono w przypadku 55 zębów u 11 polskich koni sportowych, 18 zębów u 2 kucy oraz 16 zębów u 4 koni innych ras. Wady zgryzu dotyczyły najczęściej zębów siecznych, przedtrzonowych i trzonowych we wszystkich grupach rasowych. Natomiast choroby zębów dotyczyły najczęściej kłów w grupie polskich koni sportowych (41,2%) oraz zębów siecznych w grupie kucy (40,9%) i koni innych ras (38,1%) (Tabela 5).

Tabela 5. Częstość występowania wad zgryzu i chorób zębów w grupie badanych koni w odniesieniu do rasy koni (grupa polski koni sportowy (PWB), n = 109; grupa kucy, n = 40; grupa koni innych ras, n = 57).

Rasa	Zęby	Liczba zębów	Wady zgryzu	Choroby
PWB	Sieczne	1282 (16,2)	1270 (16,1; 32,7)	55 (0,7; 32,4)
	Kły	292 (3,7)	0 (0; 0)	70 (0,9; 41,2)
	Wilcze	13 (0,2)	4 (0,1; 0,1)	2 (0,03; 1,2)
	Przedtrzonowe	1304 (16,5)	1304 (16,5; 33,5)	17 (0,2; 10,0)
	Trzonowe	1309 (16,5)	1309 (16,5; 33,7)	26 (0,3; 15,3)
Łącznie		4200 (53,1)	3887 (49,1)	170 (2,1)
Test chi-kwadrat			p < 0,0001;	p < 0,0001
Kuce	Sieczne	478 (6,0)	466 (5,9; 33,3)	18 (0,2; 40,9)
	Kły	100 (1,3)	0 (0; 0)	8 (0,1; 18,2)
	Wilcze	5 (0,1)	1 (0,01; 0,1)	0 (0; 0)
	Przedtrzonowe	476 (6,0)	464 (5,9; 33,2)	6 (0,1; 13,6)
	Trzonowe	479 (6,1)	467 (5,9; 33,4)	12 (0,2; 27,3)
Łącznie		1538 (19,4)	1398 (17,7)	1494 (18,9)
Test chi-kwadrat			p < 0,0001;	p < 0,0001
Inne	Sieczne	684 (8,6)	600 (7,6; 30,5)	16 (0,2; 38,1)
	Kły	120 (1,5)	2 (0,01; 0,1)	10 (0,1; 23,8)
	Wilcze	5 (0,1)	1 (0,01; 0,1)	0 (0; 0)
	Przedtrzonowe	682 (8,6)	682 (8,6; 34,7)	4 (0,05; 9,5)
	Trzonowe	683 (8,6)	683 (8,6; 34,7)	12 (0,2; 28,6)
Łącznie		2174 (27,5)	1968 (24,9)	42 (0,5)
Test chi-kwadrat			p < 0,0001;	p < 0,0001
Łącznie		7912	7253 (91,7)	256 (3,2)

Dane przedstawiono jako n (% wszystkich koni i % koni w stosunku do liczby zębów dotkniętych wadą / chorobą). Różnice uznano za istotne, dla p < 0,05.

Biorąc pod uwagę rasę koni, nie stwierdzono diastem u polskich koni sportowych oraz haków wśród kucy. W grupie koni innych ras nie stwierdzono przodozgryzu, diastem, oligodoncji ani przetrwałych zębów mlecznych. Spośród chorób zębów, kamień nazębny zębów siecznych w występował najczęściej w grupie polskich koni sportowych, ale nie w grupie kucy i koni innych ras. Nie stwierdzono zależnych od rasy koni różnic w występowaniu syndromu EOTRH. Częstość występowania wad zgryzu i chorób zębów pozostałych zębów w odniesieniu do ras koni omówiono szczegółowo w publikacji Górski i wsp. (2022a).

Co ciekawe, częstotliwość występowania kilku zaburzeń uzębienia wydaje się być zależna od wieku koni, a nie od płci czy rasy. Niezależnie od badanych predylekcji wady zgryzu zębów

siecznych stanowią najczęściej obserwowany problem. Wraz z wiekiem zmienia się rodzaj obserwowanych wad. Zmniejsza się liczba zaburzeń zgryzu typowych dla młodych koni na rzecz resorpcji i hipercementozy zębów w syndromie EOTRH, którego występowanie wyraźnie rośnie wraz z wiekiem konia (Rehrl i wsp., 2018; Hole i Staszyk, 2018). Wyjątek stanowiły niewyrznięte kły, ślepe zęby wilcze, złamania kłów i zębów wilczych oraz kamień nazębny kłów, które ze względu na predylekcje zależne od płci (Floyd, 1991) stwierdzano u samców, a nie u klaczy.

6.2. Obraz kliniczny i radiologiczny syndromu EOTRH

W publikacji Górski i wsp. (2021) przedstawiono przypadki kliniczne dwóch koni u których stwierdzono objawy kliniczne i radiologiczne ciężkiego syndromu EOTRH. Pierwszym opisanym przypadkiem był wałach, w wieku 21 lat, rasy szlachetnej półkrwi, o masie ciała ok. 650 kg, użytkowany rekreacyjnie. Z wywiadu wiadomo, że u konia regularnie przeprowadzano badanie jamy ustnej i korekcję zgryzu, ale mimo to od dłuższego czasu był on wybredny, nie dojadał paszy treściwej, chętnie przyjmował natomiast paszę objętościową w postaci siana oraz trawy. Już 6 lat przed opisem przypadku, a więc u konia w wieku 15 lat, właściciel zauważył pierwsze niespecyficzne objawy kliniczne syndromu EOTRH w postaci zaczerwienienia w okolicy dziąseł siekaczy. Właściciel informował również o pojawiających się w kolejnych latach objawu klinicznego syndromu EOTRH w postaci odsłonięcia fragmentu korzeni zębów siecznych. Stan zapalny tej okolicy postępował, pomimo stosowania zabiegów higienicznych. W kolejnych latach stan zębów siecznych pogarszał się. W szczegółowym badaniu jamy ustnej stwierdzono odór z jamy ustnej, nadmierne ślinienie, różnego stopnia ruchomość wszystkich siekaczy, ból podczas omacywania siekaczy, odkładanie się kamienia nazębnego oraz gromadzenie się pokarmu miedzy zębami. Stwierdzono również obniżenie linii dziąseł z jednoczesnym odsłonięciem fragmentów korony rezerwowej oraz korzeni pojedynczych zębów. W łukach zębowych żuchwy stwierdzono brak zęba 303 i 403. Dodatkowo w okolicy zęba stwierdzono 403 obecność uszypułowanego nadziąślaka wykazującego znaczną ruchomość.

Drugim opisanym przypadkiem był wałach, w wieku 24 lat, rasy szlachetnej półkrwi, o masie ciała ok. 700 kg, użytkowany rekreacyjnie. Z wywiadu wiadomo, że kontrola jamy ustnej przeprowadzana była regularnie, co 6 miesięcy. Koń od dłuższego czasu miał problemy z gryzieniem podawanych jabłek lub marchewek, okresowo pojawiał się również odór z jamy ustnej oraz nadmierne ślinienie. Przyjmowanie pozostałej paszy nie sprawiało mu problemu. W szczegółowym badaniu jamy ustnej stwierdzono nadmierne ślinienie oraz umiarkowany odór z jamy ustnej, brak zęba 103, 201 i 203, pozostałości korzeni brakujących zębów 103 i 201, nadmierne odkładanie się kamienia nazębnego na pozostałych zębach, zapalenie dziąseł,

nadmiernie wyrażone brodawki dziąseł, obniżone kieszonki dziąsłowe oraz ruchomość zębów siecznych z obecną reakcją bólową przy ich ucisku.

W obu przypadkach, w obrazie radiologicznym stwierdzono cechy radiologiczne resorpcji (przejaśnienia w rzucie zębów) oraz hipercementozy (zacienienia w rzucie zębów) zębów siecznych oraz utratę kształtu poszczególnych zębów, poszerzenie części zębodołowej części zębów i nieregularną powierzchnię zębodołową wszystkich zębów siecznych.

U obydwóch koni przeprowadzono radykalną ekstrakcję zmienionych zębów siecznych. Następnie opisano szczegółowo proces gojenia i końcowy efekt zabiegu. W obu przypadkach, po całkowitym wygojeniu się zębodołów, właściciele obserwowali znaczną poprawę zachowania i kondycji koni.

6.3. Zastosowanie macierzy poziomu szarości w ocenie objawów radiologicznych syndromu EOTRH

Spośród 837 zwróconych kombinacji protokołów filtrowania (n = 9) i cech tekstury obrazu zwróconych z zastosowaniem macierzy poziomu szarości (n = 93, w tym FOS n = 18, GLCM n = 24, NGTDM n = 5, GLDM n = 14, GLRLM n = 16 i GLSZM n = 16) 13 cech FOS, 17 cech GLCM, 4 cechy NGTDM, 10 cech GLDM, 13 cech GLRLM i 8 cech GLSZM różniło się pomiędzy stopniami zaawansowania syndromu EOTRH. Różnice te zostały omówione szczegółowo w publikacji Górski i wsp. (2022b).

Spośród 683 zwróconych kombinacji różniących się pomiędzy stopniami zaawansowania syndromu EOTRH, 410 cech rosło lub malało wraz ze stopniem syndromu EOTRH (Ryc. 18).

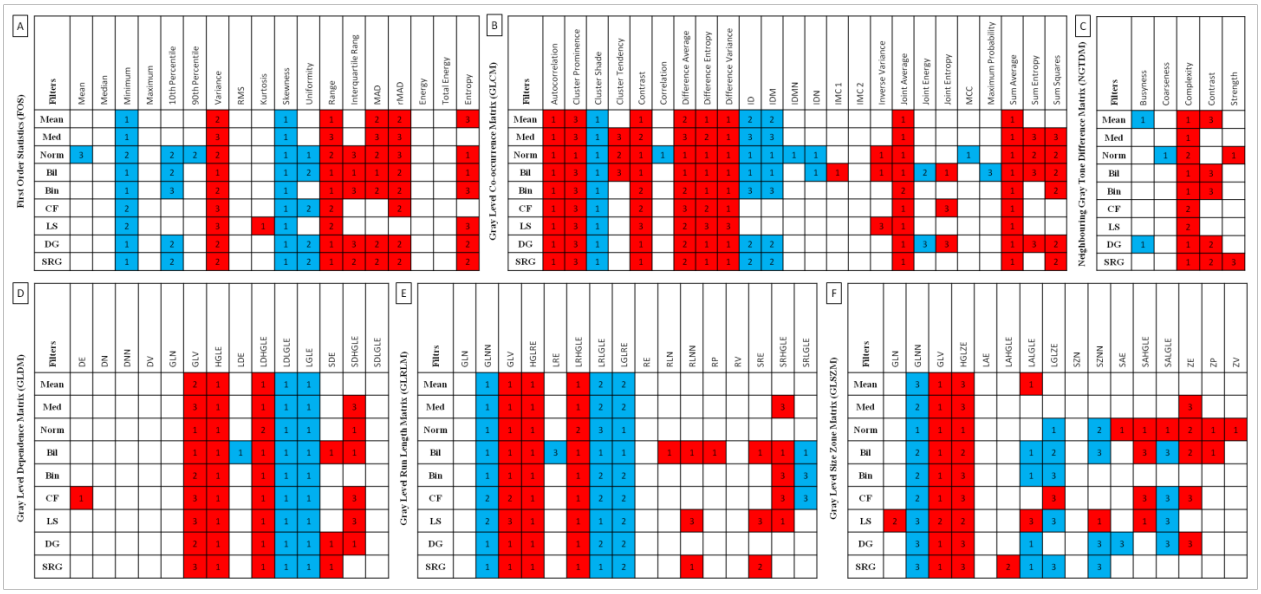

Ryc. 18. Cechy analizy tekstury obrazu z zastosowaniem (A) statystyki pierwszego rzędu (FOS), (B) macierz współwystąpień odcieni szarości (GLCM), (C) macierz sąsiednich różnic odcieni szarości (NGTDM), (D) macierz współzależności odcieni szarości (GLDM), (E) macierz długości ciągów odcieni szarości (GLRLM) i (F) macierz wielkości obszarów poziomu szarości (GLSZM). Cechy tekstury obrazu wyodrębnione z obrazów wyjściowych przefiltrowanych z wykorzystaniem filtrów: Mean, Median (Med), Normalize (Norm), Bilateral (Bil), Binomial (Bin), Curvature Flow (CF), Laplacian Sharpening (LS), Discrete Gaussian, (DG) i Smoothing Recursive Gaussian (SRG). Istotny wzrost wartości cech w zależności od stopnia zaawansowania syndromu EOTRH zaznaczono kolorem czerwonym, a istotny spadek wartości cech zaznaczono kolorem niebieskim. Liczba w komórce wskazuje stopień syndromu EOTRH, od którego zaczyna się wzrost lub spadek wartości cech.

Spośród zwróconych cech wybrano te które: (i) rosną lub malejące od stopnia 1 syndromu EOTRH dla co najmniej jednego filtra oraz (ii) rosną lub maleją w sposób powtarzalny niezależnie od zastosowanego filtrowania. W ten sposób wybrano cechy tekstury obrazu wyodrębnionych z zastosowaniem macierzy GLCM i GLRLM oraz filtracji Normalize do dalszej analizy. Szczegółowy protokół wyodrębniania protokołów filtracji i cech tekstury obrazu omówiono w publikacji Górski i wsp. (2022b). Warto zauważyć, że większość cech statystyk drugiego rzędu (GLCM, NGTDM, GLDM, GLRLM i GLSZM) różniła się pomiędzy stopniami syndromu EOTRH po przefiltrowaniu przez filtry Normalize i Bilateral (GLCM, GLDM) lub filtr Normalize (GLSZM) lub filtr Bilateral (GLRLM), podczas gdy większość cech statystyki pierwszego rzędu (FOS) różniła się pomiędzy stopniami syndromu EOTRH po przefiltrowaniu przez filtr Laplacian Sharpening. Ponieważ filtr Laplacian Sharpening zwraca obrazy wyjściowe ostrzejsze niż wejściowe (Al– meen i wsp., 2012), filtr ten wydaje się być bardziej odpowiedni

dla statystyki pierwszego rzędu niż statystyk drugiego rzędu. Co ciekawe, filtr Normalize zwiększa kontrast obrazu (Heidari i wsp., 2020), a filtr Bilateral wygładza obraz wejściowy w obszarach jednorodnych, zachowując krawędzie (Yang i wsp., 2011), co wydaje się korzystne dla statystyk drugiego rzędu. Inne zróżnicowanie zębów siecznych po przefiltrowaniu przez różne filtry może wynikać z charakterystyki poszczególnych podejść do analizy tekstury. FOS bada piksele obecne na obrazie, podczas gdy GLCM, GLDM, GLRLM i GLSZM badają rozkład przestrzenny pikseli (Jusman i wsp., 2020). Dlatego wyostrzenie obrazu lub poprawa kontrastu, zwraca większe różnice cech (Nagarajan i wsp., 2014; Kociołek i wsp., 2020). Pozostałe badane filtry zwracają obrazy wyjściowe po redukcji szumów (filtry Mean, Median i Curvature Flow), rozmyciu (filtry Mean i Discrete Gaussian), wygładzeniu (filtry Median, Curvature Flow, Discrete Gaussian i Smoothing Recursive Gaussian) lub separacja rozmycia (filtr Binomial) (Chandra i Verma, 2020), a ich zastosowanie nie zwiększało różnicowania stopni syndromu EOTRH na podstawie porównania wartości cech zarówno statystyk pierwszego i drugiego rzędu.

Spośród 24 cech GLCM wyodrębnionych z obrazów wyjściowych przefiltrowanych przez filtr Normalize, 16 cech spełniało pierwsze kryterium selekcji i rosło lub malało od stopnia 1 syndromu EOTRH były to: Autocorrelation, Cluster Prominence, Cluster Shade, Contrast, Correlation, Difference Average, Difference Entropy, Difference Variance, ID, IDM, IDMN, IDN, Inverse Variance, Joint Average, MCC oraz Sum Average (Ryc. 19). Uznano, że te cechy GLCM lepiej niż inne pozwalają na ilościową ocenę objawów radiologicznych syndromu EOTRH. W przypadku GLCM, Contrast pokazujące lokalną zmianę natężenia skali szarości, Difference Average wskazuje związek pomiędzy występowaniem par o podobnych/różnych wartościach intensywności skali szarości, Difference Entropy pokazuje losowość w sąsiedzkich różnicach wartości natężenia poziomu szarości, Join Average raportuje średni poziom intensywność rozkładu poziomów szarości a Sum Average mierzy relacje między parami o niższych/wyższych wartościach intensywności poziomów szarości (Zwanenburg i wsp., 2016). Można zauważyć, że wraz ze stopniem syndromu EOTRH wzrastają nie tylko miary intensywności skali szarości, ale także miary szorstkości (Autocorrelation) i heterogenności (Difference Variance) (Zwanenburg i wsp., 2016), co może być obiecującym wskaźnikiem zmian w obrazie radiograficznym spowodowanych resorpcją i hipercementozą zębów siecznych (Hüls i wsp., 2012; Henry i wsp., 2016; Rehrl i wsp., 2018). Jednakże rola skośności i jednorodności poziomów szarości, odzwierciedlona przez Cluster Prominence i Cluster Shade (Zwanenburg i wsp., 2016; Humeau–Heurtier, 2019), wymaga dalszych badań.

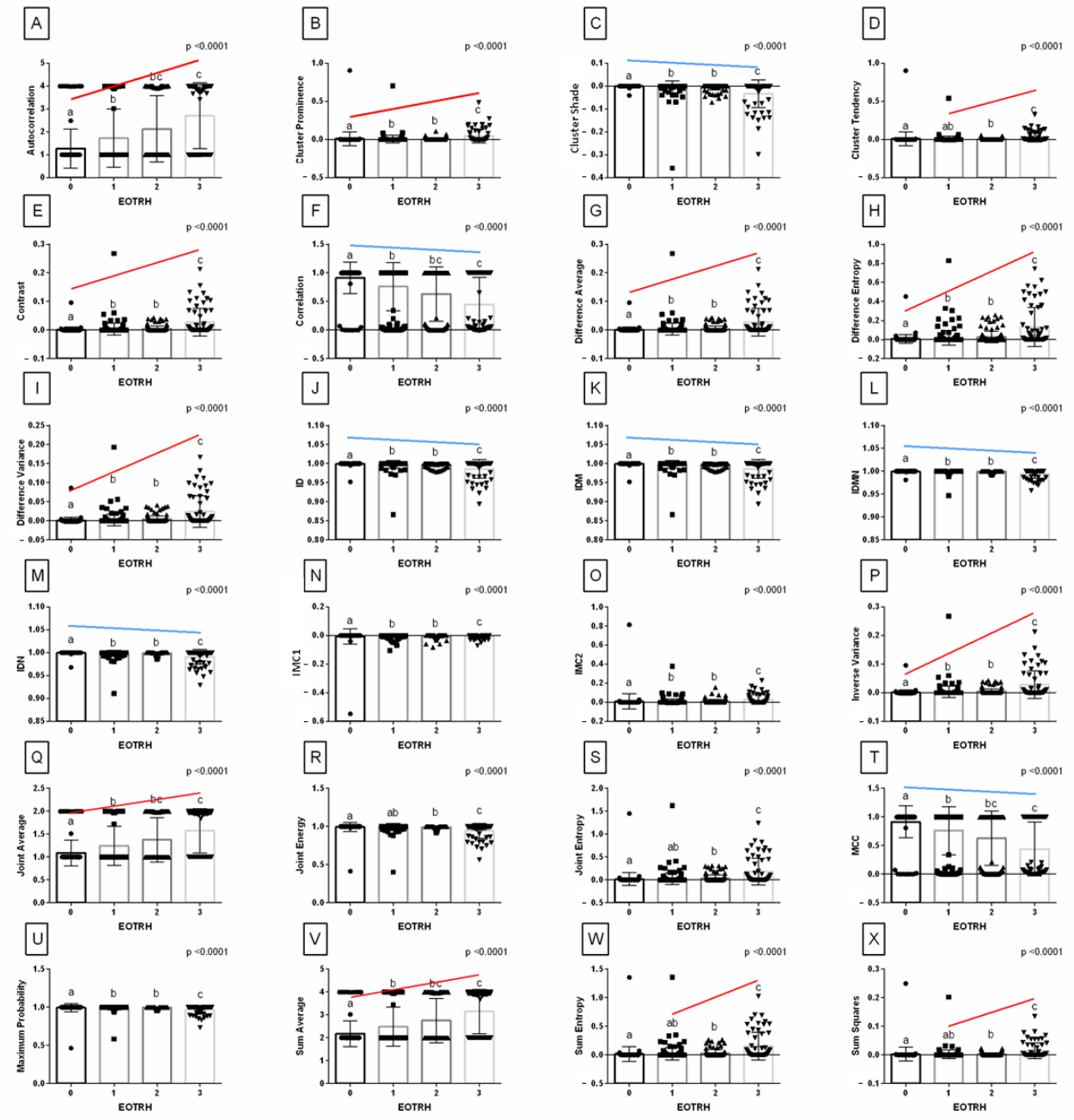

Ryc. 19. Wybrane cechy (średnia + SD) analizy tekstury obrazu wyodrębnione z zastosowaniem macierzy współwystąpień odcieni szarości (GLCM) oraz filtracji Normalize porównane w zależności od stopnia zaawansowania syndromu EOTRH. (A) Autocorrelation, (B) Cluster Prominence, (C) Cluster Shade, (D) Cluster Tendency, (E) Contrast, (F) Correlation, (G) Difference Average, (H) Difference Entropy, (I) Difference Variance, (J) Inverse difference (ID), (K) Inverse Difference Moment (IDM), (L) Inverse Difference Moment Normalized (IDMN), (M) Inverse Difference Normalized (IDN), (N) Informational Measure of Correlation 1 (IMC 1), (O) Informational Measure of Correlation 2 (IMC 2), (P) Inverse Variance, (Q) Joint Average, (R) Joint Energy, (S) Joint Entropy, (T) Maximal Correlation Coefficient (MCC), (U) Maximum Probability, (V) Sum Average, (W) Sum Entropy i (X) Sum of Squares.

Spośród 16 cech GLRLM wyodrębnionych z obrazów wyjściowych przefiltrowanych przez filtr Normalize, 4 cechy spełniły pierwsze kryterium i rosło lub malało od stopnia 1 syndromu EOTRH były to: GLNN, GLV, HGLRE i LGLRE. Uznano, że te cechy GLRLM lepiej niż inne pozwalają na ilościową ocenę objawów radiologicznych syndromu EOTRH. Potencjalne zastosowanie opisanych cech tekstury obrazów omówiono szczegółowo w publikacji Górski i wsp. (2022b).

6.4. Zastosowanie miar entropii w ocenie objawów radiologicznych syndromu EOTRH

Spośród 15 zwróconych kombinacji protokołów filtrowania (n = 3) i cech tekstury obrazu zwróconych z zastosowaniem miar entropii (n = 5), trzy miary entropii po filtracji Normalize, cztery miary entropii po filtracji Median i dwie miary entropii po filtracji Laplacian Sharpenin różniło się pomiędzy stopniami zaawansowania syndromu EOTRH. Różnice te zostały omówione szczegółowo w publikacji Górski i wsp. (2022c).

Spośród zwróconych cech wybrano te które: (i) rosną lub malejące od stopnia 0 syndromu EOTRH dla co najmniej jednego filtra oraz (ii) rosną lub maleją w sposób powtarzalny niezależnie od zastosowanego filtrowania. W ten sposób wybrano cechy tekstury obrazu wyodrębnionych z zastosowaniem DistEn2D (Ryc. 20). Uznano, że DistEn2D, wyodrębniona z obrazów wyjściowych przefiltrowanych przez filtr Normalize, lepiej niż inne miary entropii pozwalają na ilościową ocenę objawów radiologicznych syndromu EOTRH. Szczegółowy protokół wyodrębniania cech tekstury obrazu omówiono w publikacji Górski i wsp. (2022c).

Warto zauważyć, że DispEn2D zwraca wartości rosnące wraz ze stopniem syndromu EOTRH niezależnie od użytej filtracji obrazu. Spośród pięciu badanych miar entropii (Ribeiro i wsp., 2012; Da Silva i wsp., 2014; Azami i wsp., 2019; Hilal i wsp., 2019), jest to jedyna miara entropii niewrażliwa na filtrację obrazu. Obserwację tą można uznać za zaletę w porównaniu z podejściem wykorzystującym macierze poziomu szarości, w tym wybraną GLCM. Wszystkie cechy GLCM, uwzględnione w niniejszym badaniu, różniły się między stopniami syndromu EOTRH 0–3 po filtracji Normalize, ale nie po filtracji Median i Laplacian Sharpening. Filtr Laplacian Sharpening pozwala uzyskać wyjściowe radiogramy o większej ostrości (Al– meen i wsp., 2012) i sprawdza się podczas ekstrakcji cech statystyki pierwszego rzędu (Górski i wsp., 2022b). Filtr Median pozwala na wygładzenie wyjściowego radiogramu poprzez redukcję szumu (Dohoo i wsp., 2009, Chandra i Verma, 2020), co nie znalazło zastosowania w ekstrakcji cech statystyk zarówno pierwszego jak i drugiego rzędu (Górski i wsp., 2022b). Z kolei filtr Normalize zwiększa kontrast radiogramów (Heidari i wsp., 2020), co jest korzystniejsze podczas ekstrakcji cech statystyk drugiego rzędu (Górski i wsp., 2022b). Warto zauważyć, że spośród wykorzystanych

statystyk drugiego rzędu GLCM zwraca rozkład przestrzenny rozmieszczenia pikseli (Jusman i wsp., 2020), dlatego wyjściowy radiogram filtrowany algorytmem zwiększającym kontrast zwraca wartości cech GLCM o większy zróżnicowaniu pomiędzy stopniami syndromu EOTRH (Nagarajan i wsp., 2014; Kociołek i wsp., 2020).

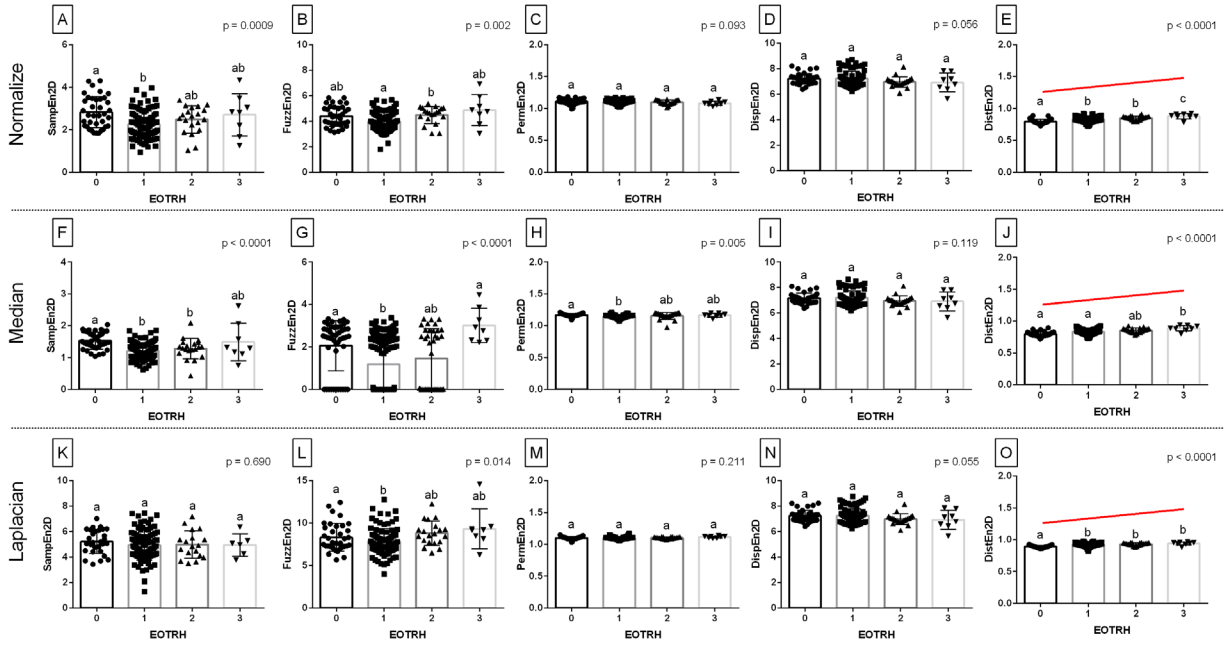

Ryc. 20. Wybrane cechy (średnia + SD) analizy tekstury obrazu wyodrębnione z zastosowaniem miar entropii oraz filtracji Normalize, Mediane i Laplacian Sharpening porównane w zależności od stopnia zaawansowania syndromu EOTRH. (A,F,K) dwuwymiarowa entropia próbki (SampEn2D); (B,G,L) dwuwymiarowa entropia rozmyta (FuzzEn2D); (C,H,M) dwuwymiarowa entropia permutacyjna (PermEn2D); (D,I,N) dwuwymiarowa entropia rozrzutu (DispEn2D); (E,J,O) dwuwymiarowa entropia rozkładu (DistEn2D).

Można przypuszczać, że ekstrakcja miar entropii umożliwi rozróżnianie stopni zaawansowania syndromu EOTRH zarówno na obrazach wyjściowych wyostrzonych po filtracji Laplacian Sharpening (Al–Ameen i wsp., 2012), o zwiększonym kontraście po filtracji Normalize (Heidari i wsp., 2020) oraz wygładzonych po filtracji Median (Dohoo i wsp., 2009, Chandra i Verma, 2020). Ponieważ miara entropii w postaci DispEn2D dostarcza ilościowego opisu nieregularności obrazów (Azami i wsp., 2017), zarówno wyostrzenie, jak i poprawa kontrastu czy redukcja szumu mogą zapewnić dobry stopień różnicowania objawów radiologicznych syndromu EOTRH.

Można również zauważyć, że w przypadku radiogramów wyjściowego po filtracji Normalize wartość nachylenia krzywej regresji DistEn2D była wyższa niż wartość nachylenia pięciu z sześciu porównywanych cech GLCM. Różnice w nachyleniu krzywych regresji,

opisane szczegółowo u publikacji Górski i wsp. (2022b), wskazują na większy wzrost wartości miary entropii niż cech GLCM w odniesieniu do nasilenia objawów radiologicznych syndromu EOTRH i sugerują większą przydatność DistEn2D niż cech GLCM. Z tego względu w następnym kroku poddano ocenie dokładność rozróżniania stopni 0 i 3 syndromu EOTRH na podstawie wartości DistEn2D oraz wybranych cech GLCM.

Dla wybranej miary entropii oraz wybranych 6 cech GLCM, które rosły od stopnia 0 syndromu EOTRH (Cluster Prominence, Contrast, Difference Average, Difference Entropy, Difference Variance, Inverse Variance) określono dokładność rozróżniania stopni 0 i 3 syndromu EOTRH (Tabela 6).

Tabela 6. Dokładność (Se – czułość; Sp – swoistość; PPV – dodatnia wartość predykcyjna; NPV – ujemna wartość predykcyjna) rozróżniania stopni 0 i 3 syndromu EOTRH na podstawie wartości wybranej miary entropii (dwuwymiarowa entropia rozkładu, DistEn2D) i wybranych cechy macierzy współwystąpień odcieni szarości (GLCM) (ClusterProminence; Contrast; DifferenceAverage; DifferenceEntropy; DifferenceVariance; Inverse Variance) oraz filtracji Normalize. Zastosowano trzy progi (średnia; średnia + SD; średnia + 2 SD).

Cechy	DistEn2D	Cluster Prominence	Contrast	Difference Average	Difference Entropy	Difference Variance	Inverse Variance
Próg 1				**średnia**			
Se	0,50	0,25	0,25	0,25	0,27	0,25	0,25
Sp	0,95	0,99	0,99	0,99	0,99	0,99	0,99
PPV	0,67	0,94	0,94	0,94	0,94	0,94	0,94
NPV	0,90	0,70	0,70	0,70	0,70	0,70	0,70
Próg 2				**średnia + SD**			
Se	0,13	0,17	0,17	0,17	0,22	0,17	0,17
Sp	1,00	0,99	0,99	0,99	0,98	0,99	0,99
PPV	1,00	0,91	0,91	0,91	0,93	0,91	0,91
NPV	0,84	0,68	0,68	0,68	0,58	0,68	0,68
Próg 3				**średnia + 2SD**			
Se	0,00	0,03	0,07	0,07	0,07	0,07	0,07
Sp	1,00	0,99	1,00	1,00	1,00	1,00	1,00
PPV	-	0,67	1,00	1,00	1,00	1,00	1,00
NPV	0,82	0,65	0,66	0,66	0,66	0,66	0,66

W przypadku DistEn2D i wszystkich sześciu cech GLCM stwierdzając, że Se i NPV maleją wraz z wyższymi wartościami progowymi (średnia > średnia + SD > średnia + 2SD), a Sp i PPV rosną wraz z wyższymi wartościami progowymi (średnia > średnia + SD > średnia + 2SD). Dla pierwszego progu (średnia), Se mieściła się w zakresie od 0,50 dla DistEn2D przez 0,27 dla Difference Entropy; do 0,25 dla pozostałych pięciu cech GLCM. Sp mieściła się w zakresie od 0,95 dla DistEn2D do 0,99 dla wszystkich cech GLCM. Dla drugiego progu (średnia + SD), Se mieściła się w zakresie od 0,13 dla DistEn2D; przez do 0,22 dla Difference

Entropy; do 0,17 dla pozostałych pięciu cech GLCM. Sp mieściła się w zakresie od 1,00 dla DistEn2D; przez 0,98 dla Difference Entropy; do 0,99 dla pozostałych pięciu cech GLCM. Dla trzeciego progu (średnia + SD), Se mieściła się w zakresie od 0,00 dla DistEn2D; przez 0,03 dla Cluster Prominence; do 0,07 dla pozostałych pięciu cech GLCM. Sp mieściła się w zakresie od 0,99 dla Cluster Prominence do 1,00 dla DistEn2D i pozostałych pięciu cech GLCM. Macierze poziomu szarości są miarami nieregularności pikseli w danym oknie oraz prawdopodobieństwa podobieństwa tych pikseli do pikseli sąsiedniego okna. W analizie tekstury obrazów z zastosowaniem macierzy poziomu szarości zliczane jest występowanie danego piksela (Szczypiński i wsp., 2014; Szczypiński i wsp., 2017). Z kolei zastosowane miary entropii są obliczane bezpośrednio na obrazie (Humeau–Heurtier, 2019), oddając powtarzalność wzorów pikseli danego obrazu, co w tym zastosowaniu jest związane z właściwościami tekstury radiogramu (Da Silva i wsp., 2018). Dlatego porównanie w którym za najbardziej czuły wskaźnikiem progresji objawów radiologicznych syndromu EORTH, spośród rozpatrywanych cech tekstury obrazu, uznano dwuwymiarową entropię rozkładu (DistEn2D), a dopiero w drugiej kolejności Difference Entropy spośród cech GLCM, jest uzasadniony. Szczegółowe porównanie przydatności miar entropii i cech wybranej macierzy poziomu szarości do kwantyfikacji objawów radiologicznych syndromu EOTRH omówiono w publikacji Górski i wsp. (2022c).

Uzyskane wyniki uzasadniają wybór filtracji Normalize, wybranej miary entropii (DistEn2D) oraz wybranej macierzy poziomu szarości (GLCM) do dalszych badań nad zautomatyzowanym wykrywaniem objawów radiologicznych syndromu EOTRH. Jednak niezbędne są dalsze badania na większym zbiorze danych, aby zweryfikować przydatność proponowanych algorytmów (Górski i wsp., 2022b; Górski i wsp., 2022c). Co więcej, należy zauważyć, że proponowane metody cyfrowego przetwarzania obrazów radiologicznych pozwalają na wykrycie objawów radiologicznych wszystkich stopni syndromu EOTRH, choć różnicowanie stopni 0 i 1, 1 i 2 oraz 2 i 3 syndromu EOTRH jest niskie (Górski i wsp., 2022b; Górski i wsp., 2022c). Dlatego dalsze poszukiwanie przydatnej metody oceny objawów radiologicznych syndromem EOTRH z zastosowaniem protokołu skalowanego liczenia pikseli (Górski i wsp., 2023) jest w pełni uzasadnione.

6.5. Zastosowanie protokołu skalowanego liczenia pikseli w ocenie objawów radiologicznych syndromem EOTRH

Wprowadzenie protokołu skalowanego liczenia pikseli do oceny objawów radiologicznych syndromu EOTRH omówiono szczegółowo w publikacji Górski i wsp. (2023). Na jego podstawie zwrócono wartości liczby pikseli dla każdego z dziesięciu stopni (S1-S10) standardu gęstości, które porównano pomiędzy stopniami zaawansowania syndromu EOTRH. Stwierdzono wzrost liczby pikseli od najniższych wartości w stopniu 0 syndromu EOTRH do najwyższych w stopniu 3 syndromu EOTRH 3 dla S1 – S8 (Ryc. 21A – H), ale nie dla S9 – S10 (Ryc. 21I–J). Można zaobserwować dwa wzorce wzrostu liczby pikseli w ocenianych radiogramach. W pierwszym wzorcu stwierdzono wzrost liczby pikseli pomiędzy stopniami 0 i 3 oraz 1 i 3 syndromu EOTRH, które zaznaczono odpowiednio liniami pomarańczowymi i czerwonymi. W drugim wzorcu stwierdzono wzrost liczby pikseli pomiędzy stopniami 0 i 3, 0 i 1 oraz 2 i 3 syndromu EOTRH, które zaznaczono odpowiednio liniami pomarańczowymi, niebieskimi i zielonymi. Pierwszy wzór rozpoznano dla S1 (Ryc. 21A), S2 (Ryc. 21B), S6 (Ryc. 21F), S7 (Ryc. 21G), i S8 (Ryc. 21H); natomiast druga dla S3 (Ryc. 21C), S4 (Ryc. 21D) i S5 (Ryc. 21E).

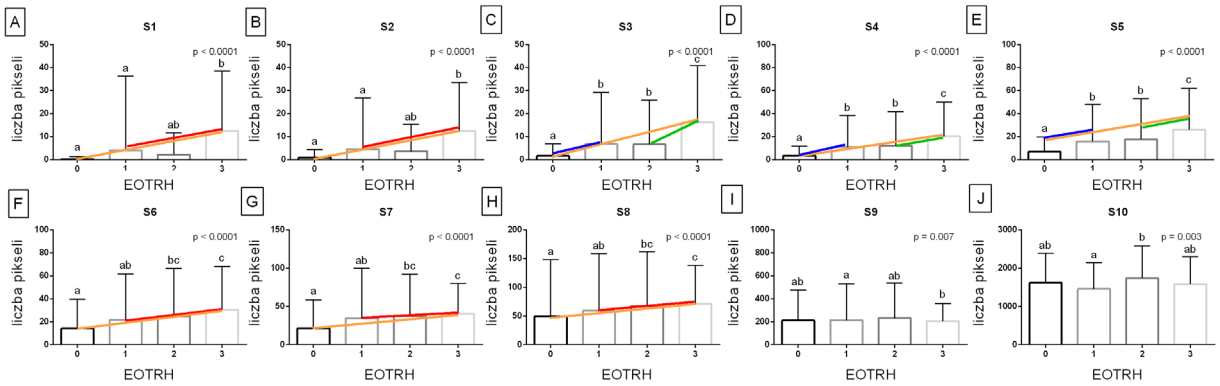

Ryc. 21. Liczba pikseli (średnia + SD) zwrócona z zastosowaniem protokołu skalowanego liczenia pikseli porównana w zależności od stopnia zaawansowania syndromu EOTRH. (A) pierwszy stopień (S1) standardu gęstości; (B) drugi stopień (S2) standardu gęstości; (C) trzeci stopień (S3) standardu gęstości; (D) czwarty stopień (S4) standardu gęstości; (E) piąty stopień (S5) standardu gęstości; (F) szósty stopień (S6) standardu gęstości; (G) siódmy stopień (S7) standardu gęstości; (H) ósmy stopień (S8) standardu gęstości; (I) dziewiąty stopień (S9) standardu gęstości; (J) dziesiąty stopień (S10) standardu gęstości.

Zastosowanie protokołu skalowanego liczenia pikseli pozwala na względną ocenę mineralnej gęstości kości, a w przypadku radiogramów wyrostków zębodołowych, również mineralnej gęstości zębów, ponieważ zęby wykazują wysoką gęstość radiologiczną i są dobrze zdefiniowane radiologicznie (Saccomanno i wsp., 2018). Mineralna gęstość kości jest ważnym wskaźnikiem wytrzymałości kości, pozwalającym na ocenę ryzyka złamań (Kamran i wsp., 2010; Cresswell i wsp., 2019) w treningu koni wyścigowych (Firth i wsp., 2005; Yamada i wsp., 2015) i sportowych (Rajão i wsp., 2019), dlatego jej nieinwazyjny pomiar był przedmiotem intensywnych badań. Podejmowano próby badania mineralnej gęstości kości przy użyciu metod wolnych od promieniowania rentgenowskiego z wykorzystaniem absorpcjometrii pojedynczych fotonów (McCarthy i Jeffcott, 1992) i ultrasonografii (Lepage i wsp., 2001). Jednak metody te okazały się mało skuteczne i dalsze badania skupiono na właściwościach materii prześwietlanej promieniowaniem rentgenowskim. W tym celu wykorzystano dwa główne podejścia, jedno obejmujące cyfrową absorpcjometrię rentgenowską wiązki o pojedynczej energii (Bell i wsp., 2001; Vaccaro i wsp., 2012; Bowen i wsp., 2013; Yamada i wsp., 2015; Górski i wsp., 2023) i drugie obejmujące dwuenergetyczną absorpcjometrię rentgenowską (McClure i wsp., 2001; Vaccaro i wsp., 2012; Yamada i wsp., 2015). Dwuenergetyczna absorpcjometria rentgenowska jest preferowaną metodą oceny mineralnej gęstości kości u ludzi (Johnson, 2012; Ulivieri i Rinaudo, 2021), jednak jej zastosowanie kliniczne u koni jest znacznie ograniczone zwłaszcza w praktyce terenowej (Bowen i wsp., 2013; Yamada i wsp., 2015). Dlatego w praktyce terenowej skupiono się na zastosowaniu cyfrowej absorpcjometrii rentgenowskiej wiązki o pojedynczej energii w konwencjonalnej radiografii (Bell i wsp., 2001; Kobayashi i wsp., 2006; Kobayashi i wsp., 2007; Bowen i wsp., 2013; Yamada i wsp., 2015; Górski i wsp., 2023). Takie podejście wymaga użycia wzorca gęstości (nazywanego również aluminiowym odpowiednikiem radiograficznym kości (Bell i wsp., 2001; Kobayashi i wsp., 2006; Kobayashi i wsp., 2007; Yamada i wsp., 2015) lub markera aluminium (Bowen i wsp., 2013) i było wykorzystane również w niniejszej pracy (Górski i wsp., 2023). Zastosowanie standardu gęstości, o znanych wymiarach i gęstości, umożliwia kalibrację skali szarości między obrazami. Skalę szarości kości i zębów można na tej podstawie określić ilościowo za pomocą indeksu jasności i ciemności (Bowen i wsp., 2013) lub liczby pikseli (NP) w określonym zakresie jasności (Górski i wsp., 2023) odnosząc je do średniej pochłanialności wiązki promieniowania zależnej od grubości standardu gęstości. Wzrost tłumienia wiązki promieni rentgenowskich jest związane ze wzrostem grubości tkanki (Laskey, 1996) i wzorca gęstości (Bowen i wsp., 2013) co zostało potwierdzone w niniejszych badaniach zębów siecznych koni poprzez stwierdzenie liniowej zależności pomiędzy wzrostem wartości NP oraz wzrostem pochłaniania wiązki promieniowania przez kolejne stopnie wzorca gęstości. Zależność ta została opisana szczegółowo w publikacji

Górski i wsp. (2023). Z tego względu zastosowanie aluminiowego wzorca gęstości do pośredniej ilościowej oceny jasności radiogramów, a tym samym zastosowanie proponowanego protokołu zliczania skalowanych pikseli do pośredniej ilościowej oceny objawów radiologicznych resorpcji i hipercementozy zębów w przebiegu syndromu EOTRH, jest w pełni uzasadnione.

Tabela 7. Dokładność (Se – czułość; Sp – swoistość; PPV – dodatnia wartość predykcyjna; NPV – ujemna wartość predykcyjna) rozróżniania stopni syndromu EOTRH (0-3) na podstawie liczby pikseli zwróconych dla poszczególnych stopni (S1-S10) standardu gęstości. Zastosowano dwa progi (średnia; |średnia - SD|).

S1-S10	**EOTRH**		**Se**	**Sp**	**PPV**	**NPV**	**Se**	**Sp**	**PPV**	**NPV**
	stopień		**Próg 1:** średnia				**Próg 2:** |średnia – SD|			
S1	0	3	0,25	1,00	1,00	0,70	0,25	1,00	1,00	0,70
S2	0	3	0,30	0,99	0,95	0,71	0,30	0,96	0,82	0,70
S3	0	3	0,31	0,96	0,83	0,71	0,41	0,96	0,86	0,74
S4	0	3	0,36	0,95	0,81	0,72	0,49	0,89	0,71	0,75
S5	0	3	0,23	0,93	0,67	0,68	0,52	0,74	0,54	0,73
S6	0	3	0,38	0,82	0,55	0,69	0,67	0,68	0,55	0,78
S7	0	3	0,38	0,79	0,51	0,69	0,97	0,40	0,48	0,95
S8	0	3	0,34	0,78	0,48	0,67	0,98	0,46	0,51	0,98
S1	1	3	0,25	0,96	0,65	0,80	0,25	0,96	0,65	0,80
S2	1	3	0,30	0,94	0,60	0,81	0,30	0,91	0,51	0,81
S6	1	3	0,38	0,79	0,36	0,80	0,67	0,57	0,33	0,85
S7	1	3	0,38	0,74	0,32	0,79	0,97	0,32	0,31	0,97
S8	1	3	0,34	0,76	0,31	0,79	0,98	0,31	0,31	0,98
S3	2	3	0,30	0,90	0,65	0,67	0,39	0,83	0,59	0,68
S4	2	3	0,34	0,85	0,59	0,67	0,46	0,74	0,53	0,68
S5	2	3	0,33	0,80	0,51	0,65	0,33	0,75	0,46	0,64
S3	0	1	0,17	0,94	0,85	0,38	0,08	0,96	0,79	0,36
S4	0	1	0,21	0,91	0,82	0,38	0,16	0,94	0,84	0,38
S5	0	1	0,25	0,80	0,70	0,36	0,23	0,82	0,70	0,36

Dla wybranych stopni standardu gęstości, których liczba pikseli rosły od stopnia 0 do 3 syndromu EOTRH (S1 – S8), od stopnia 1 do 3 syndromu EOTRH (S1, S2, S6, S7, S8), od stopnia 2 do 3 syndromu EOTRH (S3 – S5) oraz od stopnia 0 do 1 syndromu EOTRH (S3 – S5) określono dokładność rozróżniania stopni syndromu EOTRH (Tabela 7).

Dla pierwszego progu (średnia) najwyższą Se (0,38) stwierdzono dla EOTRH 0 i 3 w S6, EOTRH 1 i 3 w S6, EOTRH 0 i 3 w S7 oraz EOTRH 1 i 3 w S7. Se mieściła się w zakresie od 0,38 do 0,17 dla EOTRH 0 i 1 w S7; a Sp mieściła się w zakresie od 1,00 dla EOTRH 0 i 3 w S1 do 0,74 dla EOTRH 1 i 3 w S7. Dla drugiego progu (|średnia – SD|) najwyższą Se (0,98) stwierdzono dla EOTRH 0 i 3 w S8 oraz EOTRH 1 i 3 w S8. Se mieściła się w zakresie od 0,98 do 0,08 dla EOTRH 0 i 1 w S3; a Sp mieściła się w zakresie od 1,00 dla EOTRH 0 i 3 w S1 do 0,31 dla EOTRH 1 i 3 w S8. Spośród rozpatrywanych stopni standardu gęstości w protokole skalowanego liczenia pikseli, za najbardziej czuły wskaźnikiem progresji objawów radiologicznych syndromu EORTH uznano liczbę pikseli mierzoną dla stopni S7 i S8.

W niniejszym badaniu, wykazano różnice w wartościach NP pomiędzy stopniem 0 i 3, 0 i 2 oraz 0 i 1 syndromu EOTRH. Co więcej dokładność różnicowania stopni 0 i 1 syndromu EOTRH była wysoka, a dokładność różnicowania stopni 0 i 3 syndromu EOTRH była wyższa niż ta opisana dla analizy tekstury obrazu z zastosowaniem wybranej miary entropii (DistEn2D) oraz wybranej macierzy poziomu szarości (GLCM) (Górski i wsp., 2022c). Można więc stwierdzić, że zastosowana pośrednia ocena gęstości mineralnej zębów siecznych koni pozwala na różnicowanie wczesnych objawów radiograficznych łagodnego stopnia syndromu EOTRH (Rehrl i wsp., 2018). Biorąc pod uwagę, że objawy radiologiczne syndromu EOTRH pojawiają się wcześniej niż objawy kliniczne (Barrett i Easley, 2013; Moore i wsp., 2016; Pearce, 2020), a odpowiednio 20 i 88% koni nie wykazujących wyraźnych objawów klinicznych pomimo radiologicznych objawów odpowiednio hipercementozy i resorpcji zębów siecznych (Rehrl i wsp., 2018), wspomagane komputerowo wykrywanie wczesnych objawów radiologicznych syndromu EOTRH byłoby dużym postępem w stomatologii weterynaryjnej koni. Z tego względu zaproponowany protokół cyfrowej absorpcjometrii rentgenowskiej wiązki o pojedynczej energii zostanie wykorzystany w dalszych badaniach nad zautomatyzowanym wykrywaniem objawów radiologicznych syndromu EOTRH.

7. Wnioski

1. Wady zgryzu i choroby zębów siecznych występują odpowiednio u 32,2% i 34,8% koni w populacji reprezentującej województwo mazowieckie, a występowanie syndromu EOTRH rośnie wraz z wiekiem tak, że objawy kliniczne syndromu EOTRH stwierdzono w przypadku 3,11% zębów siecznych koni w wieku powyżej 15 lat (Górski i wsp., 2022a). W przypadku wad zgryzu, wśród siekaczy najczęściej stwierdzono nieprawidłową krzywiznę, zębów wilczych – ślepy ząb wilczy, kłów – niewyrznięty kieł, zębów przedtrzonowych i trzonowych – ostre krawędzie zębów. Wśród chorób zębów, w obrębie siekaczy najczęściej stwierdzono kamień nazębny, zębów wilczych – złamanie, kłów - kamień nazębny, a zębów przedtrzonowych i trzonowych – próchnicę;
2. Różnym objawom klinicznym syndromu EOTRH towarzyszą podobne objawy radiologiczne, a leczeniem z wyboru ciężkiej postaci syndromu EOTRH jest radykalna ekstrakcja siekaczy (Górski i wsp., 2021);
3. Objawy radiologiczne syndromu EOTRH można oceniać ilościowo z wykorzystaniem:
    a. wybranych cech macierzy współwystąpień odcieni szarości (GLCM) po filtracji zwiększającej kontrast obrazu (Górski i wsp., 2022b); a objawy radiologiczne ciężkiego syndromu EOTRH najdokładniej rozróżnia cecha Difference Entropy (Górski i wsp., 2022c);
    b. wybranych miar entropii po filtracji redukującej szumy lub zwiększającej ostrość lub kontrast obrazu, a objawy radiologiczne ciężkiego syndromu EOTRH najdokładniej rozróżnia dwuwymiarowa entropia rozkładu (DistEn2D) (Górski i wsp., 2022c);
    c. protokołu skalowanego liczenia pikseli, który umożliwia rozróżnienie objawów radiologicznych łagodnego, zaawansowanego i ciężkiego syndromu EOTRH (Górski i wsp., 2023).

8. Piśmiennictwo

1. Abdel–Nasser, M.; Moreno, A.; Puig, D. Breast cancer detection in thermal infrared images using representation learning and texture analysis methods. Electronics 2019, 8, 100.
2. Al–Ameen, Z.; Sulong, G.; Gapar, M.D.; Johar, M.D. Reducing the Gaussian blur artifact from CT medical images by employing acombination of sharpening filters and iterative deblurring algorithms. J. Theor. Appl. Inf. Technol. 2012, 46, 31–36.
3. Albers, L., Albers, J., Dullin, C., Staszyk, C., Bienert-Zeit, A. Early incisor lesions and Equine Odontoclastic Tooth Resorption and Hypercementosis: Reliability of radiographic findings. Equine Vet. J. 2023, 55(2), 261-269.
4. Anthony, J.; Waldner, C.; Grier, C.; Laycock, A.R. A survey of equine oral pathology. J. Vet. Dent. 2010, 27, 12–15.
5. Azami, H.; Da Silva, L.E.V.; Omoto, A.C.M.; Humeau–Heurtier, A. Two–dimensional dispersion entropy: An information–theoretic method for irregularity analysis of images. Signal. Process. Image Commun. 2019, 75, 178–187.
6. Azami, H.; Escudero, J.; Humeau–Heurtier, A. Bidimensional Distribution Entropy to Analyze the Irregularity of Small–Sized Textures. IEEE Signal. Proc. Lett. 2017, 24, 1338– 1342.
7. Baker, G.J. A Study of Dental Disease in the Horse. Ph.D. Thesis, The Faculty of Veterinary Medicine, University Utrecht, Utrecht, The Netherlands, 1979.
8. Baratt, R. Advances in equine dental radiology. Vet. Clin. North Am. Equine Pract. 2013, 29, 367–395.
9. Baratt, R. Equine incisor resorptive lesions. In: Proceedings of the 21st Annual Veterinary Dental Forum, Minneapolis, USA; 2007, 23–30.
10. Baratt, R. Equine odontoclastic tooth resorption and hypercementosis (EOTRH): What do we know? Equine Vet. Educ. 2016, 28(3), 131–3.
11. Baratt, R.M. Dental Radiography and Radiographic Signs of Equine Dental Disease. Vet. Clin. N. Am. Equine Pract. 2020, 36, 445–476.
12. Barrett, M.F.; Easley, J.T. Acquisition and interpretation of radiographs of the equine skull. Equine Vet. Educ. 2013, 25(12), 643–52.
13. Baxter, C. J. Veterinary dentistry: A clinician's viewpoint. Dental Update 2013, 40, 386– 390.
14. Bębas, E.; Borowska, M.; Derlatka, M.; Oczeretko, E.; Hładuński, M.; Szumowski, P.; Mojsak, M. Machine–learning–based classification of the histological subtype of non–small–cell lung cancer using MRI texture analysis. Biomed. Signal. Process. Control. 2021, 66, 102446.

15. Bell, R. A.; Nielsen, B. D.; Waite, K.; Rosenstein, D.; Orth, M. Daily access to pasture turnout prevents loss of mineral in the third metacarpus of Arabian weanlings. J. Anim. Sci. 2001, 79, 1142–1150.
16. Björnsdóttir, S.; Frey, R.; Kristjansson, T.; Lundström, T. Bit–related lesions in Icelandic competition horses. Acta Vet. Scand. 2014, 56, 40.
17. Borowska, M. Wprowadzenie do zastosowania entropii w analizie sygnałów i obrazów biomedycznych oraz jej aplikacje w medycynie i weterynarii. Oficyna wydawnicza Politechniki Białostockiej. ISBN 978-83-67185-82-0, ISBN 978-83-67185-81-3 (eBook), Białystok, 2023.
18. Borowska, M.; Maśko, M.; Jasiński, T.; Domino, M. The Role of Two–Dimensional Entropies in IRT–Based Pregnancy Determination Evaluated on the Equine Model. In Information Technology in Biomedicine. ITIB 2022. Advances in Intelligent Systems and Computing, 1st ed.; Pietka, E., Badura, P., Kawa, J.,Wieclawek,W., Eds.; Springer: Cham, Switzerland. 2022, 1429, 54–65.
19. Bowen, A. J.; Burd, M. A.; Craig, J. J.; Craig, M. Radiographic calibration for analysis of bone mineral density of the equine third metacarpal bone. J. Equine Vet. Sci. 2013, 33, 1131- 1135.
20. Brigham, E.J.; Duncanson, G.R. An equine postmortem dental study: 50 cases. Equine Vet. Educ. 2000, 12, 59–62.
21. Broman, A. How to Identify and Extract Blind Wolf Teeth. AAEP PROCEEDINGS, USA, 2021, 67, 420–423.
22. Carmalt, J. L. C. Understanding the equine diastema. Equine Vet. Educ. 2003, 15, (1), 34– 35.
23. Chandra, T.B.; Verma, K. Analysis of quantum noise–reducing filters on chest X–ray images: A review. Measurement. 2020, 153, 107426.
24. Chinkangsadarn, T.; Wilson, G.; Greer, R.; Pollitt, C.; Bird, P. An abattoir survey of equine dental abnormalities in Queensland. Australia. Aust. Vet. J. 2015, 93, 189–194.
25. Cook, W. Damage by the bit to the equine interdental space and second lower premolar. Equine Vet. Educ. 2011, 23, 355–360.
26. Cresswell, E. N.; McDonough, S. P.; Palmer, S. E.; Hernandez, C. J.; Reesink, H. L. Can quantitative computed tomography detect bone morphological changes associated with catastrophic proximal sesamoid bone fracture in Thoroughbred racehorses? Equine Vet. J. 2019, 51, 123–130.

27. Da Silva, L.E.; Duque, J.J.; Felipe, J.C.; Murta, L.O., Jr.; Humeau–Heurtier, A. Two– dimensional multiscale entropy analysis: Applications to image texture evaluation. Signal Process. 2018, 147, 224–232.
28. Da Silva, L.E.; Senra Filho, A.C.; Fazan, V.P.; Felipe, J.C.; Murta, L.O., Jr. Two– dimensional sample entropy analysis of rat sural nerve aging. In Proceedings of the 2014, 36th Annual International Conference of the IEEE Engineering in Medicine and Biology Society, Chicago, IL, USA, 26–30 August 2014, 3345–3348.
29. Dacre, I.; Kempson, S.; Dixon, P.M. Equine idiopathic cheek teeth fractures. Part 1: Pathological studies on 35 fractured cheek teeth. Equine Vet. J. 2007, 39, 310–318.
30. Dakin, S.G.; Lam, R.; Rees, E.; Mumby, C.;West, C.; Weller, R. Technical Set–up and Radiation Exposure for Standing Computed Tomography of the Equine Head: Standing CT of the Equine Head. Equine Vet. Educ. 2014, 26, 208–215.
31. Dixon, P.M.; Tremaine, W.H.; Pickles, K.; Kuhns, L.; Hawe, C.; McCann, J.; McGorum, B.; Railton, D.I .; Brammer, S. Equine dental disease part 1: a long–term study of 400 cases: disorders of the incisor, canine, and first premolar teeth. Equine Vet. J. 1999a, 31, 369–77.
32. Dixon, P.M.; Dacre, I. A review of equine dental disorders. Vet. J. 2005, 169, 165–187.
33. Dixon, P.M.; Tremaine, W.H.; Pickles, K.; Kuhns, L.; Hawe, C.; Mccann, J.; Mcgorum, B.C.; Railton, D.I.; Brammer, S. Equine dental disease. Part 3: A long–term study of 400 cases: Disorders of wear, traumatic damage and idiopathic fractures, tumours and miscellaneous disorders of the cheek teeth. Equine Vet. J. 2000, 32, 9–18.
34. Dixon, P.M.; Tremaine, W.H.; Pickles, K.; Kuhns, L.; Hawe, C.; Mccann, J.; Mcgorum, B.C.; Railton, D.I.; Brammer, S. Equine dental disease Part 2: A long–term study of 400 cases: Disorders of development and eruption and variations in position of the cheek teeth. Equine Vet. J. 1999b, 31, 519–528.
35. Dohoo, I.; Martin, W.; Stryhn, H. Veterinary Epidemiologic Research, 2nd ed.; VER Inc.: Charlottetown, PE, Canada, 2009.
36. Domino, M.; Borowska, M.; Kozłowska, N.; Trojakowska, A.; Zdrojkowski, Ł.; Jasiński, T.; Smyth, G.; Maśko, M. Selection of image texture analysis and color model in the advanced image processing of thermal images of horses following exercise. Animals 2022b, 12, 444.
37. Domino, M.; Borowska, M.; Kozłowska, N.; Zdrojkowski, Ł.; Jasiński, T.; Smyth, G.; Maśko, M. Advances in thermal image analysis for the detection of pregnancy in horses using infrared thermography. Sensors. 2022a, 22, 191.
38. Domino, M.; Borowska, M.; Zdrojkowski, Ł.; Jasiński, T.; Sikorska, U.; Skibniewski, M.; Maśko, M. Application of the Two–Dimensional Entropy Measures in the Infrared

Thermography–Based Detection of Rider: Horse Bodyweight Ratio in Horseback Riding. Sensors. 2022c, 22, 6052.

39. du Toit, N.D.; Rucker, B. The gold standard of dental care: the geriatric horse. Vet. Clin. Equine. 2013, 29, 521–7.
40. du Toit, N.D.; Burden, F.A.; Dixon, P.M. Clinical dental examinations of 357 donkeys in the UK. Part 2: Epidemiological studies on the potential relationships between different dental disorders. and between dental disease and systemic disorders. Equine Vet. J. 2009, 41, 395–400.
41. du Toit, N.D.; Burden, F.A.; Kempson, S.A.; Dixon, P.M. Pathological investigation of caries and occlusal pulpar exposure in donkey cheek teeth using computerised axial tomography with histological and ultrastructural examinations. Vet. J. 2008, 178, 387–395.
42. du Toit, N.D.; Dixon, P.M. Common dental disorders in the donkey. Equine Vet. Educ. 2012, 24, 45–51.
43. du Toit, N.D.; Rucker, B. Geriatric dentistry. In Equine Dentistry, 3rd ed.; Easley, P.; Dixon, P.; Schumacher, J.; Eds.; Elsevier: Philadelphia, PA, USA, 2011, 279–287.
44. Easley, J. A new look at dental radiography. In Proceedings of the 48th Annual Convention of the American Association of Equine Practitioners, Orlando, FL, USA, 4–8 December 2002, 48, 412–420.
45. Easley, J. Dental care and instrumentation. Vet. Clin. N. Am. Equine Pract. 1998, 14, 309– 332.
46. Firth, E.C.; Rogers, C.W. Musculoskeletal responses of 2–year–old Thoroughbred horses to early training. 7. Bone and articular cartilage response in the carpus. N. Z. Vet. J. 2005, 53, 113– 122.
47. Floyd, M.R. The modified Triadan system: Nomenclature for veterinary dentistry. J. Vet. Dent. 1991, 8, 18–19.
48. Foster, D.L. The gold standard of dental care for the adult performance horse. Vet. Clin. N. Am. Equine Pract. 2013, 29, 505–519.
49. Gere, I.; Dixon, P.M. Post mortem survey of peripheral dental caries in 510 Swedish horses. Equine Vet. J. 2010, 42, 310–315.
50. Gergeleit, H.; Bienert–Zeit, A. Complications following mandibular cheek tooth extraction in 20 horses. Front. Vet. Sci. 2020, 7, 504.
51. Gieche, J.M. How to Assess the Equine Periodontium. AAEP PROCEEDINGS, Vol. 56, USA, 2010, 441–449.
52. Girejko, G.; Borowska, M.; Szarmach, J. Statistical analysis of radiographic textures illustrating healing process after the guided bone regeneration surgery. In Proceedings

of the International Conference on Information Technologies in Biomedicine, Springer (ITIB'2018), Kamień Śląski, Poland, 18–20 June 2018, 217–226.

53. Górski, K.; Stefanik, E.; Turek, B. et al. Malocclusions and Dental Diseases in Privately Owned Horses in the Mazovia Region of Poland. Animals. 2022a, 12, 3120.
54. Górski, K.; Turek, B.; Rakowska, A.; Obrochta, B.; Żychska, M.; Bereznowski, A.; Polkowska, I. Dodatkowy ząb trzonowy u konia – przypadek kliniczny. Med. Weter. 2020, 76 (9), 548–552.
55. Górski, K.; Borowska, M.; Stefanik, E.; Polkowska, I.; Turek, B.; Bereznowski, A.; Domino, M. Selection of Filtering and Image Texture Analysis in the Radiographic Images Processing of Horses' Incisor Teeth Affected by the EOTRH Syndrome. Sensors 2022b, 22, 2920.
56. Górski, K.; Borowska, M.; Stefanik, E.; Polkowska, I.; Turek, B.; Bereznowski, A.; Domino, M. Application of Two–Dimensional Entropy Measures to Detect the Radiographic Signs of Tooth Resorption and Hypercementosis in an Equine Model. Biomedicines 2022c, 10, 2914.
57. Górski, K.; Borowska, M.; Turek, B.; Pawlikowki, M.; Jankowski, K.; Bereznowski, A.; Polkowska, I.; Domino, M. An application of the density standard and scaled–pixel–counting protocol to assess the radiodensity of equine incisor teeth affected by resorption and hypercementosis: preliminary advancement in standard in field dental radiography. BMC Veterinary Research 2023, 19, 116.
58. Górski, K.; Tremaine, H.; Obrochta, B.; Buczkowska, R.; Turek, B.; Bereznowski, A.; Rakowska, A.; Polkowska, I. EOTRH syndrome in polish half–bred horses–two clinical cases. J. Equine Vet. Sci. 2021, 101, 103428.
59. Greet, T.R.C. Oral and dental trauma. In Equine Dentistry, 1st ed.; Baker, G.J., Easley, J., Eds.;W.B. Saunders: London, UK. 1999, 60–69.
60. Gregory, R.; Fehr, J.; Bryant, J. Chronic incisor periodontal disease with cemental hyperplasia and hypoplasia in horses. In: Proceedings of AAEP Focus on Dentistry, Indianapolis, USA, 2006. 312–16.
61. Heidari, M.; Mirniaharikandehei, S.; Khuzani, A.Z.; Danala, G.; Qiu, Y.; Zheng, B. Improving the performance of CNN to predict the likelihood of COVID–19 using chest X–ray images with preprocessing algorithms. Int. J. Med. Inform. 2020, 144, 104284.
62. Henninger, W.; Frame, E.M.; Willmann, M, et al. CT features of alveolitis and sinusitis in horses. Vet Radiol Ultrasound. 2003, 44, 269–76.
63. Henry, T.J.; Puchalski, S.M.; Arzi, B.; Kass, P.H.; Verstraete, F.J.M.; Radiographic evaluation in clinical practice of the types and stage of incisor tooth resorption and hypercementosis in horses. Equine Vet. J. 2016, 4, 9(4), 4, 86–92.

64. Hilal, M.; Berthin, C.; Martin, L.; Azami, H.; Humeau–Heurtier, A. Bidimensional multiscale fuzzy entropy and its application to pseudoxanthoma elasticum. IEEE Trans. Biomed. Eng. 2019, 67, 2015–2022.
65. Hole, S.L.; Staszyk, C. Equine odontoclastic tooth resorption and hypercementosis. Equine Vet. Educ. 2018, 30 (7), 386–91.
66. Hüls, I.; Bienert, A.; Staszyk, C. Equine odontoclastic tooth resorption and hyper–cementosis (EOTRH): Röntgenologische und makroskopisch–anatomische Befunde. In Proceedings of the 10. Jahrestagung der Internationalen Gesellschaft zur Funktionsverbesserung der Pferdezähne,Wiesbaden, Germany, 3–4 March 2012.
67. Humeau–Heurtier, A. Texture feature extraction methods: A survey. IEEE Access 2019, 7, 8975–9000.
68. Ireland, J.L.; McGowan, C.M.; Clegg, P.D.; Chandler, K.J.; Pinchbeck, G.L. A survey of health care and disease in geriatric horses aged 30 years or older. Vet. J. 2012, 192, 57–64.
69. Johnson, T.R. Dual–energy CT: general principles. AJR 2012, 199, S3–S8.
70. Jusman, Y.; Tamarena, R.I.; Puspita, S.; Saleh, E.; Kanafiah, S.N.A.M. Analysis of features extraction performance to differentiate of dental caries types using gray level co–occurrence matrix algorithm. In Proceedings of the 2020 10th IEEE International Conference on Control System, Computing and Engineering (ICCSCE), Penang, Malaysia, 21–22 August 2020; 148–152.
71. Kamran, K.; Rashid, I.; Mozhdeh, E.; Mohd, Z.; Tengku, A.I. Osteoporosis and bone health. JAVA. 2010, 9, 1048–1054.
72. Kennedy, R.S.; Dixon, P.M. The aetiopathogenesis of equine periodontal disease – a fresh perspective. Equine Vet. Educ. 2018, 30(3), 161–8.
73. Kirkland, K.D.; Maretta, S.M.; Inoue, O.J.; Baker, G.J. Survey of equine dental disease and associated oral pathology. In Proceedings of the 40th Annual Convention of the American Association of Equine Practitioners, Lexington, KY, USA, 4–7 December 1994, 119–120.
74. Klugh D.O . Incisor and canine periodontal disease. In: Proceedings of the 18th Annual Veterinary Dental Forum, Fort Worth, Texas, USA. 2004, 18, 166–9.
75. Klugh, D.O. Principles of Equine Dentistry; Manson/Veterinary CRC Press: Boca Raton, FL, USA, 2010.
76. Kobayashi, M.; Ando, K.; Kaneko, M.; Inoue, Y.; Asai, Y.; Taniyama, H. Clinical usefulness of the measurement of bone mineral content by radiographic absorptiometry in the young thoroughbred. J. Equine Sci. 2007, 18, 99–106.

77. Kobayashi, M.; Ando, K.; Kaneko, M.; Inoue, Y.; Asai, Y.; Taniyama, H. Measurement of equine bone mineral content by radiographic absorptiometry using CR and ortho systems. J. Equine Sci. 2006, 17, 105–112.
78. Kociołek, M.; Strzelecki, M.; Obuchowicz, R. Does image normalization and intensity resolution impact texture classification? Comput. Med. Imaging Graph. 2020, 81, 101716.
79. Laskey, M.A. Dual–energy X–ray absorptiometry and body composition. Nutrition. 1996, 12, 45–51.
80. Lee, S. Equine odontoclastic tooth resorption and hypercementosis. Aust. Vet. J. 2010, 88, N23–4.
81. Lepage, O.M.; Carstanjen, B.; Uebelhart, D. Non–invasive assessment of equine bone: an update. Vet. J. 2001, 161, 10–22.
82. Limone, L. General clinical, oral and dental examination. In Equine Dentistry and Maxillofacial Surgery; Cambridge Scholars Publishing: Newcastle upon Tyne, UK, 2022, 302.
83. Lorello, O,; Foster, D.L.; Levine, D.G.; Boyle, A.; Engiles, J.; Orsini, J.A .Clinical treatment and prognosis of equine odontoclastic tooth resorption and hypercementosis. Equine Vet. J. 2016, 48, 188–94.
84. Luedke, L.; Rawlinson, J.E.; Sanchez, M.D.; Bass, L.; Engiles, J. True cementomas (cementoblastomas) associated with a nonvital left maxillary second premolar in an 11–year–old miniature horse. Equine Vet. Educ. 2017, 29 (12), 647–54.
85. Maillard, P. Comparing texture analysis methods through classification. Photogramm. Eng. Remote Sens. 2003, 69, 357–367.
86. Manso–Díaz, G.; García–López, J.M.; Maranda, L.; Taeymans, O. The role of head computed tomography in equine practice. Equine Vet. Educ. 2015, 27, 136–145.
87. Maśko, M.; Borowska, M.; Domino, M.; Jasiński, T.; Zdrojkowski, L.; Gajewski, Z. A novel approach to thermographic images analysis of equine thoracolumbar region: The effect of effort and rider's body weight on structural image complexity. BMC Vet. Res. 2021, 17, 99.
88. McCarthy, R. N.; Jeffcott, L. B. Effects of treadmill exercise on cortical bone in the third metacarpus of young horses. Res. Vet. Sci. 1992, 52, 28–37.
89. McClure, S.R.; Glickman, L.T.; Glickman, N.W.; Weaver, C.M. Evaluation of dual energy x–ray absorptiometry for in situ measurement of bone mineral density of equine metacarpi. Am. J. Vet. Res. 2001, 62, 752–756.
90. McGowan, C.M.; Ireland, J.L. Welfare, quality of life, and euthanasia of aged horses. Vet. Clin. N. Am. Equine Pract. 2016, 32, 355–367.

91. Mohanaiah, P.; Sathyanarayana, P.; GuruKumar, L. Image texture feature extraction using GLCM approach. Int. J. Sci. Res. 2013, 3, 1–5.
92. Moore, N.T.; Schroeder, W.; Staszyk, C. Equine odontoclastic tooth resorption and hypercementosis affecting all cheek teeth in two horses: clinical and histopathological findings. Equine Vet. Educ. 2016, 28(3), 123–30.
93. Nagarajan, M.B.; Coan, P.; Huber, M.B.; Diemoz, P.C.; Glaser, C.; Wismüller, A. Computer–aided diagnosis for phase–contrast X–ray computed tomography: Quantitative characterization of human patellar cartilage with high–dimensional geometric features. J. Digit. Imaging. 2014, 27, 98–107.
94. Nagy, A.; Boros, K.; Dyson, S. Magnetic Resonance Imaging, Computed Tomographic and Radiographic Findings in the Metacarpophalangeal Joints of 40 Non-Lame Thoroughbred Yearlings. Animals. 2023, 13(22), 3466.
95. Omura, C.M.; Drumond, B.; Júnior, J.L.R.; Coelho, C.S.; Gioso, M.A. Measurement of incisor overjet and physiologica diastemata parameters in quarter horse foals. J. Vet. Dent. 2015, 32, 173–175.
96. Pauwels, F. E.; Van der Vekens, E.; Christan, Y.; Koch, C.; Schweizer, D. Feasibility, indications, and radiographically confirmed diagnoses of standing extremity cone beam computed tomography in the horse. Veterinary surgery. 2021, 50(2), 365-374.
97. Pearce, C.J. Recent developments in equine dentistry. N. Z. Vet. J. 2020, 68, 178–186.
98. Pearson, A.M.; Mansfield, G.; Conaway, M.; Koput, K. Associated Risk Factors of Equine Odontoclastic Tooth Resorption and Hypercementosis. AAEP PROCEED– INGS. 2013, 59.
99. Pehkonen, J.; Karma, L.; Raekallio, M. Behavioral signs associated with equine periapical infection in cheek teeth. J. Equine Vet. Sci. 2019, 77, 144–150.
100. Quinn, G.C.; Tremaine, W.H.; Lane, J.G. Supernumerary cheek teeth (n = 24): Clinical features. diagnosis. treatment and outcome in 15 horses. Equine Vet. J. 2005, 37, 505–509.
101. Radostits, O.M.; Gay, C.; Hinchcliff, K.W.; Constable, P.D. Veterinary Medicine e–Book: A Textbook of the Diseases of Cattle, Horses, Sheep, Pigs and Goats; Elsevier Health Sciences: Amsterdam, The Netherlands, 2006.
102. Rahmani, V.H.; Häyinen, L.; Kareinen, I.; Ruohoniemi, M. History, clinical findings and outcome of horses with radiographical signs of equine odontoclastic tooth resorption and hypercementosis. Vet. Rec. 2019, 14, 1–7, 185(23), 730.
103. Raja, J.V.; Khan, M.; Ramachandra, V.K.; Al–Kadi, O. Texture analysis of CT images in the characterization of oral cancers involving buccal mucosa. Dentomaxillofac. Radiol. 2012, 41, 475–480.

104. Rajão, M.D.; Leite, C.S.; Nogueira, K.; Godoy, R.F.; Lima, E.M.M. The bone response in endurance long distance horse. Open Vet. J. 2019, 9, 58–64.
105. Ramzan, P.H.L. Oral endoscopy as an aid to diagnosis of equine cheek tooth infections in the absence of gross oral patholog cal changes:17 cases . Equine Vet. J. 2009, 41, 101–106.
106. Rawlinson, J.; Carmalt, J.L. Extraction techniques for equine incisor and canine teeth. Equine Vet. Educ. 2014, 26(12), 657–71.
107. Rawlinson, J.; Earley, E. Advances in the treatment of diseased equine incisor and canine teeth. Vet. Clin. North Am. Equine Pract. 2013, 29, 411–40.
108. Rehrl, S.; Schröder, W.; Müller, C.; Staszyk, C.; Lischer, C. Radiological prevalence of equine odontoclastic tooth resorption and hypercementosis. Equine Vet. J. 2018, 50(4), 481–7.
109. Ribeiro, H.V.; Zunino, L.; Lenzi, E.K.; Santoro, P.A.; Mendes, R.S. Complexity–entropy causality plane as a complexity measure for two–dimensional patterns. PLoS ONE. 2012, 7, e40689.
110. Rodrigues, J.B.; Araújo, S.; Sanroman–Llorens, F.; Bastos, E.; San Roman, F.; Viegas, C. A clinical survey evaluating the prevalence of incisor disorders in Zamorano–Leonés and Mirandês donkeys (Equus asinus). J. Equine Vet. Sci. 2013, 33, 710–718.
111. Saccomanno, S.; Passarelli, P.C.B.; Oliva, B.; Grippaudo, C. Comparison between two radiological methods for assessment of tooth root resorption: An in vitro study. Biomed Res. Int. 2018, 5152172.
112. Salem, S.E.; Townsend, N.B.; Refaai, W.; Gomaa, M.; Archer, D.C. Prevalence of orodental pathology in a working horse population in Egypt and its relation to equine health. Equine Vet. J. 2017, 49, 26–33.
113. Sangeetha, M.; Kumar, K.; Aljabr, A.A. Image processing techniques in periapical dental X–ray image detection and classification. Webology. 2021, 18, 42–53.
114. Simhofer, H.; Griss, R.; Zetner, K. The use of oral endoscopy for detection of cheek teeth abnormalities in 300 horses. Vet. J. 2008, 178, 396–404.
115. Siwińska, N.; Żak, A.; Mańkowska, M.; Drozd, M.; Borowicz, H. Częstotliwość występowania wad w obrębie zębów siecznych u koni użytkowych na terenie Polski. Med. Weter. 2017, 73, 362–365.
116. Smedley, R.C.; Earley, E.T.; Galloway, S.S.; Baratt, R.M.; Rawlinson, J.E. Equine odontoclastic tooth resorption and hypercementosis: histopathologic features. Vet. Pathol. 2015, 52(5), 903–9.
117. Sohail, A.S.M.; Bhattacharya, P.; Mudur, S.P.; Krishnamurthy, S. Local relative GLRLM–based texture feature extraction for classifying ultrasound medical images. In Proceedings

of the 2011 24th Canadian Conference on Electrical and Computer Engineering (CCECE, IEEE), Niagara Falls, ON, Canada, 8–11 May 2011, 001092–001095.

118. Staszyk, C.; Bienert, A.; Kreutzer, R.; Wohlsein, P.; Simhofer, H. Equine odontoclastic tooth resorption and hypercementosis. Vet. J. 2008, 178, 372–9.
119. Staszyk, C . Incisor lesions: equine odontoclastic tooth resorption and hypercementosis. In: Proceedings of the 49th British Equine Veterinary Association Congress 2010 – Birmingham, United Kingdom; 2010.
120. Steel, C.; Ahern, B.; Zedler, S.; Vallance, S.; Galuppo, L.; Richardson, J.; Young, A. Comparison of Radiography and Computed Tomography for Evaluation of Third Carpal Bone Fractures in Horses. Animals. 2023, 13(9), 1459.
121. Sykora, S.; Pieber, K.; Simhofer, H.; Hackl, V.; Brodesser, D.; Brandt, S. Isolation of *Treponema* and *Tannerella* spp. from equine odontoclastic tooth resorption and hypercementosis related periodontal disease. Equine Vet. J. 2014, 46, 358–63.
122. Szczypiński, P.; Klepaczko, A.; Pazurek, M.; Daniel, P. Texture and color based image segmentation and pathology detection in capsule endoscopy videos. Comput. Methods Programs Biomed. 2014, 113, 396–411.
123. Szczypiński, P.M.; Klepaczko, A.; Kociołek, M. QMaZda—Software tools for image analysis and pattern recognition. In Proceedings of the 2017 Signal Processing: Algorithms, Architectures, Arrangements, and Applications (SPA), Poznan, Poland, 20–22 October 2017, 217–221.
124. Tan, T.; Platel, B.; Mus, R.; Tabar, L.; Mann, R.M.; Karssemeijer, N. Computer–aided detection of cancer in automated 3–D breast ultrasound. IEEE TMI 2013, 32, 1698–1706.
125. Traub–Dargatz, J.L.; Salman, M.D.; Voss, J.I. Medical problems of adult horses, as ranked by equine practitioners. J. Am. Vet. Med. 1991, 198, 1745–1747.
126. Ulivieri, F.M.; Rinaudo, L. Beyond bone mineral density: a new dual X–ray absorptiometry index of bone strength to predict fragility fractures, the bone strain index. Front. Med. 2021, 7, 590139.
127. Ulivieri, F.M.; Rinaudo, L. Beyond bone mineral density: a new dual X–ray absorptiometry index of bone strength to predict fragility fractures, the bone strain index. Front. Med. 2021, 7, 590139.
128. Vaccaro, C.; Busetto, R.; Bernardini, D.; Anselmi, C.; Zotti, A. Accuracy and precision of computer–assisted analysis of bone density via conventional and digital radiography in relation to dual–energy x–ray absorptiometry. Am. J. Vet. Res. 2012, 73, 381–384.
129. van der Stelt, P.F. Filmless imaging: The uses of digital radiography in dental practice. J. Am. Dent. Assoc. 2005, 136, 1379–1387.

130. van Griethuysen, J.J.M.; Fedorov, A.; Parmar, C.; Hosny, A.; Aucoin, N.; Narayan, V.; Beets–Tan, R.G.H.; Fillon–Robin, J.C.; Pieper, S.; Aerts, H.J.W.L. Computational radiomics system to decode the radiographic phenotype. Cancer Res. 2017, 77, e104–e107.
131. Vemming, D.C.; Steenkamp, G.; Carstens, A.; Olorunju, S.A.S.; Stroehle, R.M.; Page, P.C. Prevalence of dental disorders inan abattoir population of horses in South Africa by oral examination of intact and bisected heads. Vet. J. 2015, 205, 110–112.
132. Vidal, P.L.; de Moura, J.; Novo, J.; Ortega, M. Multi–stage transfer learning for lung segmentation using portable X–ray devices for patients with COVID–19. Expert Syst. Appl. 2021, 173, 114677.
133. Walker, H.; Chinn, E.; Holmes, S.; Barwise–Munro, L.; Robertson, V.; Mould, R.; Bradley, S.; Shaw, D.J.; Dixon, P.M. Prevalence and some clinical characteristics of equine cheek teeth diastemata in 471 horses examined in a UK first–opinion equine practice (2008 to 2009). Vet. Rec. 2012, 171, 44.
134. Wazarkar, S.; Keshavamurthy, B.N. A survey on image data analysis through clustering techniques for real world applications. J. Vis. Commun. Image Represent. 2018, 55, 596–626.
135. Weller, R.; Livesey, L.; Maierl, J. et al. Comparison of radiography and scintigraphy in the diagnosis of dental disorders in the horse. Equine Vet. J. 2001, 33, 49–58.
136. Yamada, K.; Sato, F.; Higuchi, T.; Nishihara, K.; Kayano, M.; Sasaki, N.; Nambo, Y. Experimental investigation of bone mineral density in Thoroughbreds using quantitative computed tomography. J. Equine Sci. 2015, 26, 81–87.
137. Yang, X.; Sechopoulos, I.; Fei, B. Automatic tissue classification for high–resolution breast CT images based on bilateral filtering. Proc. SPIE. 2011, 7962, 79623H.
138. Zarychta, P. Application of fuzzy image concept to medical images matching. In Information Technology in Biomedicine. ITIB 2018. Advances in Intelligent Systems and Computing, 1st ed.; Pietka, E., Badura, P., Kawa, J., Wiecławek, W., Eds.; Springer: Cham, Switzerland, 2019, 762, 27–38.
139. Zhang, H.; Hung, C.L.; Min, G.; Guo, J.P.; Liu, M.; Hu, X. GPU–accelerated GLRLM algorithm for feature extraction of MRI. Sci. Rep. 2019, 9, 10883.
140. Zwanenburg, A.; Leger, S.; Vallieres, M.; Lock, S. Image biomarker standardisation initiative for image biomarker standardisation initiative. arXiv 2016, arXiv:1612.07003. (accessed on 12 January 2022).

9. Załączniki

9.1. Artykuły naukowe wchodzące w skład rozprawy doktorskiej

Journal of Equine Veterinary Science 101 (2021) 103428

Contents lists available at ScienceDirect

Journal of Equine Veterinary Science

journal homepage: www.j-evs.com

Case Report

EOTRH Syndrome in Polish Half-Bred Horses - Two Clinical Cases

Kamil Górski[a,*], Henry Tremaine[b], Bartłomiej Obrochta[a], Roma Buczkowska[a], Bernard Turek[a], Andrzej Bereznowski[c], Alicja Rakowska[c], Izabela Polkowska[d]

[a] Department of Large Animals Diseases with Clinic, Warsaw University of Life Sciences, Poland
[b] B&W Equine Clinic, UK
[c] Department of Veterinary Epidemiology and Economics, Faculty of Veterinary Medicine, Warsaw University of Life Sciences, Poland
[d] Department and Clinic of Animal Surgery, Faculty of Veterinary Medicine, University of Life Sciences in Lublin, Poland

ARTICLE INFO

Article history:
Received 7 October 2020
Received in revised form 12 January 2021
Accepted 22 February 2021
Available online 24 February 2021

Keywords:
Incisors
Extraction
Tooth resorption
Hypercementosis
EOTRH

ABSTRACT

The aim of this paper is to thoroughly describe the etiology, diagnostic processes and recommended treatment of equine odontoclastic tooth resorption and hypercementosis (EOTRH). It is a relatively recently described disease. Most recent reports show that it is a common problem involving older equine patients. The most common and significant symptom of EOTRH is oral pain. The main clinical signs include periodontitis and gingivitis with a gingival recession, alveolar bone protrusion, periodontic fistulas and soreness of the incisors. When establishing the final diagnosis, it is necessary to compare the results of the clinical and radiological examination, because in the early stage, the disease may not show any symptoms. Authors used two clinical cases of Polish Half-Bred horses to present some aspects of diagnostic and surgical techniques. The knowledge presented in the paper may be valuable for equine practitioners working in the field to achieve more beneficial outcomes and provide a higher level of welfare for their equine patients. Nevertheless, further research and observations are necessary, since the etiology of the disease remains unclear.

1. Introduction

Incisor disorders are relatively rare in horses, making up about 11% of stomatologic problems in this species. However, if these cases occur, 75% of them concern at least two incisor teeth. To compare, canine teeth pathology makes up less than 1.25% of reported cases [1]. One of these disorders is a recently described disease termed Equine Odontoclastic Tooth Resorption and Hypercementosis (EOTRH).

Clinical symptoms of this disease were described for the first time in 2004 by Klugh as a rare and unidentified illness of canines and incisors in horses [2]. Additional cases of incisor disorders connected with tooth resorption and bulbous enlargement of the alveolar part of the teeth were described in following years [3]. However, the name of the disease was already suggested in 2008 by Staszyk et al., who described two pathological processes involved – tooth tissue resorption and unregulated deposition of cement [4, 5]. EOTRH is commonly associated with concurrent periodontal disease [3, 6, 7, 8, 9, 10, 11]. The disease has been described worldwide, including in Europe, United States of America, and Australia [6, 7, 12, 13, 14].

The disease may be described as teeth-damaging and pain-causing, mainly affecting a horse's incisors and less frequently their canines [12, 15, 16]. Recently, cases of infected premolars and molars have also been observed [3, 17, 18].

Horses above the age of 15 are mainly affected [3], although the most current research reports cases showing the mild form of the disease even in 10-year old animals [19]. Literature data has proposed that breed and sex may be risk factors associated with the development of EOTRH [13, 20].

The objective of this study was to summarize some current knowledge about etiology, diagnosis, and treatment strategy for EOTRH, followed by a presentation of two clinical cases.

2. Etiology

The cause of the disease has not yet been fully described but some theories suggesting its emergence and development have been mentioned [3]. One theory involves an immunological basis,

Animal welfare/ethical statement: According to national law, the study did not require formal approval by an ethics committee.

Conflict of interest statement: The authors declare no conflict of interest concerning the publication of this case report.

* Corresponding author at: Kamil Górski, Department of Large Animal Diseases with Clinic, Faculty of Veterinary Medicine, Warsaw University of Life Sciences, ul. Nowoursynowska 100, 02-797 Warsaw, Poland
E-mail address: kamil_gorski@sggw.edu.pl (K. Górski).

https://doi.org/10.1016/j.jevs.2021.103428
0737-0806/

analogical to those occurring in people (MIRR - Multiple Idiopathic Root Resorption) and in cats (FORLs – Feline Odontoclastic Resorptive Lesions) [3-5, 6, 12]. In both of these cases, similarly to EOTRH, tooth tissue resorption and an unknown etiology of the illness are typical [3]. Resorption can affect all of the dental tissues, i.e. cement, enamel, dentine, and sporadically, dental pulp [4]. In horses, clinical changes mainly have a proliferative character with a dominance of hypercementosis [3]. In severe cases of the disease, bulbous enlargements of reserve crown may appear along with multiple enlargements of the tooth crown, in comparison with a healthy tooth [4, 6].

Furthermore, involvement of *Treponema* spp. and *Tannerella spp*., which were isolated from the oral cavity of affected horses, have been taken into consideration as possible factors triggering EOTRH [3, 4, 7, 21, 22].

Some authors suggest that Polish Half-Bred horses, Thoroughbreds and Warmbloods may be more prone to this disease [16], but it has not been fully confirmed [19]. Some studies also propose that sex and breed may influence the development of the disease [13, 20]. A few reports suggest that geldings are most often affected [13, 20, 22].

Other potential predispositions have also been enumerated: ischaemic necrosis of the tooth root and the tooth reserve crown, genetic background, influence of the diet, systemic factors, i.e.: hypervitaminosis A, fluorosis, hypocalcaemia, hyperparathyroidism,pituitary pars intermedia dysfunction (PPID), metabolic syndrome, severe paradentium inflammation, idiopathic background, and also iatrogenic causes, connected with erroneous correction of incisors and canines [3, 6, 16, 19].

According to Staszyk et al., a factor which most probably initiates EOTRH and the most probable cause of the pathological process is the excessive mechanical stress put on the periodontal ligaments during prehension [3, 16]. It refers particularly to older horses, where the number of periodontal ligaments decreases in relation to the occlusal surface. However, the masticatory load imposed on these structures remains the same as in young horses.

Some authors claim that excessive mechanical loading of periodontal ligaments causes focal necrosis and secretion of cytokines, which leads to an influx and activation of odontoclasts and resorption of tooth tissues. This process triggers a reconstructive reaction, which comprises of the deposition of cement by the cementoblasts [3]. Furthermore, canine teeth may also be affected by this pathology, although they do not take part in prehension. Hence, they are not subjected to excessive pressure, which may explain their less advanced deformations. However, conducted simulations of straining and deforming the incisors revealed that the excessive pressure is transferred through fragments of the maxilla and mandible, located on the *Margo interalveolaris*, to canine periodontal ligaments, even though this pressure is definitely weaker than in the case of the incisors [3]. Also histopathological research indicates that the illness is caused by biomechanical strains and deformations as well as microbial secondary infections [3, 7].

3. Clinical signs and diagnosis

The diagnosis is based on radiological signs in the presence of clinical signs [3]. EOTRH syndrome is a pain-causing disease [15, 19, 23]. First unspecific signs are usually noticed by the horse's owner. They manifest by difficulties during prehension or rejecting meals such as hard fruits and vegetables, namely apples or carrots. The other clinical signs are excessive salivation, halitosis, oversensitivity to the bit, difficulties in being lead, especially while turning during riding, tilting or trembling of the horse's head, oversensitivity to touch, periodical decline of condition, and weight loss [15, 19, 22, 24]. Moreover, foregoing or limiting the use of incisors while grazing or prehending hay can be noticed, with horses compensating by using the lips [15]. Examination of the oral cavity can be difficult to conduct, because manipulating and pressing the affected teeth can trigger the pain reaction [15]. One should be particularly cautious during inserting a full mouth speculum that loads the incisors. It can cause excessive pain and an unexpected reaction of the horse, even after using a significant amount of sedatives. Local symptoms of the disease include periodontal inflammation, gingivitis of different degrees and gingival recession, denuding of *lamina dura dentis* [4], deposition of tooth calculus, accumulation of food remains, instability of the teeth, fractures of *lamina dura*, fractures of tooth reserve crown or their complete loss [3, 6, 13, 19]. One of the characteristic signs is visible defects in maxillary and mandibular gingivae, between intra-alveolar appendages. Some authors also describes prominent juga as a depressions between the ridges of bone formed by roots in the alveolar process on the maxilla or the mandibula [13, 15]. Dental abscesses and periodontal fistulation resulting from infected tooth, periodontal disease or osteomyelitis are also described [4, 6, 13, 15, 19]. Moreover, mandibular lymph nodes can be enlarged [15, 16]. In older horses, tooth defects connected with their resorption can also be seen under the calculus on canines, especially those localized on the mandible [13, 15]. In some cases, for example in well-trained horses or in the early stage of the disease, clinical signs may not be apparent, at least until periodontal inflammation connected with resorptive or proliferative changes occur [3, 15].

Table 1
Radiological system of classifying changes to the incisors according to Hüls et al.

Picture	Degree	The Extent of Radiological Changes
SEVERE	III	Loss of the shape of the tooth / intra-alveolar tooth part is wider than a clinical crown / tooth fractured Intra-alveolar surface irregular / rough
MODERATE	II	Tooth shape mostly preserved / intra-alveolar tooth part is wider than a clinical crown/ clearly blunt tooth's peak of the root
MILD	I	Tooth shape preserved / Slightly blunt peak of the root Irregular / intra-alveolar tooth part of surface / rough
NORMAL	0	Lack of perceptible radiological changes

Apart from clear clinical signs, radiological examination is essential to obtain definite diagnosis, since similar symptoms may occur in other dental problems, such as periapical abscess. Moreover, it is necessary to assess the stage of the disease, especially in its initial phase, when the majority of the changes affect the subgingival layer [3, 19]. This can also present some advantages in planning the treatment and a probable extraction of infected teeth [15]. Hüls et al. [28] developed a radiological system of classifying changes of incisors in horses. It was modified by S. Rehrl et al. – Table 1. [19].

Radiographs confirm which teeth should be extracted, determine the extent of changes and allow to illustrate the condition of surrounding soft tissues and bone structures which is particularly helpful for later extraction [15]. Before radiological examination it is advised to sedate the horse. To visualize the condition of the incisors properly, it is essential to take intraoral radiographs with a bisecting angle technique using the dorsoventral projection for the maxillary teeth and ventrodorsal projection for the mandibular teeth [17, 22, 25].

The x-ray beam is aimed at a 90° to the plate where an imaginary line bisects the angle made by the tooth and cassette [3, 7, 15, 19, 25, 26]. Oblique views can be used to provide better visualization and separation of the third incisors and canine teeth, particularly in males, through the reduction of superimposition [25, 26]. This allow for complete assessment of the incisors, especially considering the finding that for some types of resorption, the third incisors are most often affected [25]. A cassette should be put hor-

izontally into the oral cavity, as caudally as possible. In geriatric horses, the teeth and incisive processes are more angled, such that the x-ray beam can be almost perpendicular to the plate, whereas this positioning results in foreshortening of the incisors in young horses [26]. Using a cassette protector and a head-rest for stabilization can be helpful. This projection seems to be the most diagnostic since the lateral projections result in dental superimposition. It may also be necessary to take additional projections of every canine tooth [19]. In this situation, the x-ray beam is angled around 45 degrees to the plate, and perpendicular to the long axis of the head [26].

Moreover, the range of changes from completely healthy teeth to advanced pathological changes can be seen in incisors and canines in the same horse [15]. The literature shows that most cases with clear clinical signs present more advanced radiographic changes than can be expected from an oral examination alone. Additionally, the impression of completely healthy teeth during clinical examination, with evident clinical signs and radiological picture was more often noted in mandibles than incisive bones [22]. Two radiological images can be distinguished and occur simultaneously: tooth resorption and bulbous enlargement of the intra-alveolar part of the teeth [6]. However, the radiological picture can also show widening of the periodontal ligament space, root resorption, erosion of the apical part of the root, root and reserve crown enlargement due to hypercementosis, irregular and/or rough surface of an intra-alveolar part, disruption of *lamina dura*, osteomyelitis, atrophy or other pathology in the course of a pulp canal, or fractures of the root and the reserve crown [4, 17, 19].

4. Treatment

According to the literature, no other treatment other than exodontia is currently available for severe cases of EOTRH. Shortening of the incisors and daily cleaning with chlorhexidine solution may have some positive effect and decrease inflammatory signs [3, 22, 27]. Whereas the incisors can be carefully shortened to provide optimal occlusion contact and reduce abnormal forces appearing in overlong sectors, some authors claim that shortening of incisal teeth in EOTRH cases rarely brings improvement or enhances the animal's comfort of life [3, 4, 23]. They even consider incisor reduction to make a horse nearly five times more likely to subsequent development of hypercementosis or resorption process [16]. It is essential to remember that at present the extraction of pathologically changed teeth is the only effective solution and the method of choice [3, 4, 23].

5. Postoperative Care

Even before making a decision about extracting affected tooth/teeth, the horse's owner should be informed about postoperative care, proper diet, possible complications and expected results [15]. Removal of all the incisors requires suitable instrumentation and it is advised to be conducted by an experienced veterinary surgeon or an equine dentist [15, 22]. While extraction of the incisors can be conducted in a stable, removal of canines usually requires more advanced techniques with denuding a significant fragment of gingiva and alveolar bone, preferably conducted in a clinical setting. Attention should be paid to the necessity of more frequent monitoring and increased probability of stomatologic procedures after incisors extraction. Removing a tooth will result in the lack of rubbing the antagonist tooth, causing clinical crown overgrowth, which leads to hindering the process of food fragmentation, soft tissue damages in the oral cavity, emergence or exacerbating of already existing stomatologic defects and sometimes fractures of a tooth crown. Therefore, it is necessary to regularly check the oral cavity and possibly correct the dentition every six months. This usually consists of removing a fragment of overlong tooth crown. Modification of the diet is necessary as it enables to maintain the appropriate condition of the animal [23]. In the case of pathologies or lack of incisors, one should eliminate or drastically limit hay with long stalks, which will minimize the risk of choking or intestinal obstruction. Soaking the hay softens the stalks and facilitates biting through the hunks. Soaked beet pulp may be a good alternative, since it contains a significant amount of digestible fiber and is usually eagerly eaten by horses. The addition of medicago (alfalfa) in the form of chaff or granulat (preferably soaked earlier), is a good source of protein. It can also be advantageous to give haylage or chopped hay. However some research shows that short fragments of fiber might potentiate layering and covering the interdental spaces with food in the case of diastemas, which causes the exacerbation of periodontal disease. Introduction of crushed grain, mainly oats, which remarkably increases their digestibility or commercial feed blends for older horses should be considered. During the spring to autumn period, the best solution for horses with stomatologic problems is to graze. Grass is a source of fodder and is easy to bite and digest [23].

6. Clinical Cases

6.1. Case 1

Twenty-one-year old, 650 kg Polish Half-Bred gelding used for pleasure riding was bought by the present owner at the age of 13, without any information about earlier examination of oral cavity or correction of the dentition. From the purchase of the horse, neck stiffness and problems with a snaffle bit were observed during riding. According to the owner the horse was choosy, did not finish eating rich fodder, but eagerly ate roughage in the form of hay and grass. The first correction of the dentition was conducted. It consisted of rasping the sharp edges of the mandibular and maxillary premolars and molars and removal of the calculus from canines and incisors. Oral cavity examination and correction of the dentition were conducted every six months. When the horse was 15, the owner noticed redness in the gingiva around the incisors. At the age of 17, in the area of the gingival papilla, gingival recession of a maxillary incisor's root occurred. Inflammation of this area developed even though hygienic procedures were implied. At the age of 19, an epulis appeared in the area of the mandibular incisors. For the next two years, the condition of the incisors declined, halitosis appeared and gingival recession and tooth fractures occurred, which lead to damage of the gingiva. During routine blood examinations, decreased levels of zinc and copper were detected for years, along with a periodically decreased level of potassium. The horse was also diagnosed with headshaking syndrome.

At the age of 21, the horse was presented for dental evaluation. At this time, overall parameters were situated within physiological limits. During the oral cavity examination, halitosis and excessive salivation were noticed. Different degrees of movement involving the incisors was revealed. During palpation, the horse's defence reaction connected with pain occurred. Accumulation of calculus and food remains in between interdental spaces were present. One could observe gingival recession and irregular, deformed gingival papilla of the maxillary and mandiblular incisors. Moreover, fragments of reserve crown and roots of individual incisors of the maxilla and mandible were denuded. In the mandible teeth arches, teeth 303 and 403 were lacking. Additionally, in the proximity to tooth 402, an epulis was localized and was characterized with prominent movement (Fig. 1 and 2.).

The Hausmann speculum, dental mirror and headlight source were used for further examination of the oral cavity. The overgrowth and movement of tooth 106, overgrowth of tooth 206, malocclusion – mainly in teeth arcades of the maxilla; carries on the infundibulum of tooth 109, lack of tooth 406; excessive loss of tooth 306 up to the gingival line; sharp edges of the cheek teeth of maxilla (tooth 08–11) and

Fig. 1. Case 1- The condition before extraction of the mandibular incisors; teeth 303 and 403 were absent; deformation of the area surrounding the alveolar process; pedunculated epulis close to the tooth 402; fragments of reserve crown and roots of tooth 301 were denuded.

Fig. 2. Case 1 - Pedunculated fragment of an epulis located near tooth 402.

mandible (tooth 07–11) and erosion of the cheek mucosa were identified. During radiological examination of the maxilla, a decreased opacity of the incisors' roots and reserve crowns was observed, as well as the lamina dura of the alveolar processes of maxillary and mandibular incisors was noted. EOTRH was the definite diagnosis. Because of the present condition and developing disease, the decision to extract the incisors was made. The procedure was divided into two stages, with a 45-day break in between. During the first stage the maxillary incisors were removed, while during the second stage, the mandibular ones. In both stages, the premedication was conducted with detomidine (20 μg/kg m.c.) and butorphanol (20 μg/kg m.c.) given intravenously. Before removing teeth 101, 102, 103, 201, 202, 203 both infraorbital nerves were anaesthetized with 0,5% bupivacaine hydrochloride and surrounding gingiva was locally anaesthetized with 2% lignocaine hydrochloride. Initially, gingivae were separated from the clinical crowns of the incisors with chisels and LECLUSE and BEIN type root levers (Fig. 3).

Liston type forceps were used to loosen the tooth. For this purpose, forceps were applied and left within the interdental space for 2-3 minutes then moved to the opposite side of the tooth. This process was repeated several times, which allowed to disrupt the periodontal ligament [15]. During the next step, the teeth were removed by progressive separation of the alveolar ligaments and loosening of the tooth with chisels for equine incisor extraction. Teeth were pulled out from the alveoli with special forceps, starting from the outermost teeth. In some cases, usage of a more aggressive technique was necessary, therefore a mallet and chisel were used to cut off the periodontal ligaments precisely. When the crown breaks, the alveolus should be thoroughly palpated for retained fragments. In such circumstances, any remaining fragments should be removed with a bone curette or small rongeur. Post-operative radiographs are recommended. Small root fragments firmly embedded in the alveolus can be left in place with no detrimental effects or removed a few days later, during bandage changing. The horse should be kept without food and water for 4 hours after the extraction. A simple disposable muzzle may be used for that purpose.

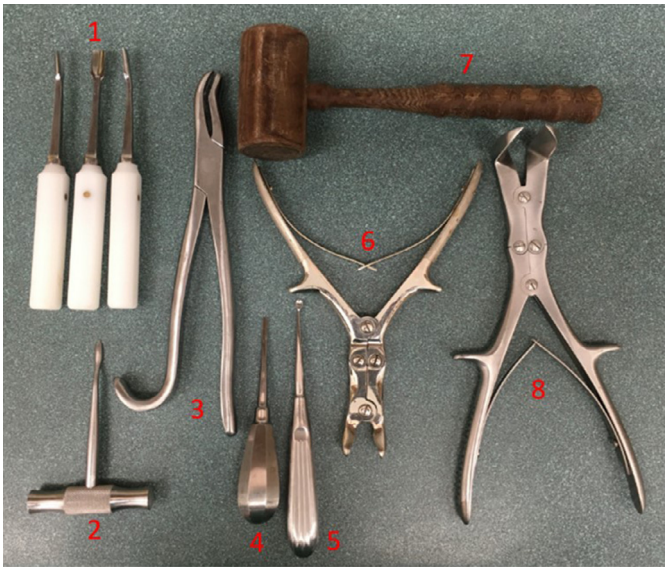

Fig. 3. Incisor extraction set instruments: 1 – chisels set for incisor extraction; 2 -LECLUSE type elevator; 3 – forceps for incisor extraction; 4- BEIN type elevator; 5 – bone curette; 6 – bone rounger; 7 – mallet; 8 – curved LISTON forceps.

Correction of the dentition was conducted with the mechanical rasp. The sharp edges of the maxillary and mandibular cheek teeth were ground, firstly with the diamond disc followed by the apple core burr to thoroughly smooth out the teeth. Moreover, their overgrown crowns were shortened approximately 3 mm to provide better movement of the mandible and therefore, improved food grinding. Sharp enamel points on the buccal side of the maxillary cheek teeth and lingual side of the mandibular cheek teeth are a sign of pathology and may cause damages to the mucous membrane of the cheeks or tongue. They also reduce a range of motion during the chewing cycle.

An overall chemotherapy had been implemented in the form of dihydrostreptomycin (8000 I.U./kg m.c.) with procaine penicillin (8 mg/kg m.c.) for six days and phenylbutazone (2.2 mg/kg m.c.) for the first two days. After the extraction, the loose gingival margins were left unsutured and the wound was managed as an infected one. The bandage placed in the intra-alveolar area was first changed after 3 days, then again in 7-day intervals, until full coverage with granulation tissue was obtained (Fig. 4).

Preparation of the second stage of the procedure was identical. After desensitisation of left and right mental nerves, teeth 301, 302, 401, 402 were removed (Figure 5).

Furthermore, the pedunculated fragment of the epulis located near tooth 402 was removed. Subsequently, the gingivae were stitched with two situational sutures made of polyglicolic acid. Post-operative care

Fig. 4. Case 1 -The incisor area immediately after extraction of the incisors and 5 days after.

was conducted in an analogical way. In both cases it was advised to rinse the oral cavity with 0,12 % solution of chlorhexidine gluconate repeatedly every day, and for several days to give the horse grass pellets pulp as well as to avoid feeding with oats grain. After both stages of the procedure, the overall parameters remained within the physiological limits. The horse ate both roughage and properly prepared rich fodder without any problems. Complete filling of the intra-alveolar area with granulation tissue occurred and the wounds healed prior to 30 days following the procedures (Figs. 6 and 7).

Such a long time of recovery could have been caused by continuous irritation of the tissues by ingested food and chronic inflammatory changes in this area. After extraction of the teeth and healing of the wounds the horse's condition significantly improved. The animal was able to ingest the food better, put on weight and halitosis disappeared. The horse learnt to use its lips to bite the grass bits, sometimes helping itself with the gingiva. The owner noticed that the amount of undigested fragments of rich fodder and long fibers in faeces decreased, which could be attributed to the pain reduction, which escalated during an attempt to close the incisors, and correction of the cheek teeth disorders. The risk of the tongue protrusion happens sporadically and lasts only temporarily. After the procedure the horse was not used under the saddle, because of its orthopedic problems.

6.2. Case 2

Twenty-four-year old, 700 kg Polish Half-Bred gelding used for pleasure riding was known to have oral cavity control conducted regularly, every six months. Dental correction was conducted whenever it was needed. During a control visit, two movable incisors were removed and one fell out by itself. For a while the horse had problems with biting apples and carrots and periodically halitosis and excessive salivation appeared. Eating other fodder was not problematic.

Fig. 6. Case 1 - Sixty-two days after the removal of the maxillary incisors and 17 days after removal of the mandibular incisors; the incisor area of the mandible during granulation with visible suturing.

During the examination, all of the overall parameters remained within the physiological limits. Salivation and halitosis were present. Buccal cavity examination indicated: lack of teeth 103, 201, and 203, fragments of tooth 103 and 201, accumulation of calculus and cement on the other teeth, gingivitis, fragments of the roots of lacking teeth, excessively expressed gingival papilla, gingival recession, and movement of the incisors along with a pain reaction when they were touched (Fig. 8).

It was also noted: lack of teeth 306, 406, overlong teeth 106 and 206, sharp edges of the maxillary and mandibular cheek teeth, and small erosions on cheek mucosa. During radiological examination of the maxilla it was noted: an acquired oligodontia, decreased opacity of the roots and reserve crown areas of other incisors as well as the lamina dura of the alveolar processes of maxillary and mandibular incisors (Figs. 9 and 10).

After analysing the signs and the result of the radiological examination, the decision was made to extract the maxillary incisors, and in the later stage – the mandibular incisors.

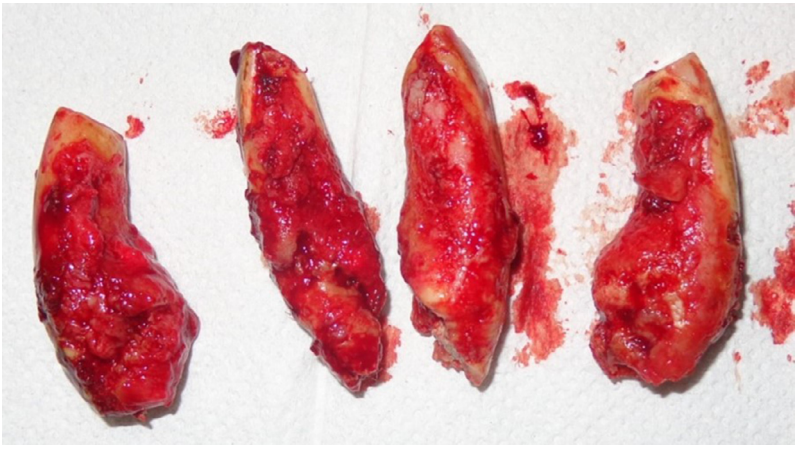

Fig. 5. Case 1 - Mandibular incisors after extraction; an evident widening of the alveolar part, especially the external teeth.

Fig. 7. Case 1 - Healed area of the maxilla and mandible respectively 46 and 135 days after extraction.

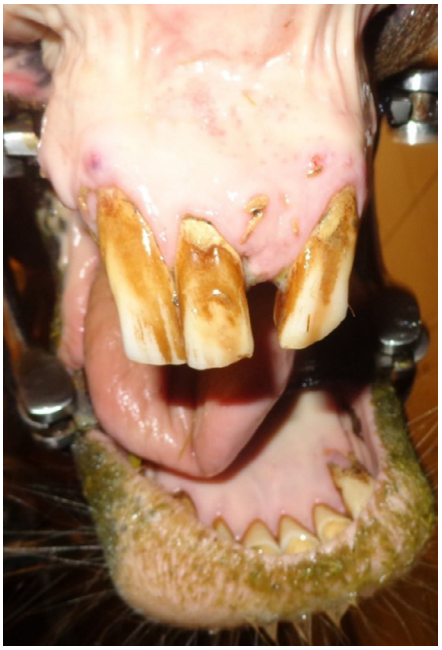

Fig. 8. Case 2 - Condition before surgery; teeth 103, 201, and 203 were absent; remains of teeth 103, 201; deposition of calculus; maxillary incisal deformation area with numerous fistulas.

Extraction of the incisors and post-operative care were conducted similarly to Case 1. Removed teeth had greater tendency to crumble and fracture which was a main difference (Fig. 11). Especially in that situation it was reasonable to take a radiographic check (Fig. 12). The gingival healing lasted about 4 weeks (Fig. 13).

After full recovery of the wounds, the horse was given fodder, halitosis and salivation from the oral cavity disappeared and the animal put on weight. Sporadically protrusion of the tongue occurs. Because of improvement in functioning and in the animal's condition the owner decided to postpone the extraction of the mandibular incisors. Three months after the procedure, applying pressure to the incisors was not painful anymore for the horse. The gingivitis had almost disappeared. Because of the orthopedic problems the horse has not been used under the saddle.

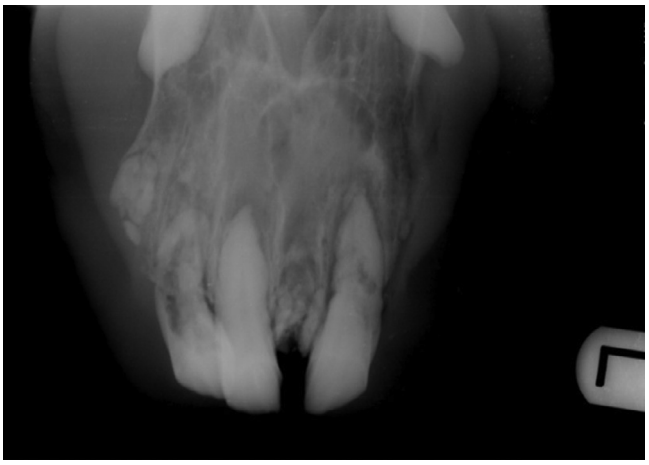

Fig. 9. Case 2 - Intraoral radiograph of maxillary incisor teeth; no teeth 103, 201, and 203; fragments of 103, 201; teeth roots lysis; inflammatory resorption with loss of teeth and alveolar bone structure.

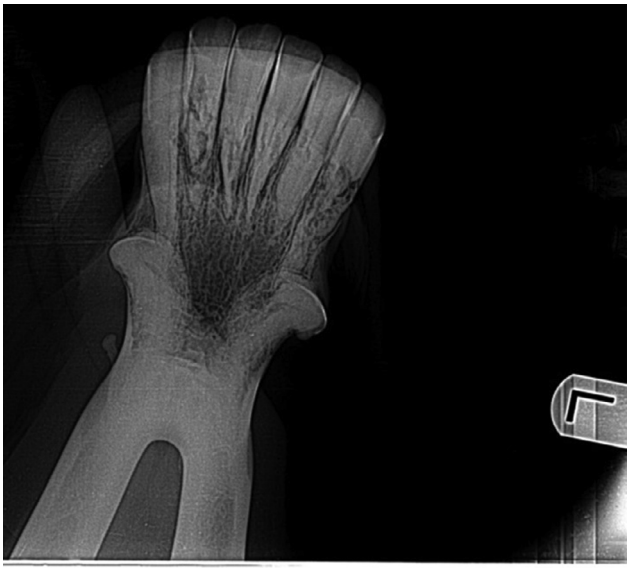

Fig. 10. Case 2 - Intraoral radiograph of mandibular incisor teeth; surface irregular/rough; odontoclastic lesions were present in the reserve crown as mottled radiolucent areas.

7. Prognosis and Prevention

Hitherto, an effective method of preventing this disease was not found. Some authors suggest to x-ray the incisors together with their assessment to evaluate the level of resorption and accommodation of cement, in horses 15 years of age or older [25]. The sole fact of being aware of the eventual development of the disease would enable close observation, formulation of a treatment plan, and directing of future actions.

The EOTRH syndrome is a developing disease [3]. With advanced clinical signs the extraction of infected teeth is the method of choice [3, 4, 23]. Described attempts of using fodder supplements on the basis of mushrooms (Equident), and even daily cleaning of the incisors with a brush with added disinfectant, for example chlorhexidine, together with shortening the incisors' crowns, brought positive results in the form of limiting the inflammatory reaction, but this was only a palliative solution, possible during

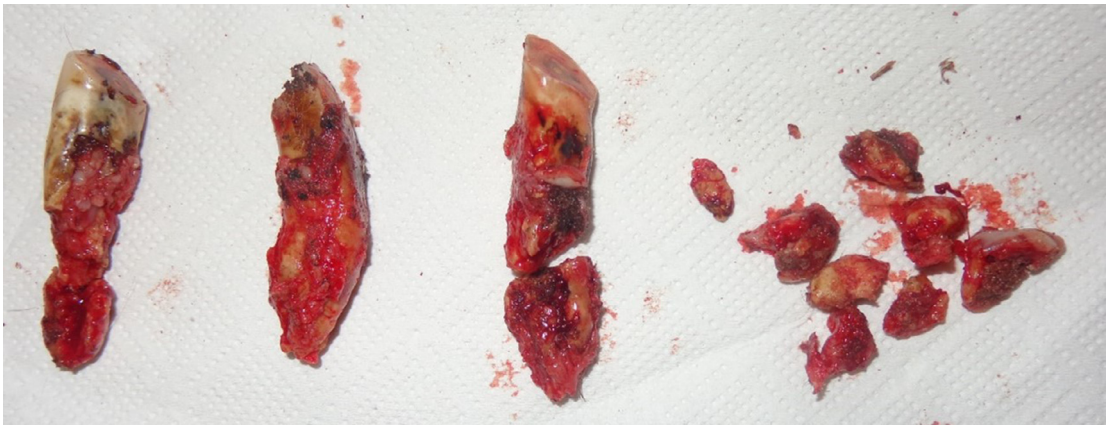

Fig. 11. Case 2 - Incisors' condition after removal. Some incisors were fully extracted, some had a tendency to crumble and fracture.

Figure 12. Case 2 – The radiographs were taken after extraction for documentation and confirmation that the entire tooth was extracted. The picture shows small pieces of teeth roots.

Figure 13. Case 2 - Two days after maxillary incisors extractions; swabs have stuck in the teeth sockets; the gingivae have shrunk.

less developed stages of the illness [4]. Taking into consideration the fact that the disease is very painful, even such a radical solution as removal of all the incisors, remarkably improves the comfort of the animal in the further perspective. The owners' reluctance to extract several incisors can be an obstacle. However, it can be explained by the concerns about further functioning of the horse and ingestion of food. The observations show that even after total removal of the incisors, horses can adapt to the new situation and ingest food including hay or grass [22]. The side effect of removing all the incisors can be tongue protrusion, which is often a cosmetic defect.

8. Summary

The etiopathogenesis of the illness has not been fully explained. An effective method of preventing the disease or of conservative treatment has not been established [3, 22]. The treatment of choice would be the extraction of the teeth exhibiting clinical and radiological changes, which remarkably diminishes the chronic pain and other symptoms connected with this oral cavity malfunction. Hopefully, effective methods of preventing or slowing down the development of this devastating disease will emerge. Until then, the proper dental and radiological evaluation made by an experienced clinician and extraction of the affected teeth seems to be the best and most efficient method of treating the disease [3, 22].

Sources of Funding

This research did not receive any specific grant from funding agencies in the public, commercial, or not-for-profit sectors.

Author Contributions

All the authors had a significant impact on conduction of this study as well as have read and agreed to the published version of the manuscript.

References

[1] Dixon PM, Tremaine WH, Pickles K, Kuhns L, Hawe C, McCann J, McGorum B, Railton DI, Brammer S. Equine dental disease part 1: a long-term study of 400 cases: disorders of the incisor, canine, and first premolar teeth. Equine Vet. J. 1999;31:369–77.
[2] Klugh DO. Incisor and canine periodontal disease. In: Proceedings of the 18th Annual Veterinary Dental Forum, Fort Worth, Texas, USA., 18; 2004. p. 166–9.
[3] Hole SL, Staszyk C. Equine odontoclastic tooth resorption and hypercementosis. Equine vet. Educ. 2018;30(7):386–91.
[4] Moore NT, Schroeder W, Staszyk C. Equine odontoclastic tooth resorption and hypercementosis affecting all cheek teeth in two horses: clinical and histopathological findings. Equine vet. Educ. 2016;28(3):123–30.

[5] Baratt R. Equine odontoclastic tooth resorption and hypercementosis (EOTRH): What do we know? *Equine vet. Educ.*, 2016;28(3):131–3.
[6] Staszyk C, Bienert A, Kreutzer R, Wohlsein P, Simhofer H. Equine odontoclastic tooth resorption and hypercementosis. Vet J 2008;178:372–9.
[7] Sykora S, Pieber K, Simhofer H, Hackl V, Brodesser D, Brandt S. Isolation of *Treponema* and *Tannerella* spp. from equine odontoclastic tooth resorption and hypercementosis related periodontal disease. Equine Vet. J 2014;46:358–63.
[8] Gregory R, Fehr J, Bryant J. Chronic incisor periodontal disease with cemental hyperplasia and hypoplasia in horses. In: Proceedings of AAEP Focus on Dentistry, Indianapolis, USA; 2006. p. 312–16.
[9] Baratt R. Equine incisor resorptive lesions. In: Proceedings of the 21st Annual Veterinary Dental Forum, Minneapolis, USA; 2007. p. 23–30.
[10] Rawlinson J, Earley E. Advances in the treatment of diseased equine incisor and canine teeth. Vet. Clin. North Am. Equine Pract. 2013;29:411–40.
[11] du Toit N, Rucker B. The gold standard of dental care: the geriatric horse. Vet. Clin. Equine 2013;29:521–7.
[12] Staszyk C. Incisor lesions: equine odontoclastic tooth resorption and hypercementosis. In: Proceedings of the 49th British Equine Veterinary Association Congress 2010 - Birmingham, United Kingdom; 2010.
[13] Smedley RC, Earley ET, Galloway SS, Baratt RM, Rawlinson JE. Equine odontoclastic tooth resorption and hypercementosis: histopathologic features. Vet. Pathol. 2015;52(5):903–9.
[14] Lee S. Equine odontoclastic tooth resorption and hypercementosis. Aust Vet J 2010;88:N23–4.
[15] Rawlinson J, Carmalt JL. Extraction techniques for equine incisor and canine teeth. Equine vet. Educ. 2014;26(12):657–71.
[16] Pearson AM, Mansfield G, Conaway M, Koput K. Associated Risk Factors of Equine Odontoclastic Tooth Resorption and Hypercementosis. AAEP PROCEEDINGS 2013;59.
[17] Barrett MF, Easley JT. Acquisition and interpretation of radiographs of the equine skull. Equine vet. Educ. 2013;25(12):643–52.
[18] Luedke L, Rawlinson JE, Sanchez MD, Bass L. Engiles J True cementomas (cementoblastomas) associated with a nonvital left maxillary second premolar in an 11-year-old miniature horse. *Equine vet. Educ.*, 2017;29(12):647–54.
[19] Rehrl S, Schröder W, Müller C, Staszyk C, Lischer C. Radiological prevalence of equine odontoclastic tooth resorption and hypercementosis. Equine Vet. J 2018;50(4):481–7.
[20] Rahmani VH, Häyinen L, Kareinen I, Ruohoniemi M. History, clinical findings and outcome of horses with radiographical signs of equine odontoclastic tooth resorption and hypercementosis. Vet Rec 2019;14:1–7 185(23):730.
[21] Kennedy RS, Dixon PM. The aetiopathogenesis of equine periodontal disease – a fresh perspective. Equine vet. Educ. 2018;30(3):161–8.
[22] Lorello O, Foster DL, Levine DG, Boyle A, Engiles J, Orsini JA. Clinical treatment and prognosis of equine odontoclastic tooth resorption and hypercementosis. Equine Vet. J 2016;48:188–94.
[23] Jarvis N, Paradis MR, Harris P. Nutrition considerations for the aged horse. Equine vet. Educ. 2017;31:102–10.
[24] Pimentel LF, Zoppa AL. Analysis of the relationship between occlusal and clinical parameters and the need for incisor reduction in confined horses - a retrospective study. Cienc. Rural 2014;44(11):2052–7.
[25] Henry TJ, Puchalski SM, Arzi B, Kass PH, Verstraete FJM. Radiographic evaluation in clinical practice of the types and stage of incisor tooth resorption and hypercementosis in horses. Equine Vet. J 2016;49(4):486–92.
[26] Baratt R. Advances in equine dental radiology. Vet. Clin. North Am. Equine Pract. 2013;29:367–95.
[27] Earley E, Rawlinson JT. A new understanding of oral and dental disorders of the equine incisor and canine teeth. Vet. Clin. North Am. Equine Pract. 2013;29:273–300.
[28] Hüls I, Bienert A, Staszyk C. Equine odontoclastic tooth resorption and hypercementosis (EOTRH): Röntgenologische und makroskopisch – anatomische Befunde. Proceedings. 10. Jahrestagung der Internationalen Gesellschaft zur Funktionsverbesserung der Pferdezähne (IGFP) 2012.

animals

MDPI

Article

Malocclusions and Dental Diseases in Privately Owned Horses in the Mazovia Region of Poland

Kamil Górski [1,*], Elżbieta Stefanik [1], Bernard Turek [1], Andrzej Bereznowski [2], Michał Czopowicz [2], Izabela Polkowska [3] and Małgorzata Domino [1,*]

[1] Department of Large Animal Diseases and Clinic, Institute of Veterinary Medicine, Warsaw University of Life Sciences, 02-787 Warsaw, Poland
[2] Division of Veterinary Epidemiology and Economics, Institute of Veterinary Medicine, Warsaw University of Life Sciences, Nowoursynowska 159c, 02-776 Warsaw, Poland
[3] Department and Clinic of Animal Surgery, Faculty of Veterinary Medicine, University of Life Sciences in Lublin, 20-950 Lublin, Poland
* Correspondence: kamil_gorski@sggw.edu.pl (K.G.); malgorzata_domino@sggw.edu.pl (M.D.); Tel.: +48-22-593-61-91 (M.D.)

Simple Summary: Dental care is an integral part of equine veterinary practice and has a significant impact on the welfare and body condition score of horses. Regular and detailed examination of the oral cavity allows for diagnosis of malocclusions and dental disease and the implementation of appropriate treatment. As predispositions for individual dental diseases differ among horse populations and age groups, this study aims to characterize the prevalence and frequency distribution of selected malocclusions and dental diseases among horses housed in the Mazovia region of Poland, using the prevalence and frequency distribution of selected malocclusions and dental diseases. Routine veterinary dental examinations were carried out on 206 horses, and the presenting signs of specific malocclusions and dental diseases were recorded for the incisor, canine, wolf, premolar, and molar teeth. Ninety-five percent of examined horses presented with a dental disorder in at least one tooth, with malocclusions more prevalent than dental disease in the incisors, premolars, and molars alike. Curvatures and calculus were the most commonly reported pathologies in incisor teeth, whereas sharp enamel points and caries predominated in cheek teeth.

Abstract: Dental disorders, a term encompassing both malocclusion and dental disease, constitute a serious health problem in horses worldwide. As horse populations differ among countries and regions, a geographically specific characterization of the occurrence of various dental disorders may be helpful for local equine practitioners. This study investigated the prevalence and frequency distribution of selected malocclusions and dental diseases in horses housed in the Mazovia region of Poland, with attention paid to variations among age, gender, and breed categories. Routine dental examinations were conducted on 206 privately owned horses (n = 206). Disorders were recorded using a dental chart and classified as either malocclusions or dental diseases. Out of all examined horses, 95% demonstrated at least one dental disorder, with a roughly equal distribution of these disorders among incisor teeth (31%) and cheek teeth (31% each for premolars and molars). More specifically, there were disorders noted in 14 incisors, 3 canines, 2 wolf teeth, and 15 cheek teeth. Across all age, gender, and breed groups, malocclusions of incisor, premolar, and molar teeth occurred with a higher prevalence than did dental diseases. Curvatures and calculus were the most commonly reported pathologies in incisor teeth, whereas sharp enamel points and caries predominated in cheek teeth.

Keywords: equine dentistry; dental disorders; malocclusion; occurrence; horse

Citation: Górski, K.; Stefanik, E.; Turek, B.; Bereznowski, A.; Czopowicz, M.; Polkowska, I.; Domino, M. Malocclusions and Dental Diseases in Privately Owned Horses in the Mazovia Region of Poland. *Animals* **2022**, *12*, 3120. https://doi.org/10.3390/ani12223120

Academic Editor: Clive J. C. Phillips

Received: 21 September 2022
Accepted: 8 November 2022
Published: 11 November 2022

1. Introduction

It is widely accepted that oral cavity diseases and their sequalae constitute a serious health problem in horses worldwide [1]. Both routine [2–4] and post mortem [5,6] examinations of the oral cavity have revealed that dental diseases are the most commonly diagnosed oral cavity pathology. As previously indicated by Salem et al. [7], most studies of equine dental disease type and incidence are based on clinical cases of hospitalized horses or autopsies of equine heads obtained from slaughterhouses [3,5,8–10]. Kirkland [11] examined 500 horse skulls isolated from cadavers and confirmed 80% showed evidence of dental problems. In a similar but smaller post mortem study of 50 skulls, Brigham et al. found a 74% rate of dental disease [3]. In North America, dental diseases are among the five most common health problems in adult horses [12], affecting 79% of the local horse population [6]. In England, 42% of owners reported their horse suffered from a known dental disorder [13]. In Scotland, 87% of the local horse population is suspected to have a dental disease [14]. In Australia, out of 400 horses referred to clinics due to dental complaints, 87% had a primary disorder in the area of the cheek teeth, 13% had a serious disorder resulting from significant tooth wear, and 11% did not show clinical signs [15]. Out of 400 horse heads examined in an Australian slaughterhouse, 94% showed at least one tooth defect [15]. Similarly, when 556 horse cadavers were examined in a Canadian slaughterhouse, 70% had at least one type of dental abnormality in the cheek teeth [12].

In Poland, apart from one study documenting the frequency of incisor defects [16], the incidence of equine dental abnormalities has not yet been reported. However, given the prevalence of dental diseases in other countries and the horse population in Poland, one can expect to find similar rates of occurrence in Polish horses. According to data provided by the Polish Horse Breeders Association (PHBA-PZHK), there were 271,324 horses in Poland in 2019, including 131,661 cold-blooded horses, 93,852 Polish sport horses, and 45,881 ponies [17]. Among these horses, 37,397 were registered in the Mazovian Voivodeship [18] as sport horses associated with equestrian centers [19] or were privately owned and housed on small horse farms [18]. According to the same dataset, 111 equestrian centers were registered in Mazovia Voivodeship, with each housing an average of 50 horses [19]. It can therefore be estimated that about 5550 horses in Mazovia are sport horses under specific veterinary care, while the remaining 31,847 horses are privately owned. According to the data provided by the Central Statistical Office (CSO-GUS), there are 4550 small horse farms registered in Mazovia, with an average of 7 horses stabled at each. Among the 5,358,000 people of Mazovia Voivodeship, it is estimated 0.08% keep horses for pleasure [18]. As the majority of horses in the region (~85%) are privately owned, the privately owned horses included in this study constitute a reasonably representative group. Moreover, in accordance with veterinary guidelines [7], all privately owned horses should undergo a routine dental examination once a year to determine the health status of the teeth and to perform any necessary corrections. Such annual examinations are advised due to the continuous growth rate of equine teeth and the anisognathic mandible and maxilla conformation, which can lead to irregular wear [1,6].

Examination of dental charts of horses presented for routine dentistry over the years reveal an increase in the percentage of horses manifesting dental problems. Disorders of the incisor teeth, for example, were diagnosed in 11% of horses in the study in 1999 [20], in 20% in 2005 [21], and in 26% in 2008 [22]. One of the reasons for the observed increased incidence of dental disease is improved recognition, due to greater acceptance among owners of the importance of a regularly scheduled dental examination [23], the availability of advanced diagnostic imaging, such as computed tomography (CT) and magnetic resonance imaging (MRI) [24,25], as well as the increased proclivity of veterinarians to specialize in equine dentistry [25–27]. In light of the growing understanding of the impact of proper dental care on the horse's ability to properly chew and grind fodder [3], on equine welfare [28,29], and on sport and working horse usage [30–32], emphasis on odontology as a means of diagnosing, treating, and preventing oral cavity diseases is also increasing [27].

Dental diseases are generally painful [33,34], and thus greatly impact both the horses' quality of life [28] and the owner's ability to use the animal [31,32]. Consequences of dental disease such as pain, discomfort, and altered feed intake have a negative impact on a horse's well-being and are part of the equine welfare monitoring system assessment protocol [29]. This protocol requires the assessor to note the presence of any abnormal wear of the incisors, which might negatively affect feed intake, and asks with what frequency the horse's teeth are being inspected by an equine dental veterinarian [29]. With respect to horse usage, wolf teeth and hooks of the premolar teeth may interfere with the bit, affecting rein tension-related response and consequently the ride ability of the horse [31]. If wolf teeth are present and cause biting issues, they should be removed as early as possible in the horse's career in order to reduce training disturbances [31]. Similarly, if hooks are present, especially on the upper second premolars, they should be corrected to avoid discomfort associated with the bit [31]. In domestic sport and working horses, erosive lesions and fractures of the lower second premolar dental hard tissues and canine teeth are common [30,32]. When dental disease is diagnosed, specific treatment and often a break in riding, training, and competition is required. Moreover, in the case of aggravations or complications, treatment is prolonged, and the financial costs are significantly higher [35]. Thus, both the outright financial losses for the owner and the disruption to the horse's training plan make dental disease an important issue in the equine industry.

Salem et al. [7] highlighted the integral role of field investigations in determining the prevalence of oral cavity and dental disorders and noted that these data contribute to veterinarian and owner knowledge regarding the impact of dental disease on horse health and welfare. Therefore, this study describes the prevalence and frequency distribution of selected malocclusions and dental diseases in a population group of privately owned horses housed in the Mazovia region of Poland, taking into consideration age, gender, and breed.

2. Materials and Methods

2.1. Horses

The study population includes 206 privately owned horses (n = 206) (age mean ± SD: 16.9 ± 7.0; 114 geldings, 78 mares, 14 stallions), presented to a dental veterinarian by their owners for the annual routine dental examination between January and December 2019. The horses were housed in a total of 45 different private stables, all located in Mazovia Voivodeship in Poland, with each stable contributing an average of 4.6 horses to the study. Therefore, horses from 1% (n = 45) of private stables located in the studied region (n = 4550) were examined. At each stable, all horses were inspected as part of a routine annual dental check-up, independent of oral health status. Owners provided written consent to the inclusion of their horses' data in the current study.

The prevalence of malocclusions and dental disease was considered with respect to three variables: age, gender, and breed. The horses were divided into four age groups: (i) 0–5 years old (n = 20; 9 geldings, 6 stallions, 5 mares), (ii) 6–10 years old (n = 75; 45 geldings, 4 stallions, 26 mares), (iii) 11–15 years old (n = 57; 30 geldings, 3 stallions, 24 mares), and (iv) > 15 years old (n = 54; 30 geldings, 1 stallion, 23 mares). Additionally, horses were assigned to one of two gender groups: males (n = 128; 114 geldings, 14 stallions) and females (n = 78; 78 mares). Finally, the horses, all from warm-blooded breeds, were divided into three sub-groups: (i) Polish warmblood (n = 109; 69 geldings, 4 stallions, 36 mares), (ii) pony (n = 40; 22 geldings, 3 stallions, 15 mares), and (iii) "other" (n = 57; 23 geldings, 7 stallions, 27 mares). The Polish warmblood group comprised four breeds: the Polish Halfbred (n = 73), the Wielkopolska (n = 10), the Malopolska (n = 17), and Schlesisches Warmblood (n = 9). The pony group included warm-blooded mixed-breed ponies (n = 27), Arabian horses (n = 5), Carpathian ponies (n = 4), Welsh ponies (n = 1), Welsh ponies (n = 2), and Halfinger ponies (n = 2). The "other" group included warm-blooded mix-breeds (n = 24), Thoroughbreds (n = 15), Spanish Warmbloods (n = 7), Dutch Warmbloods (n = 4), Hanoverians (n = 4), and Holsteiners (n = 3).

As the dental examinations were standard veterinary diagnostic procedures, no ethical approval was required.

2.2. Dental Examination

The veterinary diagnostic procedure began with a basic clinical examination. The internal temperature, heart rate, respiratory rate, mucous membrane color and moistness, capillary refill time, and lymph nodes were evaluated in accordance with international veterinary standards [36]. A detailed examination of the oral cavity was performed following the relevant professional guidelines [7,37,38].

In order to facilitate a complete oral, dental, and radiological examination, horses were sedated with detomidine hydrochloride (Domosedan; Orion Corporation, Espoo, Finland; 0.01 mg/kg bwt i.v.), xylazine hydrochloride (Xylapan; Vetoquinol Biowet Sp. Zo.o., Gorzów Wielkopolski, Poland; 0.4 mg/kg bwt i.v.), or a combination of both, with some requiring the additional of butorphanol tetrate (Torbugesic; Zoetis Polska Sp. z o.o., Warsaw, Poland; 0.01 mg/kg bwt i.v.). The dose and composition of the sedation was determined on the basis of the horse's body weight and temperament.

A detailed dental examination was performed using the following equipment: Haussmann's mouth speculum (to open the oral cavity for visual examination and digital palpation); a 400 mL syringe (to rinse the oral cavity with water and remove the remaining food); a headlamp (for illumination of the oral cavity during visual examination); a dental mirror (for more accurate observation of occlusal changes and for examination of the interdental spaces, the condition of the gums, and the mucosa of the cheeks and tongue, especially in the caudal part of the oral cavity); a periodontal probe (to examine the interdental spaces); and a dental hook (to examine the occlusal surfaces of the teeth) (Figure 1).

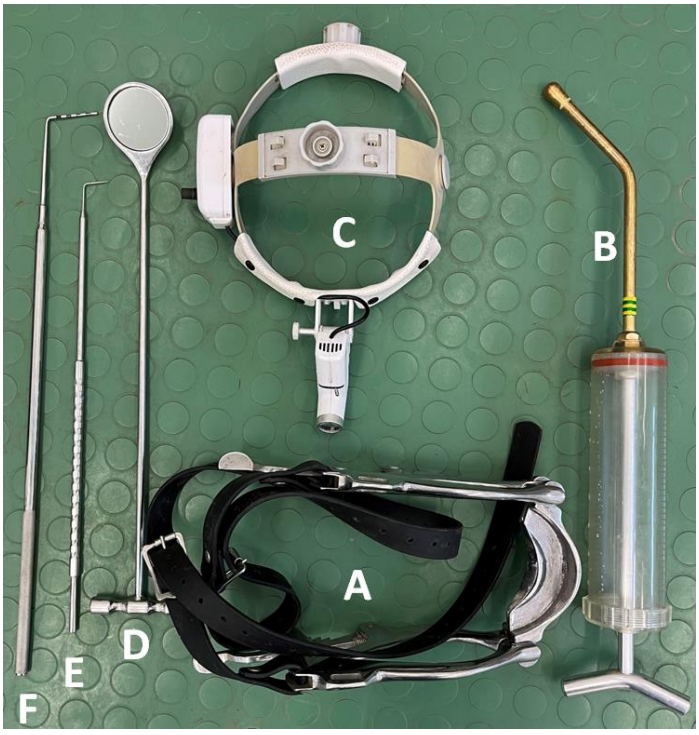

Figure 1. The equipment used in a detailed dental examination. Haussmann's mouth speculum (**A**); 400 mL syringe (**B**); headlamp (**C**); dental mirror (**D**); dental hook (**E**); and periodontal probe (**F**).

The detailed dental examination included both visual observation and digital palpation, and the findings were recorded using a dental chart presented in Supplementary Figure S1 and available online. The equine dental nomenclature was unified following the modified Triadan system [39]. In the maxilla, the right-hand quadrant was identified as

"1" and the left-hand quadrant as "2". Teeth were numbered consecutively beginning with 01 at the midline and proceeding distally. In the mandible, the left-hand quadrant was identified as "3" and the right-hand as "4", and the teeth were numbered as in the maxilla.

Oral cavity inspection began with a visual examination and digital palpation of the incisor teeth (upper right: 101, 102, 103; upper left: 201, 202, 203; lower left: 301, 302, 303; lower right: 401, 402, 403) [39]. The line created by the occlusal surfaces of the maxillary and mandibular incisors was evaluated. The occurrence of underbite or overbite, as well as ventral, dorsal, diagonal, or irregular curvature was noted. Missing or supernumerary teeth, retained milk teeth, and diastemata were marked. Additionally, indications of Equine Odontoclastic Tooth Resorption and Hypercementosis (EOTRH) syndrome, such as periodontal inflammation, gingivitis of different degrees and gingival recession, denuding of lamina dura dentis, deposition of tooth calculus, accumulation of food remains, tooth instability, dental abscesses, and periodontal fistulation were evaluated [34,37].

Next, visual examination and digital palpation of any canine teeth (upper right: 104; upper left: 204; lower left: 304; lower right: 404) [39] was performed. Calculus deposition and associated gingivitis, canine fracture, peripheral caries and non-erupted canines were considered [38].

Subsequently, the Hausmann speculum was utilized to open the oral cavity, which was then rinsed with plenty of water using a drencher. After rinsing, visual examination and digital palpation of the cheek teeth was performed, including: the vestigial first premolars (wolf teeth; upper right: 105; upper left: 205; lower left: 305; lower right: 405); premolar teeth (upper right: 106, 107, 108; upper left: 206, 207, 208; lower left: 306, 307, 308; lower right: 406, 407, 408), and molar teeth (upper right: 109, 110, 111; upper left: 209, 210, 211; lower left: 309, 310, 311; lower right: 409, 410, 411) [39]. A detailed assessment of the occlusal surface of the cheek teeth was facilitated by use of a dental mirror and the direct light of a headlamp. All tooth surfaces—buccal, palatine, lingual, labial, and occlusal [15]—were assessed. Diastema, retained milk teeth fragments, fractures, infandibulum and peripheral caries, calculus, gingivitis, gum recession and periodontal pockets, erosions, ulcers, as well as lacerations of the buccal or lingual mucous membrane were evaluated [40,41]. Moreover, the tongue was examined for signs of any possible inflammation or trauma, and oral mucous membranes were examined for signs of injuries such as ulcerations, buccal calluses (loss of superficial epithelium with evidence of necrosis or areas of mucosal epithelial hyperplasia) and/or lacerations (tears in the oral mucosa). Lingual scarring was defined as evidence of old lacerations or other healed tongue injuries with resultant scar tissue formation, e.g., due to inappropriate bits or use of tongue twitches [7].

2.3. Malocclusions and Dental Disease Classification

Based on the signs detected during the detailed dental examination, the following malocclusions (i) and dental diseases (ii) were diagnosed for the incisor, canine, wolf, premolar, and molar teeth, respectively (Figure 2). The definitions of selected disorders are summarized in Supplementary Tables S1–S4 available online.

For the incisor teeth, detected malocclusions (i) included the following: underbite, overbite, curvature (ventral, dorsal, slant, or irregular), diastema, oligodontia, polydontia, retained deciduous teeth (RDT), EOTRH, and hooks. In addition, dental diseases (ii) included the following: supernumerary teeth, loose teeth, fractures (marginal, transverse, sagittal, and undefined), caries (infundibular and peripheral), and calculus.

For the canine teeth, malocclusions (i) included non-erupted canines, and dental diseases (ii) included fractures (marginal, transverse, sagittal, and undefined) and calculus.

For the wolf teeth, malocclusions (i) included blind wolf teeth and dental disease (ii) included fractures.

The same malocclusions (i) and dental diseases (ii) are applicable to the premolar and molar teeth, and include the following: (i) sharp enamel points, overgrown teeth, wave mouth, step mouth, displaced teeth, diastema, oligodontia, polydontia, RDT, excessive

transverse ridges (ETR), and hooks; (ii) loose teeth, fractures (marginal, transverse, sagittal, and undefined), caries (infundibular and peripheral), and calculus.

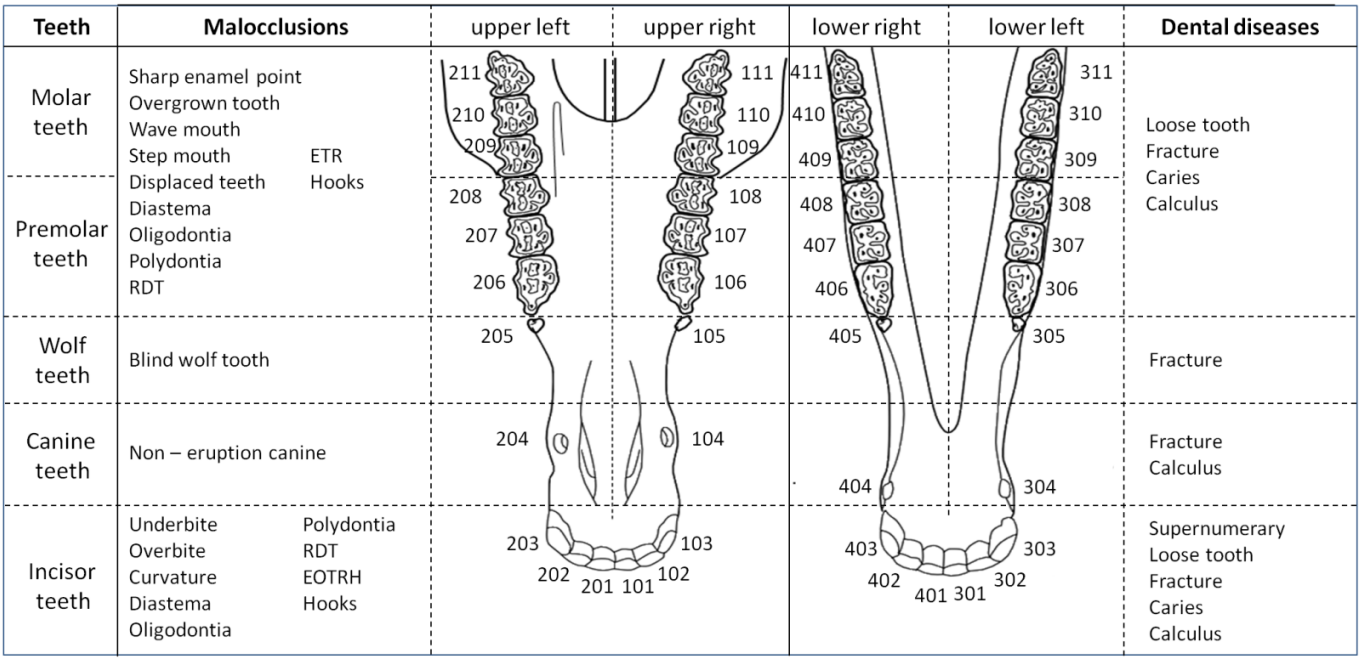

Figure 2. Classification of the malocclusions and dental diseases of the incisor (101, 102, 103, 201, 202, 203, 301, 302, 303, 401, 402, and 403); canine (104, 204, 304, and 404); wolf (105, 205, 305, and 405); premolar (106, 107, 108, 206, 207, 208, 306, 307, 308, 406, 407, and 408); and molar (109, 110, 111, 209, 210, 211, 309, 310, 311, 409, 410, and 411) teeth in horses. ETR—excessive transverse ridges; RDT—retained deciduous teeth; EOTRH—Equine Odontoclastic Tooth Resorption and Hypercementosis syndrome.

2.4. Statistical Analysis

The statistical analysis was conducted following the model used by Huang and Chen [42] to report the prevalence of signs of selected dental diseases in a limited population of people.

The prevalences of dental malocclusions and diseases were calculated for the population of studied horses as a whole, as well as for each sub-grouping according to age, gender, and breed. The data were evaluated by Chi-square analysis, where expected and observed values were entered as percentages representing malocclusions and dental disease distributions, respectively. The part of whole comparison was conducted twice, in relation to the whole horses' group and concerning the number of affected teeth. Differences were considered significant when $p < 0.05$.

The frequency distributions of teeth malocclusions and dental diseases were calculated for the studied horse population in its entirety as well as for each individual sub-grouping according to the variables of age, gender, and breed. For the calculation of frequency distribution, each horse was represented as one realization where values <0; 12> for incisor, premolar, and molar teeth, <0; 4> for canine teeth, and <0; 2> for wolf teeth were assigned to each malocclusion or dental disease for individual teeth. Thus, each realization ranged from 0 to 2, from 0 to 4, or from 0 to 12, where 0 meant no signs of malocclusion or dental disease and values > 0 indicated the presence of signs in individual teeth. Next the values for incisor, premolar, and molar teeth were compared using the Kruskal–Wallis test followed by Dunn's multiple comparisons test, as no Gaussian distributions of consecutive data series were demonstrated by the Shapiro–Wilk normality test. On the other hand, the of values for canine teeth dental diseases were compared using the Mann–Whitney test, as again, no Gaussian distributions of even one data series were demonstrated by the Shapiro–Wilk

normality test. The data were presented in tables with mean with the range, and various superscripts mark statistical differences. Differences among distributions of consecutive malocclusions or dental diseases were indicated with individual *p*-values when $p < 0.05$.

3. Results

3.1. The Total Prevalence of Malocclusions and Dental Diseases

A total of 7912 teeth were examined in this study (Table 1). The specimens consisted of 2444 incisor teeth, 2462 premolar teeth, and 2471 molar teeth, as oligodontia was noted in the case of 28 incisors, 10 premolars, and 3 molars. Moreover, polydontia was observed in the case of 2 molar teeth. Canine teeth were observed in male horses only, with 512 canine teeth examined in all. Finally, a total of 23 wolf teeth were seen in 16 horses.

Table 1. The prevalence of malocclusions and dental diseases in 7912 examined teeth of 206 horses.

Teeth	No. of Teeth	Teeth with Malocclusions	Teeth with Dental Diseases
Incisor	2444 (30.9)	2336 (29.5; 32.2)	89 (1.1; 34.8)
Canine	512 (6.5)	2 (0.03; 0.03)	88 (1.1; 34.4)
Wolf	23 (0.3)	6 (0.1; 0.1)	2 (0.03; 0.8)
Premolar	2462 (31.1)	2450 (31.0; 33.8)	27 (0.3; 10.5)
Molar	2471 (31.2)	2459 (31.1; 33.9)	50 (0.6; 19.5)
Total	7912	7253 (91.7; 100.0)	256 (3.2; 100.0)
Chi-square test		$p < 0.0001$; $p < 0.0001$	

Data are presented as n (% of all horses supported with *p* and % of horses in relation to the number of affected teeth supported with *p*). Differences were considered significant when $p < 0.05$.

At least one malocclusion was found in 2336 incisor teeth from a total of 191 horses, meaning only 9 horses were free of incisor malocclusions. Malocclusion of canine teeth was found in 2 teeth in 2 different horses, thus 126 male and all female horses were free from this condition. Malocclusion of wolf teeth was present in six teeth in four horses, so two two-sided conditions were noted. Only 1 horse lacked premolar malocclusions, with at least one premolar malocclusion detected each of the remaining 205 horses, affecting a combined total of 2450 teeth. Similarly, only 1 horse was free of molar malocclusions, while 205 horses exhibited molar malocclusions in a total of 2459 teeth. At least one malocclusion was found to affect 7253 teeth, which constitutes over 91.7% of all examined teeth.

Disease was observed in 89 incisor teeth in 17 horses, while 189 horses appeared to be free of incisor diseases. Diseases of canine teeth were found in 88 teeth in 44 horses, thus 84 male and all female horses were clear. Only two diseased wolf teeth were found in different horses. Diseases of premolar and molar teeth were present in 27 and 50 teeth in 20 and 33 horses, respectively, thus 186 and 173 horses were free of these conditions. In total, at least one disease was found in 256 teeth, which constitutes only 3.2% of all examined teeth. Thus, the prevalence of malocclusions was notably different than that of dental diseases. Among the studied population, the prevalence of dental malocclusions with the exception of those affecting canine teeth was higher than the prevalence of dental diseases ($p < 0.0001$). Concerning the number of affected teeth, dental diseases most often affected incisors (34.8%) and canines (34.4%), whereas malocclusions were most commonly observed in incisors (32.2%), premolars (33.8%), and molars (33.9%) ($p < 0.0001$) (Table 1).

3.2. The Age-Related Prevalence of Malocclusions and Dental Diseases

In the group of horses up to 5 years old, at least 1 malocclusion was found in 143 incisor teeth from 12 horses, thus 8 horses were free of incisor malocclusions. No malocclusions of canine teeth were seen. Malocclusions of wolf teeth were noted in two teeth in one horse. Malocclusions were noted in all 240 premolar and 240 molar teeth of all 20 horses. Dental disease affected only one wolf tooth, while all remaining incisor, canine, premolar, and molar teeth were free from clinical signs of disease.

In the group of horses between 6 and 10 years of age, at least one malocclusion was found in all incisor, premolar, and molar teeth, affecting 900, 899, and 900 teeth of 20 horses, respectively. Malocclusions were noted in one canine tooth in one horse and four wolf teeth in three horses. Dental diseases were noted in five incisor, one wolf, four premolar, and five molar teeth, in four, one, three, and four horses, respectively. Dental diseases of canine teeth were observed in 28 teeth in 14 horses.

Among horses between 11 and 15 years of age, of all incisor, premolar, and molar teeth, only one incisor showed no signs of malocclusion. Malocclusion was additionally found in one canine tooth. In the case of wolf teeth, no malocclusions or disease were noted. Dental diseases were observed in 17 incisors, 10 premolars, and 14 molars, in 6, 6, and 10 horses, respectively. Canine tooth disease was again common, appearing in 34 teeth in 17 horses.

In the oldest group of horses, those over 15 years of age, not all incisors, premolars, or molars were affected by malocclusions. However, only 610, 627, and 634 teeth of the respective type were affected in the case of 53 horses. No malocclusions were noted in canine or wolf teeth, and wolf teeth were additionally free of dental disease. Dental diseases were, however, evident in 67 incisor, 26 canine, 13 premolar, and 31 molar teeth, in 7, 18, 11, and 19 horses, respectively.

In total, malocclusions and dental diseases were seen in 625 teeth and 1 tooth in the youngest group, 2704 and 43 teeth in the young group, 2053 and 75 teeth in the old group, as well as 1871 and 137 teeth in the oldest group. The prevalence of malocclusions differed significantly from the prevalence of dental diseases across all four age groups. In all age groups, the prevalence of malocclusions was higher ($p < 0.0001$) for incisor, premolar, and molar teeth. Canine teeth were affected more often by dental diseases than malocclusions in the three groups of horses over 5 years old. Wolf teeth were affected more often by malocclusions than by dental diseases in the two groups of horses up to 10 years old, while in the older horses no sign of either ailment appeared. Dental diseases were most often related to canine teeth in horses between 6–10 years old (65.1%) and those between 11–15 years old (45.3%), whereas in the oldest group of horses, diseases of the incisors were the most frequently reported (48.9%), followed by the molars (22.6%), and then the canines (19.0%). Malocclusions were most often related to the incisor, premolar, and molar teeth in all examined age groups, ranging from 22.9% to 38.4% of all affected teeth in individual groups ($p < 0.0001$) (Table 2).

Table 2. The prevalence of malocclusions and dental diseases in 7912 examined teeth of 206 horses by horses' age (n = 20, 0–5 years; n = 75, 6–10 years; n = 57, 11–15 years; n = 54, > 15 years).

Age	Teeth	No. of Teeth	Teeth with Malocclusions	Teeth with Dental Diseases
0–5 years	Incisor	239 (3.0)	143 (1.8; 22.9)	0 (0; 0)
	Canine	60 (0.8)	0 (0; 0)	0 (0; 0)
	Wolf	5 (0.1)	2 (0.03; 0.3)	1 (0.01; 100.0)
	Premolar	240 (3.0)	240 (3.0; 38.4)	0 (0; 0)
	Molar	240 (3.0)	240 (3.0; 38.4)	0 (0; 0)
Total		784 (9.9)	625 (7.9)	1 (0.01)
Chi-square test			$p < 0.0001$; $p < 0.0001$	
6–10 years	Incisor	900 (11.4)	900 (11.4; 33.3)	5 (0.1; 11.6)
	Canine	196 (2.5)	1 (0.01; 0.04)	28 (0.35; 65.1)
	Wolf	12 (0.2)	4 (0.1; 0.1)	1 (0.01; 2.3)
	Premolar	899 (11.4)	899 (11.4; 33.2)	4 (0.05; 9.3)
	Molar	900 (11.4)	900 (11.4; 33.3)	5 (0.1; 11.6)
Total		2907 (36.7)	2704 (34.2)	43 (0.5)
Chi-square test			$p < 0.0001$; $p < 0.0001$	

Table 2. *Cont.*

Age	Teeth	No. of Teeth	Teeth with Malocclusions	Teeth with Dental Diseases
11–15 years	Incisor	684 (8.6)	683 (8.6; 33.3)	17 (0.2; 22.7)
	Canine	132 (1.7)	1 (0.01; 0.05)	34 (0.4; 45.3)
	Wolf	1 (0.01)	0 (0; 0)	0 (0; 0)
	Premolar	684 (8.6)	684 (8.6; 33.3)	10 (0.1; 13.3)
	Molar	685 (8.7)	685 (8.7; 33.4)	14 (0.2; 18.7)
Total		2185 (26.7)	2053 (25.9)	75 (0.9)
Chi-square test			$p < 0.0001$; $p < 0.0001$	
>15 years	Incisor	622 (7.9)	610 (7.7; 32.6)	67 (0.9; 48.9)
	Canine	124 (1.6)	0 (0; 0)	26 (0.3; 19.0)
	Wolf	5 (0.1)	0 (0; 0)	0 (0; 0)
	Premolar	639 (8.1)	627 (7.9; 33.5)	13 (0.2; 9.5)
	Molar	646 (8.2)	634 (8.0; 33.9)	31 (0.4; 22.6)
Total		2036 (25.7)	1871 (23.6)	137 (1.7)
Chi-square test			$p < 0.0001$; $p < 0.0001$	
Total		7912	7253 (91.7)	256 (3.2)

Data are presented as n (% of all horses supported with *p* and % of horses in relation to the number of affected teeth supported with *p*). Differences were considered significant when $p < 0.05$.

3.3. The Gender-Related Prevalence of Malocclusions and Dental Diseases

Among male horses, at least one malocclusion was found in 1449 incisor teeth from 122 horses, leaving only 6 male horses free of incisor malocclusion. Malocclusion of canine teeth was found in 2 teeth in 2 male horses, so the remaining 126 horses were free from this condition. Malocclusion was noted in six wolf teeth in four male horses. Only one male horse was free from malocclusions of premolar and molar teeth, with these conditions noted in 127 male horses in 1521 and 1525 teeth, respectively. Diseases of incisor teeth were observed in 45 incisors in 11 male horses, while 117 male horses remained unaffected. Diseases of canine teeth were noted in each of the previously reported horses. Disease was found in only one wolf tooth in one male horse. Diseases of premolar and molar teeth were noted in 16 and 24 teeth in 12 and 18 horses, respectively, thus 116 and 110 horses were free of cheek teeth diseases.

Among female horses, at least one malocclusion was found in 887 incisor teeth from 75 horses, so the incisors of 3 female horses were free of malocclusions. No malocclusions were found in canine or wolf teeth. All studied horses were affected with malocclusions of premolar and molar teeth, thus 929 and 934 affected teeth were noted, respectively. Dental diseases were noted in 44 incisors, 1 wolf tooth, 11 premolars, and 26 molars, in 6, 1, 8, and 16 female horses, respectively. In total, malocclusions were evident in 4503 teeth of male horses and 2750 of females, which constitutes 56.9% and 34.8% of all examined teeth. Dental diseases were noted in 174 and 80 teeth of the respective gender groups, corresponding to 2.2% and 1.0% of all examined teeth. The prevalence of malocclusions differed significantly from the prevalence of dental diseases in both male and female groups. In both gender groups, the prevalence of malocclusions was higher ($p < 0.0001$) for incisor, premolar, and molar teeth. The canine teeth in males were affected more often by dental diseases than by malocclusions, whereas in female horses, the presence of these teeth was not recorded. Concerning the distribution of the observed pathologies, dental diseases most often affected canines in male horses (50.6%) and incisors in females (53.7%), whereas malocclusions predominantly affected incisors (male: 32.2%; female: 32.3%), premolars (male: 33.8%; female: 33.8%), and molars (male: 33.9%; female: 34.0%) ($p < 0.0001$) (Table 3).

Table 3. The prevalence of malocclusions and dental diseases in 7912 examined teeth of 206 horses by horses' gender (n = 128, male; n = 78, female).

Gender	Teeth	No. of Teeth	Teeth with Malocclusions	Teeth with Dental Diseases
Male	Incisor	1521 (19.2)	1449 (18.3; 32.2)	45 (0.6; 25.9)
	Canine	512 (6.5)	2 (0.03; 0.04)	88 (1.1; 50.6)
	Wolf	14 (0.2)	6 (0.1; 0.1)	1 (0.01; 0.6)
	Premolar	1533 (19.4)	1521 (19.2; 33.8)	16 (0.2; 9.2)
	Molar	1537 (19.4)	1525 (19.3; 33.9)	24 (0.3; 13.8)
Total		5117 (64.7)	4503 (56.9)	174 (2.2)
Chi-square test			$p < 0.0001$; $p < 0.0001$	
Female	Incisor	923 (11.7)	887 (11.2; 32.3)	44 (0.6; 53.7)
	Canine	0 (0)	0 (0; 0)	0 (0; 0)
	Wolf	9 (0.1)	0 (0; 0)	1 (0.01; 1.2)
	Premolar	929 (11.7)	929 (11.7; 33.8)	11 (0.1; 13.4)
	Molar	934 (11.8)	934 (11.8; 34.0)	26 (0.3; 31.7)
Total		2795 (35.3)	2750 (34.8)	82 (1.0)
Chi-square test			$p < 0.0001$; $p < 0.0001$	
Total		7912	7253 (91.7)	256 (3.2)

Data are presented as n (% of all horses supported with p and % of horses in relation to the number of affected teeth supported with p). Differences were considered significant when $p < 0.05$.

3.4. The Breed-Related Prevalence of Malocclusions and Dental Diseases

Among Polish warmbloods, at least one malocclusion was found in 1270 incisor teeth from 108 horses, so only 1 horse was malocclusion free. No malocclusions of canine teeth were noted, and malocclusions of wolf teeth were observed in only four teeth in two horses. Malocclusions of premolars and molars were observed in all examined horses in this group, affecting 1304 and 1309 teeth, respectively. Disease was observed in 55 incisors in 11 horses and 70 canines in 38 horses, while 98 and 35 Polish warmbloods were unaffected. Only two wolf teeth in two horses were found to be diseased. Diseases of premolars and molars were noted in the case of 17 and 26 teeth in 17 and 26 horses, respectively, thus 95 and 90 horses were free of cheek teeth diseases.

In the group of ponies, at least one malocclusion was found in all incisor, premolar, and molar teeth, affecting 466, 464, and 467 teeth, respectively, in 39 horses. Thus, for each tooth type only one horse was malocclusion free. No malocclusions of canine teeth were noted, and malocclusions of wolf teeth were observed in only one tooth in one horse. Dental diseases were noted in 18 incisors, 8 canines, 6 premolars, and 12 molars, in 2, 4, 3, and 6 horses, respectively, whereas no dental disease was observed in wolf teeth.

In the group comprising "other" horse breeds, at least one malocclusion was found in 600 incisor teeth from 50 horses, with the incisors of 7 horses appearing malocclusion free. Malocclusions were noted in two canine teeth in two horses and one wolf tooth in one horse. All horses in this group were affected with premolar and molar malocclusions, thus 682 and 683 affected teeth were noted, respectively. Dental diseases were noted in 16 incisors, 10 canines, 4 premolars, and 12 molars, in 4, 4, 3, and 8 horses, respectively. No dental disease of wolf teeth was found in this group.

In total, malocclusions and dental diseases were evident in 3887 and 170 teeth of Polish warmblood horses, 1398 and 44 teeth of ponies, and in 1968 and 42 teeth "other" breeds. The prevalence of malocclusions and dental diseases differed significantly within the three breed-based groups. In all breed-related groups, the prevalence of malocclusions was higher ($p < 0.0001$) for incisor, wolf, premolar, and molar teeth. Similarly, in all breed-related groups, the prevalence of dental diseases was higher ($p < 0.0001$) for canine teeth. Concerning the number of affected teeth, malocclusions were most often related to the incisor, premolar, and molar teeth in the group of Polish warmblood horses (32.7%, 33.5%, and 33.7%), in the group of ponies (33.3%, 33.2%, and 33.4%), as well as in the group of

"other" breeds of horses (30.5%, 34.7%, and 34.7%). Dental diseases were most often related to canine teeth in the group of Polish warmblood horses (41.2%) and to incisor teeth in the groups of ponies (40.9%) and "other" breeds of horses (38.1%) ($p < 0.0001$) (Table 4).

Table 4. The prevalence of malocclusions and dental diseases in 7912 examined teeth of 206 horses by horses' breed ($n = 109$, Polish warmblood; $n = 40$, pony; $n = 57$, "other").

Breed	Teeth	No. of Teeth	Teeth with Malocclusions	Teeth with Dental Diseases
Polish warmblood	Incisor	1282 (16.2)	1270 (16.1; 32.7)	55 (0.7; 32.4)
	Canine	292 (3.7)	0 (0; 0)	70 (0.9; 41.2)
	Wolf	13 (0.2)	4 (0.1; 0.1)	2 (0.03; 1.2)
	Premolar	1304 (16.5)	1304 (16.5; 33.5)	17 (0.2; 10.0)
	Molar	1309 (16.5)	1309 (16.5; 33.7)	26 (0.3; 15.3)
Total		4200 (53.1)	3887 (49.1)	170 (2.1)
Chi-square test			$p < 0.0001$; $p < 0.0001$	
Pony	Incisor	478 (6.0)	466 (5.9; 33.3)	18 (0.2; 40.9)
	Canine	100 (1.3)	0 (0; 0)	8 (0.1; 18.2)
	Wolf	5 (0.1)	1 (0.01; 0.1)	0 (0; 0)
	Premolar	476 (6.0)	464 (5.9; 33.2)	6 (0.1; 13.6)
	Molar	479 (6.1)	467 (5.9; 33.4)	12 (0.2; 27.3)
Total		1538 (19.4)	1398 (17.7)	1494 (18.9)
Chi-square test			$p < 0.0001$; $p < 0.0001$	
"Other"	Incisor	684 (8.6)	600 (7.6; 30.5)	16 (0.2; 38.1)
	Canine	120 (1.5)	2 (0.01; 0.1)	10 (0.1; 23.8)
	Wolf	5 (0.1)	1 (0.01; 0.1)	0 (0; 0)
	Premolar	682 (8.6)	682 (8.6; 34.7)	4 (0.05; 9.5)
	Molar	683 (8.6)	683 (8.6; 34.7)	12 (0.2; 28.6)
Total		2174 (27.5)	1968 (24.9)	42 (0.5)
Chi-square test			$p < 0.0001$; $p < 0.0001$	
Total		7912	7253 (91.7)	256 (3.2)

Data are presented as n (% of all horses supported with p and % of horses in relation to the number of affected teeth supported with p). Differences were considered significant when $p < 0.05$.

3.5. The Frequency Distribution of Malocclusions and Dental Diseases of the Incisor Teeth

The curvature occurred with a significantly higher frequency than did other malocclusions of the incisor teeth, regardless of the studied group ($p < 0.0001$). One may observe that in all incisor teeth no polydontia appeared. Moreover, no overbite, diastema, EOTRH, or hooks were found in the youngest group of horses, those up to 5 years old. In the group of young horses between 6 and 10 years of age, no oligodontia or EOTRH were noted. In the groups of horses between 11–15 years old and those over 15 years of age, no underbite, diastema, or RDT were observed. In the gender-based groups, while polydontia was absent among both males and females, the female group also lacked signs of diastema. Similarly, in the breed-based groups, no diastema was noted in Polish warmblood horses. Among the ponies, no hooks were observed, while in the group of "other" breeds, no underbite, diastema, oligodontia, or RDT were recognized. No significant differences were found among the distributions of the remaining malocclusions (Table 5; Figure 3).

Table 5. The frequency distribution of malocclusions of incisor teeth in the total 7912 examined teeth of 206 horses.

	Underbite	Overbite	Curvature	Diastema	Oligodontia	Polydontia	RDT	EOTRH	Hooks	*p*
Total	0.12 (12) a	1.17 (12) a	11.29 (12) b	0.01 (2) a	0.14 (12) a	0 (0) a	0.01 (1) a	0.87 (12) a	0.02 (2) a	<0.0001
0–5 years	0.60 (12) a	0 (0) a	7.15 (12) b	0 (0) a	0.05 (1) a	0 (0) a	0.05 (1) a	0 (0) a	0 (0) a	<0.0001
6–10 years	0.16 (12) a	1.76 (12) a	12.00 (12) b	0.01 (1) a	0 (0) a	0 (0) a	0.01 (1) a	0 (0) a	0.01(1) a	<0.0001
11–15 years	0 (0) a	1.05 (12) a	12.00 (12) b	0 (0) a	0.02 (1) a	0 (0) a	0 (0) a	0.21 (12) a	0.04(2) a	<0.0001
>15 years	0 (0) a	0.89 (12) a	11.09 (12) b	0 (0) a	0.48 (12) a	0 (0) a	0 (0) a	3.11 (12) a	0.04 (2) a	<0.0001
Male	0.09 (12) a	1.41 (12) a	11.33 (12) b	0.01 (1) a	0.12 (12) a	0 (0) a	0.02 (1) a	1.03 (12) a	0.02 (2) a	<0.0001
Female	0.15 (12) a	0.77 (12) a	11.23 (12) b	0 (0) a	0.17 (12) a	0 (0) a	0 (0) a	0.62 (12) a	0.03 (2) a	<0.0001
PWB	0.11 (12) a	1.21 (12) a	11.55 (12) b	0 (0) a	0.24 (12) a	0 (0) a	0.01 (12) a	1.21 (1) a	0.03(2) a	<0.0001
Pony	0.30 (12) a	0.90 (12) a	11.68 (12) b	0.03 (1) a	0.05 (1) a	0 (0) a	0.03 (1) a	0.60 (12) a	0 (0) a	<0.0001
"Other"	0 (0) a	1.26 (12) a	10.53 (12) b	0 (0) a	0 (0) a	0 (0) a	0 (0) a	0.42 (12) a	0.04 (2) a	<0.0001

Data are presented as mean (with the range). Different letters in consecutive cells were statistically different when $p < 0.05$. PWB—Polish warmblood; RDT—retained deciduous teeth; EOTRH—Equine Odontoclastic Tooth Resorption and Hypercementosis syndrome.

Figure 3. The samples of the malocclusions of the incisor teeth in horses. Underbite (**A**); overbite (**B**); curvature (**C**); diastema (**D**); oligodontia (**E**); polydontia (**F**); retained deciduous teeth (RDT) (**G**); the Equine Odontoclastic Tooth Resorption and Hypercementosis (EOTRH) syndrome (**H**); and hooks (**I**).

Calculus occurred with a significantly higher frequency than other dental diseases of the incisor teeth in the groups of all studied horses ($p = 0.0007$), the oldest horses ($p = 0.0005$), the male horses ($p = 0.021$), and the Polish warmblood horses ($p = 0.009$), but not in the remaining sub-groups. No supernumerary incisor teeth appeared in any group. Moreover, no dental diseases were found in the group of the youngest horses up to 5 years old. No loose teeth were noted in groups of horses between 6–10 years old or 11–15 years

old, or in male horses, ponies, or "other" breeds. Additionally, no fractures were found in groups of horses over 15 years old, in ponies, or in "other" breeds. Finally, no caries was observed in horses between 11–15 years old or older in female horses, Polish warmbloods, or ponies. No significant differences were found among the distributions of the remaining malocclusions (Table 6; Figure 4).

Table 6. The frequency distribution of dental diseases of incisor teeth in the total 7912 examined teeth of 206 horses.

	Supernumerary	Loose Teeth	Fractures	Caries	Calculus	*p*
Total	0 (0) a	0.001 (1) a	0.02 (1) a	0.01 (1) a	0.40 (12) b	0.0007
0–5 years	0 (0)	0 (0)	0 (0)	0 (0)	0 (0)	nc
6–10 years	0 (0) a	0 (0) a	0.01 (1) a	0.03 (1) a	0.03 (2) a	0.476
11–15 years	0 (0) a	0 (0) a	0.05 (1) a	0 (0) a	0.25 (6) a	0.057
>15 years	0 (0) a	0.02 (1) a	0 (0) a	0 (0) a	1.22 (12) b	0.0005
Male	0 (0) a	0 (0) a	0.02 (1) ab	0.02 (1) ab	0.31 (12) b	0.021
Female	0 (0) a	0.01 (1) a	0.01 (1) a	0 (0) a	0.54 (12) a	0.056
PWB	0 (0) a	0.01 (1) ab	0.01 (1) ab	0 (0) a	0.46 (12) b	0.009
Pony	0 (0) a	0 (0) a	0 (0) a	0 (0) a	0.45 (12) a	0.090
"Other"	0 (0) a	0 (0) a	0 (0) a	0.04 (1) a	0.25 (12) a	0.194

Data are presented as mean (with the range). Different letters in consecutive cells were statistically different when $p < 0.05$; nc—not calculable; PWB—Polish warmblood.

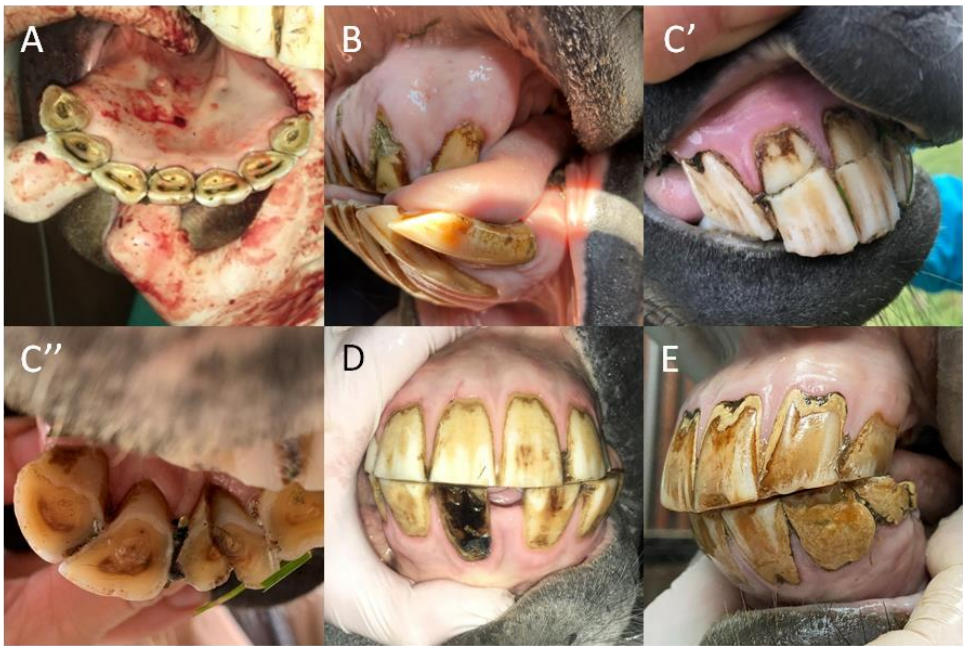

Figure 4. The samples of the dental diseases of the incisor teeth in horses. Supernumerary (**A**); loose teeth (**B**); fractures ((**C**): transverse fracture, (**C'**); sagittal fracture, (**C''**)); caries (**D**); and calculus (**E**).

3.6. The Frequency Distribution of Malocclusions and Dental Diseases of Canine and Wolf Teeth

Regarding malocclusions, non-erupted canines occurred in groups of horses between 6 and 10 years old, and 11 and 15 years old, in male horses, and in "other" breeds, whereas blind wolf teeth occurred in groups of horses 0–5 years old, between 6–10 years-old, in male horses, and in all studied breeds. With respect to dental diseases, fractures of canine teeth did not appear in horses 0–5 years of age or 6–10 years of age in either gender group, or among Polish warmbloods. Moreover, calculus of the canines did not occur in the youngest

group up to 5 years old or in female horses (in whom canines were absent altogether). In all other groups, calculus appeared more frequently than fractures (Table 7; Figure 5).

Table 7. The frequency distribution of malocclusions and dental diseases of canine * and wolf ** teeth in the total 7912 examined teeth of 206 horses.

	Non-Erupted Canines *	Blind Wolf Tooth **	Fractures *	Calculus *	*p*	Fractures **
Total	0.01 (1)	0.03 (2)	0 (0) a	0.43 (2) b	<0.0001	0.01 (1)
0–5 years	0 (0)	0.10 (2)	0 (0)	0 (0)	nc	0.05 (1)
6–10 years	0.01 (1)	0.05 (2)	0 (0) a	0.37 (2) b	<0.0001	0.01 (1)
11–15 years	0.02 (1)	0 (0)	0 (0) a	0.60 (2) b	<0.0001	0 (0)
>15 years	0 (0)	0 (0)	0 (0) a	0.48 (2) b	<0.0001	0 (0)
Male	0.02 (1)	0.05 (2)	0 (0) a	0.69 (2) b	<0.0001	0.01 (1)
Female	0 (0)	0 (0)	0 (0)	0 (0)	nc	0.02 (1)
PWB	0 (0)	0.04 (2)	0 (0) a	0.64 (2) b	<0.0001	0.02 (1)
Pony	0 (0)	0.03 (1)	0 (0) a	0.20 (2) a	0.116	0 (0)
"Other"	0.04 (1)	0.02 (1)	0 (0) a	0.17 (2) a	0.057	0 (0)

Data are presented as mean (with the range). Different letters in consecutive cells were statistically different when $p < 0.05$; nc—not calculable; PWB—Polish warmblood.

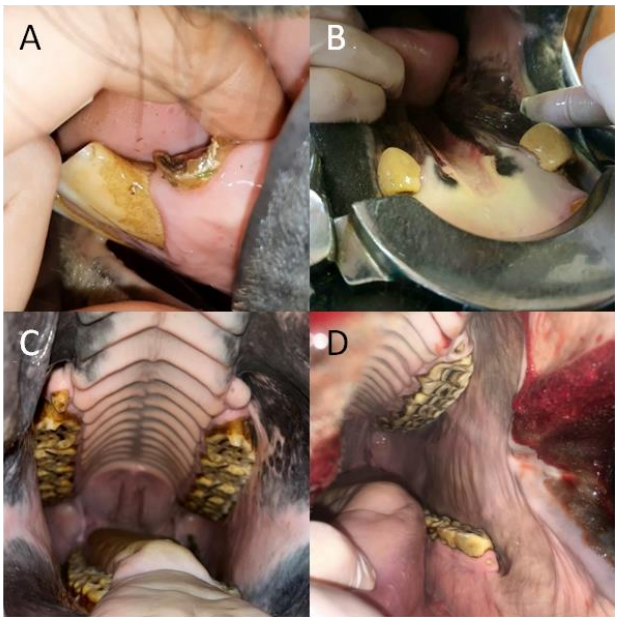

Figure 5. The samples of the malocclusions and dental diseases of the canine and wolf teeth in horses. For the canine teeth: fractures (**A**) and calculus (**B**). For the wolf teeth: blind wolf tooth (**C**) and fractures (**D**).

3.7. The Frequency Distribution of Malocclusions and Dental Diseases of Cheek Teeth

Sharp enamel points occurred with a significantly higher frequency than other malocclusions of the premolar and molar teeth, irrespective of the studied group ($p < 0.0001$). No polydontia of the premolars appeared in any group, and no molars affected by RDT occurred. The remaining malocclusions occurred in both premolar and molar teeth with varying frequency among for the studied groups. In the youngest horses up to 5 years old, overgrown and displaced teeth, RDT, and ETR were found to affect premolar teeth, while only ETR and hooks appeared to affect molars. Regarding premolar teeth, the same malocclusions (overgrown tooth, wave mouth, diastema, ETR, and hooks) were noted in groups of horses 6–10 and 11–15 years old, except for oligodontia, which only appeared in the group of 6–10 years old (Table 8; Figure 6).

Figure 6. The samples of the malocclusions of the premolar and molar teeth in horses. Sharp enamel points (**A**); overgrown tooth (**B**); wave mouth (**C**); step mouth (**D**); displaced teeth (**E**); diastema (**F**); oligodontia (**G**); polydontia (**H**); retained deciduous teeth (RDT) (**I**); excessive transverse ridges (ETR) (**J**); and hooks (**K'**,**K"**).

Similarly, regarding molar teeth, in groups of horses between 6–10 and 11–15 years old, the same malocclusions (overgrown teeth, wave mouth, displaced teeth, diastema, ETR, and hooks) were observed, with the exception of polydontia, which only appeared in horses 11–15 years old. In the group of the oldest horses, those over 15 years of age, all malocclusions were recognized, except for premolar polydontia and RDT and molar RDT. In the gender-based groups, in addition to the lack of either premolar polydontia or molar RDT, there were no signs of premolar step mouth or RDT females. Moreover, no signs of molar oligodontia were seen in males or molar step mouth in females. Similarly, in the breed-related groups, except for lack of premolar polydontia and molar RDT, all other premolar and molar malocclusions were noted among Polish warmbloods. Among the ponies, no premolar step mouth, displaced teeth, RDT, or ETR were observed, and none had molar step mouth, polydontia, or ETR. Finally, in the group of "other" breeds, no premolar or molar step mouth, polydontia, or RDT were recognized (Table 9).

Table 8. The frequency distribution of malocclusions of premolar teeth in the total 7912 examined teeth of 206 horses.

	Sharp e.	Overgrown t.	Wave m.	Step m.	Displaced t.	Diastema	Oligodontia	Polydontia	RDT	ETR	Hooks	*p*
Total	11.90(12) a	0.68 (12) b	0.52 (12) c	0.06 (12) c	0.02 (2) c	0.15 (2) bc	0.05 (4) c	0 (0) c	0.01(2) c	0.58 (12) bc	0.19 (2) b	<0.0001
0–5 years	12.00 (12) a	0.30 (2) b	0 (0) b	0 (0) b	0.20(2) b	0 (0) b	0 (0) b	0 (0) b	0.10(2) b	0.60(12) b	0 (0) b	<0.0001
6–10 years	12.00 (12) a	0.53 (4) b	0.31 (12) c	0 (0) c	0 (0) c	0.08 (2) bc	0.01(1) c	0 (0) c	0 (0) c	0.96 (12) bc	0.20 (2) bc	<0.0001
11–15 years	12.00 (12) a	0.93 (12) b	0.21(12) c	0 (0) c	0 (0) c	0.09 (2) c	0 (0) c	0 (0) c	0 (0) c	0.21(12) c	0.21(2) c	<0.0001
>15 years	11.61 (12) a	0.78 (4) b	1.33 (12) bc	0.22 (12) c	0.02 (1) c	0.35 (2) bc	0.17 (4) bc	0 (0) c	0 (0) c	0.44 (12) bc	0.22 (2) bc	<0.0001
Male	11.89 (12) a	0.63 (4) b	0.37 (12) c	0.09 (12) c	0.03 (2) c	0.13 (2) c	0.02 (1) c	0 (0) c	0.02 (2) c	0.56 (12) c	0.18 (2) c	<0.0001
Female	11.91 (12) a	0.77 (12) b	0.77 (12) bc	0 (0) c	0.01 (1) c	0.18 (2) bc	0.09 (4) c	0 (0) c	0 (0) c	0.62(12) c	0.21 (2) bc	<0.0001
PWB	11.98 (12) a	0.68(4) b	0.55 (12) c	0.09 (12) c	0.02 (2) c	0.18 (2) c	0.03 (1) c	0 (0) c	0.03 (2) c	0.38 (12) c	0.19 (2) c	<0.0001
Pony	11.60 (12) a	0.73 (4) b	0.30 (12) c	0 (0) c	0 (0) c	0.05 (1) c	0.10 (4) c	0 (0) c	0 (0) c	0 (0) c	0.13 (2) bc	<0.0001
"Other"	11.96 (12) a	0.68 (12) b	0.63 (12) b	0 (0) b	0.05 (2) b	0.09 (2) b	0.04 (2) b	0 (0) b	0 (0) b	1.47 (12) b	0.18 (2) b	<0.0001

Data are presented as mean (with the range). Different letters in consecutive cells were statistically different when $p < 0.05$. PWB—Polish warmblood; sharp e.—sharp enamel points; overgrown t.—overgrown tooth; wave m.—wave mouth; step m.—step mouth; displaced t.—displaced teeth; RDT—retained deciduous teeth; ETR—excessive transverse ridges.

Table 9. The frequency distribution of malocclusions of molar teeth in the total 7912 examined teeth of 206 horses.

	Sharp e.	Overgrown t.	Wave m.	Step m.	Displaced t.	Diastema	Oligodontia	Polydontia	RDT	ETR	Hooks	*p*
Total	11.93 (12) a	0.19 (4) b	0.53 (12) b	0.06 (12) b	0.03 (2) b	0.05 (2) b	0.01 (1) b	0.01(1) b	0(0) b	0.58(12) b	0.32(2) b	<0.0001
0–5 years	12 (12) a	0 (0) b	0 (0) b	0 (0) b	0 (0) b	0 (0) b	0 (0) b	0 (0) b	0 (0) b	0.60 (12) b	0.10 (2) b	<0.0001
6–10 years	12.00 (12) a	0.11 (2) b	0.32 (12) b	0 (0) b	0.01 (1) b	0.01 (1) b	0 (0) b	0 (0) b	0 (0) b	0.96 (12) b	0.28(2) b	<0.0001
11–15 years	12.00 (12) a	0.21 (2) b	0.21 (12) b	0 (0) b	0.09 (2) b	0.04 (2) b	0 (0) b	0.02 (1) b	0 (0) b	0.21 (12) b	0.21 (2) b	<0.0001
>15 years	11.72 (12) a	0.35 (4) b	1.37 (12) b	0.23 (12) b	0.02 (1) b	0.13 (2) b	0.06 (1) b	0.02 (1) b	0 (0) b	0.44 (12) bc	0.56 (2) c	<0.0001
Male	11.91 (12) a	0.23 (4) b	0.38 (12) b	0.09 (12) b	0.03 (2) b	0.05 (2) b	0 (0) b	0.01 (1) b	0 (0) b	0.56 (12) b	0.29 (2) b	<0.0001
Female	11.96 (12) a	0.12 (2) b	0.79 (12) b	0 (0) b	0.04 (2) b	0.05 (2) b	0.04 (1) b	0.01 (1) b	0(0) b	0.62 (12) b	0.36 (2) b	<0.0001
PWB	11.99 (12) a	0.24 (4) bc	0.57 (12) bc	0.11 (12) b	0.02 (2) b	0.06 (2) bc	0.01 (1) b	0.02 (1) b	0(0) b	0.33 (12) bc	0.33 (2) c	<0.0001
Pony	11.68 (12) a	0.13 (2) b	0.30 (12) b	0(0) b	0.10 (2) b	0.05 (1) b	0.03 (1) b	0(0) b	0(0) b	0(0) b	0.18 (2) b	<0.0001
"Other"	11.98 (12) a	0.14 (2) b	0.63 (12) b	0(0) b	0.02 (1) b	0.02 (1) b	0.02 (1) b	0(0) b	0(0) b	1.47 (12) b	0.39 (2) b	<0.0001

Data are presented as mean (with the range). Different letters in consecutive cells were statistically different when $p < 0.05$. PWB—Polish warmblood; sharp e.—sharp enamel points; overgrown t.—overgrown tooth; wave m.—wave mouth; step m.—step mouth; displaced t.—displaced teeth; RDT—retained deciduous teeth; ETR—excessive transverse ridges.

In all studied horses, dental diseases occurred with the same frequency distribution in premolar teeth ($p = 0.059$), whereas in molar teeth, caries occurred with a significantly higher frequency than loose teeth or calculus ($p < 0.0001$). Concerning premolars among sub-groups, caries was noted with a higher frequency than other dental diseases in horses 6–10 years old ($p = 0.028$), as well as with a higher frequency than calculus in horses over 15 years of age ($p = 0.036$). Concerning molar teeth among the sub-groups, caries was recognized with a higher frequency than other dental diseases in horses 11–15 years old ($p = 0.004$), in male horses ($p = 0.002$), and in Polish warmbloods ($p < 0.0001$), as well as with a higher frequency than calculus in horses over 15 years of age ($p = 0.003$) and in female horses ($p = 0.028$). In the case of cheek teeth, no calculus was observed. Moreover, no dental diseases were found in the cheek teeth of horses up to 5 years old. In addition to a lack of calculus, no loose premolars were noted in horses 6–10 years old or 11–15 years old. Similarly, no loose molars were observed in the horses from the "other" breeds group. Additionally, no premolar fractures were recognized in horses 6–10 years old, in ponies, or in the "other" breeds (Table 10; Figure 7).

Table 10. The frequency distribution of dental diseases of premolar * and molar ** teeth in the total 7912 examined teeth of 206 horses.

	Loose t. *	Fractures *	Caries *	Calculus *	*p*	Loose t. **	Fractures **	Caries **	Calculus **	*p*
Total	0.04 (2) a	0.02 (1) a	0.07 (2) a	0 (0) a	0.059	0.04 (5) a	0.06 (2) ab	0.14 (2) b	0 (0) a	<0.0001
0–5 years	0 (0)	0 (0)	0 (0)	0 (0)	nc	0 (0)	0 (0)	0 (0)	0 (0)	nc
6–10 years	0 (0) a	0 (0) a	0.05 (2) b	0 (0) a	0.028	0 (0) a	0.03 (1) a	0.04 (2) a	0 (0) a	0. 257
11–15 years	0.02 (1) a	0.02 (1) a	0.14 (2) a	0 (0) a	0.098	0 (0) a	0.09 (2) ab	0.16 (2) b	0 (0) a	0.004
>15 years	0.13 (2) a	0.07 (1) ab	0.04 (2) a	0 (0) b	0.036	0.17 (5) ab	0.11 (2) ab	0.30 (2) a	0 (0) b	0.003
Male	0.03 (1) a	0.02 (1) a	0.07 (2) a	0 (0) a	0.185	0.02 (1) a	0.04 (2) a	0.14 (2) b	0 (0) a	0.0002
Female	0.05 (2) a	0.03 (1) a	0.06 (2) a	0 (0) a	0.378	0.09 (5) ab	0.10 (2) ab	0.14 (2) a	0 (0) b	0.028
PWB	0.05 (1) a	0.05 (1) a	0.06 (2) a	0 (0) a	0.175	0.03 (1) a	0.04 (2) a	0.17 (2) b	0 (0) a	<0.0001
Pony	0.05 (2) a	0 (0) a	0.10 (2) a	0 (0) a	0.294	0.15 (5) a	0.05 (1) a	0.10 (2) a	0 (0) a	0.559
"Other"	0.02 (1) a	0 (0) a	0.05 (2) a	0 (0) a	0.294	0 (0) a	0.12 (2) a	0.08 (2) a	0 (0) a	0.051

Data are presented as mean (with the range). Different letters in consecutive cells were statistically different when $p < 0.05$. PWB—Polish warmblood. Different superscripts in consecutive cells were statistically different. Loose t.—loose teeth; nc—not calculable.

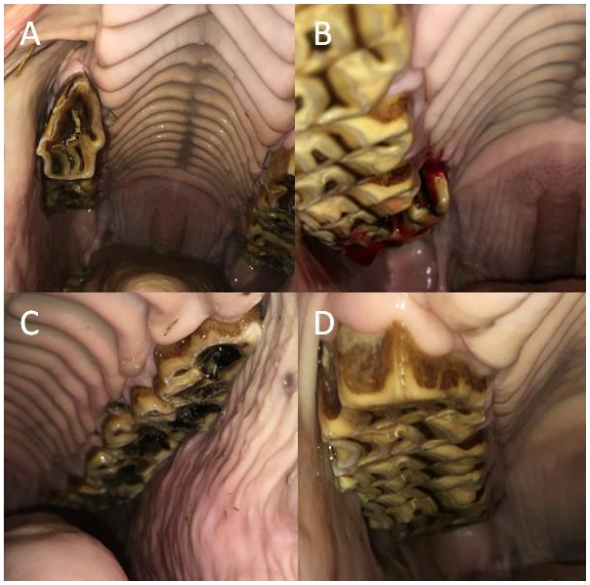

Figure 7. The samples of the dental diseases of the premolar and molar teeth in horses. Loose teeth (**A**); fractures (**B**); caries (**C**); and calculus (**D**).

4. Discussion

To the best of our knowledge, the current paper presents for the first time a descriptive study of the prevalence and frequency distribution of malocclusions and dental diseases of all types of teeth in a select population of horses housed in the Mazovia region of Poland. As horse populations differ among countries and regions, a specific characterization of dental disorder occurrence may be helpful for local equine practitioners. In the current study, 31% of examined horses presented with dental disorders in the area of the incisor teeth, which is less than the previously reported 53% of Polish horses [16]. No data regarding the prevalence of dental disorders of the cheek teeth have been previously reported in Poland. However, 70% of examined horses in Canada [12] and 87% in Australia [15] demonstrated dental disorders in the area of the cheek, which is more than the 62% reported herein. In the current study, dental disorders occurred in at least one tooth in 95% of examined horses, which is close to the prevalence reported in Australia (94%) [15] and Scotland (87%) [14], and higher than the prevalence reported in the USA (80%) [11] and UK (from 79% [3] to 42% [13]). Given the variability in the reported prevalence in a single geographic location such as the UK, other factors such as the dental examination protocol, equipment, and type of study design employed should be taken into consideration as the cause of variability in the incidence of malocclusions and dental disease.

Regardless of the study group, malocclusions of incisor, premolar, and molar teeth occurred with a higher prevalence than did dental diseases. As previously referenced authors [3,11,13–16] did not differentiate dental problems into malocclusions and dental diseases, the findings of the current study provide valuable clinical evidence justifying the need for periodic dental examination of horses. In many cases, malocclusions can be corrected using simple procedures, and this can prevent the development and consequences of very advanced disorders including dental diseases [43]. Some congenital disorders, such as underbite and overbite, which are easily diagnosed in young foals, can be corrected early [43,44], preventing the development of further dental disorders. Moreover, the event of underbite or overbite or conformational variations in the cheek teeth may also occur, which may result in the possible formation of hooks of the maxillar or mandibular teeth [31]. This is consistent with the current observation that no dental diseases were noted in the youngest age group. Notably, the prevalence of dental diseases, but not malocclusions, increased with age. Given that some dental disorders, especially dental diseases, are common to geriatric horses, educating older horse owners and recommending prophylactic dental treatments for this age group are key to minimizing the impact of debilitating dental disease [45]. Interestingly, the prevalence of incisor and cheek teeth malocclusions was similar across divisions in both gender-based and in breed-based groups when the percentage of horses was considered in relation to the number of affected teeth in each group. In contrast, the prevalence of both malocclusions and dental diseases of canine and wolf teeth was higher in the male than female group, as no canine teeth were present in mares [39].

Regarding the distribution of specific malocclusions for each tooth, curvatures most frequently affected incisor teeth while sharp enamel points plagued cheek teeth. In the case of incisor teeth, the line created by the occlusal surfaces between the maxillary and mandibular incisors should lie on the horizontal plane, and any deviation thereof, be it ventral, dorsal, diagonal, or irregular, constitutes an abnormality [46]. In the current study, ventral curvature was found in 157 horses. Irregular curvature and diagonal bite were found in 21 and 10 horses respectively, whereas dorsal curvature was not observed. Depending on recent reports, ventral curvature may be considered an acquired, age-related disorder, probably secondary to cheek teeth disorders [46] or correct conformation [9]. However, regardless of this characterization, the gradual correction of ventral curvature is recommended to restore the correct conformation of the incisors, thus avoiding the development of an abnormal occlusal surface [46], which may affect the horse's chewing ability [47]. In the current study, sharp edges were found in 204 horses on the buccal surface of the maxillary cheek teeth and the lingual surface of the mandibular cheek teeth, posing

a risk to the cheek or tongue mucosa, respectively. The extent of the mucosal damage at the site of irritation may involve its partial destruction (i.e., erosion) or damage to the full thickness of the mucosa (i.e., ulceration). In extreme cases, laceration may occur, involving complete rupture of the mucosa over a considerable length. As a result of long-term irritation to the mucosa, buccal calluses may form. In such cases, there is loss of superficial epithelium together with necrotic signs or areas of excessive mucosal epithelial growth [7]. The anatomical arrangement of the teeth in the lower and upper dental arches is such that the curvature of the upper arch does not fully match that of the lower arch, the lower arch is straighter, and the distance between the right and the left arch is smaller in the mandible in comparison to the maxilla [48]. Furthermore, the cheek teeth of the mandible are physiologically narrower than their antagonists in the maxilla. This arrangement of the teeth and their anatomical dependence on each other causes uneven abrasion of the occlusal surfaces, predisposing to the formation of sharp points on the buccal edges of the maxillary cheek teeth and the lingual edges of the mandibular cheek teeth, which in turn leads to mechanical damage to the cheek mucosa or the tongue [49,50].

With respect to the distribution of specific dental diseases for each tooth, calculus was most frequently observed on incisor teeth and caries in cheek teeth. Calculus, the accumulation of tartar, occurs as a result of the mineralization of the bacterial plaque flora on the teeth [51]. The canine and incisor teeth of the mandible are most frequently predisposed to calculus deposition [51], which is in line with the observations in the present study. On the other hand, maxillary cheek teeth are most frequently predisposed to caries, as each maxillary cheek tooth contains two semicircular funnel-like infundibula filled with cementum [51]. In the current study, infundibular caries was found in 26 horses, most often in the first molars. However, the grading of caries was not investigated in this study. Clinically, a 4-grade scale of infundibular caries advancement is used to describe the process and the structures involved. In grade 1, only the cementum is affected. In grade 2, the cementum and adjacent enamel are affected. In grade 3, the cementum, enamel, and dentin are affected. In grade 4, the integrity of the tooth is affected [46]. In many cases, the presence of infundibular caries mechanically weakens the clinical crown of the cheek tooth and thus predisposes to increased wear. Consequently, the opposing mandibular tooth tends to protrude excessively [47]. Advanced infundibular caries of the maxillary cheek teeth often predisposes to midline sagittal fractures and apical infection [52,53].

Interestingly, the frequency distribution of a few dental disorders seems to be age-related, rather than gender- or breed-related. The exceptions were non-erupted canines, blind wolf teeth, fractures of canine and wolf teeth, and calculus of canine teeth, which, due to the gender-dependent occurrence of canine and to some extent wolf teeth [39], were found in males and not in females. In the case of incisor teeth, EOTRH and calculus did not appear in horses up to 5 years old but appeared frequently in horses over 15 years of age. The current observations are in line with the previous study on age predilection in the occurrence of both malocclusion [54] and disease [51]. The age-related risk of EOTRH occurrence was confirmed in a subsequent study [34,55]. In the case of cheek teeth, wave mouth, step mouth, fractures, and caries were absent in horses up to 5 years of age but appeared frequently in horses over 15 years old. The etiology of wave mouth is unclear, but an age-related component has been postulated [14]. The eruption of a horse's cheek teeth depends on the continuous relaxation and contraction of the periodontal fibers. During periodontal disease and aging, subsequent fiber loss may delay the eruption of affected teeth and thus lead to the formation of a wave mouth [14]. On the other hand, a step mouth is an abnormal bite, which most often appears as a result of the overgrowth of a cheek tooth due to the lack or fracture of its antagonist [56,57]. Therefore, an increased occurrence of check teeth fractures may predispose to step mouth [14,58], which is in keeping with the current observations.

Limitations

In this study, the reader's attention should be paid to several limitations that should be taken into account when assessing the value of the presented results. As indicated at the beginning of the discussion section, the horse populations as well as the occurrence of dental disorders differ among countries and regions [3,11–16]. One should note that this paper presents a descriptive study of the prevalence and frequency distribution of dental disorders in a select population of horses housed in the Mazovia region of Poland. Thus, the presented results are of much greater local importance, especially for local equine practitioners, than of general relevance.

Moreover, this study was conducted on a specific and restricted population, not on a region-wide reference population of local horses as assumed in population screening. In recent studies, two methods have been used to obtain data on the occurrence of dental disorder in horse populations. The first approach involves screening horses' teeth at slaughter [5,6], while the second involves screening horses' teeth during annual routine examination of the oral cavity [2–4]. Post mortem examinations of equine heads obtained from slaughterhouses [5,6,8–10] evaluate sample groups that may be considered representative of the larger study population, whereas routine examinations of live horses [2–4,7] satisfy the criteria of descriptive studies. Each method of study group selections has its own limitations. The use of horse heads obtained from slaughterhouses is constrained by the limited availability of sensitive data. Slaughterhouses in Poland are not legally permitted to provide private information, even for scientific purposes, regarding the origin, pedigree, age, or reason for slaughter of horses. Therefore, even though the group of slaughtered horses is more representative of the local population, legal restrictions significantly impede any effort to classify data according to age, gender, or breed. On the other hand, the use of live horses presented for dental examinations by consenting owners provides access to a complete set of sensitive data. However, such studies may nonetheless be limited by inferior representation, as horses presented for dental examinations may, for various reasons, not exhibit the same prevalence of dental disease as those not included in such a study. Therefore, for the purpose of the current study, routine inspection during the annual dental check-up was performed in all horses housed in 45 private stables, 1% of all small horse farms (4550) registered in the Mazovian Voivodeship [18], regardless of their oral health status [7]. Moreover, demographic data were provided to substantiate the representative nature of the sample group. Among 37,397 horses registered in the Mazovian Voivodeship [18], approximately 15% (5550 horses) are housed in smaller-scale (111) equestrian centers [19], whereas about 85% (31,847 horses) are kept in (4550) private small horse farms [18]. The annual routine dental examination on small horse farms is generally easier to perform due to the smaller number of horses housed in a single stable (an average of 4–6 horses per stable in this study) compared with large equestrian centers (averaging 50 horses per stable). Furthermore, private owners place greater emphasis on the welfare of their horses and are willing to spend more time on routine inspection during an annual dental check-up, regardless of oral health status. Thus, the observations described below should be considered with respect to the selected group of privately owned horses housed in the Mazovia region of Poland.

5. Conclusions

In a select group of privately owned horses housed in the Mazovia region of Poland, 95% demonstrated dental disorders, with a similar percentage of pathology observed in the incisor teeth (31%) and the cheek teeth (31% each for premolars and molars). Irrespective of age, gender, and breed groupings, malocclusions of incisor, premolar, and molar teeth occurred with a higher prevalence than did dental diseases. Curvatures and sharp enamel points were the most frequently occurring malocclusions of the incisor and cheek teeth, respectively, while calculus and caries were the most frequently distributed dental diseases of the incisor and cheek teeth, respectively.

Supplementary Materials: The following are available online at https://www.mdpi.com/article/10.3390/ani12223120/s1. Figure S1: An equine dental chart used during the detailed dental examination, Table S1: The definitions of selected disorder (malocclusions and dental diseases) of the incisor teeth, Table S2: The definitions of selected disorder (malocclusion and dental diseases) of the canine teeth, Table S3: The definitions of selected disorder (malocclusion and dental disease) of the wolf teeth, Table S4: The definitions of selected disorder (malocclusions and dental diseases) of the cheek (premolar and molar) teeth.

Author Contributions: Conceptualization, K.G. and M.D.; methodology, K.G. and E.S.; software, M.C. and M.D.; validation, B.T. and I.P.; formal analysis, K.G., M.C. and M.D.; investigation, K.G., E.S., B.T., A.B., I.P. and M.D.; resources, K.G.; data curation, K.G.; writing—original draft preparation, K.G., E.S., M.C. and M.D.; writing—review and editing, B.T., A.B. and I.P.; visualization, K.G. and M.D.; supervision, I.P.; project administration, K.G.; funding acquisition, K.G. All authors have read and agreed to the published version of the manuscript.

Funding: This research received no external funding.

Institutional Review Board Statement: The research, using the results of veterinary clinical examinations, does not fall under the legislation for the protection of animals used for scientific purposes, national decree-law Dz. U. 2015 poz. 266 and 2010-63-EU directive. No ethical approval was needed according to the list of exemptions of the II Local Committee for Ethics in Animal Research of Warsaw University of Life Sciences—SGGW.

Informed Consent Statement: Not applicable.

Data Availability Statement: The data presented in this study are available on request from the corresponding author.

Conflicts of Interest: The authors declare no conflict of interest.

References

1. Kirkland, K.D.; Marretta, S.M.; Inoue, O.J.; Baker, G.J. Survey of equine dental disease and associated oral pathology. *Proc. Annu. Conv. Am. Assoc. Equine Pract.* **1994**, *119*, 120.
2. Vemming, D.C.; Steenkamp, G.; Carstens, A.; Olorunju, S.A.S.; Stroehle, R.M.; Page, P.C. Prevalence of dental disorders in an abattoir population of horses in South Africa by oral examination of intact and bisected heads. *Vet. J.* **2015**, *205*, 110–112. [CrossRef] [PubMed]
3. Brigham, E.J.; Duncanson, G.R. An equine postmortem dental study: 50 cases. *Equine Vet. Educ.* **2000**, *12*, 59–62. [CrossRef]
4. Walker, H.; Chinn, E.; Holmes, S.; Barwise-Munro, L.; Robertson, V.; Mould, R.; Bradley, S.; Shaw, D.J.; Dixon, P.M. Prevalence and some clinical characteristics of equine cheek teeth diastemata in 471 horses examined in a UK first-opinion equine practice (2008 to 2009). *Vet. Rec.* **2012**, *171*, 44. [CrossRef]
5. Gere, I.; Dixon, P.M. Post mortem survey of peripheral dental caries in 510 Swedish horses. *Equine Vet. J.* **2010**, *42*, 310–315. [CrossRef]
6. Anthony, J.; Waldner, C.; Grier, C.; Laycock, A.R. A survey of equine oral pathology. *J. Vet. Dent.* **2010**, *27*, 12–15. [CrossRef]
7. Salem, S.E.; Townsend, N.B.; Refaai, W.; Gomaa, M.; Archer, D.C. Prevalence of oro-dental pathology in a working horse population in Egypt and its relation to equine health. *Equine Vet. J.* **2017**, *49*, 26–33. [CrossRef]
8. Toit, N.D.; Burden, F.A.; Kempson, S.A.; Dixon, P.M. Pathological investigation of caries and occlusal pulpar exposure in donkey cheek teeth using computerised axial tomography with histological and ultrastructural examinations. *Vet. J.* **2008**, *178*, 387–395. [CrossRef]
9. Toit, N.D.; Burden, F.A.; Dixon, P.M. Clinical dental examinations of 357 donkeys in the UK. Part 2: Epidemiological studies on the potential relationships between different dental disorders. and between dental disease and systemic disorders. *Equine Vet. J.* **2009**, *41*, 395–400. [CrossRef]
10. Baker, G.J. A Study of Dental Disease in the Horse. Ph.D. Thesis, The Faculty of Veterinary Medicine, University Utrecht, Utrecht, The Netherlands, 1979.
11. Baxter, C. J. Veterinary dentistry: A clinician's viewpoint. *Dental Update* **2013**, *40*, 386–390. [CrossRef]
12. Traub-Dargatz, J.L.; Salman, M.D.; Voss, J.I. Medical problems of adult horses, as ranked by equine practitioners. *J. Am. Vet. Med.* **1991**, *198*, 1745–1747.
13. Ireland, J.L.; McGowan, C.M.; Clegg, P.D.; Chandler, K.J.; Pinchbeck, G.L. A survey of health care and disease in geriatric horses aged 30 years or older. *Vet. J.* **2012**, *192*, 57–64. [CrossRef] [PubMed]
14. Dixon, P.M.; Tremaine, W.H.; Pickles, K.; Kuhns, L.; Hawe, C.; Mccann, J.; Mcgorum, B.C.; Railton, D.I.; Brammer, S. Equine dental disease. Part 3: A long-term study of 400 cases: Disorders of wear, traumatic damage and idiopathic fractures, tumours and miscellaneous disorders of the cheek teeth. *Equine Vet. J.* **2000**, *32*, 9–18. [CrossRef] [PubMed]

15. Chinkangsadarn, T.; Wilson, G.; Greer, R.; Pollitt, C.; Bird, P. An abattoir survey of equine dental abnormalities in Queensland. Australia. *Aust. Vet. J.* **2015**, *93*, 189–194. [CrossRef] [PubMed]
16. Siwińska, N.; Zak, A.; Mańkowska, M.; Drozd, M.; Borowicz, H. Częstotliwość występowania wad w obrębie zębow siecznych u koni uzytkowych na terenie Polski. *Med. Weter.* **2017**, *73*, 362–365.
17. Polish Horse Breeders Association: Pogłowie Koni w Polsce. 2019. Available online: https://www.pzhk.pl/hodowla/poglowie-koni-polsce/ (accessed on 10 May 2021).
18. Central Statistical Office: Pogłowie Koni w Województwie Mazowieckim. 2019. Available online: https://bdl.stat.gov.pl/ (accessed on 10 May 2021).
19. Polish Equestrian Federation: Liczba zarejestrowanych klubów Sportowych w Województwie Mazowieckim. 2022. Available online: https://wmzj.waw.pl/ (accessed on 14 October 2022).
20. Dixon, P.M.; Tremaine, W.H.; Pickles, K.; Kuhns, L.; Hawe, C.; McCann, J.; McGorum, B.; Railton, D.I.; Brammer, S. Equine dental disease Part 1: A longterm study of 400 cases: Disorders of incisor, canine and first premolar teeth. *Equine Vet. J.* **1999**, *31*, 369–377. [CrossRef]
21. Wilson, G.J.; Liyou, O.J. Examination of dental charts of horses presented for routine dentistry over a 12 month period. *Aust. Equine Vet.* **2005**, *24*, 79–83.
22. Maslauskas, K.; Tulamo, R.M.; McGowan, T.; Kučinskas, A. A descriptive study of the dentition of Lithuanian heavy-drought horses. *Vet. Zootech.* **2008**, *43*, 62–67.
23. Ramzan, P.H.L. Oral endoscopy as an aid to diagnosis of equine cheek tooth infections in the absence of gross oral patholog cal changes:17 cases . *Equine Vet. J.* **2009**, *41*, 101–106.
24. Schumacher, J. The present state of equine dentistry. *Equine Vet. J.* **2001**, *33*, 2–3. [CrossRef]
25. Pearce, C.J. Recent developments in equine dentistry. *N. Z. Vet. J.* **2020**, *68*, 178–186. [CrossRef] [PubMed]
26. Knottenbelt, D.C. Equine dentistry—The state of the art and the state of the science. *Vet. J.* **2005**, *169*, 159–161. [CrossRef] [PubMed]
27. Jáuregui, H.; Briones, R. Identificación de Patologías Dentales Encaballos de Tiro Urbano en la Comuna de Padre las Casas, Región de la Araucanía, Chile. Ph.D. Thesis, The Faculty of Veterinary Medicine, Universidad Mayor, Santiago, Chile, 2016.
28. McGowan, C.M.; Ireland, J.L. Welfare, quality of life, and euthanasia of aged horses. *Vet. Clin. N. Am. Equine Pract.* **2016**, *32*, 355–367. [CrossRef] [PubMed]
29. Wageningen, U.R. Welfare monitoring system—Assessment protocol for horses, version 2.0. *Wagening. UR Livest. Res.* **2012**, *44*, 1–44.
30. Cook, W. Damage by the bit to the equine interdental space and second lower premolar. *Equine Vet. Educ.* **2011**, *23*, 355–360. [CrossRef]
31. Foster, D.L. The gold standard of dental care for the adult performance horse. *Vet. Clin. N. Am. Equine Pract.* **2013**, *29*, 505–519. [CrossRef]
32. Björnsdóttir, S.; Frey, R.; Kristjansson, T.; Lundström, T. Bit-related lesions in Icelandic competition horses. *Acta Vet. Scand.* **2014**, *56*, 40. [CrossRef]
33. Pehkonen, J.; Karma, L.; Raekallio, M. Behavioral signs associated with equine periapical infection in cheek teeth. *J. Equine Vet. Sci.* **2019**, *77*, 144–150. [CrossRef]
34. Rehrl, S.; Schröder, W.; Müller, C.; Staszyk, C.; Lischer, C. Radiological prevalence of equine odontoclastic tooth resorption and hypercementosis. *Equine Vet. J.* **2018**, *50*, 481–487. [CrossRef]
35. Gergeleit, H.; Bienert-Zeit, A. Complications following mandibular cheek tooth extraction in 20 horses. *Front. Vet. Sci.* **2020**, *7*, 504. [CrossRef]
36. Radostits, O.M.; Gay, C.; Hinchcliff, K.W.; Constable, P.D. *Veterinary Medicine e-Book: A Textbook of the Diseases of Cattle, Horses, Sheep, Pigs and Goats*; Elsevier Health Sciences: Amsterdam, The Netherlands, 2006.
37. Quinn, G.C.; Tremaine, W.H.; Lane, J.G. Supernumerary cheek teeth (n = 24): Clinical features. diagnosis. treatment and outcome in 15 horses. *Equine Vet. J.* **2005**, *37*, 505–509. [CrossRef] [PubMed]
38. Casey, M.B.; Tremaine, W.H. The prevalence of secondary dentinal lesions in cheek teeth from horses with clinical signs of pulpitis compared to controls. *Equine Vet. J.* **2010**, *42*, 30–36. [CrossRef] [PubMed]
39. Floyd, M.R. The modified Triadan system: Nomenclature for veterinary dentistry. *J. Vet. Dent.* **1991**, *8*, 18–19. [CrossRef] [PubMed]
40. Simhofer, H.; Griss, R.; Zetner, K. The use of oral endoscopy for detection of cheek teeth abnormalities in 300 horses. *Vet. J.* **2008**, *178*, 396–404. [CrossRef] [PubMed]
41. Casey, M.B.; Tremaine, W.H. Dental diastemata and periodontal disease secondary to axially rotated maxillary cheek teeth in three horses. *Equine Vet. Educ.* **2010**, *22*, 439–444. [CrossRef]
42. Huang, L.G.; Chen, G. A histological and radiographic study of pulpal calcification in periodontally involved teeth in a Taiwanese population. *J. Dent. Sci.* **2016**, *11*, 405–410. [CrossRef]
43. Omura, C.M.; Drumond, B.; Júnior, J.L.R.; Coelho, C.S.; Gioso, M.A. Measurement of incisor overjet and physiologica diastemata parameters in quarter horse foals. *J. Vet. Dent.* **2015**, *32*, 173–175. [CrossRef]
44. Easley, J. Dental care and instrumentation. *Vet. Clin. N. Am. Equine Pract.* **1998**, *14*, 309–332. [CrossRef]

45. Toit, N.D.; Rucker, B. Geriatric dentistry. In *Equine Dentistry*, 3rd ed.; Easley, P., Dixon, P., Schumacher, J., Eds.; Elsevier: Philadelphia, PA, USA, 2011; pp. 279–287.
46. Rodrigues, J.B.; Araújo, S.; Sanroman-Llorens, F.; Bastos, E.; San Roman, F.; Viegas, C. A clinical survey evaluating the prevalence of incisor disorders in Zamorano-Leonés and Mirandês donkeys (*Equus asinus*). *J. Equine Vet. Sci.* **2013**, *33*, 710–718. [CrossRef]
47. Dixon, P.M.; Dacre, I. A review of equine dental disorders. *Vet. J.* **2005**, *169*, 165–187. [CrossRef]
48. Baker, G.J.; Easley, J. Dental physiology. In *Equine Dentistry*, 1st ed.; W.B. Saunders Co. Ltd.: London, UK, 1999; pp. 30–33.
49. Rucker, B.A. Utilizing cheeck teeth angle of occlusio to determine length of incisor shortening. In Proceedings of the 48th AAEP Annual Convention, Orlando, FL, USA, 4–8 December 2002; pp. 448–452.
50. Dixon, P.M.; Kennedy, R.; Reardon, R.J.M. Equine "idiopathic" and infundibular caries-related cheek teeth fractures: A long-term study of 486 fractured teeth in 300 horses. *Front. Vet. Sci.* **2021**, *8*, 646870. [CrossRef] [PubMed]
51. Klugh, D.O. *Principles of Equine Dentistry*; Manson/Veterinary CRC Press: Boca Raton, FL, USA, 2010.
52. Pearce, D.J.; Brown, J.A. Extraction of 22 equine cheek teeth with displaced sagittal fractures using polymethylmethacrylate stabilisation (2011–2016). *Equine Vet. Educ.* **2019**, *31*, 421–426. [CrossRef]
53. Borkent, D.; Smith, S.; Dixon, P.M. A histological and ultrastructural study of equine peripheral caries. *Equine Vet. J.* **2020**, *52*, 104–111. [CrossRef] [PubMed]
54. Staszyk, C.; Bienert, A.; Kreutzer, R.; Wohlsein, P.; Simhofer, H. Equine odontoclastic tooth resorption and hypercementosis. *Vet. J.* **2008**, *178*, 372–379. [CrossRef] [PubMed]
55. Hole, S.L.; Staszyk, C. Equine odontoclastic tooth resorption and hypercementosis. *Equine Vet. Educ.* **2018**, *30*, 386–391. [CrossRef]
56. Dixon, P.M.; Tremaine, W.H.; Pickles, K.; Kuhns, L.; Hawe, C.; Mccann, J.; Mcgorum, B.C.; Railton, D.I.; Brammer, S. Equine dental disease Part 2: A long-term study of 400 cases: Disorders of development and eruption and variations in position of the cheek teeth. *Equine Vet. J.* **1999**, *31*, 519–528. [CrossRef]
57. Dacre, I.; Kempson, S.; Dixon, P.M. Equine idiopathic cheek teeth fractures. Part 1: Pathological studies on 35 fractured cheek teeth. *Equine Vet. J.* **2007**, *39*, 310–318. [CrossRef]
58. Toit, N.D.; Dixon, P.M. Common dental disorders in the donkey. *Equine Vet. Educ.* **2012**, *24*, 45–51. [CrossRef]

sensors

MDPI

Article

Selection of Filtering and Image Texture Analysis in the Radiographic Images Processing of Horses' Incisor Teeth Affected by the EOTRH Syndrome

Kamil Górski [1], Marta Borowska [2], Elżbieta Stefanik [1], Izabela Polkowska [3], Bernard Turek [1], Andrzej Bereznowski [4] and Małgorzata Domino [1,*]

[1] Department of Large Animal Diseases and Clinic, Institute of Veterinary Medicine, Warsaw University of Life Sciences, 02-787 Warsaw, Poland; kamil_gorski@sggw.edu.pl (K.G.); elzbieta_stefanik@sggw.edu.pl (E.S.); bernard_turek@sggw.edu.pl (B.T.)
[2] Institute of Biomedical Engineering, Faculty of Mechanical Engineering, Białystok University of Technology, 15-351 Bialystok, Poland; m.borowska@pb.edu.pl
[3] Department and Clinic of Animal Surgery, Faculty of Veterinary Medicine, University of Life Sciences in Lublin, 20-950 Lublin, Poland; izabela.polkowska@up.lublin.pl
[4] Department of Veterinary Epidemiology and Economics, Faculty of Veterinary Medicine, Warsaw University of Life Sciences, 02-787 Warsaw, Poland; andrzej_bereznowski@sggw.edu.pl
* Correspondence: malgorzata_domino@sggw.edu.pl

Abstract: Equine odontoclastic tooth resorption and hypercementosis (EOTRH) is one of the horses' dental diseases, mainly affecting the incisor teeth. An increase in the incidence of aged horses and a painful progressive course of the disease create the need for improved early diagnosis. Besides clinical findings, EOTRH recognition is based on the typical radiographic findings, including levels of dental resorption and hypercementosis. This study aimed to introduce digital processing methods to equine dental radiographic images and identify texture features changing with disease progression. The radiographs of maxillary incisor teeth from 80 horses were obtained. Each incisor was annotated by separate masks and clinically classified as 0, 1, 2, or 3 EOTRH degrees. Images were filtered by *Mean*, *Median*, *Normalize*, *Bilateral*, *Binomial*, *CurvatureFlow*, *LaplacianSharpening*, *DiscreteGaussian*, and *SmoothingRecursiveGaussian* filters independently, and 93 features of image texture were extracted using *First Order Statistics* (FOS), *Gray Level Co-occurrence Matrix* (GLCM), *Neighbouring Gray Tone Difference Matrix* (NGTDM), *Gray Level Dependence Matrix* (GLDM), *Gray Level Run Length Matrix* (GLRLM), and *Gray Level Size Zone Matrix* (GLSZM) approaches. The most informative processing was selected. GLCM and GLRLM return the most favorable features for the quantitative evaluation of radiographic signs of the EOTRH syndrome, which may be supported by filtering by filters improving the edge delimitation.

Keywords: equine odontoclastic tooth resorption and hypercementosis; filtering; texture analysis; digital image processing; dental care

Citation: Górski, K.; Borowska, M.; Stefanik, E.; Polkowska, I.; Turek, B.; Bereznowski, A.; Domino, M. Selection of Filtering and Image Texture Analysis in the Radiographic Images Processing of Horses' Incisor Teeth Affected by the EOTRH Syndrome. *Sensors* **2022**, *22*, 2920. https://doi.org/10.3390/s22082920

Academic Editors: Robert Martí and Joan Martí Bonmatí

Received: 28 February 2022
Accepted: 8 April 2022
Published: 11 April 2022

1. Introduction

Dental diseases are known to significantly affect horses' health [1–6], affecting not only the body condition [1] but also the functioning of the whole body [2] and predisposing horses to life-threatening colic [5,6]. Dental diseases are the third most common problem in equine veterinary medicine [7,8]. It is estimated that 24% of young horses, even without clinical signs of oral disease, have oral abnormalities [9]. In Dixon and Tremaine's study [7], 11% of the examined horses showed disorders in the area of the incisor teeth. In Wilson and Liyou's study [10], 20% of the examined horses had abnormalities in their incisor teeth. In the Maslauskas et al. study [11], 26% of the Lithuanian dray horses demonstrated signs of incisor tooth disorders. Moreover, the teeth pathology concerned more often the incisor teeth of the maxilla than the mandible, and more than one tooth [7,8]. Since incisor

teeth, unlike the cheek teeth, are easier to visually assess due to the rostral position [8], any abnormalities can be diagnosed and corrected at an early stage [11]. However, just in the early stages of the disease, a detailed dental examination, including radiographic imaging, is necessary to make the correct diagnosis [12,13] and to plan and choose the treatment [14], as most of the early changes concern the alveolar part of the teeth [12,13].

The Equine odontoclastic tooth resorption and hypercementosis (EOTRH) syndrome is one of the important diseases affecting the incisor teeth [12,15–18], whose etiopathogenesis remains not fully understood. The EOTRH syndrome may be diagnosed based on the anamnestic data and careful clinical examination; however, only the radiological signs are determinant, often exclusive and usually conclusive [19]. Therefore, it is widely accepted that the careful evaluation of the radiological images of the incisor teeth provides valuable data on the advancement of the disease [13]. Moreover, the changes in the radiographic image of the incisal processes appear earlier than the clinical symptoms [13,20,21]. As teeth demonstrate high radiodensity, they are extremely radiopaque and radiographically well-defined [19]. Therefore, their radiological images are visually inspected for the presence of signs of tooth resorption and bulbous enlargement of the intra-alveolar part of the teeth [13,18]. Moreover, the radiological images reveal the signs of widening of the periodontal ligament space, root resorption, erosion of the apical part of the root, root and reserve crown enlargement due to hypercementosis, irregular and/or rough surface of an intra-alveolar part, disruption of the lamina dura, osteomyelitis, atrophy or other pathology in the course of a pulp canal, or fractures of the root and the reserve crown [18]. In general, these symptoms are related to the following two ongoing processes of varying intensity: resorption and hypercementosis, which are involved in the pathogenesis of EOTRH. As resorption is sometimes present without hypercementosis, whereas hypercementosis is never present alone, hypercementosis seems to be a reparative or secondary process [22]. Therefore, the pathological features of both processes were included in the radiological classification system designed specifically for the detection of signs of EOTRH [23]. The visual classification system, introduced by Hüls et al. [23], uses radiological criteria (shape, contour, radiodensity, and delineation of the periodontal space) as well as macroscopical criteria (shape, surface structure, contour, and consistency) to classify EOTRH affected teeth as mild, moderate, or severely altered [13]. A more detailed clinical classification of the incisor tooth resorption and hypercementosis processes in horses was introduced by Henry et al. [22] based on the humans' and canines' classification methods. Most of the previous studies focus on the description of the disease, whereas the problem arising from the difficulty of EOTRH diagnosis, especially at an early stage, remains unsolved.

Therefore, the statistical decryptions of the radiographic digital image are proposed here, as the large field of medical applications [24,25] and good results for images where the textures are visually easily separable [26], were reported. The first- and second-order descriptive statistics have successfully been used in human medicine to improve the extraction of texture features of ultrasound images [27], thermal images [28], magnetic resonance images [29,30], computed tomography images [31], and radiographic images [32,33]. In equine medicine, they have been recently applied to the detailed characteristics of the thermal images reflected the increase in the metabolic activity in response to the pregnancy [34] as well as single [35] or multiple [36] exercise. The approaches to feature extraction from digital images represent seven major classes: statistical approaches, structural approaches, transform-based approaches, model-based approaches, graph-based approaches, learning-based approaches, and entropy-based approaches [37,38]. The statistical approach enables the description of the image by a set of statistical quantitative features such as intensity histogram-based and texture matrix-based features. The matrix-based features are subdivided into the following classes: Gray Level Co-occurrence Matrix (GLCM), Neighbouring Gray Tone Difference Matrix (NGTDM), Gray Level Dependence Matrix (GLDM), Gray Level Run Length Matrix (GLRLM), and Gray Level Size Zone Matrix (GLSZM) [37], whereas intensity histogram-based features are represented by First Order Statistics (FOS) [37]. When the matrices resulting from the texture analysis are

calculated for each direction vector, the average values are returned, and the texture matrices become invariant to rotation and translation [37]. Such matrices can be useful in biomedical applications and their features can be calculated based on original images or filtered images [39,40].

Different approaches of the image feature extraction and image processing steps can affect quantified characteristics of the image [38]. One may observe that the image features can be calculated based on original images or filtered images. However, it should be kept in mind that the values of texture features received after different filtering will not be the same. Therefore, the filtrating algorithms are concerned in terms of a specific objective [38]. For example, in human dentistry, digital radiographic images are routinely filtered and used to enhance brightness, contrast, and edges, carrying the potential for increasing their diagnostic value [41,42]. Minimal filtering, the most commonly used in this type of analysis, was applied to remove outliers (*Median* filter), increase contrast (*Normalization* filter), preserve edges (*Bilateral* filter), highlight regions of rapid intensity change (*Laplacian* filter), and gently smear to remove noise (*DiscreteGaussian* and *Smoothingrecursive Gaussian* filters) [41,42]. In equine dentistry, a similar image filtering has not yet been applied, whereas the processes of tooth resorption and hypercementosis are similar in humans and horses. Moreover, the comparison between different radiological methods for assessment of tooth root resorption [19] and statistical analysis of radiographic textures illustrating teeth [32] was performed in humans, but not in horses. Therefore, we hypothesized the effect of resorption and hypercementosis processes on the appearance of a tooth radiograph may be similar, thus human approaches can be successfully applied to veterinary medicine. However, both image filtering methods and texture analysis approaches have to be tested on the equine specimen in order to demonstrate the effect of digital image processing on the basic features quantification. To the best of our knowledge, this is the first report on equine tooth texture analysis assessing its usefulness in diagnosing equine-specific dental diseases [12,13].

Based on the presented background, we hypothesize that the radiographic signs of the EOTRH syndrome could be successively quantified using the statistical decryptions of the radiographic digital image. Therefore, this study aimed to examine nine filtering algorithms and six texture analysis approaches to indicate the features of the descriptive statistics that change with the EOTRH degree. The identified features are preliminary to introducing digital image processing into the quantification of radiographic signs of the EOTRH syndrome and will be used in future research investigating the application of texture analysis in equine dental veterinary medicine.

2. Materials and Methods

2.1. Horses

The study was carried out on eighty privately owned horses (n = 80) (age mean ± SD: 16.9 ± 7.0; 37 geldings, 43 mares), presented to a dental veterinarian by their owner and underwent a routine dental examination from July 2021 to December 2021. The horses represented predominantly warmblood breeds (n = 76) including mostly three Polish warmblood breeds (n = 41) in it: Polish Halfbred horse (n = 30), Wielkopolska (n = 8), and Malopolska (n = 3) breeds. Moreover, Arabian horses (n = 13), Schlesisches Warmblood horses (n = 10), Dutch Warmblood (n = 7), Thoroughbred horses (n = 5), and Polish coldblooded horses (n = 4) were also included. The experimental protocol was approved by the II Local Ethical Committee on Animal Testing in Warsaw on behalf of the National Ethical Committees on Animal Testing (No WAW2/091/2020 approved on 29 July 2020).

2.2. Image Collection

Horses were sedated with detomidine, xylazine, or a combination of both, with some cases given additional butorphanol was administered intravenously. The dose and composition of the sedation were determined on the basis of the horse's body weight and temperament. The Haussmann's halter retractor was used to open the oral cavity for visual

examination and digital palpation. Then, the oral cavity was rinsed with 400 mL of water to remove the remainder of the food. The detailed dental examination was conducted following the previously used standard protocol. The results of the oral cavity examination were documented using an equine dental chart [18]. The intraoral radiographic image was obtained using a bisecting angle technique and the dorsoventral projection for the maxillary teeth [18,20,22], following the standard, previously described protocol and under the same settings of the x-ray tube [18].

Based on the dental examination including the radiological signs, each maxillary incisor tooth was classified as normal (0), mild (1), moderate (2), and severe (3) EOTRH affected. The visual classification system, introduced by Hüls et al. [23] with Rehrl et al. modification [13] was used. The radiological criteria included shape, contour, radiodensity and delineation of the periodontal space. The macroscopical criteria included shape, surface structure, contour, and consistency. Based on the findings obtained, the incisor teeth were assigned to the normal group (EOTRH 0; n = 105), the mild EOTRH group (EOTRH 1; n = 195), the moderate EOTRH group (EOTRH 2; n = 111), or the severe EOTRH group (EOTRH 3; n = 61). The total number of incisors for all groups was 472; therefore, 8 incisors were excluded due to tooth fractures.

2.3. Image Processing

Processing steps for radiographic image texture analysis included (i) image acquisition; (ii) masks annotation and image segmentation; (iii) input image filtering using nine filtering algorithms: *Mean*, *Median*, *Normalize*, *Bilateral*, *Binomial*, *CurvatureFlow*, *LaplacianSharpening*, *DiscreteGaussian*, and *SmoothingRecursiveGaussian;* (iv) image texture features extraction from output filtered images using six analytical approaches: *First Order Statistics* (FOS), *Gray Level Co-occurrence Matrix* (GLCM), *Neighbouring Gray Tone Difference Matrix* (NGTDM), *Gray Level Dependence Matrix* (GLDM), *Gray Level Run Length Matrix* (GLRLM), and *Gray Level Size Zone Matrix* (GLSZM) (Figure 1). The image texture analysis, including steps iii and iv, was applied to regions of interest (ROIs) annotated by the masks during image segmentation in step ii. Each ROI was considered separately.

2.3.1. Masks Annotation and Image Segmentation

The masks representing 6 maxillary incisor teeth were manually annotated. The modified Triadan system for equine dental nomenclature was used [43]. In the maxilla, the quadrant was identified with 1 on the right and 2 on the left, and the incisor teeth were numbered consecutively, beginning with 01 at the midline and proceeding distally. Thus, 103, 102, 101, 201, 202 and 203 incisor teeth were annotated separately (Figure 1C). The masks segmented each image into six ROIs representing the consecutive incisor teeth. The masks were annotated from a high radiodensity line representing the edge of the rubbing surface of the incisor toot along the lateral and medial surfaces of the tooth to the tooth root. The masks were individually fitted to the separate teeth and did not include lips, mucous membranes, and the bone of the incisal processes. The masks were annotated using the ImageJ software (version 1.46r, Wayne Rasband, National Institutes of Health, USA).

2.3.2. Filtering

The following nine different filtering algorithms were used to reduce the noise in the radiographic images (Figure 2). The filtering algorithms were implemented in SimpleITK toolkit in Python language [39,40,44].

(*i*) *Mean filter* is a linear filter. The pixels of the output image are the average values of the pixels in the neighborhood of the input pixel being calculated. The parameter of this filter is the window containing the neighborhood of the calculated pixel (w = 3) [40,45].

(*ii*) *Median filter* is a non-linear filter. The pixels of the output image are the medians of the pixels in the neighborhood of the input pixel being calculated. This filter requires a neighborhood size (w = 3) [45].

(*iii*) *Normalize filter* is a linear filter, when the normalizing image involves setting its mean to zero and its variance to one. The output image is a rescaled image in which the pixels have zero mean and unit variance [45].
(*iv*) *Bilateral filter* is a non-linear filter that consists of a domain filter and a range filter. The output image contains the new pixel value calculated based on the pixels similar to a pixel in the image domain and similar to a pixel in the image range. Two Gaussian kernels are used in both image domain and image range [46]. In these filter settings, the sigma in the image domain was 4.0 and the sigma in the image range was 50.
(*v*) *Binomial filter* is a linear filter, which separable blur on each image dimension. The output image is closer to performing a spline operation with a Gaussian window, after n iterations calculating the average of the nearest neighbors along each direction [47].
(*vi*) *CurvatureFlow filter* is a linear filter that reduces the noise using curvature-based flow. The output image is displayed as a set of brightness levels calculated using curvature-based speed function [48]. In these filter settings, the number of update iterations to perform was 5 and the interval between each update was 0.05.
(*vii*) *LaplacianSharpening filter* is a non-linear filter, that sharpens an image using a Laplacian. The output image is produced after a pixel convolution with a Laplacian operator, which results in change of the regions of rapid intensity and highlights the edges [49].
(*viii*) *DiscreteGaussian filter* is a linear filter that calculates derivatives using discrete Gaussian derivative operator (kernel). The output image contains a disjoint spline of the input image with a kernel where the variance and standard deviation (sigma) are evaluated as physical units [50].
(*ix*) *SmoothingRecursiveGaussian filter* is a linear that uses Gaussian kernels implemented as IIR filter. The output image is produced after convolution of the input image with Gaussian kernels. In these filter settings, the sigma parameter was 3 [51].

2.3.3. Extraction of Image Texture Features

The following six texture analysis approaches [37] were used to extract 93 texture features of the radiographic image from each of the six segmented ROIs, separately (Figure 1E). Texture features were calculated independently for individual filtrated output images using PyRadiomics, an open-source python package for the extraction of features from radiographic images [52].

(*i*) *First Order Statistics* (FOS) describe the distribution of pixel intensity using the first-order histogram statistics of images. FOS returns the following 18 features: mean, median, minimum, maximum, 10th percentile, 90th percentile, variance, root mean squared (RMS), kurtosis, skewness, uniformity, range, interquartile range, mean absolute deviation (MAD), robust mean absolute deviation (rMAD), energy, total energy, and entropy [37].
(*ii*) *Gray Level Co-occurence Matrix* (GLCM) describes the second-order joint probability function of the image defined as P(*i,j*). Each element of this matrix represents the mutual spatial relationship between pairs of pixels with specific intensity levels in different directions along angle θ and at different distances δ of pixel pairs [53]. GLCM returns the following 24 features: autocorrelation, cluster prominence, cluster shade, cluster tendency, contrast, correlation, difference average, difference entropy, difference variance, inverse difference (ID), inverse difference moment (IDM), inverse difference moment normalized (IDMN), inverse difference normalized (IDN), informational measure of correlation 1 (IMC 1), informational measure of correlation 2 (IMC 2), inverse variance, joint average, joint energy, joint entropy, maximal correlation coefficient (MCC), maximum probability, sum average, sum entropy, and sum of squares [53].
(*iii*) *Neighbouring Gray Tone Difference Matrix* (NGTDM) describes the difference between a gray value and the average gray value of its neighbors within a Chebyshew distance δ using the second-order statistic. Matrix contains the sum of the absolute differences

in gray level [54]. NGTDM returns the following 5 features: busyness, coarseness, complexity, contrast, and strength [54].

(*iv*) *Gray Level Dependence Matrix* (GLDM) describes dependencies of gray level in the image using the second-order statistic. A gray level dependency is defined as the number of connected pixels within distance δ, which are dependent on the center pixel. Each element of the gray level dependence matrix P(*i,j*) describes the number of times appearance a pixel with gray level *i* with *j* dependent pixels in its neighbourhood [55]. GLDM returns the following 14 features: dependence entropy (DE), dependence non-uniformity (DN), dependence non-uniformity normalized (DNN), dependence variance (DV), gray level non-uniformity (GLN), gray level variance (GLV), high gray level emphasis (HGLE), large dependence emphasis (LDE), large dependence high gray level emphasis (LDHGLE), large dependence low gray level emphasis (LDLGLE), low gray level emphasis (LGLE), small dependence emphasis (SDE), small dependence high gray level emphasis (SDHGLE), and small dependence low gray level emphasis (SDLGLE) [55].

(*v*) *Gray Level Run Length Matrix* (GLRLM) describes gray level runs in the image using the second-order statistic. A gray level run is defined as the length of the number of consecutive pixels with the same gray level values. Each element in the gray level run length matrix P(*i,j*) describes the number of runs with the gray level *i* and the length *j* in different directions along angle θ [56,57]. GLRLM returns the following 16 features: gray level non-uniformity (GLN), gray level non-uniformity normalized (GLNN), gray level variance (GLV), high gray level run emphasis (HGLRE), long run emphasis (LRE), long run high gray level emphasis (LRHGLE), long run low gray level emphasis (LRLGLE), low gray level run emphasis (LGLRE), run entropy (RE), run length non-uniformity (RLN), run length non-uniformity normalized (RLNN), run percentage (RP), run variance (RV), short run emphasis (SRE), short run high gray level emphasis (SRHGLE), and short run low gray level emphasis (SRLGLE) [56,57].

(*vi*) *Gray Level Size Zone Matrix* (GLSZM) describes gray-level zones in the image using the second-order statistic. A gray-level zone is defined as the number of connected pixels with the same gray-level intensity. Each element in the gray level size zone matrix P(*i,j*) describes the number of zones with gray level *i* and size *j* [58]. GLSZM returns the following 16 features: gray level non-uniformity (GLN), gray level non-uniformity normalized (GLNN), gray level variance (GLV), high gray level zone emphasis (HGLZE), large area emphasis (LAE), large area high gray level emphasis (LAHGLE), large area low gray level emphasis (LALGLE), low gray level zone emphasis (LGLZE), size-zone non-uniformity (SZN), size-zone non-uniformity normalized (SZNN), small area emphasis (SAE), small area high gray level emphasis (SAHGLE), small area low gray level emphasis (SALGLE), zone entropy (ZE), zone percentage (ZP), and zone variance (ZV) [58].

2.4. Statistical Analysis

Statistical analysis was performed using GraphPad Prism software, version 6, (GraphPad Software Inc., San Diego, CA, USA). Data were presented as data series for each filtering independently, where each incisor tooth represented one realization. The numerical data in Supplementary Tables S1–S54 were presented as mean ± standard deviation (SD). Data series were tested independently for univariate distributions using a Shapiro–Wilk normality test. Data analysis was performed in the following three steps: (i) testing the differences between data series of the EOTRH classes; (ii) testing the increase or decrease with the EOTRH; (iii) calculating the coefficient of variation for the consecutive features in each of each texture analysis approach including all filters used.

Figure 1. Processing steps for radiographic image texture analysis. Clinical examination (**A**); radiographic image acquisition (**B**); masks annotation and image segmentation with regions of interest (ROIs) marked with yellow lines (**C**); input image filtering (**D**); image texture features extraction from output filtered images (**E**).

The comparisons between (i) data series representing EOTRH classes were assessed using the ordinary one-way ANOVA for Gaussian data and the Kruskal–Wallis for non-Gaussian data. The alpha value was established as $\alpha = 0.05$. On the corresponding summarizing plot, when a feature differed between EOTRH classes the cell was marked with gray and the number of features that differed between classes was given in each row. Statistical analysis was performed using GraphPad Prism6 software (GraphPad Software Inc., San Diego, CA, USA).

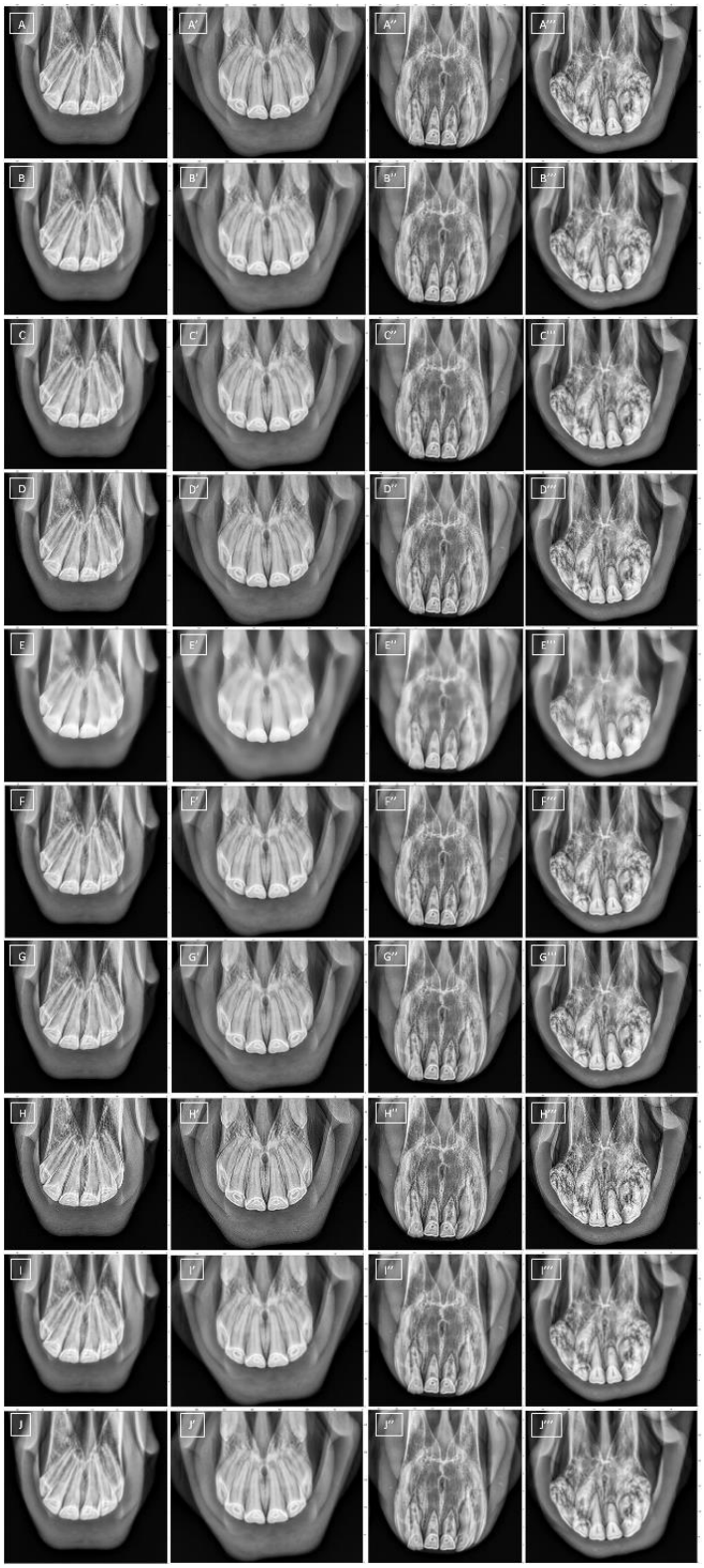

Figure 2. The samples of radiographic images representing normal maxillary incisor teeth (EOTRH 0, **A**–**F**) and mild (EOTRH 1, **A′**–**F′**), moderate (EOTRH 2, **A″**–**F″**), and severe (EOTRH 3, **A‴**–**F‴**) Equine odontoclastic tooth resorption and hypercementosis (EOTRH) syndrome. The input images (**A**–**A‴**) and output images filtered by *Mean* (**B**–**B‴**), *Median* (**C**–**C‴**), *Normalize* (**D**–**D‴**), *Bilateral* (**E**–**E‴**), *Binomial* (**F**–**F‴**), *CurvatureFlow* (**G**–**G‴**), *LaplacianSharpening* (**H**–**H‴**), *DiscreteGaussian* (**I**–**I‴**), and *SmoothingRecursiveGaussian* (**J**–**J‴**) filters, respectively.

The comparisons between (ii) the mean rank of each EOTRH class with the mean rank of every other EOTRH class were assessed using the Ordinary one-way ANOVA followed by Tukey's multiple comparisons test for Gaussian data and the Kruskal–Wallis test followed by the Dunn's multiple comparisons test for non-Gaussian data. The alpha value was established as $\alpha = 0.05$. On the corresponding summarizing plot, when a feature was found to significantly increase or decrease with the degree of the EOTRH, the cell was marked with red or blue, respectively. The number in the cell indicates the degree of EOTRH from which the increase or decrease in the values of the features begins. The selected filtering and texture analysis approaches were presented on scatter plots with bars using mean ± SD and dots representing each realization. Statistical analysis was performed using GraphPad Prism6 software (GraphPad Software Inc., San Diego, CA, USA).

The coefficient of variation (iii) was calculated for the consecutive features of FOS, GLCM, NGTDM, GLDM, GLRLM, and GLSZM using data set containing all filtrated output images. The coefficient of variation was presented on plots independently for consecutive texture analysis approaches, where the red dashed line indicates the mean value of the feature for the total data set of consecutive texture analysis approaches. The features that differed between EOTRH degrees regardless of the filtering used were marked with an asterisk and the percentage of these features was shown in the right lower corner of each plot.

3. Results

Among 837 returned combinations of filtering (n = 9) and image texture features (n = 93, including FOS n = 18, GLCM n = 24, NGTDM n = 5, GLDM n = 14, GLRLM n = 16, and GLSZM n = 16), considering all filters used at least 13 features of FOS, 17 features of GLCM, 4 features of NGTDM, 10 features of GLDM, 13 features of GLRLM, and 8 features differed between the EOTRH classes. These differences were summarized in Figure 3 and considered for further analysis. For FOS, the most features differed after filtering by *LaplacianSharpening* filter (n = 16) and the least after filtering by the *Normalize* filter (n = 13). For GLCM, the most features differed after filtering by *Normalize* and *Bilateral* filters (n = 24) and the least after filtering by the *LaplacianSharpening* filter (n = 17). For NGTDM, only after filtering by the *LaplacianSharpening* filter, not all features (n = 4) differed between the EOTRH classes. For GLDM n = 14, the most features differed after filtering by *Normalize* and *Bilateral* filters (n = 13) and the least after filtering by *Median*, *Binomial*, *CurvatureFlow*, and *LaplacianSharpening* filters (n = 10). For GLRLM, the most features differed after filtering by a *Bilateral* filter (n = 16) and the least after filtering by *Median*, *Normalize*, *CurvatureFlow*, and *LaplacianSharpening* filters (n = 13). For GLSZM, the most features differed after filtering by the *Normalize* filter (n = 16) and the least after filtering by the *Median* filter (n = 8). The mean ± SD values of extracted features were calculated and presented in Supplementary Tables S1–S9 for FOS, Tables S10–S18 for GLCM, Tables S19–S27 for NGTDM, Tables S28–S36 for GLDM, Tables S37–S45 for GLRLM, and Tables S46–S54 for GLSZM, available online.

Among 683 returned combinations that basically differed between the EOTRH classes, 410 features increased or decreased with the degree of the EOTRH (including FOS n = 76, GLCM n = 123, NGTDM n = 19, GLDM n = 56, GLRLM n = 71, and GLSZM n = 65) (Figure 4). Then two criteria were used to indicate these features, which clearly correlate with the following EOTRH degrees: (i) the features that increase or decrease from class 1 of the EOTRH for at least one filter and (ii) the features that increase or decrease repeatable in each output images data set, regardless of the applied filtering. For FOS, the first criterion (an increase from class 1 of the EOTRH) passed: Variance, Kurtosis, Range, Interquartile range, MAD, and Entropy; as well as (a decrease from class 1 of the EOTRH): Minimum, Skewness, and Uniformity. For GLCM, the first criterion (an increase from class 1 of the EOTRH) was passed for the following: Autocorrelation, Cluster Prominence, Contrast, Difference Average, Difference Entropy, Difference Variance, IMC1, Inverse Variance, Joint Average, Joint Energy, and Sum Average; as well as (a decrease from class 1 of the EOTRH):

Cluster Shade, Correlation, ID, IDM, IDMN, IDN, and MCC. For NGTDM, the first criterion (an increase from class 1 of the EOTRH) was passed for the following: Complexity and Strength; as well as (a decrease from class 1 of the EOTRH): Busyness and Coarseness. For GLDM, the first criterion (an increase from class 1 of the EOTRH) was passed for the following: DE, GLV, HGLE, LDHGLE, SDE, and SDHGLE; as well as (a decrease from class 1 of the EOTRH): LDE, LDLGLE, and LGLE. For GLRLM, the first criterion (an increase from class 1 of the EOTRH) was passed for the following: GLV, HGLR, LRHGLR, RLN, RLNN, RP, SRE, and SRHGLE; as well as (a decrease from class 1 of the EOTRH): GLNN, LRLGL, LGLRE, and SRLGLE. Finally, for GLSZM, the first criterion (an increase from class 1 of the EOTRH) was passed for the following: GLV, HGLZE, LALGLE, SZNN, SAE, SAHGLE, SALGLE, ZP, and ZV; as well as (a decrease from class 1 of the EOTRH): GLNN, LALGLE, and LGLZE.

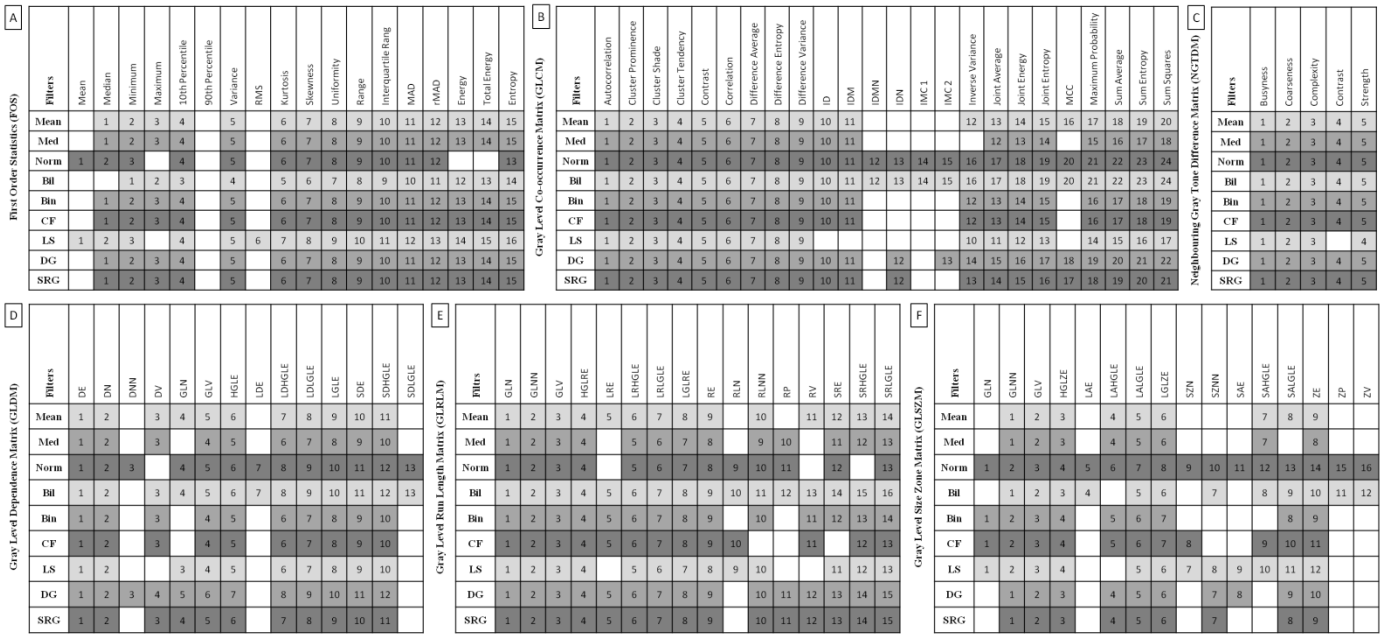

Figure 3. Features of First Order Statistics (FOS, **A**), Gray Level Co-occurrence Matrix (GLCM, **B**), Neighbouring Gray Tone Difference Matrix (NGTDM, **C**), Gray Level Dependence Matrix (GLDM, **D**), Gray Level Run Length Matrix (GLRLM, **E**), and Gray Level Size Zone Matrix (GLSZM, **F**) extracted from examined output images, filtered by Mean, Median (Med), Normalize (Norm), Bilateral (Bil), Binomial (Bin), CurvatureFlow (CF), LaplacianSharpening (LS), DiscreteGaussian (DG), and SmoothingRecursiveGaussian (SRG) filters, found to be significantly different between the Equine odontoclastic tooth resorption and hypercementosis classes (EOTRH 0–3). The number in the cell indicates the number of features in the row that differ between classes.

One may observe that the part of the listed features passed the second criterion (increase or decrease repeatable in each output image data set, regardless of the applied filtering) and thus were considered to clearly correlate with the EOTRH degree. For FOS, the second criterion passed four of the following nine listed features: Variance, Range, Maximum, and Skewness. For GLCM, the second criterion passed 9 of the following 18 listed features: Autocorrelation, Cluster Prominence, Contrast, Difference Average, Difference Entropy, Difference Variance, Joint Average, Sum Average, and Cluster Shade. For NGTDM, the second criterion passed one of the following four listed features: Complexity. For GLDM, the second criterion passed five of the following nine listed features: GLV, HGLE, LDHGLE, LDLGLE, and LGLE. From GLRLM, the second criterion passed 6 of the following 12 listed features: GLV, HGLRE, LRHGLE, GLNN, LRLGLE, and LGLRE. Finally, for GLSZM, the second criterion passed 3 of the following 12 listed features increase: GLV, HGLZE, and GLNN.

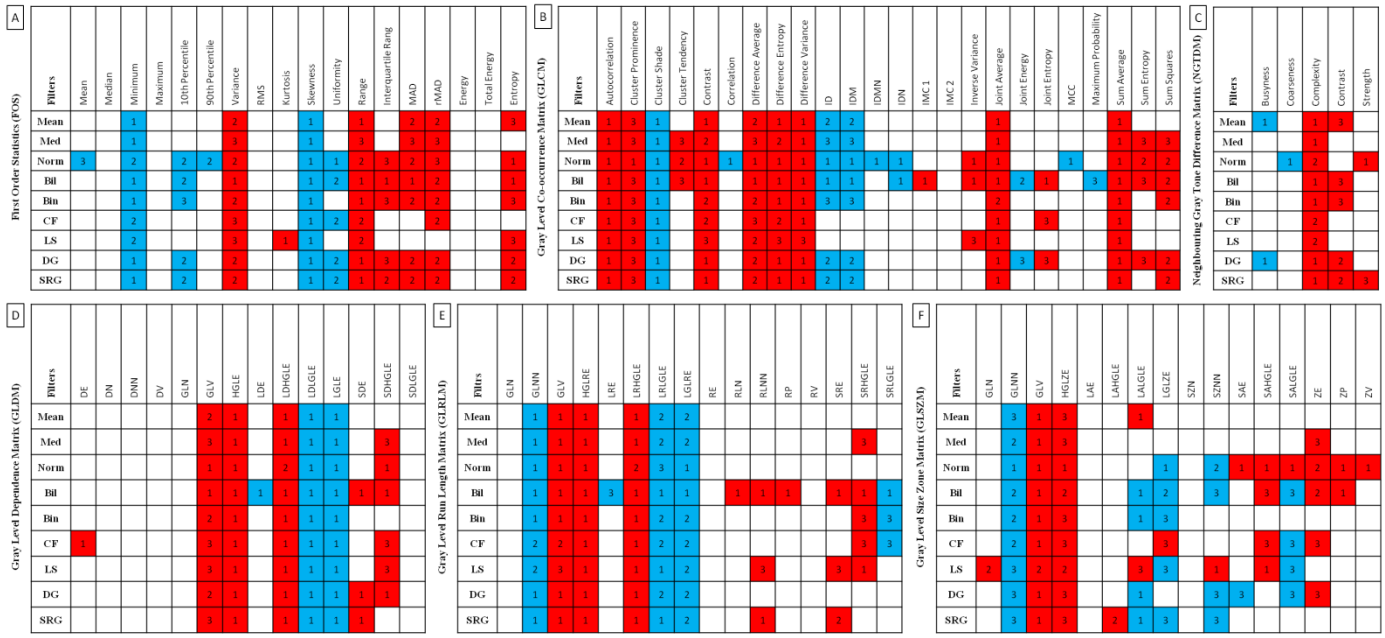

Figure 4. Features of First Order Statistics (FOS, **A**), Gray Level Co-occurrence Matrix (GLCM, **B**), Neighbouring Gray Tone Difference Matrix (NGTDM, **C**), Gray Level Dependence Matrix (GLDM, **D**), Gray Level Run Length Matrix (GLRLM, **E**), and Gray Level Size Zone Matrix (GLSZM, **F**) extracted from examined output images, filtered by Mean, Median (Med), Normalize (Norm), Bilateral (Bil), Binomial (Bin), CurvatureFlow (CF), LaplacianSharpening (LS), DiscreteGaussian (DG), and SmoothingRecursiveGaussian (SRG) filters, found to significantly increase (red cell) or decrease (blue cell) with the degree of the Equine odontoclastic tooth resorption and hypercementosis syndrome (EOTRH 0–3). The number in the cell indicates the degree of EOTRH from which the increase or decrease in the values of the features begins.

Then, the coefficient of variation was used to indicate which understudied texture analysis approaches could be most favorable used in further research for the quantification of radiographic signs of the EOTRH syndrome. The texture features that passed both criteria indicating the EOTRH degree (FOS $n = 4$, GLCM $n = 9$, NGTDM $n = 1$, GLDM $n = 5$, GLRLM $n = 6$, and GLSZM $n = 3$) were marked with the asterisks on the plots in Figure 5. One may observe that the coefficient of variation of the selected features was partially lower and partially higher than the mean value of the feature for the total data set of consecutive texture analysis approaches, marked with the red dashed. For FOS, one feature was lower and three features were higher than the mean coefficient of variation of FOS, and repetitively variable features accounted for 20.2% of all extracted FOS features. For GLCM, four features were lower, and five features were higher than the mean coefficient of variation of GLCM, and repetitively variable features accounted for 37.5% of all extracted GLCM features. For NGTDM, the only one feature was lower than the mean coefficient of variation of NGTDM and accounted for 20.0% of all extracted NGTDM features. For GLDM, three features were lower, and two features were higher than the mean coefficient of variation of GLDM, and repetitively variable features accounted for 35.7% of all extracted GLDM features. For GLRLM, four features were lower and five features were higher than the mean coefficient of variation of GLRLM, and repetitively variable features accounted for 37.5% of all extracted GLRLM features. Finally, for GLSZM, three features were lower than the mean coefficient of variation of GLSZM, and repetitively variable features accounted for 18.8% of all extracted GLSZM features. One may observe that GLCM and GLRLM return the most favorable features for the quantitative evaluation of radiographic signs of the EOTRH syndrome, and thus could be used in further research on the advanced radiographic diagnosis of equine dental diseases.

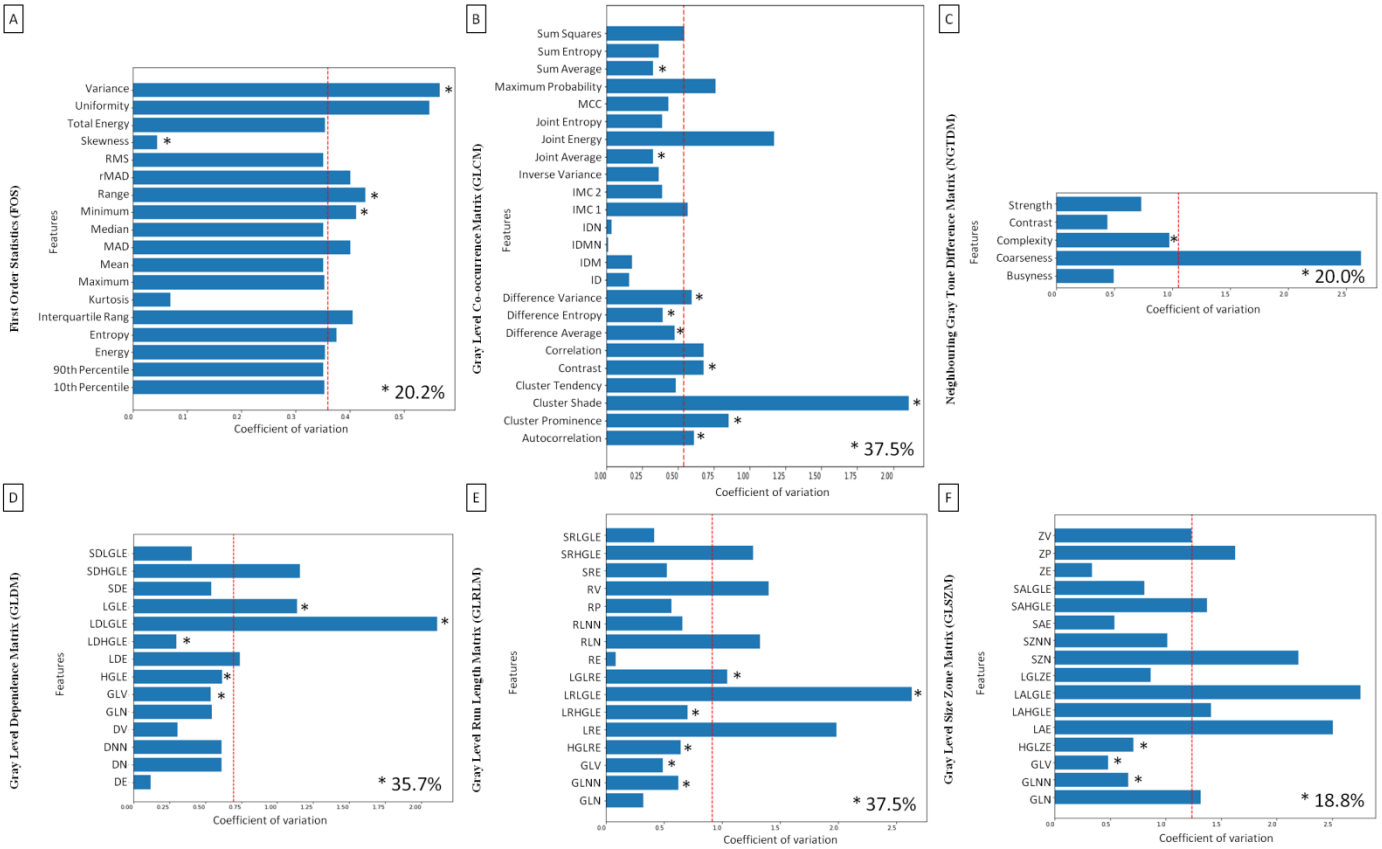

Figure 5. Coefficient of variation for the consecutive features of First Order Statistics (FOS, **A**), Gray Level Co-occurrence Matrix (GLCM, **B**), Neighbouring Gray Tone Difference Matrix (NGTDM, **C**), Gray Level Dependence Matrix (GLDM, **D**), Gray Level Run Length Matrix (GLRLM, **E**), and Gray Level Size Zone Matrix (GLSZM, **F**) including nine filters used. The red dashed line indicates the mean value of the feature for the total data set of consecutive texture analysis approaches. The asterisk indicates the features that differed between Equine odontoclastic tooth resorption and hypercementosis (EOTRH) degree regardless of the filtering used. The percentage of features marked with an asterisk is shown in the right low corner of each plot.

Synthetically summarizing the above results, one may observe that features of GLCM and GLRLM extracted from the output images filtered by the *Normalize* filter are considered to be the best for imaging radiological symptoms of EOTRH. Therefore, the detailed comparisons of these features (Figures 6 and 7) between EOTRH degrees have been presented as an example that can be used in future research.

Among the 24 features of GLCM extracted from the output images filtered by the *Normalize* filter, 16 features passed the first criterion of correlation with the EOTRH degree and increased or decreased from class 1 of the EOTRH: Autocorrelation, Cluster Prominence, Cluster Shade, Contrast, Correlation, Difference Average, Difference Entropy, Difference Variance, ID, IDM, IDMN, IDN, Inverse Variance, Joint Average, MCC, and Sum Average (Figure 6). These GLCM features were considered better than others to quantify the radiographic signs of the EOTRH syndrome.

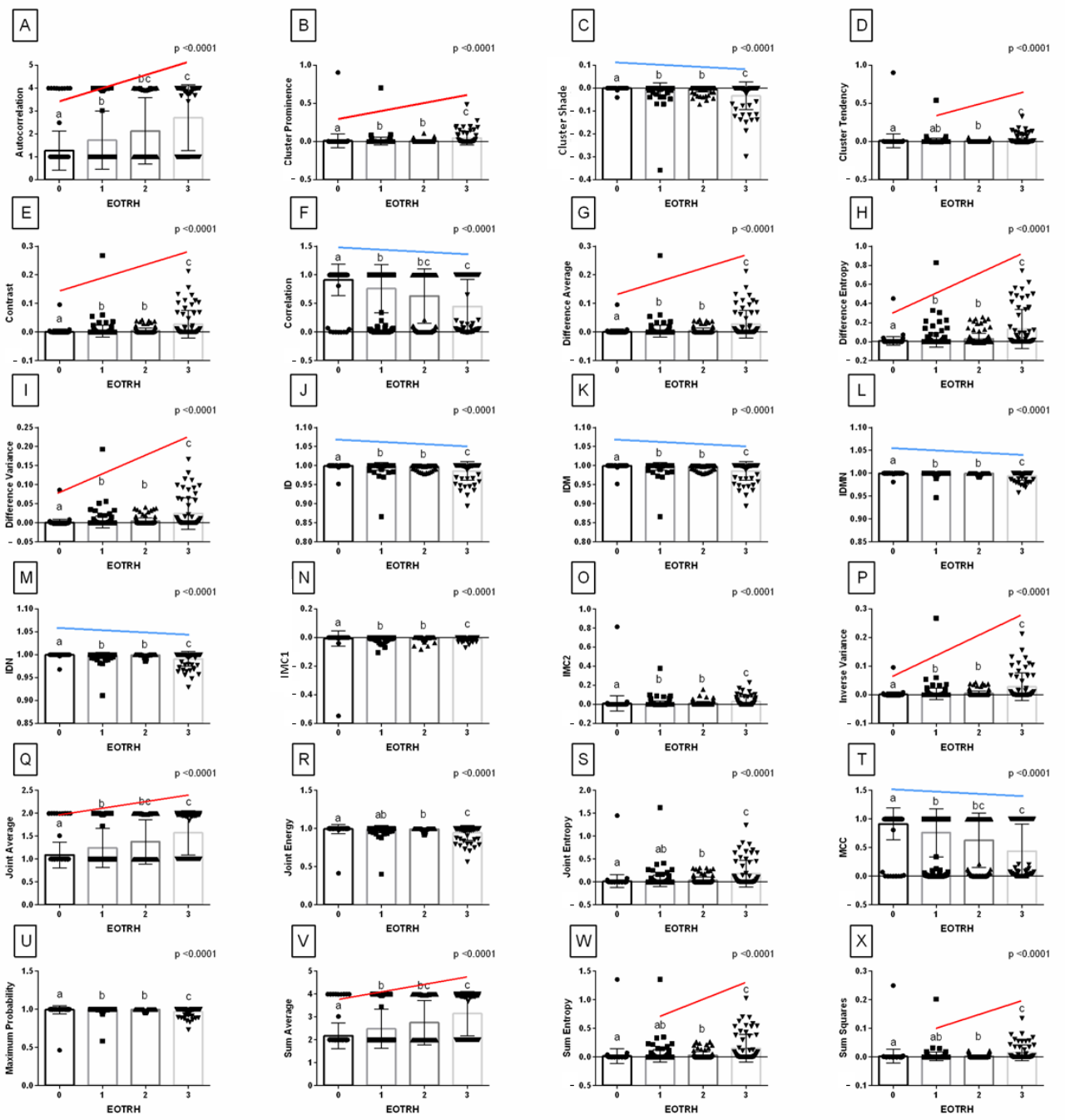

Figure 6. Features (mean ± SD) of *Gray Level Co-occurrence Matrix* (GLCM) extracted from examined output images, filtered by *Normalize* filter compared between the degrees of the Equine odontoclastic tooth resorption and hypercementosis syndrome (EOTRH 0–3). Autocorrelation (**A**), Cluster Prominence (**B**), Cluster Shade (**C**), Cluster Tendency (**D**), Contrast (**E**), Correlation (**F**), Difference Average (**G**), Difference Entropy (**H**), Difference Variance (**I**), Inverse difference (ID, **J**), Inverse Difference Moment (IDM, **K**), Inverse Difference Moment Normalized (IDMN, **L**), Inverse Difference Normalized (IDN, **M**), Informational Measure of Correlation 1 (IMC 1, **N**), Informational Measure of Correlation 2 (IMC 2, **O**), Inverse Variance (**P**), Joint Average (**Q**), Joint Energy (**R**), Joint Entropy (**S**), Maximal Correlation Coefficient (MCC, **T**), Maximum Probability (**U**), Sum Average (**V**), Sum Entropy (**W**), and Sum of Squares (**X**). Lower case letters (a–c) indicate differences between classes for $p < 0.05$ independently for each feature. The significant increase or decrease with the degree of the EOTRH 0–3 is marked with red and blue lines respectively. Single realizations are marked with dots.

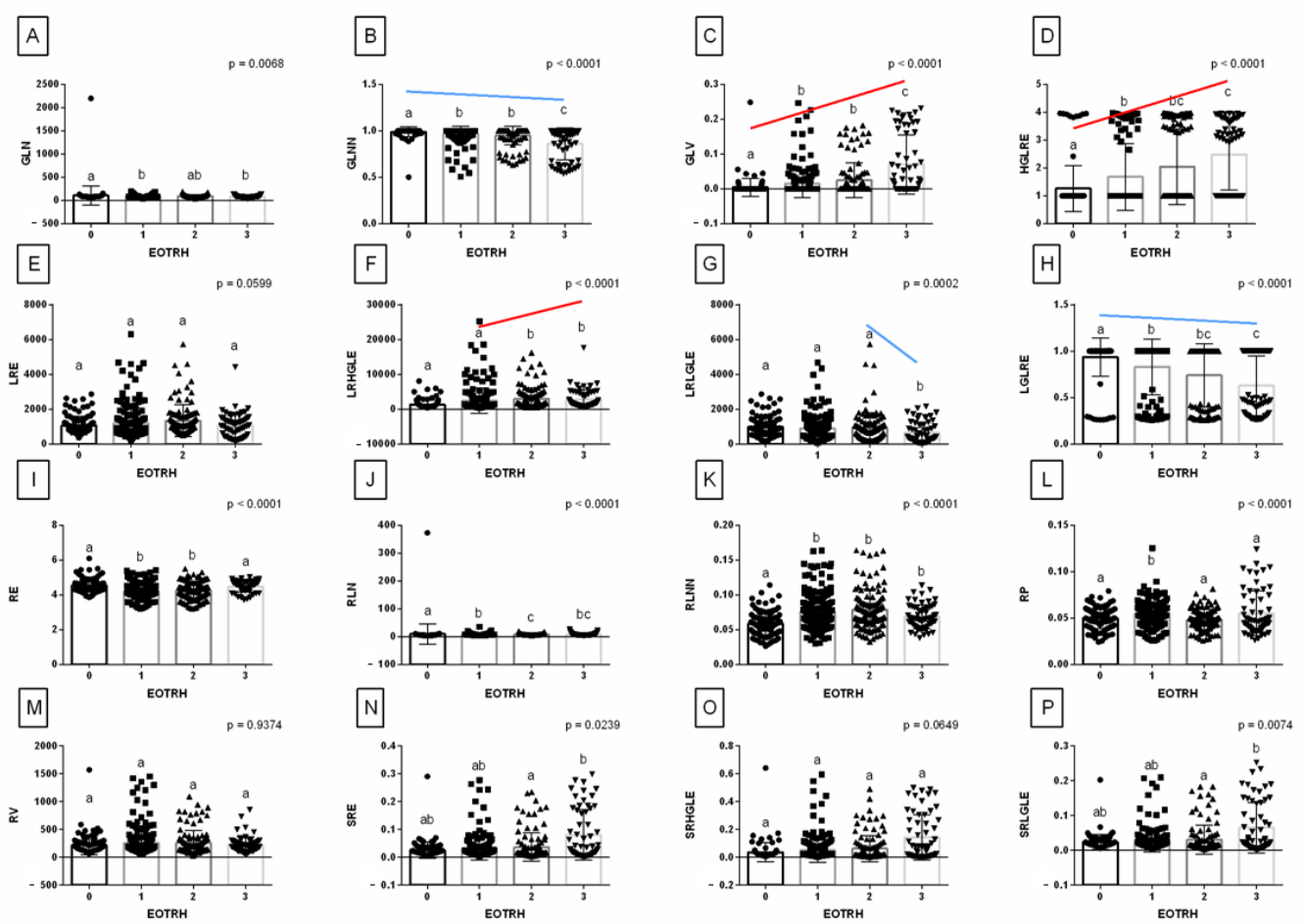

Figure 7. Features (mean ± SD) of *Gray Level Run Length Matrix (GLRLM)* extracted from examined output images, filtered by *Normalize* filter compared between the degrees of the Equine odontoclastic tooth resorption and hypercementosis syndrome (EOTRH 0–3). Gray Level Non-uniformity (GLN, **A**), Gray Level Non-uniformity Normalized (GLNN, **B**), Gray Level Variance (GLV, **C**), High Gray Level Run Emphasis (HGLRE, **D**), Long Run Emphasis (LRE, **E**), Long Run High Gray Level Emphasis (LRHGLE, **F**), Long Run Low Gray Level Emphasis (LRLGLE, **G**), Low Gray Level Run Emphasis (LGLRE, **H**); Run Entropy (RE, **I**), Run Length Non-uniformity (RLN, **J**), Run Length Non-uniformity Normalized (RLNN, **K**), Run Percentage (RP, **L**), Run Variance (RV, **M**), Short Run Emphasis (SRE, **N**), Short Run High Gray Level Emphasis (SRHGLE, **O**), Short Run Low Gray Level Emphasis (SRLGLE, **P**). Lower case letters (a–c) indicate differences between classes for $p < 0.05$ independently for each feature. The significant increase or decrease with the degree of the EOTRH 0–3 is marked with red and blue lines respectively. Single realizations are marked with dots.

Among 16 features of GLRLM extracted from the output images filtered by the *Normalize* filter, the following 4 features passed the first criterion of correlation with the EOTRH degree and increased or decreased from class 1 of the EOTRH: GLNN, GLV, HGLRE, and LGLRE (Figure 8). These GLRLM features were considered better than others to quantify the radiographic signs of the EOTRH syndrome.

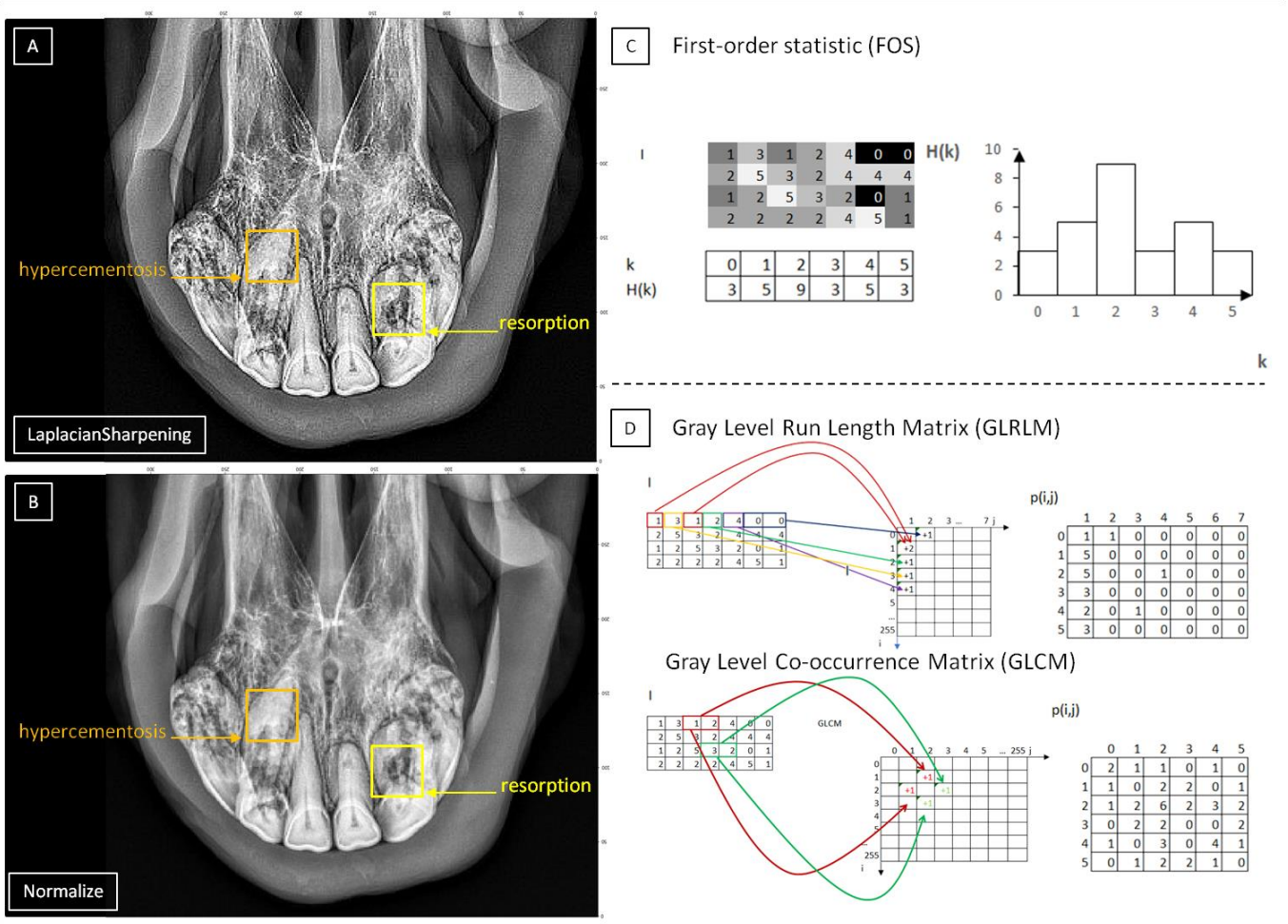

Figure 8. The samples of radiographic images representing severe Equine odontoclastic tooth resorption and hypercementosis (EOTRH 3) syndrome. The output images filtered by *LaplacianSharpening* (**A**) and *Normalize* (**B**) filters with marked signs of resorption (yellow square) and hypercementosis (orange square). The filtered images compiled with diagrams of optimal approaches of texture analysis, the first-order statistic (FOS) for *LaplacianSharpening* filter (**C**) and the second-order statistic for *Normalize* filter (**D**).

4. Discussion

In both studies, the previous [13,16,18,22] and current resorptive lesions of variable degree and mild to severe hypercementosis were radiographically recognized. The impact of the resorption and hypercementosis processes on the texture of the radiological images is visually easily separable [13,18,22]. The tooth resorption process involves the cementum, enamel, dentine, and occasionally the pulp cavity [15], which is visible on the radiological images as a loss of the radiodensity of dental tissue and alveolar bone. Radiographically, the widening of the periodontal ligament space is visible as a radiolucent line and the alveolar bone appears as a delicate radiodense line, which is typical [22]. The hypercementosis reflects the cement accumulation, which often appears as radiopaque bulbous enlargements of the apex of the tooth [59]. In the cases of cement accumulation, the extensive bulbs are created within an increase in density in this place, so the radiological images show mottled radiolucent areas [60]. Thus, we hypothesize that the radiographic signs of the EOTRH syndrome could be successively quantified as the statistical decryptions of the medical digital image give very good results in a large field of applications [24], especially when the textures are visually easily separable [26].

Most features of the second-order statistic (GLCM, NGTDM, GLDM, GLRLM, and GLSZM) differed between the EOTRH classes after filtering by the *Normalize* and *Bilateral*

filters (GLCM, GLDM) or the *Normalize* filter (GLSZM) or the *Bilateral* filter (GLRLM), contrary to the features of first-order statistic (FOS) where they differed least after filtering by *Normalize* filter. On the other hand, the least features of the second-order statistic differed between the EOTRH classes after filtering by the *LaplacianSharpening* filter (GLCM, NGTDM, GLDM, and GLRLM), which was the most differential filter, was just the *LaplacianSharpening* filter. As the *LaplacianSharpening* filter returns output images sharper than the input one [61], this filter appears to be more suitable for the first-order statistic than the second-order one. Interestingly, moreover, the *Normalize* filter increases the contrast of the image [62] and *Bilateral* filter smooths the input image in the homogeneous areas while preserving the edges [63], which seems to be favorable for the second-order statistic (Figure 8).

This other differentiation of the incisor teeth after filtering by various filters may be caused by the characteristics of particular approaches to texture analysis. The FOS examines the pixels that are present in the image, while the GLCM and the other second-order matrices examine the spatial distribution of the pixels [64]. Therefore, when the filter returns the output images after sharpening or improving the contrast, the feature differences will be greater [65,66]. On the contrary, other filters tested in the current study, which returns the output images after noise reduction (*Mean*, *Median,* and *CurvatureFlow* filters), blurring (*Mean* and *DiscreteGaussian* filters), smoothing (*Median, CurvatureFlow*, *DiscreteGaussian,* and *SmoothingRecursiveGaussian* filters), or blur separation (*Binomial* filter) [67]. This means that if the second-order statistical approaches are chosen for the texture analysis of the radiographic image, the use of one or both filters that improve the edge delimitation is advisable, as the other examined filters appear to be less desirable in the quantification of radiographic signs of the EOTRH syndrome.

Concerning the texture features that increase or decrease repeatability regardless of the applied filtering, each applied texture analysis approach returns the specific feature profile. Beginning from the lowest percentage of selected features, GLSZM (18.8%), NGTDM (20.0%), FOS (20.2%), GLDM (35.7%), and equally, GLRLM (37.5%) and GLCM (37.5%) were ranked. For GLSZM, the increase in GLV and HGLZE, as well as the decrease in GLNN with the increase in the EOTRH degree, were noted. Although the GLV indicates the increase in the variance in gray level intensities for the zones [37], the role of the other two features requires further study. HGLZE counts the distribution of lower/higher gray-level size zones together with LGLZE, whereas GLNN measures the variability of gray-level intensity values together with GLN [37]. As LGLZE and GLN did not change repetitively, GLSZM should not be the recommended approach for the quantitative EOTRH evaluation. For NGTDM, only Complexity, the measure of the occurrence of many primitive components in the image [37], increased repetitively. Thus, the NGTDM approach is also difficult to recommend. For FOS, with the increase in the EOTRH degree, the increase in Variance, which is the mean of squared distances between each pixel and the mean value of pixels [37], and the increase in Range, which is the difference between the maximum and minimum values of pixels [37], were noted. Moreover, with the increase in the EOTRH degree, a decrease in the Minimum and Skewness was observed. As the Minimum describes the specific intensity values in the image [37], with its decrease, the increase in Range is justified, especially since no similar differences were found for Maximum, 10th percentile, and 90th percentile, the other indicators of specific intensity. Likewise, the increase in Skewness, which is an indicator of the asymmetry of the distribution of values from the mean value [38], may be related to the Variance increase, as these two features are negatively correlated [37]. Therefore, recommending the FOS approach for the quantitative EOTRH evaluation is also questionable. The pattern of GLDM features appears to be much more reproducible, as the related features increase (HGLE and LDHGLE) and decrease (LGLE and LDLGLE) with the EOTRH degree, respectively. It should be noted that LGLE and HGLE are measures of the distribution of low/high gray level values [38], whereas LDLGLE and LDHGLE are measures the joint distribution of large dependences with low/high gray-level values [37]. Moreover, GLV measuring variance in gray level [37] also increased with the EOTRH degree, which may suggest the diversity of grayscale distribution in the radiographic images [68]

typical for tooth resorption and hypercementosis [13,22,23], which requires further study. A similar, though broader, pattern was represented by GLRLM features, where the related features increased (HGLRE and LRHGLE) and decreased (LGLRE and LRLGLE) with the EOTRH degree, as was shown in the *Normalize* filtered sample of detailed comparisons. It should be noted that LGLRE and HGLRE are measures of the distribution of low/high gray level values [37], whereas LRLGLE and LRHGLE are measures of the joint distribution of long run lengths with low/high gray level values [37]. Moreover, similarly to GLDM, the increase in GLV, measuring of the variance in gray level intensity for the runs [38], and additionally, the decrease in GLNN, measuring the similarity of gray-level intensity values in the image [37], were noted. One may conclude that such a repetition, in GLDM and GLRLM, of similar measures the diversity of grayscale distribution in the radiographic images may be an important direction in the quantification of radiographic signs of the EOTRH syndrome [13,22,23]. For GLCM, with the increase in the EOTRH degree, the increase in Autocorrelation, Cluster Prominence, Contrast, Difference Average, Difference Entropy, Difference Variance, Joint Average, and Sum Average was noted. The most selected features, such as Contrast showing the local intensity variation, Difference Average indicating the relationship between the occurrence of pairs with similar/differing intensity values, Difference Entropy, showing the randomness in neighbourhood intensity value differences, Joint Average, reporting the mean level intensity of the *i* distribution, and Sum Average, measuring the relation between pairs with lower/higher intensity values [37], reflect the intensity of the pixels of the radiographic images. One may observe that not only the intensity measures but also the coarseness (Autocorrelation) and heterogeneity (Difference Variance) measures [37] increased with the EOTRH degree, which may be a promising indicator of changes in the radiographic image caused by tooth resorption and hypercementosis [13,22,23]. However, the role of the skewness/asymmetry/uniformity of the GLCM, reflected by Cluster Prominence and Cluster Shade [37,38], requires further research.

Given the presented volatility of the coefficient of variation and the percentage of the repetitively variable features within the consecutive approaches and their specific patterns, one may state that the selection of the filtering algorithms and texture analysis approaches for the quantification of radiographic signs of the EOTRH syndrome should include GLCM and GLRLM analysis of the output images received after filtering by the *Normalize* or *Bilateral* filters. However, further research is needed to evaluate the usefulness of the texture analysis of radiographic images of equine incisor teeth concerning clinical symptoms such as varying degrees of oral pain, periodontitis, gingivitis, gingival hyperplasia or recession, fistulas, often in combination with a focal subepithelial swelling (referred to as parulis or gum boils), bulbous enlargement of dental structures, tooth mobility, tooth fractures, and missing teeth [13,69,70]. Moreover, the optimal filtering and texture analysis approaches should be established for the detection of other equine tooth diseases and malocclusions such as sharp edges on the cheek teeth, hooks, excessively protruding clinical crowns, excessive transverse ridges, wave mouth, step mouth, diastemata, persistent milk teeth, loose teeth, tooth fractures, angled teeth, periodontitis, caries, oligodontia, polydontia, calculus, tooth deformities, underbite, overbite, erosions or ulcers on the cheek or tongue mucosa, curvature of the incisors, unerupted canines, and wolf teeth [7,10]. However, the computed tomography imaging of a horse's head is preferred to limit the radiological superimposition arising from the anatomical structure of the horse's skull [20], since the diagnostic accuracy of computed tomography of equine cheek teeth is much higher compared with radiography for this disorder [71]. Thus, one may concern with the current two-dimensional imaging and analysis as the preliminary before the further three-dimensional study, as the incisor teeth, unlike the cheek teeth, are easier to visually and radiography assess due to the rostral position [8].

5. Conclusions

The radiographic images of the equine maxillary incisor teeth may be successfully digitally processed using different filtering algorithms and then analyzed by texture features

extraction based on the first- and second-order statistics. Within six studied texture analysis approaches, GLCM and GLRLM return the most favorable features for the quantitative evaluation of radiographic signs of the EOTRH syndrome. Based on the GLCM analysis, one may suggest that the measures of the radiographic image intensity, coarseness, and heterogeneity increase with the EOTRH degree. Moreover, based on the GLRLM analysis, one may observe that the diversity of grayscale distribution reflected by the opposing texture features may reveal the advancement of both the tooth resorption and hypercementosis processes visible on the radiographic images. It is worth noting that the application of GLCM and GLRLM as the most advisable for the quantification of radiographic signs of the EOTRH syndrome may be supported by filtering by filters improving the edge delimitation, such as *Normalize* or *Bilateral* filters.

Supplementary Materials: The following are available online at https://www.mdpi.com/article/10.3390/s22082920/s1. Table S1: The values of features of *First Order Statistics* (FOS) of output images, filtrated by *Mean* filter between four classes of the EOTRH syndrome, Table S2: The values of features of *First Order Statistics* (FOS) of output images, filtrated by *Median* filter between four classes of the EOTRH syndrome, Table S3: The values of features of *First Order Statistics* (FOS) of output images, filtrated by *Normalize* filter between four classes of the EOTRH syndrome, Table S4: The values of features of *First Order Statistics* (FOS) of output images, filtrated by *Bilateral* filter between four classes of the EOTRH syndrome, Table S5: The values of features of *First Order Statistics* (FOS) of output images, filtrated by *Binomial* filter between four classes of the EOTRH syndrome, Table S6: The values of features of *First Order Statistics* (FOS) of output images, filtrated by *CurvatureFlow* filter between four classes of the EOTRH syndrome, Table S7: The values of features of *First Order Statistics* (FOS) of output images, filtrated by *LaplacianSharpening* filter between four classes of the EOTRH syndrome, Table S8: The values of features of *First Order Statistics* (FOS) of output images, filtrated by *DiscreteGaussian* filter between four classes of the EOTRH syndrome, Table S9: The values of features of *First Order Statistics* (FOS) of output images, filtrated by *SmoothingRecursiveGaussian* filter between four classes of the EOTRH syndrome, Table S10: The values of features of *Gray Level Co-occurence Matrix* (GLCM) of output images, filtrated by *Mean* filter between four classes of the EOTRH syndrome, Table S11: The values of features of *Gray Level Co-occurence Matrix* (GLCM) of output images, filtrated by *Median* filter between four classes of the EOTRH syndrome, Table S12: The values of features of *Gray Level Co-occurence Matrix* (GLCM) of output images, filtrated by *Normalize* filter between four classes of the EOTRH syndrome, Table S13: The values of features of *Gray Level Co-occurence Matrix* (GLCM) of output images, filtrated by *Bilateral* filter between four classes of the EOTRH syndrome, Table S14: The values of features of *Gray Level Co-occurence Matrix* (GLCM) of output images, filtrated by *Binomial* filter between four classes of the EOTRH syndrome, Table S15: The values of features of *Gray Level Co-occurence Matrix* (GLCM) of output images, filtrated by *CurvatureFlow* filter between four classes of the EOTRH syndrome, Table S16: The values of features of *Gray Level Co-occurence Matrix* (GLCM) of output images, filtrated by *LaplacianSharpening* filter between four classes of the EOTRH syndrome, Table S17: The values of features of *Gray Level Co-occurence Matrix* (GLCM) of output images, filtrated by *DiscreteGaussian* filter between four classes of the EOTRH syndrome, Table S18: The values of features of *Gray Level Co-occurence Matrix* (GLCM) of output images, filtrated by *SmoothingRecursiveGaussian* filter between four classes of the EOTRH syndrome, Table S19: The values of features of *Neighbouring Gray Tone Difference Matrix* (NGTDM) of output images, filtrated by *Mean* filter between four classes of the EOTRH syndrome, Table S20: The values of features of *Neighbouring Gray Tone Difference Matrix* (NGTDM) of output images, filtrated by *Median* filter between four classes of the EOTRH syndrome, Table S21: The values of features of *Neighbouring Gray Tone Difference Matrix* (NGTDM) of output images, filtrated by *Normalize* filter between four classes of the EOTRH syndrome, Table S22: The values of features of *Neighbouring Gray Tone Difference Matrix* (NGTDM) of output images, filtrated by *Bilateral* filter between four classes of the EOTRH syndrome, Table S23: The values of features of *Neighbouring Gray Tone Difference Matrix* (NGTDM) of output images, filtrated by *Binomial* filter between four classes of the EOTRH syndrome, Table S24: The values of features of *Neighbouring Gray Tone Difference Matrix* (NGTDM) of output images, filtrated by *CurvatureFlow* filter between four classes of the EOTRH syndrome, Table S25: The values of features of *Neighbouring Gray Tone Difference Matrix* (NGTDM) of output images, filtrated by *LaplacianSharpening* filter between four classes of the EOTRH

syndrome, Table S26: The values of features of *Neighbouring Gray Tone Difference Matrix* (NGTDM) of output images, filtrated by *DiscreteGaussian* filter between four classes of the EOTRH syndrome, Table S27: The values of features of *Neighbouring Gray Tone Difference Matrix* (NGTDM) of output images, filtrated by *SmoothingRecursiveGaussian* filter between four classes of the EOTRH syndrome, Table S28: The values of features of *Gray Level Dependence Matrix* (GLDM) of output images, filtrated by *Mean* filter between four classes of the EOTRH syndrome, Table S29: The values of features of *Gray Level Dependence Matrix* (GLDM) of output images, filtrated by *Median* filter between four classes of the EOTRH syndrome, Table S30: The values of features of *Gray Level Dependence Matrix* (GLDM) of output images, filtrated by *Normalize* filter between four classes of the EOTRH syndrome, Table S31: The values of features of *Gray Level Dependence Matrix* (GLDM) of output images, filtrated by *Bilateral* filter between four classes of the EOTRH syndrome, Table S32: The values of features of *Gray Level Dependence Matrix* (GLDM) of output images, filtrated by *Binomial* filter between four classes of the EOTRH syndrome, Table S33: The values of features of *Gray Level Dependence Matrix* (GLDM) of output images, filtrated by *CurvatureFlow* filter between four classes of the EOTRH syndrome, Table S34: The values of features of *Gray Level Dependence Matrix* (GLDM) of output images, filtrated by *LaplacianSharpening* filter between four classes of the EOTRH syndrome, Table S35: The values of features of *Gray Level Dependence Matrix* (GLDM) of output images, filtrated by *DiscreteGaussian* filter between four classes of the EOTRH syndrome, Table S36: The values of features of *Gray Level Dependence Matrix* (GLDM) of output images, filtrated by *SmoothingRecursiveGaussian* filter between four classes of the EOTRH syndrome, Table S37: The values of features of *Gray Level Run Length Matrix* (GLRLM) of output images, filtrated by *Mean* filter between four classes of the EOTRH syndrome, Table S38: The values of features of *Gray Level Run Length Matrix* (GLRLM) of output images, filtrated by *Median* filter between four classes of the EOTRH syndrome, Table S39: The values of features of *Gray Level Run Length Matrix* (GLRLM) of output images, filtrated by *Normalize* filter between four classes of the EOTRH syndrome, Table S40: The values of features of *Gray Level Run Length Matrix* (GLRLM) of output images, filtrated by *Bilateral* filter between four classes of the EOTRH syndrome, Table S41: The values of features of *Gray Level Run Length Matrix* (GLRLM) of output images, filtrated by *Binomial* filter between four classes of the EOTRH syndrome, Table S42: The values of features of *Gray Level Run Length Matrix* (GLRLM) of output images, filtrated by *CurvatureFlow* filter between four classes of the EOTRH syndrome, Table S43: The values of features of *Gray Level Run Length Matrix* (GLRLM) of output images, filtrated by *LaplacianSharpening* filter between four classes of the EOTRH syndrome, Table S44: The values of features of *Gray Level Run Length Matrix* (GLRLM) of output images, filtrated by *DiscreteGaussian* filter between four classes of the EOTRH syndrome, Table S45: The values of features of *Gray Level Run Length Matrix* (GLRLM) of output images, filtrated by *SmoothingRecursiveGaussian* filter between four classes of the EOTRH syndrome, Table S46: The values of features of *Gray Level Size Zone Matrix* (GLSZM) of output images, filtrated by *Mean* filter between four classes of the EOTRH syndrome, Table S47: The values of features of *Gray Level Size Zone Matrix* (GLSZM) of output images, filtrated by *Median* filter between four classes of the EOTRH syndrome, Table S48: The values of features of *Gray Level Size Zone Matrix* (GLSZM) of output images, filtrated by *Normalize* filter between four classes of the EOTRH syndrome, Table S49: The values of features of *Gray Level Size Zone Matrix* (GLSZM) of output images, filtrated by *Bilateral* filter between four classes of the EOTRH syndrome, Table S50: The values of features of *Gray Level Size Zone Matrix* (GLSZM) of output images, filtrated by *Binomial* filter between four classes of the EOTRH syndrome, Table S51: The values of features of *Gray Level Size Zone Matrix* (GLSZM) of output images, filtrated by *CurvatureFlow* filter between four classes of the EOTRH syndrome, Table S52: The values of features of *Gray Level Size Zone Matrix* (GLSZM) of output images, filtrated by *LaplacianSharpening* filter between four classes of the EOTRH syndrome, Table S53: The values of features of *Gray Level Size Zone Matrix* (GLSZM) of output images, filtrated by *DiscreteGaussian* filter between four classes of the EOTRH syndrome, Table S54: The values of features of *Gray Level Size Zone Matrix* (GLSZM) of output images, filtrated by *SmoothingRecursiveGaussian* filter between four classes of the EOTRH syndrome.

Author Contributions: Conceptualization, K.G. and M.D.; methodology, K.G., M.B. and M.D.; software, M.B.; validation, E.S. and I.P.; formal analysis, K.G., M.B. and M.D.; investigation, K.G., M.B., E.S., I.P., B.T., A.B. and M.D.; resources, K.G. and M.B.; data curation, K.G. and M.D.; writing—original draft preparation, K.G., M.B., E.S. and M.D.; writing—review and editing, I.P., B.T. and A.B.; visualization, K.G. and M.D.; supervision, I.P.; project administration, K.G. and M.D.; funding acquisition, K.G. All authors have read and agreed to the published version of the manuscript.

Funding: The study was performed as part of the projects WI/WM-IIB/2/2021 and was partially financed with funds from the Polish Ministry of Science and Higher Education.

Institutional Review Board Statement: The animal protocols used in this work were evaluated and approved by the II Local Ethical Committee on Animal Testing in Warsaw on behalf of the National Ethical Committees on Animal Testing (protocol code WAW2/091/2020 approved on 29 July 2020). They are in accordance with FELASA guidelines and the National law for Laboratory Animal Experimentation (Dz. U. 2015 poz. 266 and 2010-63-EU directive).

Informed Consent Statement: Not applicable.

Data Availability Statement: The data presented in this study are available on request from the corresponding author.

Conflicts of Interest: The authors declare no conflict of interest. The funders had no role in the design of the study; in the collection, analyses, or interpretation of data; in the writing of the manuscript, or in the decision to publish the results.

References

1. Dixon, P.M.; Dacre, I. A review of equine dental disorders. *Vet. J.* **2005**, *169*, 165–187. [CrossRef] [PubMed]
2. Knottenbelt, D.C. The systemic effects of dental disease. In *Equine Dentistry*, 1st ed.; Baker, G.J., Easley, J., Eds.; Elsevier/Saunders: Philadelphia, PA, USA, 1999; pp. 127–138.
3. Kirkland, K.D.; Maretta, S.M.; Inoue, O.J.; Baker, G.J. Survey of equine dental disease and associated oral pathology. In Proceedings of the 40th Annual Convention of the American Association of Equine Practitioners, Lexington, KY, USA, 4–7 December 1994; pp. 119–120.
4. Lowder, M.Q.; Mueller, P.O.E. Dental disease in geriatric horses. *Vet. Clin. North Amer. Equine Pract.* **1998**, *14*, 365–380. [CrossRef]
5. Peters, J.W.E.; de Boer, B.; Broeze-ten, G.B.M.; Broeze, J.; Wiemer, P.; Sterk, T.; Spoormakers, T.J.P. *Survey of Common Dental Abnormalities in 483 Horses in the Netherlands, Proceedings of the American Association of Equine Practitioners-Equine Dentistry Focus Meeting, Indianapolis, IN, USA, 1 August 2006*; AAEP American Association of Equine Practitioners: Indianapolis, IN, USA, 2006.
6. Pimentel, L.F.R.O.; Zopa, A.; Alves, G.E.S.; Amaral, R.F. Equine dental disorders: Review of 607 cases. *Pesqui. Vet. Bras.* **2007**, *27*, 109–110.
7. Dixon, P.M.; Tremaine, W.H.; Pickles, K.; Kuhns, L.; Hawe, C.; McCann, J.; McGorum, B.; Railton, D.I.; Brammer, S. Equine dental disease Part 1: A longterm study of 400 cases: Disorders of incisor, canine and first premolar teeth. *Equine Vet. J.* **1999**, *31*, 369–377. [CrossRef]
8. Dixon, P.M.; Tremaine, W.H.; Pickles, K.; Kuhns, L.; Hawe, C.; McCmn, J.; McGorum, B.C.; Railton, D.I.; Brammer, S. Equine dental disease Part 3: A long term study of 400 case: Disorders of wear, traumatic and idiopathic fractures, tumours and miscellaneous disorders of the cheek teeth. *Equine Vet. J.* **1999**, *32*, 9–18. [CrossRef]
9. Uhlinger, C. Survey of selected dental abnormalities in 233 horses. In Proceedings of the 33rd Annual Meeting of the Association of Equine Practitioners, Lexington, KY, USA, 2 May 1987; pp. 577–583.
10. Wilson, G.J.; Liyou, O.J. Examination of dental charts of horses presented for routine dentistry over a 12 month period. *Austr. Equine Vet.* **2005**, *24*, 79–83.
11. Maslauskas, K.; Tulamo, R.M.; McGowan, T.; Kučinskas, A. A descriptive study of the dentition of Lithuanian heavy-drought horses. *Vet. Ir Zootech.* **2008**, *43*, 62–67.
12. Hole, S.L.; Staszyk, C. Equine odontoclastic tooth resorption and hypercementosis. *Equine Vet. Educ.* **2018**, *30*, 386–391. [CrossRef]
13. Rehrl, S.; Schröder, W.; Müller, C.; Staszyk, C.; Lischer, C. Radiological prevalence of equine odontoclastic tooth resorption and hypercementosis. *Equine Vet. J.* **2018**, *50*, 481–487. [CrossRef]
14. Rawlinson, J.; Carmalt, J.L. Extraction techniques for equine incisor and canine teeth. *Equine Vet. Educ.* **2014**, *26*, 657–671. [CrossRef]
15. Staszyk, C.; Bienert, A.; Kreutzer, R.; Wohlsein, P.; Simhofer, H. Equine odontoclastic tooth resorption and hypercementosis. *Vet. J.* **2008**, *178*, 372–379. [CrossRef] [PubMed]
16. Sykora, S.; Pieber, K.; Simhofer, H.; Hackl, V.; Brodesser, D.; Brandt, S. Isolation of Treponema and Tannerella spp. from equine odontoclastic tooth resorption and hypercementosis related periodontal disease. *Equine Vet. J.* **2014**, *46*, 358–363. [CrossRef] [PubMed]

17. Rahmani, V.H.; Häyinen, L.; Kareinen, I.; Ruohoniemi, M. History, clinical findings and outcome of horses with radiographical signs of equine odontoclastic tooth resorption and hypercementosis. *Vet. Rec.* **2019**, *185*, 730. [CrossRef] [PubMed]
18. Górski, K.; Tremaine, H.; Obrochta, B.; Buczkowska, R.; Turek, B.; Bereznowski, A.; Rakowska, A.; Polkowska, I. EOTRH syndrome in polish half-bred horses-two clinical cases. *J. Equine Vet. Sci.* **2021**, *101*, 103428. [CrossRef]
19. Saccomanno, S.; Passarelli, P.C.B.; Oliva, B.; Grippaudo, C. Comparison between two radiological methods for assessment of tooth root resorption: An in vitro study. *Biomed Res. Int.* **2018**, *2018*, 5152172. [CrossRef]
20. Barrett, M.F.; Easley, J.T. Acquisition and interpretation of radiographs of the equine skull. *Equine Vet. Educ.* **2013**, *25*, 643–652. [CrossRef]
21. Moore, N.T.; Schroeder, W.; Staszyk, C. Equine odontoclastic tooth resorption and hypercementosis affecting all cheek teeth in two horses: Clinical and histopathological findings. *Equine Vet. Educ.* **2016**, *28*, 123–130. [CrossRef]
22. Henry, T.J.; Puchalski, S.M.; Arzi, B.; Kass, P.H.; Verstraete, F.J.M. Radiographic evaluation in clinical practice of the types and stage of incisor tooth resorption and hypercementosis in horses. *Equine Vet. J.* **2016**, *49*, 486–492. [CrossRef]
23. Hüls, I.; Bienert, A.; Staszyk, C. Equine odontoclastic tooth resorption and hyper-cementosis (EOTRH): Röntgenologische und makroskopisch-anatomische Befunde. In Proceedings of the 10. Jahrestagung der Internationalen Gesellschaft zur Funktionsverbesserung der Pferdezähne, Wiesbaden, Germany, 3–4 March 2012.
24. Mohanaiah, P.; Sathyanarayana, P.; GuruKumar, L. Image texture feature extraction using GLCM approach. *Int. J. Sci. Res.* **2013**, *3*, 1–5.
25. Wazarkar, S.; Keshavamurthy, B.N. A survey on image data analysis through clustering techniques for real world applications. *J. Vis. Commun. Image Represent.* **2018**, *55*, 596–626. [CrossRef]
26. Maillard, P. Comparing texture analysis methods through classification. *Photogramm. Eng. Remote Sens.* **2003**, *69*, 357–367. [CrossRef]
27. Sohail, A.S.M.; Bhattacharya, P.; Mudur, S.P.; Krishnamurthy, S. Local relative GLRLM-based texture feature extraction for classifying ultrasound medical images. In Proceedings of the 2011 24th Canadian Conference on Electrical and Computer Engineering (CCECE, IEEE), Niagara Falls, ON, Canada, 8–11 May 2011; pp. 001092–001095.
28. Abdel-Nasser, M.; Moreno, A.; Puig, D. Breast cancer detection in thermal infrared images using representation learning and texture analysis methods. *Electronics* **2019**, *8*, 100. [CrossRef]
29. Bębas, E.; Borowska, M.; Derlatka, M.; Oczeretko, E.; Hładuński, M.; Szumowski, P.; Mojsak, M. Machine-learning-based classification of the histological subtype of non-small-cell lung cancer using MRI texture analysis. *Biomed. Signal. Process. Control.* **2021**, *66*, 102446. [CrossRef]
30. Zhang, H.; Hung, C.L.; Min, G.; Guo, J.P.; Liu, M.; Hu, X. GPU-accelerated GLRLM algorithm for feature extraction of MRI. *Sci. Rep.* **2019**, *9*, 10883. [CrossRef]
31. Raja, J.V.; Khan, M.; Ramachandra, V.K.; Al-Kadi, O. Texture analysis of CT images in the characterization of oral cancers involving buccal mucosa. *Dentomaxillofac. Radiol.* **2012**, *41*, 475–480. [CrossRef]
32. Girejko, G.; Borowska, M.; Szarmach, J. Statistical analysis of radiographic textures illustrating healing process after the guided bone regeneration surgery. In Proceedings of the International Conference on Information Technologies in Biomedicine, Springer (ITIB'2018), Kamień Śląski, Poland, 18–20 June 2018; pp. 217–226.
33. Sangeetha, M.; Kumar, K.; Aljabr, A.A. Image processing techniques in periapical dental X-ray image detection and classification. *Webology* **2021**, *18*, 42–53. [CrossRef]
34. Domino, M.; Borowska, M.; Kozłowska, N.; Zdrojkowski, Ł.; Jasiński, T.; Smyth, G.; Maśko, M. Advances in thermal image analysis for the detection of pregnancy in horses using infrared thermography. *Sensors* **2022**, *22*, 191. [CrossRef]
35. Masko, M.; Borowska, M.; Domino, M.; Jasinski, T.; Zdrojkowski, L.; Gajewski, Z. A novel approach to thermographic images analysis of equine thoracolumbar region: The effect of effort and rider's body weight on structural image complexity. *BMC Vet. Res.* **2021**, *17*, 99. [CrossRef]
36. Domino, M.; Borowska, M.; Kozłowska, N.; Trojakowska, A.; Zdrojkowski, Ł.; Jasiński, T.; Smyth, G.; Maśko, M. Selection of image texture analysis and color model in the advanced image processing of thermal images of horses following exercise. *Animals* **2022**, *12*, 444. [CrossRef]
37. Zwanenburg, A.; Leger, S.; Vallieres, M.; Lock, S. Image biomarker standardisation initiative for image biomarker standardisation initiative. *arXiv* **2016**, arXiv:1612.07003. Available online: https://arxiv.org/abs/1612.07003 (accessed on 12 January 2022).
38. Humeau-Heurtier, A. Texture feature extraction methods: A survey. *IEEE Access* **2019**, *7*, 8975–9000. [CrossRef]
39. Lowekamp, B.C.; Chen, D.T.; Ibáñez, L.; Blezek, D. The design of SimpleITK. *Front. Neuroinform.* **2013**, *7*, 45. [CrossRef] [PubMed]
40. Yaniv, Z.; Lowekamp, B.C.; Johnson, H.J.; Beare, R. SimpleITK image-analysis notebooks: A collaborative environment for education and reproducible research. *J. Digit. Imaging* **2018**, *31*, 290–303. [CrossRef] [PubMed]
41. Belém, M.D.F.; Ambrosano, G.M.B.; Tabchoury, C.P.M.; Ferreira-Santos, R.I.; Haiter-Neto, F. Performance of digital radiography with enhancement filters for the diagnosis of proximal caries. *Braz. Oral Res.* **2013**, *27*, 245–251. [CrossRef] [PubMed]
42. Geetha, V.; Aprameya, K.S. Textural analysis based classification of digital X-ray images for dental caries diagnosis. *Int. J. Eng. Manuf.* **2019**, *9*, 44–45.
43. Floyd, M.R. The modified Triadan system: Nomenclature for veterinary dentistry. *J. Vet. Dent.* **1991**, *8*, 18–19. [CrossRef] [PubMed]

44. Beare, R.; Lowekamp, B.; Yaniv, Z. Image segmentation, registration and characterization in R with SimpleITK. *J. Stat. Soft.* **2018**, *86*, 8. [CrossRef]
45. Lim, J.S. *Two-Dimensional Signal and Image Processing*, 1st ed.; Prentice Hall: Englewood Cliffs, NJ, USA, 1990.
46. Tomasi, C.; Manduchi, R. Bilateral filtering for gray and color images. In Proceedings of the Sixth International Conference on Computer Vision (IEEE Cat. No. 98CH36271), Bombay, India, 7 January 1998; pp. 839–846.
47. Aubury, M.; Luk, W. Binomial filters. *J. VLSI Signal Process. Syst. Signal Image Video Technol.* **1996**, *12*, 35–50. [CrossRef]
48. Sethian, J.A. *Level Set Methods and Fast Marching Methods: Evolving Interfaces in Computational Geometry, Fluid Mechanics, Computer Vision, and Materials Science*, 2nd ed.; Cambridge University Press: Cambridge, UK, 1999; Volume 3.
49. Gonzalez, R.C.; Eddins, S.L.; Woods, R.E. *Digital Image Publishing Using MATLAB*, 1st ed.; Prentice Hall: Upper Saddle River, NJ, USA, 2004.
50. Lindeberg, T. Discrete Scale-Space Theory and the Scale-Space Primal Sketch. Ph.D. Thesis, Department of Numerical Analysis and Computing Science, Royal Institute of Technology, Stockholm, Sweden, 1991.
51. Deriche, R. Recursively implementating the gaussian and its derivatives. In Proceedings of the IEEE International Conference on Image Processing (ICIP), Singapore, 7–11 September 1992; pp. 263–267.
52. van Griethuysen, J.J.M.; Fedorov, A.; Parmar, C.; Hosny, A.; Aucoin, N.; Narayan, V.; Beets-Tan, R.G.H.; Fillon-Robin, J.C.; Pieper, S.; Aerts, H.J.W.L. Computational radiomics system to decode the radiographic phenotype. *Cancer Res.* **2017**, *77*, e104–e107. [CrossRef]
53. Haralick, R.; Shanmugan, K.; Dinstein, I. Textural features for image classification. *IEEE Trans. Syst. Man Cybern.* **1973**, *6*, 610–621. [CrossRef]
54. Amadasun, M.; King, R. Textural features corresponding to textural properties. *IEEE Trans. Syst. Man Cybern.* **1989**, *19*, 1264–1274. [CrossRef]
55. Sun, C.; Wee, W.G. Neighboring gray level dependence matrix for texture classification. *Comput. Vis. Graph. Image Process.* **1983**, *23*, 341–352. [CrossRef]
56. Galloway, M.M. Texture analysis using gray level run lengths. *Comput. Gr. Image Process.* **1975**, *4*, 172–179. [CrossRef]
57. Chu, A.; Sehgal, C.M.; Greenleaf, J.F. Use of gray value distribution of run length for texture analysis. *Pattern Recognit. Lett.* **1990**, *11*, 415–419. [CrossRef]
58. Thibault, G.; Fertil, B.; Navarro, C.; Pereira, S.; Cau, P.; Levy, N.; Sequeira, J.; Mari, J.L. Texture indexes and gray level size zone matrix. application to cell nuclei classification. In Proceedings of the 10th International Conference on Pattern Recognition and Information Processing, PRIP 2009, Minsk, Belarus, 19–21 May 2009; pp. 140–145.
59. Smedley, R.C.; Earley, E.T.; Galloway, S.S.; Baratt, R.M.; Rawlinson, J.E. Equine odon-toclastic tooth resorption and hypercementosis: Histopathologic features. *Vet. Pathol.* **2015**, *52*, 903–909. [CrossRef] [PubMed]
60. Baratt, R. Advances in equine dental radiology. *Vet. Clin. North Am. Equine Pract.* **2013**, *29*, 367–395. [CrossRef] [PubMed]
61. Al-Ameen, Z.; Sulong, G.; Gapar, M.D.; Johar, M.D. Reducing the Gaussian blur artifact from CT medical images by employing a combination of sharpening filters and iterative deblurring algorithms. *J. Theor. Appl. Inf. Technol.* **2012**, *46*, 31–36.
62. Heidari, M.; Mirniaharikandehei, S.; Khuzani, A.Z.; Danala, G.; Qiu, Y.; Zheng, B. Improving the performance of CNN to predict the likelihood of COVID-19 using chest X-ray images with preprocessing algorithms. *Int. J. Med. Inform.* **2020**, *144*, 104284. [CrossRef]
63. Yang, X.; Sechopoulos, I.; Fei, B. Automatic tissue classification for high-resolution breast CT images based on bilateral filtering. *Proc. SPIE* **2011**, *7962*, 79623H.
64. Jusman, Y.; Tamarena, R.I.; Puspita, S.; Saleh, E.; Kanafiah, S.N.A.M. Analysis of features extraction performance to differentiate of dental caries types using gray level co-occurrence matrix algorithm. In Proceedings of the 2020 10th IEEE International Conference on Control System, Computing and Engineering (ICCSCE), Penang, Malaysia, 21–22 August 2020; pp. 148–152.
65. Nagarajan, M.B.; Coan, P.; Huber, M.B.; Diemoz, P.C.; Glaser, C.; Wismüller, A. Computer-aided diagnosis for phase-contrast X-ray computed tomography: Quantitative characterization of human patellar cartilage with high-dimensional geometric features. *J. Digit. Imaging* **2014**, *27*, 98–107. [CrossRef]
66. Kociołek, M.; Strzelecki, M.; Obuchowicz, R. Does image normalization and intensity resolution impact texture classification? *Comput. Med. Imaging Graph.* **2020**, *81*, 101716. [CrossRef] [PubMed]
67. Chandra, T.B.; Verma, K. Analysis of quantum noise-reducing filters on chest X-ray images: A review. *Measurement* **2020**, *153*, 107426. [CrossRef]
68. Alzubaidi, M.A.; Otoom, M. A comprehensive study on feature types for osteoporosis classification in dental panoramic radiographs. *Comput. Methods Programs Biomed.* **2020**, *188*, 105301. [CrossRef] [PubMed]
69. Lorello, O.; Foster, D.L.; Levine, D.G.; Boyle, A.; Engiles, J.; Orsini, J.A. Clinical treatment and prognosis of equine odontoclastic tooth resorption and hypercementosis. *Equine Vet. J.* **2016**, *48*, 188–194. [CrossRef] [PubMed]
70. Earley, E.; Rawlinson, J.T. A new understanding of oral and dental disorders of the equine incisor and canine teeth. *Vet. Clin. North Am. Equine Pract.* **2013**, *29*, 273–300. [CrossRef] [PubMed]
71. Liuti, T.; Smith, S.; Dixon, P.M. Radiographic, computed tomographic, gross pathological and histological findings with suspected apical infection in 32 equine maxillary cheek teeth (2012–2015). *Equine Vet. J.* **2018**, *50*, 41–47. [CrossRef]

biomedicines

MDPI

Article

Application of Two-Dimensional Entropy Measures to Detect the Radiographic Signs of Tooth Resorption and Hypercementosis in an Equine Model

Kamil Górski [1,*], Marta Borowska [2], Elżbieta Stefanik [1], Izabela Polkowska [3], Bernard Turek [1], Andrzej Bereznowski [4] and Małgorzata Domino [1,*]

[1] Department of Large Animal Diseases and Clinic, Institute of Veterinary Medicine, Warsaw University of Life Sciences, 02-787 Warsaw, Poland
[2] Institute of Biomedical Engineering, Faculty of Mechanical Engineering, Białystok University of Technology, 15-351 Bialystok, Poland
[3] Department and Clinic of Animal Surgery, Faculty of Veterinary Medicine, University of Life Sciences, 20-950 Lublin, Poland
[4] Division of Veterinary Epidemiology and Economics, Institute of Veterinary Medicine, Warsaw University of Life Sciences, Nowoursynowska 159c, 02-776 Warsaw, Poland
* Correspondence: kamil_gorski@sggw.edu.pl (K.G.); malgorzata_domino@sggw.edu.pl (M.D.)

Abstract: Dental disorders are a serious health problem in equine medicine, their early recognition benefits the long-term general health of the horse. Most of the initial signs of Equine Odontoclastic Tooth Resorption and Hypercementosis (EOTRH) syndrome concern the alveolar aspect of the teeth, thus, the need for early recognition radiographic imaging. This study is aimed to evaluate the applicability of entropy measures to quantify the radiological signs of tooth resorption and hypercementosis as well as to enhance radiographic image quality in order to facilitate the identification of the signs of EOTRH syndrome. A detailed examination of the oral cavity was performed in eighty horses. Each evaluated incisor tooth was assigned to one of four grade–related EOTRH groups (0–3). Radiographs of the incisor teeth were taken and digitally processed. For each radiograph, two–dimensional sample (SampEn2D), fuzzy (FuzzEn2D), permutation (PermEn2D), dispersion (DispEn2D), and distribution (DistEn2D) entropies were measured after image filtering was performed using Normalize, Median, and LaplacianSharpening filters. Moreover, the similarities between entropy measures and selected Gray–Level Co–occurrence Matrix (GLCM) texture features were investigated. Among the 15 returned measures, DistEn2D was EOTRH grade–related. Moreover, DistEn2D extracted after Normalize filtering was the most informative. The EOTRH grade–related similarity between DistEn2D and Difference Entropy (GLCM) confirms the higher irregularity and complexity of incisor teeth radiographs in advanced EOTRH syndrome, demonstrating the greatest sensitivity (0.50) and specificity (0.95) of EOTRH 3 group detection. An application of DistEn2D to Normalize filtered incisor teeth radiographs enables the identification of the radiological signs of advanced EOTRH with higher accuracy than the previously used entropy–related GLCM texture features.

Keywords: radiographs; texture analysis; entropy–based approaches; equine odontoclastic tooth resorption and hypercementosis; dental care

Citation: Górski, K.; Borowska, M.; Stefanik, E.; Polkowska, I.; Turek, B.; Bereznowski, A.; Domino, M. Application of Two-Dimensional Entropy Measures to Detect the Radiographic Signs of Tooth Resorption and Hypercementosis in an Equine Model. *Biomedicines* **2022**, *10*, 2914. https://doi.org/10.3390/biomedicines10112914

Academic Editors: Gianluca Gambarini, Giuseppe Minervini and Gianmarco Abbadessa

Received: 1 October 2022
Accepted: 11 November 2022
Published: 13 November 2022

1. Introduction

Dental disorders, including complications related to cases of oral cavity disease, constitute a serious health problem in equine medicine [1]. As equine hypsodont teeth slowly erupt over most of the horse's life [2], simple dental rasping is able to improve the welfare and possibly food digestion as well as biting behaviour of more than 70% of horses presenting dental disorders [3]. Thus, dental disorders are of major importance in equine veterinary practice, with up to 10% of practice time involving dental–related work [1].

The current standard of care in equine dentistry includes performing a complete visual oral examination, including general and dental history taking, observation and general physical examination, as well as comprehensive oral and dental examination [4]. However, radiography and possibly other imaging of dental apices and reserve crowns is essential in the evaluation of primary incisor and canine teeth disease affected by resorption and hypercementosis of the reserve crown [5,6], secondary periodontal disease with remodelling and lysis of the alveolar bone [1,7,8], traumatic disorders of teeth [1,9,10], as well as apical infections such as cheek teeth apical abscessation [1,9]. The welfare of the horse depends on skilled and knowledgeable veterinarians who can characterize normal and abnormal findings relative to the oral cavity [4], including frequently occurring dental disorders [1]. Therefore, the digital processing of dental radiographs is proposed here to enhance the quality of the image so that the veterinarians can more easily identify the radiographic signs of disease. As radiography is useful in the diagnosis of tooth resorption and hypercementosis [5,6], bone remodelling and lysis [1,7,8], as well as tooth fractures [1,9,10] and infections [1,9], these preliminary studies focus on the example of Equine Odontoclastic Tooth Resorption and Hypercementosis (EOTRH) syndrome. EOTRH requires radiographic imaging in the early stages to visualize the alveolar aspect of the teeth, where the signs are typically more advanced than is suggestive by the external appearance of the teeth [5,11]. Moreover, the radiographic signs of EOTRH appear earlier than the clinical signs [12–14], as 88% of horses with no apparent clinical signs demonstrated radiographic signs of incisor teeth resorption and 20% of horses demonstrated signs of incisor teeth hypercementosis [5]. Resorption and hypercementosis are two ongoing processes that progressively affect the structure of the tooth starting from the alveolar aspect (root and the reserve crown) [15]. Both processes are radiographically well–defined, as teeth demonstrate high radiodensity [16], where low radiopaque signs of resorption and high radiopaque signs of hypercementosis are alternately visible, thus, presenting the high irregularity and complexity of the image texture of radiographs [17].

The complete visual examination of the oral cavity allows the veterinarian to identify and manage dental problems and diagnose early stages of disease, benefiting the long–term general health of the horse and improving its quality of life [4], whereas the main aim of using digital processing of digital radiographs is to enhance the automated detection of early signs of EOTRH disease that might be missed by solely visual evaluation. Thus, the introduction of digital processing to the equine dental radiographs aims to improve the detection of specific signs of dental diseases which are not recognizable during the preliminary visual examination. It has been shown that raw radiographs collected directly from the X–ray scanner, which have not been digitally processed, are less effective in incisor teeth radiographic texture quantification than those that have been digitally processed. Due to the presence of noise, the radiographic filtering by filters improves the edge delimitation, such as Normalize or Bilateral filters, which increases the recognition of the radiographic signs of EOTRH syndrome [17]. However, the specific detection of grade 1, grade 2, and grade 3 EOTRH radiological signs remains challenging.

With the rapid advances in diagnostic imaging in equine dentistry [17–19], high–resolution detailed digital images [20] as well as a vast and ever–growing amount of data [17] are more readily available. Digital image processing is increasingly used to select and provide diagnostically important data [21] to avoid information noise that is difficult to evaluate. As the development of the computer–aided detection of image differences is a multi–stage process [22,23], the first two steps towards achieving the main goal have already been attained. The first step, concerning the preliminary demonstration of the possibility of quantifying the texture features of horses' incisor radiographs, has been previously published [17]. The second step is presented in this study. This second step concerns the advancement in image regularity evaluation, comparison of the novel and recent image regularity indicators, and demonstration of the detection accuracy of radiographic signs of teeth resorption and hypercementosis in both novel and recent experiments. To achieve this intermediate goal, the two–dimensional entropy measures [24],

which are relatively recent methods of image irregularity and complexity quantification, have been proposed to obtain relevant and insightful data from equine dental radiographs, which could be applied in early EOTRH diagnosis. As entropy–based measurements represent a new class of easy–to–implement methods [25], their evaluation in different types of clinical applications [26] is advisable. In equine medicine, the entropy–based measurements have been successfully applied for the analysis of the texture of equine thermal images in pregnancy determination [27] and the rider:horse body weight ratio detection in horseback riding [28]. In the study examining the pregnancy model, four entropy–based measurements were used [27], however, in the horses' back load assessment model, a fifth measurement was added [28]. These five entropy–based measurements included: two–dimensional sample entropy (SampEn2D) [29], two–dimensional fuzzy entropy (FuzzEn2D) [30], two–dimensional permutation entropy (PermEn2D) [31], two–dimensional dispersion entropy (DispEn2D) [32], and two–dimensional distribution entropy (DistEn2D) [33]. These five aforementioned entropy–based measurements have been implemented in the current study. We hypothesize that the quantitative description of incisor tooth radiographs, by using filtrations and entropy measurement extraction, imply the specific detection of the radiological signs of grade 1, grade 2, and grade 3 EOTRH syndrome, which could be used in the future development of the automated detector of early signs of the disease.

Therefore, the study aimed to evaluate the applicability of entropy measures to quantify the radiological signs of tooth resorption and hypercementosis and to enhance the quality of the radiograph to improve the identification of the radiographic signs of EOTRH syndrome. To achieve this goal, the measures of five entropy–based measurements were extracted from radiographs of equine incisor teeth. Then, combinations of measures and filters were used to identify changes associated with the EOTRH grades. Next, the selected entropy measures and filters were compared with recently reported features of gray–level matrices texture analysis approaches to find similarities. Finally, for the selected measures and features, the detection accuracy of the radiographic signs of EOTRH syndrome was calculated.

2. Materials and Methods

2.1. Horses

Eighty privately owned horses (n = 80) (age mean ± SD: 16.9 ± 7.0; 37 geldings, 43 mares; 30 Polish Halfbred horses, 13 Arabian horses, 10 Schlesisches Warmblood horses, 8 Wielkopolska breed horses, 7 Dutch Warmblood horses, 5 Thoroughbred horses, 4 Polish coldblooded horses, and 3 Malopolska breed horses) were enrolled in the current study. The owners presented their horses for the standard veterinary diagnostic procedure including a basic clinical examination [34], a detailed examination of the oral cavity [35], and an additional examination [5]. In the current study, examination data collected from July 2021 to December 2021 were used.

A basic clinical examination was conducted following standard protocol [34], which allowed for the collection of the internal temperature, heart rate, respiratory rate, mucous membranes, capillary refill time, and lymph node evaluation. After a basic clinical examination–based qualification prior to the sedation procedure, the horses received a dose of detomidine hydrochloride (Domosedan; Orion Corporation, Espoo, Finland; 0.01 mg/kg bwt i.v.), xylazine hydrochloride (Xylapan; Vetoquinol Biowet Sp. z o.o., Gorzów Wielkopolski, Poland; 0.4 mg/kg bwt i.v.), or a combination of both. In some cases, the additional dose of butorphanol tartrate (Torbugesic; Zoetis Polska Sp. z o.o., Warsaw, Poland.; 0.01 mg/kg bwt i.v.) was required. No clinical contraindication to the sedation procedure was found in any of the examined horses.

A detailed examination of the oral cavity was conducted following standard protocol and included a visual examination and digital palpation of the teeth [35]. The Haussmann's mouth speculum was used to ensure the safety of the horse and veterinarian during a detailed examination. A 400 mL syringe was used to flush the oral cavity in order to remove

any food which remained on, around, and between teeth. The periodontal probe was used for the evaluation of the interdental spaces. All clinical signs, including the condition of teeth, interdental spaces, gums, and mucosa of the cheeks and tongue, were documented on the equine dental chart [15] (Figure 1A).

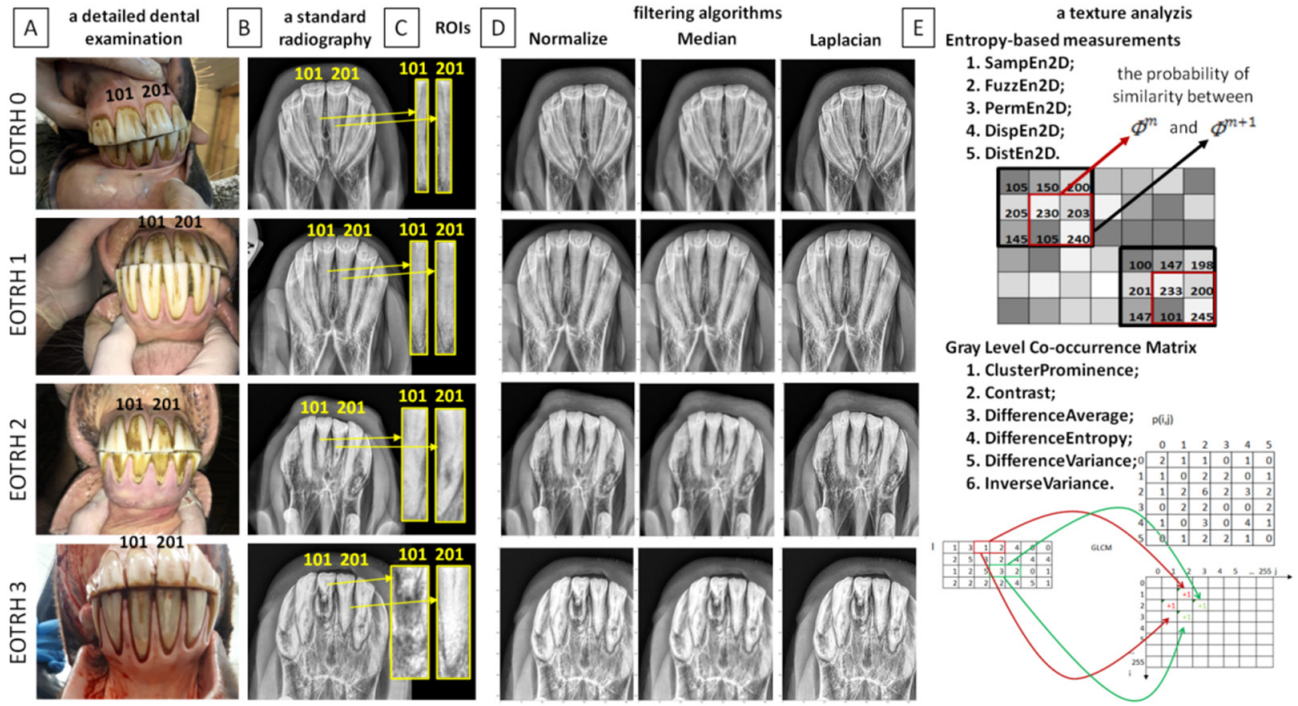

Figure 1. Scheme of radiographic–based detection of the signs of the Equine Odontoclastic Tooth Resorption and Hypercementosis (EOTRH) syndrome. A detailed dental examination (**A**); a standard radiography (**B**); segmentation of input radiographs with regions of interest (ROIs) of the first upper right incisor tooth (101) and the first upper left incisor tooth (201) marked with yellow lines (**C**); filtering of input radiographs by three filters—Normalize, Median, and Laplacian Sharpening (**D**); a texture analysis of output radiographs after filtering using entropy–based measures (five measures: SampEn2D—two–dimensional sample entropy, FuzzEn2D—two–dimensional fuzzy entropy, PermEn2D—two–dimensional permutation entropy, DispEn2D—two–dimensional dispersion entropy, DistEn2D—two–dimensional distribution entropy) and Gray–Level Co–occurrence Matrix (six selected features: Cluster Prominence, Contrast, Difference Average, Difference Entropy, Difference Variance, Inverse Variance) (**E**).

An additional examination allowed for radiography of the incisor teeth [5]. The radiographs were obtained by intraoral presentation, which required insertion of the protected radiographic cassette into the opened oral cavity of the horse, following the guidelines of the bisecting angle technique [13]. The dorsoventral projection for the maxillary teeth [15] was achieved by using the following settings: 2.5 mAs; 65 kV; of the x–ray tube (Orange 9020HF, Ecoray Co., Ltd.; 3F, Urbanlight B/D, 630, Eonju–ro, Gangnam–gu, Seoul, Korea) and the same distance (80 cm) to the radiographic cassette (Saturn 8000, Vievorks Co., Ltd., 41–3, Burim–ro, 170beon–gil, Dongan–gu, Anyang–si, Gyeonggi–do, 14055 Korea. The radiographs were acquired on HP portable computer (HP Inc UK Ltd., Earley West, 300 Thames Valley Park Drive, UK) using DxWorks software (Vievorks Co., Ltd., 41–3, Burim–ro, 170beon–gil, Dongan–gu, Anyang–si, Gyeonggi–do, 14055 Korea) and saved as .jpg files (Figure 1B).

The study was approved by the II Local Ethical Committee on Animal Testing in Warsaw on behalf of the National Ethical Committees on Animal Testing (No WAW2/091/2020 approved on 29 July 2020). The owners agreed to use the horses' data in the current study.

2.2. Radiographs Classification

Based on the clinical and radiological signs achieved from the standard veterinary diagnostic procedure, four grade–related EOTRH groups (0–3) were annotated. The radiological classification system introduced by Hüls et al. [36] and modified by Rehl et al. [5] was used. This classification system includes the evaluation of shape, surface structure, contour, and consistency of incisor teeth as well as contour, radiodensity, and delineation of the periodontal space of incisor teeth. As the preliminary application of two–dimensional entropy measures in the radiographic–based detection of the signs of EOTRH syndrome was tested, the central maxillary incisor teeth showing the best presentation in the radiographs obtained in the dorsoventral projection and the lowest superimposition of rounding tissues, were selected for testing. Following the modified Triadan system for equine dental nomenclature [37], the test incisor teeth were numbered as 101 (the first upper right incisor tooth) and 201 (the first upper left incisor tooth). On each selected incisor tooth, the representative rectangular region of interest (ROI) was manually annotated. Each ROI covers the largest possible area of the tooth crown and the largest possible area of the tooth root. Each ROI was individually fitted to the consecutive, separate teeth as shown on Figure 1C. Each ROI was edged by four high–radiodensity lines representing: (i) the occlusal side of the incisor tooth, (ii) the medial side of the incisor tooth, (iii) the apical side of the incisor tooth, and (iv) the lateral side of the incisor tooth, respectively. The ROIs were annotated using the ImageJ software version 1.46r (Wayne Rasband, National Institutes of Mental Health, Bethesda, MD, USA) and saved as .png files.

Based on above criteria, 101 and 201 maxillary incisor teeth were classified to grade 0 (normal teeth; $n = 37$), grade 1 (mildly EOTRH affected teeth; $n = 94$), grade 2 (moderately EOTRH affected teeth; $n = 20$), and grade 3 (severely EOTRH affected teeth; $n = 8$). The total number of incisors for all groups was 159; as 1 incisor was excluded due to tooth fractures.

2.3. Digital Radiograph Processing

Radiographs were digitally processed in two steps including input image filtering (Figure 1D) and output image texture analysis (Figure 1E). For the image filtering, three filtering algorithms were chosen: Normalize, Median, and Laplacian Sharpening based on the previously described findings of equine incisor teeth radiographs evaluation [17]. For the image texture analysis, five entropy–based texture measures were considered: two–dimensional sample entropy (SampEn2D), two–dimensional fuzzy entropy (FuzzEn2D), two–dimensional permutation entropy (PermEn2D), two–dimensional dispersion entropy (DispEn2D), and two–dimensional distribution entropy (DistEn2D), based on the previously described applicability in the equine image evaluation [27,28]. Both processing steps were conducted one after the other for the annotated ROIs, so that for each ROI, fifteen filtering–entropy combinations were returned. Each ROI was considered separately. Additionally, the currently presented entropy–based texture measures were compared with the selected, previously reported Gray–Level Co–occurrence Matrix data [17].

One may observe in Górski et al. [17] that the data from the combination of nine filtering algorithms (Mean, Median, Normalize, Bilateral, Binomial, Curvature Flow, Laplacian Sharpening, Discrete Gaussian, and Smoothing Recursive Gaussian) and six texture analysis approaches (First Order Statistics (FOS), Gray–Level Co–occurrence Matrix (GLCM), Neighbouring Gray Tone Difference Matrix (NGTDM), Gray–Level Dependence Matrix (GLDM), Gray–Level Run Length Matrix (GLRLM), and Gray–Level Size Zone Matrix (GLSZM) were returned using PyRadiomics—an open–source python package for the extraction of features from radiographic images [38]—and presented in relation to the radiological signs of EOTRH syndrome grades. The raw data of six selected GLCM features selected in a previous study [17] (Cluster Prominence, Contrast, Difference Average, Difference Entropy, Difference Variance, Inverse Variance) were used in the current study to find similarities with the current raw data of entropy–based texture measures. For the details of the protocol of GLCM features extraction, see Górski et al. [17].

2.3.1. Filtering

Three filtering algorithms were implemented to reduce the noise in the radiographs using SimpleITK toolkit in Python language [39,40]. The used filtering algorithms differ depending on the linearity of the filter, type of output image, and result of filtering, as shown in Table 1.

Table 1. The comparison of details (linearity of the filter, type of output image, and result of filtering) of three filtering algorithms (Normalize filter, Median filter, and Laplacian Sharpening filter) used in the study.

Filter	Linearity	Output Image	Result
Normalize filter [41]	Linear filter	A rescaled image in which the pixels have zero mean and unit variance	An increase in the contrast of the image
Median filter [41]	Non–linear filter	A recalculated image in which the pixels are represented by the medians of the pixels in the neighbourhood of the input pixel	A reduction in the noise
Laplacian Sharpening filter [42]	Non–linear filter	A produced image in which the pixels are convoluted with a Laplacian operator	A change of the regions of rapid intensity and highlights the edges

2.3.2. Extraction of the Entropy–Based Measures

The five entropy–based texture analyses were conducted separately, returning five entropy measures, using Python, version 3.8.5 64–bit using package EntopyHub [43]. The extracted entropy measures differed depending, i.e., on the definition, relations between the values and the irregularity/complexity of the image, and application of measures, as shown in Table 2. For more details and equations of the entropy measures extraction, see Domino et al. [28].

2.4. Statistical Analysis

Five entropy measures (SampEn2D, FuzzEn2D, PermEn2D, DispEn2D, DistEn2D) and six selected GLCM features (Cluster Prominence, Contrast, Difference Average, Difference Entropy, Difference Variance, Inverse Variance) were presented as a data series, where each tooth of each horse represented one realization. The entire data set was divided into four EOTRH grade–related groups, thus, four EOTRH grade–labelled data series were extracted. The extracted data series were tested independently for univariate distributions using a Shapiro–Wilk normality test.

EOTRH grade–labelled data series were then compared between EOTRH grades using the ordinary one–way ANOVA followed by Tukey's multiple comparisons test for Gaussian data and the Kruskal–Wallis test, followed by the Dunn's multiple comparisons test for non–Gaussian data, and for each entropy measure and GLCM feature independently. The alpha value was established as $\alpha = 0.05$. On the respective plot, when a measure value was found to significantly increase with the EOTRH grades, the red line was additionally marked. The entropy measures and GLCM features were presented on scatter plots with bars using mean $\pm$ SD and dots representing each realization, where lower case letters indicate differences between EOTRH grades.

EOTRH grade–labelled data series were then compared between used filtering algorithms using the ordinary one–way ANOVA followed, by Tukey's multiple comparisons test for Gaussian data and the Kruskal–Wallis test, followed by the Dunn's multiple comparisons test for non–Gaussian data, and for each entropy measure and GLCM feature independently. The alpha value was established as $\alpha = 0.05$. The entropy measures and GLCM features were presented on scatter plots with bars using mean $\pm$ SD and dots representing each realization, where lower case letters indicate differences between filtering algorithms.

Table 2. The comparison of details (definition, relations between the values and the irregularity/complexity of the image, and application of measures) of five entropy measures (SampEn2D, FuzzEn2D, PermEn2D, DispEn2D, DistEn2D) used in the study.

Entropy Measures	Definition	Values	Application
SampEn2D [29,44]	The negative natural logarithm of the probability of similarity of patterns of length m with patterns of length $m + 1$ $$\text{SampEn2D} = -\ln \frac{\Phi^{m+1}}{\Phi^{m}}$$	Low: regular patterns or periodic structures, as they have the same number of patterns for both m and $m + 1$ High: irregular patterns	A measure of the irregularity in the pixel patterns
FuzzEn2D [30,45]	The negative natural logarithm of the conditional probability $$\text{FuzzyEn2D} = -\ln \frac{\Phi^{m+1}(r)}{\Phi^{m}(r)}$$	Low: regular patterns or periodic structures High: irregular patterns or non-periodic structures	A measure of the irregularity in pixel patterns but using a continuous exponential function to determine the degree of similarity
PermEn2D [31,46]	The concept of counting permutation patterns π, where the permutation patterns are obtained after ordering the positions of the initial image patterns $$\text{PermEn2D} = -\frac{1}{(n-d_n+1)(m-d_m+1)} \sum_{\pi=1}^{d_n!\times d_m!} p(\pi)\ln p(\pi)$$	Low: regular patterns with the pixels always appearing in the same order High: irregular patterns with the highly disordered image pixels	An identification of irregular structure of the image
DispEn2D [32,45]	The conception of using the sigmoid function relies on mapped to c classes and the values of image pixels form $z_{i,j}^{c} = round(c \times v(i,j) + 0.5)$, where $v(i,j)$ $$\text{DispEn2D} = -\frac{1}{(n-d_n+1)(m-d_m+1)} \sum_{\pi=1}^{d_n!\times d_m!} p(\pi_v)\ln p(\pi_v)$$	Low: regular patterns with the low probability of dispersion patterns High: irregular image with the high probability of dispersion patterns	An assessment of the regularity of images with no indeterminacy of small–sized images
DistEn2D [33,47]	The amount of similarity between two windows by measuring the distance between the corresponding windows based on the distance matrix used to estimate the empirical probability density function $(ePDF)$ $$\text{DistEn2D} = -\sum_{t=1}^{M} p_t log_2(p_t)$$	Low: regular patterns of the small size images High: irregular patterns of the small size images	A quantitative description of the irregularities of the images, taking into account the small size of the image

SampEn2D—two–dimensional sample entropy; FuzzEn2D—two–dimensional fuzzy entropy; PermEn2D—two–dimensional permutation entropy; DispEn2D—two–dimensional dispersion entropy; DistEn2D—two–dimensional distribution entropy.

Based on the received differences, only for the most EOTRH–related entropy measures and GLCM features were linear regressions calculated. On regression plots, two regression equations were displayed, including one selected entropy measure and one for Cluster Prominence, Contrast, Difference Average, Difference Entropy, Difference Variance, or Inverse Variance. Equations were supported with the measure of the difference of linearity. All the slopes were significantly non–zero ($p < 0.0001$). For non–significant differences between the slopes ($p > 0.05$), one slope was calculated and the intercepts were compared. For non–significant differences between the intercepts ($p > 0.05$), one intercept was calculated. When the slope value of the entropy measure was higher than the slope value of the GLCM features, the plot was additionally marked by dashed frames. GraphPad Prism6 software (GraphPad Software Inc., San Diego, CA, USA) was used for all statistical analyses.

Based on the received differences, for the most EOTRH–related entropy measures and GLCM features only, the detection accuracy of EOTRH 0 and EOTRH 3 was calculated using three thresholds for gradually increasing measures (mean, mean + SD, mean + 2SD). The radiograph was annotated as EOTRH 0 when the individually measured value was above the threshold and annotated as EOTRH 3 when below it. The same annotation was carried out for the both EOTRH grade–related groups. The sensitivity (Se), specificity (Sp), positive predictive value (PPV), and negative predictive value (NPV) were estimated. The values of Se, Sp, PPV, and NPV were calculated across the range from 0.1 to 1.0 using standard formulae [48].

3. Results

Among the 15 returned combinations of entropy measures ($n = 5$) and filtering algorithms ($n = 3$), three entropy measures for Normalize filtering output radiographs, four entropy measures for Median filtering output radiographs, and two entropy measures for Laplacian Sharpening filtering output radiographs differed significantly between the EOTRH grades (Figure 2). Although some EOTRH grade–related differences were noted for SampEn2D (Normalize filtering, $p = 0.0009$, Figure 2A and Median filtering, $p < 0.0001$, Figure 2F), FuzzEn2D (Normalize filtering, $p = 0.002$, Figure 2B; Median filtering, $p < 0.0001$, Figure 2G; and Laplacian Sharpening filtering, $p = 0.0014$, Figure 2L), and PermEn2D (Median filtering, $p = 0.005$, Figure 2H), only DistEn2D significantly increased with the EOTRH grades. DistEn2D extracted from the Normalize filtering output radiographs was the lowest in the EOTRH 0 group, higher in the EOTRH 1 and 2 groups, and the highest in the EOTRH 3 group, with no differences between the EOTRH 1 and 2 groups ($p < 0.0001$, Figure 2E). DistEn2D extracted from the Median filtering output radiographs was lower in the EOTRH 0 group compared to the EOTRH 3 group, with no differences between the EOTRH 0–2 groups and EOTRH 2–3 groups ($p < 0.0001$, Figure 2J). DistEn2D extracted from Laplacian Sharpening filtering output radiographs was lower in the EOTRH 0 group compared to EOTRH 1–3 groups with no differences between EOTRH 1–3 groups ($p < 0.0001$, Figure 2O). The significance of this step was to extract entropy–based measurements from the radiographs of equine incisor teeth, and select those combinations of measures and filters that changed with the EOTRH grades.

When comparing entropy measures between the filtering algorithms, the same differences in consecutive EOTRH groups were noted for SampEn2D ($p < 0.0001$, Figure 3A,F,K,P), FuzzEn2D ($p < 0.0001$, Figure 3B,G,L,Q), PermEn2D ($p < 0.0001$, Figure 3C,H,M,R), and DistEn2D ($p < 0.0001$, Figure 3E,J,O,T), respectively, but not for DispEn2D ($p > 0.05$, Figure 3D,I,N,S). In each EOTRH group, SampEn2D and FuzzEn2D were always the lowest after Median filtering, higher after Normalize filtering, and the highest after Laplacian Sharpening filtering. Similarly, in each EOTRH group, PermEn2D was higher after Median filtering than after Normalize and Laplacian Sharpening filtering, whereas DistEn2D was higher after Laplacian Sharpening filtering than after Normalize and Median filtering. This step demonstrates how the use of filtering algorithms affects the values of the entropy–based measurements received from the consecutive EOTRH groups.

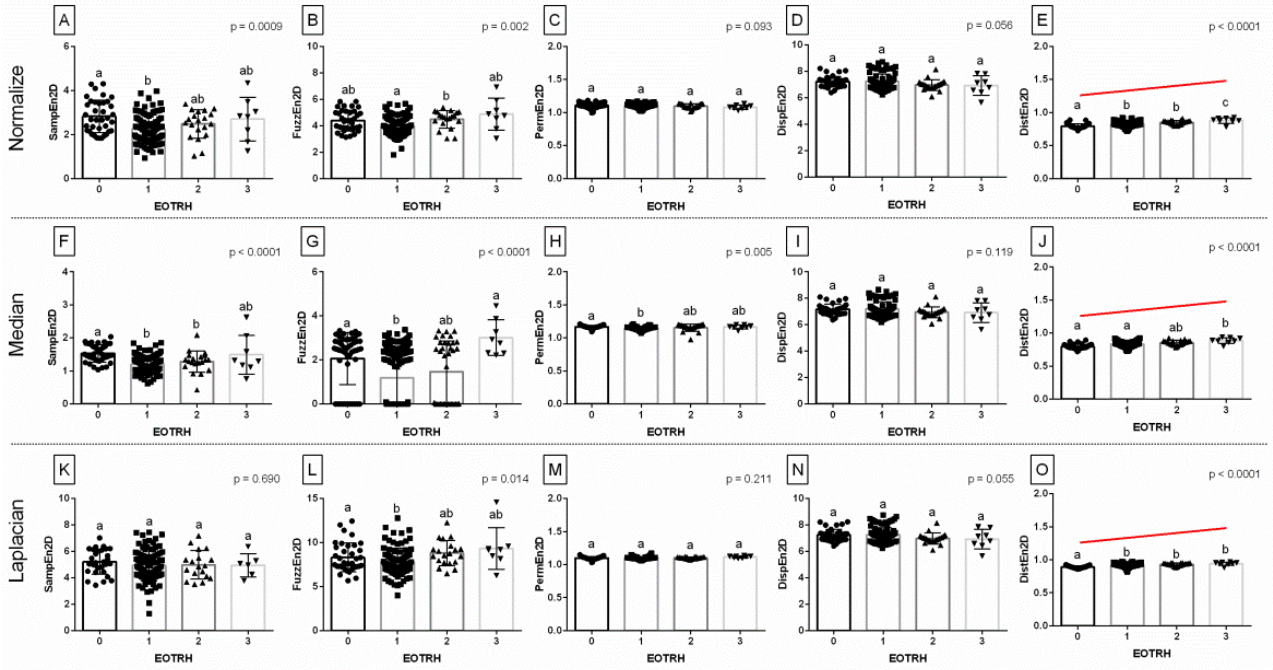

Figure 2. The comparison of the entropy measures between the EOTRH grades (0–3). The following entropy measures are considered: SampEn2D—two–dimensional sample entropy (**A**,**F**,**K**), FuzzEn2D—two–dimensional fuzzy entropy (**B**,**G**,**L**), PermEn2D—two–dimensional permutation entropy (**C**,**H**,**M**), DispEn2D—two–dimensional dispersion entropy (**D**,**I**,**N**), DistEn2D—two–dimensional distribution entropy (**E**,**J**,**O**). The output radiographs filtered by Normalize (**A**–**E**), Median (**F**–**J**), and Laplacian Sharpening (**K**–**O**) filtering algorithms are separated by dashed horizontal lines. Lower case letters (a–c) indicate differences between groups for $p < 0.05$ independently for each measure. The significant increase with the EOTRH grades is marked with a red line. Single realizations are marked with dots.

Among the 18 returned combinations of selected GLCM features ($n = 6$) and filtering algorithms ($n = 3$), all combinations differed significantly between the EOTRH grades and significantly increased with the EOTRH grades (Figure 4). Although some EOTRH grade–related increases were found between EOTRH 0 and 1 groups (Difference Variance after Median filtering, $p < 0.0001$, Figure 4K), between EOTRH 2 and 3 groups (Cluster Prominence after Median filtering, $p < 0.0001$, Figure 4G and Laplacian Sharpening filtering, $p < 0.0001$, Figure 4M; Contrast after Laplacian Sharpening filtering, $p = 0.010$, Figure 4N; Difference Average after Median filtering, $p = 0.004$, Figure 4I and Laplacian Sharpening filtering, $p = 0.029$, Figure 4O; Difference Entropy after Laplacian Sharpening filtering, $p = 0.006$, Figure 4P; Difference Variance after Laplacian Sharpening filtering, $p = 0.0009$, Figure 4Q; Inverse Variance after Median filtering, $p = 0.018$, Figure 4L and Laplacian Sharpening filtering, $p = 0.002$, Figure 4R), and EOTRH 1 and 3 groups (Contrast after Median filtering, $p = 0.0009$, Figure 4H; Difference Entropy after Median filtering, $p = 0.0002$, Figure 4J), all GLCM features significantly increased with the EOTRH grades from EOTRH 0 to 3 after Normalize filtering ($p < 0.0001$, Figure 4A–F). All examined GLCM features extracted from Normalize filtering output radiographs were the lowest in the EOTRH 0 group, higher in the EOTRH 1 and 2 groups, and the highest in the EOTRH 3 group, with no differences between the EOTRH 1 and 2 groups ($p < 0.0001$, Figure 4A–F). This step extracted the GLCM features from the radiographs of equine incisor teeth, and selected those combinations of features and filters that changed with each EOTRH grade.

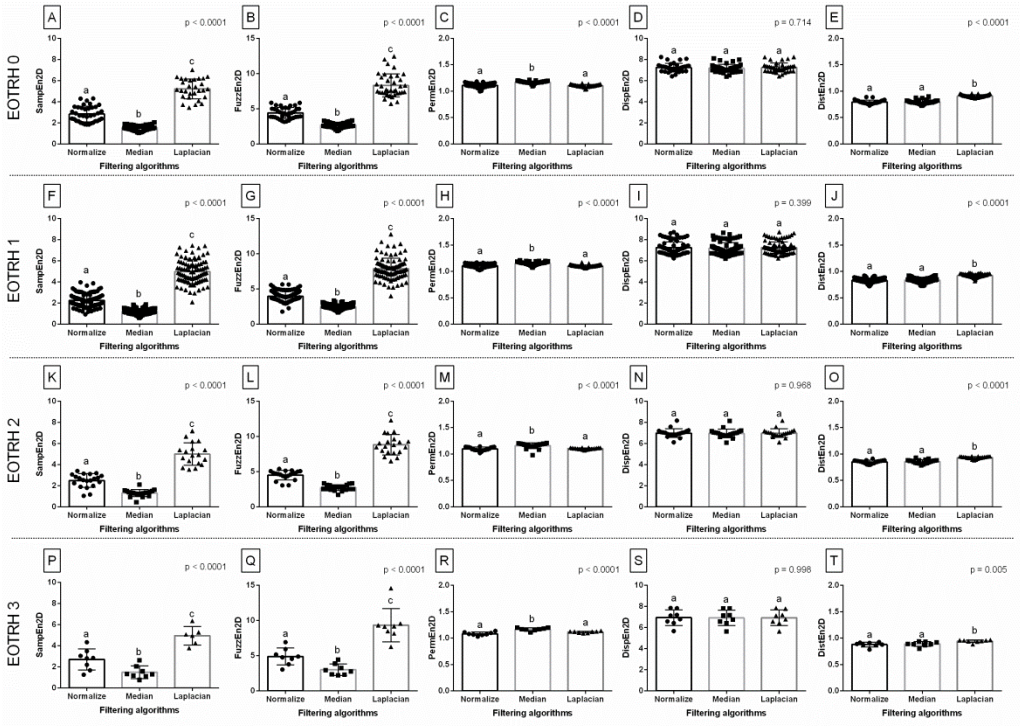

Figure 3. The comparison of the entropy measures between the filtering algorithms. The following entropy measures are considered: SampEn2D—two–dimensional sample entropy (**A**,**F**,**K**,**P**), FuzzEn2D—two–dimensional fuzzy entropy (**B**,**G**,**L**,**Q**), PermEn2D—two–dimensional permutation entropy (**C**,**H**,**M**,**R**), DispEn2D—two–dimensional dispersion entropy (**D**,**I**,**N**,**S**), DistEn2D—two–dimensional distribution entropy (**E**,**J**,**O**,**T**). The radiographs classified to EOTRH 0 grade (**A**–**E**), EOTRH 1 grade (**F**–**J**), EOTRH 2 grade (**K**–**O**), and EOTRH 3 grade (**P**–**T**) are separated by dashed horizontal lines. Lower case letters (a–c) indicate differences between groups for $p < 0.05$ independently for each measure. Single realizations are marked with dots.

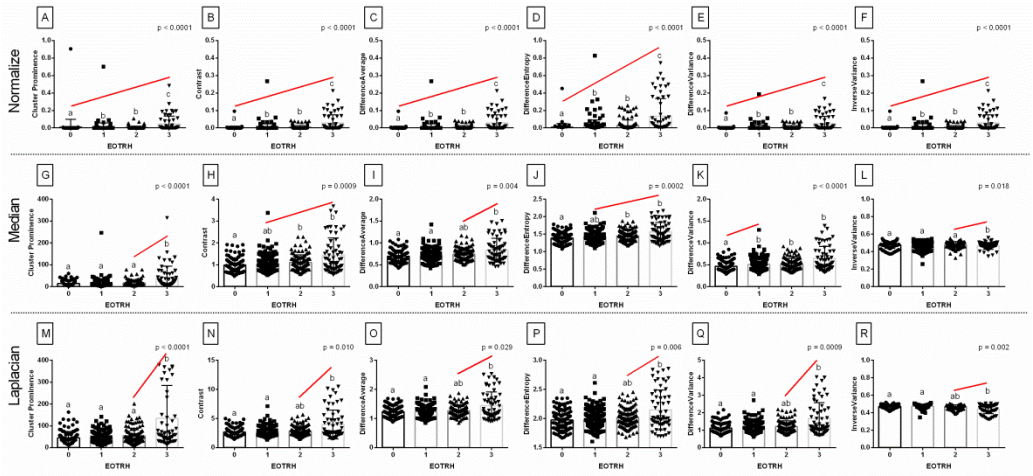

Figure 4. The comparison of the selected Gray–Level Co–occurrence Matrix (GLCM) features between the EOTRH grades (0–3). The following GLCM features are considered: Cluster Prominence (**A**,**G**,**M**), Contrast (**B**,**H**,**N**), Difference Average (**C**,**I**,**O**), Difference Entropy (**D**,**J**,**P**), Difference Variance (**E**,**K**,**Q**), Inverse Variance (**F**,**L**,**R**). The output radiographs filtered by Normalize (**A**–**F**), Median (**G**–**L**), and Laplacian Sharpening (**M**–**R**) filtering algorithms are separated by dashed horizontal lines. Lower case letters (a–c) indicate differences between groups for $p < 0.05$ independently for each feature. The significant increase with the EOTRH grades is marked with a red line. Single realizations are marked with dots.

When comparing selected GLCM features between the filtering algorithms, the same differences in consecutive EOTRH groups were noted for Cluster Prominence ($p < 0.0001$, Figure 5A,G,M,S), Contrast ($p < 0.0001$, Figure 5B,H,N,T), Difference Average ($p < 0.0001$, Figure 5C,I,O,U), Difference Entropy ($p < 0.0001$, Figure 5D,J,P,V), Difference Variance ($p < 0.0001$, Figure 5E,K,Q,W), and Inverse Variance ($p < 0.0001$, Figure 5F,L,R,X), respectively. In each EOTRH group, Cluster Prominence, Contrast, Difference Average, Difference Entropy, and Difference Variance were always the lowest after Normalize filtering, higher after Median filtering, and highest after Laplacian Sharpening filtering. Similarly, in each EOTRH group, Inverse Variance was higher after Median and Laplacian Sharpening filtering than after Normalize filtering. This demonstrated the effects that the filtering algorithms had on the select GLCM features received from the consecutive EOTRH groups.

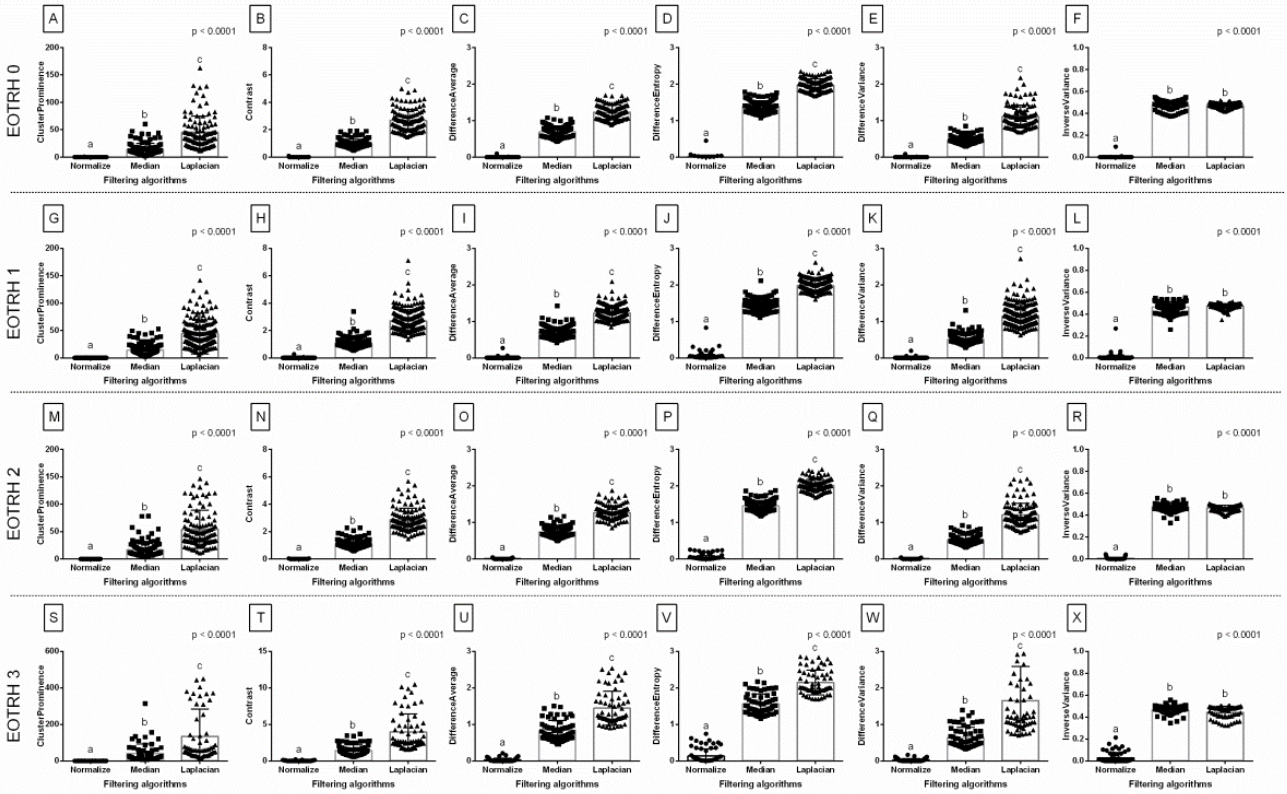

Figure 5. The comparison of the selected Gray–Level Co–occurrence Matrix (GLCM) features between the filtering algorithms. The following GLCM features are considered: Cluster Prominence (**A**,**G**,**M**,**S**), Contrast (**B**,**H**,**N**,**T**), Difference Average (**C**,**I**,**O**,**U**), Difference Entropy (**D**,**J**,**P**,**V**), Difference Variance (**E**,**K**,**Q**,**W**), Inverse Variance (**F**,**L**,**R**,**X**). The radiographs classified to EOTRH 0 grade (**A**–**F**), EOTRH 1 grade (**G**–**L**), EOTRH 2 grade (**M**–**R**), and EOTRH 3 grade (**S**–**X**) are separated by dashed horizontal lines. Lower case letters (a–c) indicate differences between groups for $p < 0.05$ independently for each measure. Single realizations are marked with dots.

Based on the received differences, the similarities were tested for DistEn2D and all six GLCM features, of which were only extracted from Normalize filtering output radiographs. The slope of the linear regression equations for DistEn2D compared to the slopes of GLCM features were not significantly different, and one slope measurement was calculated only for Difference Entropy ($p = 0.578$; one slope = 0.033; Figure 6D). The intercept within this data pair was compared and considered significant ($p < 0.0001$), thus, one intercept was not calculated. For all the other compared data pairs, the slopes were significantly different ($p < 0.05$; Figure 6A–C,E,F). The slope value of DistEn2D (slope = 0.028) was higher than the slope value of GLCM features for Cluster Prominence (slope = 0.009; Figure 6A), Contrast (slope = 0.007; Figure 6B), Difference Average (slope = 0.007; Figure 6C), Difference Entropy

(slope = 0.006; Figure 6E), and Inverse Variance (slope = 0.007; Figure 6F); but not for Difference Entropy (slope = 0.034; Figure 6D). Here, similarities between the selected entropy measures and GLCM features after subsequent selected types of filtering can be observed.

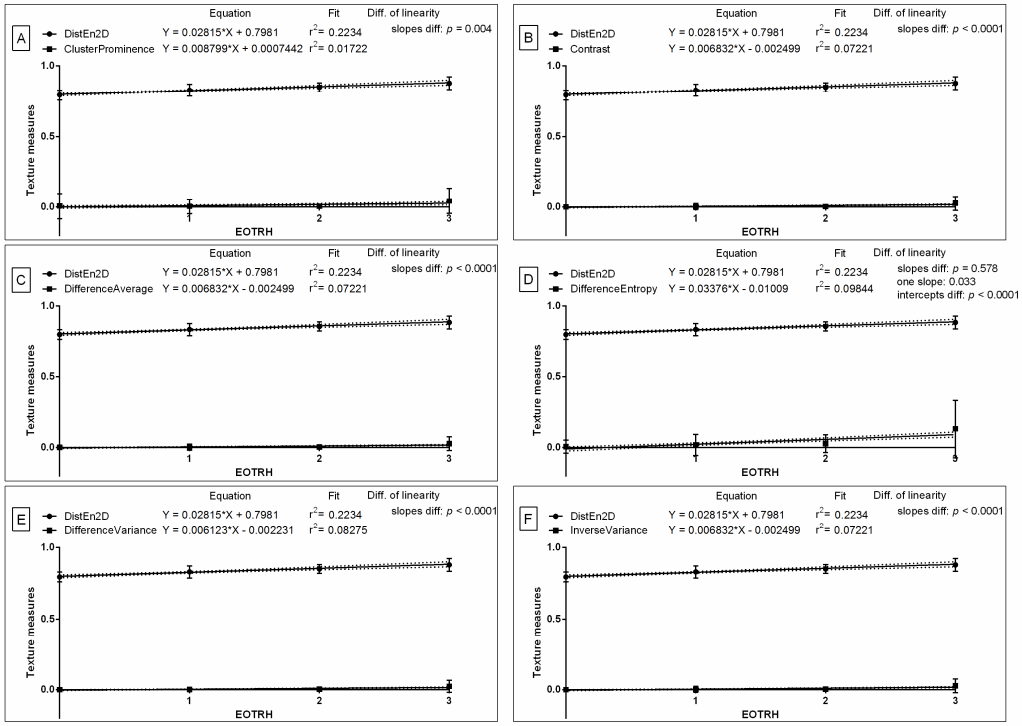

Figure 6. Comparison of selected entropy measure (DistEn2D–two–dimensional distribution entropy) and selected Gray–Level Co–occurrence Matrix (GLCM) features (Cluster Prominence (**A**), Contrast (**B**), Difference Average (**C**), Difference Entropy (**D**), Difference Variance (**E**), Inverse Variance (**F**)) throughout the EOTRH grades. Measure and features were extracted from the output radiographs after Normalize filtering. Similarity was tested using linear regressions. A $p < 0.05$ was considered significant. If the difference between slopes was not significant, a single slope measurement was calculated. Plot where the slope value of the entropy measure was higher than the slope value of the GLCM features was marked by dashed frames.

Based on the received differences, the detection accuracy of EOTRH 0 and EOTRH 3 was tested for DistEn2D and all six GLCM features extracted from Normalize filtering output radiographs (Table 3). For DistEn2D and all six GLCM features, a salient observation was made, identifying that the Se and NPV decreased with higher threshold values (mean > mean + SD > mean + 2SD) and the Sp and PPV increased with higher threshold values (mean > mean + SD > mean + 2SD). For the first threshold (mean), Se ranged from 0.50 for DistEn2D; 0.27 for Difference Entropy; to 0.25 for the remaining five GLCM features. Additionally, Sp ranged from 0.95 for DistEn2D to 0.99 for all GLCM features. For the second threshold (mean + SD), Se ranged from 0.13 for DistEn2D; to 0.22 for Difference Entropy; through 0.17 for the remaining five GLCM features. Moreover, Sp ranged from 1.00 for DistEn2D; to 0.98 for Difference Entropy; through to 0.99 for the remaining five GLCM features. For the third threshold (mean + SD), Se ranged from 0.00 for DistEn2D; 0.03 for Cluster Prominence; to 0.07 for the remaining five GLCM features. Furthermore, Sp ranged from 0.99 for Cluster Prominence to 1.00 for DistEn2D and the remaining five GLCM features. This step allowed for the summarization of the detection accuracy of the radiographic signs of EOTRH syndrome based on the selected entropy measures and GLCM features.

Table 3. The accuracy (Se—sensitivity; Sp—specificity; PPV—positive predictive value; NPV—negative predictive value) of the detection of EOTRH 0 and EOTRH 3 based on the selected entropy measure (DistEn2D—two–dimensional distribution entropy) and the selected Gray–Level Co–occurrence Matrix (GLCM) features (ClusterProminence; Contrast; DifferenceAverage; DifferenceEntropy; DifferenceVariance; Inverse Variance) extracted from the output images filtered by Normalize filter. Three thresholds (mean; mean + SD; mean + 2SD) were used.

Measures	DistEn2D	Cluster Prominence	Contrast	Difference Average	Difference Entropy	Difference Variance	Inverse Variance
Threshold				**mean**			
Se	0.50	0.25	0.25	0.25	0.27	0.25	0.25
Sp	0.95	0.99	0.99	0.99	0.99	0.99	0.99
PPV	0.67	0.94	0.94	0.94	0.94	0.94	0.94
NPV	0.90	0.70	0.70	0.70	0.70	0.70	0.70
Threshold				**mean + SD**			
Se	0.13	0.17	0.17	0.17	0.22	0.17	0.17
Sp	1.00	0.99	0.99	0.99	0.98	0.99	0.99
PPV	1.00	0.91	0.91	0.91	0.93	0.91	0.91
NPV	0.84	0.68	0.68	0.68	0.58	0.68	0.68
Threshold				**mean + 2SD**			
Se	0.00	0.03	0.07	0.07	0.07	0.07	0.07
Sp	1.00	0.99	1.00	1.00	1.00	1.00	1.00
PPV	-	0.67	1.00	1.00	1.00	1.00	1.00
NPV	0.82	0.65	0.66	0.66	0.66	0.66	0.66

4. Discussion

The benefit of using imaging processing in the radiological assessment of EOTRH will come from the enhanced automated detection of early signs of the disease that might be missed by a mere personal evaluation. As the formation of the computed–aided detector is a multi–stage process requiring extensive basic research, the current study presents the second step towards achieving this main goal. In this paper, the novel quantitative description of incisor tooth radiographs was used to enhance the quality of the radiograph to make identifying the radiographic signs of EOTRH syndrome easier, and if possible, to enhance the specific detection of the radiological signs of grade 1, grade 2, and grade 3 EOTRH syndrome.

Recently, filtering algorithms and texture analysis based on the first– and second–order statistics have been successfully used in the digital processing of the equine maxillary incisor teeth radiographs [17]. As the recent report was focused only on maxillary, not maxillary and mandibulary incisor teeth, the current study was focused similarly to provide the appropriate data sets required for the evaluation of similarities. In the previous study, the GLCM application—supported by filtering by the Normalize filter—improved edge delimitation, and was concluded to be the most advisable for the quantification of radiographic signs of EOTRH syndrome [17]. In the current study, the EOTRH grade–related increase level and accuracy of the EOTRH grade differentiation were compared between the previous digital processing approach and the new one, showing a higher slope of the linear regression equations and a higher sensitivity of radiographic sign detection for entropy–based measures than gray–level matrix–based features. As the same radiographs were used in both approaches, one may uphold the current hypothesis, that digital radiograph processing, including filtering and entropy measures extraction, may be considered as the enhancement of the quantitative description of incisor teeth radiographs and the advancement of field dental radiography. The research undertaken meets Zarychta's [26] statement that the applicability of entropy measures should be evaluated for various specimens and should highlight advances in the development, testing, and application of radiograph–processing algorithms to standard veterinary dental radiography.

In the case of EOTRH syndrome, two opposing pathological processes, resorption and hypercementosis, affect the incisor teeth [5,11]. In both processes, a variable grade of tooth

resorption and mild–to–severe hypercementosis were radiographically recognized in most publications devoted to the radiological diagnosis of EOTRH syndrome [5,6,15,49,50]—resorption shows low radiopaque signs, whereas hypercementosis shows high radiopaque signs on the background of the high radiodensity tooth structure [16,17]. Both processes may involve the whole tooth structure, although resorption signs mainly appear in the enamel, cementum, dentine, and pulp cavity [11], whereas hypercementosis is most commonly found in the apex of the tooth, with bulbous enlargements of cement accumulation [51]. The alternating occurrence of radiological signs of resorption and hypercementosis gives a mosaic pattern of the tooth structure that is separable visually [5,6,15] and quantifiable with second–order descriptive statistics [17]. This quantification, based on the Gray–Level Co–occurrence Matrix evaluation, counts the randomness in the radiograph using the differences in the intensity value of the respective pixels or their surroundings [17]. Precisely, the irregularity of pixels in a given window and the likelihood of similarity of these pixels and the pixels of the next window are the basis of the creation of a matrix where the occurrence of a given pixel is counted [52,53]. Contrarily, all currently used entropy measures are calculated directly on the image [24], returning the repeatability of pixel patterns of the image, which in this application, is related to the texture properties of the radiograph [25]. In a currently considered type of application, the values returned from the radiographs are directly related to the predictability or uncertainty of the radiograph's spatial patterns and are directly related to the radiograph's irregularity or complexity [29–32]. Therefore, one may observe that the approaches based on calculating features from the matrix obtained from the processing step applied to the image, such as GLCM, represent the disorder of the intermediate matrix rather than the irregularity of the image [54], whereas, in the case of the EOTRH radiological signs, measures of irregularity and complexity [29–32] rather than features of disorder [52] of radiograph texture may be extracted as more relevant and insightful. This hypothesis is supported by the current results, which indicate that measures of irregularity and complexity, such as DispEn2D, are more accurate in the differentiation of the EOTRH radiological signs than the features of the disorder, such as Cluster Prominence, Contrast, Difference Average, Difference Entropy, Difference Variance, and Inverse Variance. It should be highlighted that DispEn2D, rather than GLCM features, may be considered in further automated detection developments, which ultimately aim to improve EOTRH detection.

In the current study, the ROIs annotated on the incisor teeth pass the criterion of being a small size image, thus, one may suspect DispEn2D and DistEn2D rather than SampEn2D, FuzzEn2D, and PermEn2D to be effective in this type of application, especially considering that both DispEn2D and DistEn2D have been shown to be the most suitable for the entropy–based texture analysis of small ROIs which were extracted from thermographs in the equine applications of pregnancy [27] and back load [28] detection. Interestingly, in the current study, only DistEn2D, not DispEn2D, demonstrated the most favourable EOTRH grade–related differences. DistEn2D extracted from Normalize filtering output radiographs was the lowest in the EOTRH 0 group, higher in the EOTRH 1 and 2 groups, and the highest in the EOTRH 3 group. One may observe that the concept of counting the amount of similarity between two windows by measuring the distance between the corresponding windows, used in DistEn2D [33,47], is more suitable for the texture analysis of small regions of the radiographs of equine incisor teeth than the concept of using the sigmoid function, as used in DispEn2D [32,45]. The DistEn2D algorithm is invariant to rotation [33,44], whereas the DispEn2D algorithm is the least sensitive to rotation, translation, and image size, out of the five currently studied measures of entropy [45]. Thus, it appears that the concept of a measure, and not the rotation, is essential to the usefulness of the DistEn2D algorithm in this application. These findings justified the choice to use the DispEn2D for further automated detection development.

One may note that the DistEn2D value was lower after Normalize and Median filtering than after Laplacian Sharpening filtering, and the DispEn2D algorithm was the least sensitive to filtering out of the five currently studied measures of entropy [29–32]. This

can be considered a benefit over the GLCM approach. All GLCM features considered in the current study differed between EOTRH grades 0–3 after filtering by the Normalize filter but not after Median and Laplacian Sharpening filtration. The Laplacian Sharpening filter returns the output radiographs with a sharper quality than the input radiograph [55], and has been considered more suitable for the first–order than the second–order statistic extracted from equine radiographs [17]. The Normalize filter increases the contrast of the radiographs [56], which seems to be more favourable for the GLCM approaches than other filtering algorithms [17]. As the GLCM approach returns the spatial distribution of the pixel disorder [57], the output radiograph, after filtering by the contrast–improved algorithm, demonstrates a greater grade of differentiation [58,59]. Contrarily, as the DispEn2D measure returns a quantitative description of the irregularities of the images [33], both the contrast improvement by Normalize filter and the noise reduction by Median [48] may provide a good grade of differentiation for EOTRH radiological signs. One may also observe that for the Normalize filtering output radiograph, the slope value of DistEn2D was higher than the slope value of five from six compared GLCM features. These differences in the slopes of the regression curves indicate a greater increase in the value of the entropy measure than GLCM features with regard to the severity of the radiological signs of EOTRH, and suggest a greater usefulness of DistEn2D than GLCM, which was confirmed by the detection accuracy of EOTRH 0 and EOTRH 3. These findings justified the choice of the Normalize and Median filtering for the further automated detection development.

Finally, one may discern that the proposed method of digital processing of radiographs allows to detect the radiological signs of all grades of EOTRH syndrome, although it does not adequately support the differentiation between EOTRH 0 and 1, EOTRH 1 and 2, as well as EOTRH 2 and 3. Although the DistEn2D–based differentiation between EOTRH 0 and 3 was more accurate than GLCM–based differentiation, further studies on a bigger data set are required to verify the applicability of the proposed algorithms. Within the benefit of using imaging processing in the radiological assessment of EOTRH in horses, the enhancement of the quality of the radiograph to facilitate the identification of identifying the radiographic signs of EOTRH syndrome should be highlighted.

5. Conclusions

From the entropy measures recently applied in the equine image analysis, only DistEn2D showed the EOTRH grade–related differences which could be introduced to the advanced veterinary diagnostic procedure for incisor teeth disorders. These observed differences were the least susceptible to the use of radiograph filtering algorithms, returning the same values after Normalize and Median filtering. As the EOTRH grade–related differences were the most favourable for DistEn2D extraction from the Normalize filtering output radiographs, this combination of digital radiograph processing may be carefully advised in equine incisor teeth radiography. Interestingly, the considered GLCM features demonstrated a higher susceptibility for filtering than the entropy measures, showing, similar to DistEn2D, the most favourable differences after Normalize filtering. Moreover, both the evidence of similarity and the highest EOTRH grade–related increase level were noted for DistEn2D and Difference Entropy after Normalize filtering. As these two measures also demonstrated the highest accuracy of the EOTRH grade differentiation, one may suggest that they could be introduced as advancements into the field equine dentistry.

Author Contributions: Conceptualization, K.G. and M.D.; methodology, K.G., M.B. and M.D.; software, M.B.; validation, E.S. and I.P.; formal analysis, K.G., M.B. and M.D.; investigation, K.G., M.B., E.S., I.P., B.T., A.B. and M.D.; resources, K.G. and M.B.; data curation, K.G. and M.D.; writing—original draft preparation, K.G., M.B., E.S. and M.D.; writing—review and editing, I.P., B.T. and A.B.; visualization, K.G. and M.D.; supervision, I.P.; project administration, K.G. and M.D.; funding acquisition, K.G. All authors have read and agreed to the published version of the manuscript.

Funding: The study was supported by the National Science Centre, Poland, "Miniatura 6" Project, No. 2022/06/X/ST6/00431.

Institutional Review Board Statement: The animal protocols used in this work were evaluated and approved by the II Local Ethical Committee on Animal Testing in Warsaw on behalf of the National Ethical Committees on Animal Testing (protocol code WAW2/091/2020 approved on 29 July 2020). They are in accordance with FELASA guidelines and the National law for Laboratory Animal Experimentation (Dz. U. 2015 poz. 266 and 2010–63–EU directive).

Informed Consent Statement: Not applicable.

Data Availability Statement: The data presented in this study are available on request from the corresponding author.

Conflicts of Interest: The authors declare no conflict of interest. The funders had no role in the design of the study; in the collection, analyses, or interpretation of data; in the writing of the manuscript, or in the decision to publish the results.

References

1. Dixon, P.M.; Dacre, I. A review of equine dental disorders. *Vet. J.* **2005**, *169*, 165–187. [CrossRef] [PubMed]
2. Dixon, P.M. The Gross, Histological, and Ultrastructural Anatomy of Equine Teeth and Their Relationship to Disease. In Proceedings of the 49th Annual Convention of the American Association of Equine Practitioners, New Orleans, LA, USA, 21–25 November 2003; Volume 48, pp. 421–437.
3. Brigham, E.J.; Duncanson, G.R. An equine postmortem dental study: 50 cases. *Equine Vet. Educ.* **2000**, *12*, 59–62. [CrossRef]
4. Limone, L. General clinical, oral and dental examination. In *Equine Dentistry and Maxillofacial Surgery*; Cambridge Scholars Publishing: Newcastle upon Tyne, UK, 2022; p. 302.
5. Rehrl, S.; Schröder, W.; Müller, C.; Staszyk, C.; Lischer, C. Radiological prevalence of equine odontoclastic tooth resorption and hypercementosis. *Equine Vet. J.* **2018**, *50*, 481–487. [CrossRef] [PubMed]
6. Henry, T.J.; Puchalski, S.M.; Arzi, B.; Kass, P.H.; Verstraete, F.J.M. Radiographic evaluation in clinical practice of the types and stage of incisor tooth resorption and hypercementosis in horses. *Equine Vet. J.* **2016**, *49*, 486–492. [CrossRef] [PubMed]
7. Easley, J. A new look at dental radiography. In Proceedings of the 48th Annual Convention of the American Association of Equine Practitioners, Orlando, FL, USA, 4–8 December 2002; Volume 48, pp. 412–420.
8. Barakzai, S.Z.; Dixon, P.M. A study of open-mouthed oblique radiographic projections for evaluating lesions of the erupted (clinical) crown. *Equine Vet. Edu.* **2003**, *15*, 143–148. [CrossRef]
9. Greet, T.R.C. Oral and dental trauma. In *Equine Dentistry*, 1st ed.; Baker, G.J., Easley, J., Eds.; W.B. Saunders: London, UK, 1999; pp. 60–69.
10. Dixon, P.M.; Tremaine, W.H.; Pickles, K.; Kuhns, L.; Hawe, C.; McCann, J.; McGorum, B.; Railton, D.I.; Brammer, S. Equine dental disease Part 1: A longterm study of 400 cases: Disorders of incisor, canine and first premolar teeth. *Equine Vet. J.* **1999**, *31*, 369–377. [CrossRef]
11. Staszyk, C.; Bienert, A.; Kreutzer, R.; Wohlsein, P.; Simhofer, H. Equine odontoclastic tooth resorption and hypercementosis. *Vet. J.* **2008**, *178*, 372–379. [CrossRef] [PubMed]
12. Pearce, C.J. Recent developments in equine dentistry. *N. Z. Vet. J.* **2020**, *68*, 178–186. [CrossRef]
13. Barrett, M.F.; Easley, J.T. Acquisition and interpretation of radiographs of the equine skull. *Equine Vet. Educ.* **2013**, *25*, 643–652. [CrossRef]
14. Moore, N.T.; Schroeder, W.; Staszyk, C. Equine odontoclastic tooth resorption and hypercementosis affecting all cheek teeth in two horses: Clinical and histopathological findings. *Equine Vet. Educ.* **2016**, *28*, 123–130. [CrossRef]
15. Górski, K.; Tremaine, H.; Obrochta, B.; Buczkowska, R.; Turek, B.; Bereznowski, A.; Rakowska, A.; Polkowska, I. EOTRH syndrome in polish half-bred horses-two clinical cases. *J. Equine Vet. Sci.* **2021**, *101*, 103428. [CrossRef] [PubMed]
16. Saccomanno, S.; Passarelli, P.C.B.; Oliva, B.; Grippaudo, C. Comparison between two radiological methods for assessment of tooth root resorption: An in vitro study. *BioMed Res. Int.* **2018**, *2018*, 5152172. [CrossRef]
17. Górski, K.; Borowska, M.; Stefanik, E.; Polkowska, I.; Turek, B.; Bereznowski, A.; Domino, M. Selection of Filtering and Image Texture Analysis in the Radiographic Images Processing of Horses' Incisor Teeth Affected by the EOTRH Syndrome. *Sensors* **2022**, *22*, 2920. [CrossRef]
18. Manso-Díaz, G.; García-López, J.M.; Maranda, L.; Taeymans, O. The role of head computed tomography in equine practice. *Equine Vet. Educ.* **2015**, *27*, 136–145. [CrossRef]
19. Baratt, R.M. Dental Radiography and Radiographic Signs of Equine Dental Disease. *Vet. Clin. N. Am. Equine Pract.* **2020**, *36*, 445–476. [CrossRef] [PubMed]
20. Dakin, S.G.; Lam, R.; Rees, E.; Mumby, C.; West, C.; Weller, R. Technical Set-up and Radiation Exposure for Standing Computed Tomography of the Equine Head: Standing CT of the Equine Head. *Equine Vet. Educ.* **2014**, *26*, 208–215. [CrossRef]
21. van der Stelt, P.F. Filmless imaging: The uses of digital radiography in dental practice. *J. Am. Dent. Assoc.* **2005**, *136*, 1379–1387. [CrossRef]
22. Tan, T.; Platel, B.; Mus, R.; Tabar, L.; Mann, R.M.; Karssemeijer, N. Computer-aided detection of cancer in automated 3-D breast ultrasound. *IEEE TMI* **2013**, *32*, 1698–1706. [CrossRef] [PubMed]

23. Vidal, P.L.; de Moura, J.; Novo, J.; Ortega, M. Multi-stage transfer learning for lung segmentation using portable X-ray devices for patients with COVID-19. *Expert Syst. Appl.* **2021**, *173*, 114677. [CrossRef]
24. Humeau-Heurtier, A. Texture feature extraction methods: A survey. *IEEE Access* **2019**, *7*, 8975–9000. [CrossRef]
25. Silva, L.E.; Duque, J.J.; Felipe, J.C.; Murta, L.O., Jr.; Humeau-Heurtier, A. Two-dimensional multiscale entropy analysis: Applications to image texture evaluation. *Signal Process.* **2018**, *147*, 224–232. [CrossRef]
26. Zarychta, P. Application of fuzzy image concept to medical images matching. In *Information Technology in Biomedicine. ITIB 2018. Advances in Intelligent Systems and Computing*, 1st ed.; Pietka, E., Badura, P., Kawa, J., Wieclawek, W., Eds.; Springer: Cham, Switzerland, 2019; Volume 762, pp. 27–38.
27. Borowska, M.; Maśko, M.; Jasiński, T.; Domino, M. The Role of Two-Dimensional Entropies in IRT-Based Pregnancy Determination Evaluated on the Equine Model. In *Information Technology in Biomedicine. ITIB 2022. Advances in Intelligent Systems and Computing*, 1st ed.; Pietka, E., Badura, P., Kawa, J., Wieclawek, W., Eds.; Springer: Cham, Switzerland, 2022; Volume 1429, pp. 54–65.
28. Domino, M.; Borowska, M.; Zdrojkowski, Ł.; Jasiński, T.; Sikorska, U.; Skibniewski, M.; Maśko, M. Application of the Two-Dimensional Entropy Measures in the Infrared Thermography-Based Detection of Rider: Horse Bodyweight Ratio in Horseback Riding. *Sensors* **2022**, *22*, 6052. [CrossRef]
29. Da Silva, L.E.; Senra Filho, A.C.; Fazan, V.P.; Felipe, J.C.; Murta, L.O., Jr. Two-dimensional sample entropy analysis of rat sural nerve aging. In Proceedings of the 2014 36th Annual International Conference of the IEEE Engineering in Medicine and Biology Society, Chicago, IL, USA, 26–30 August 2014; pp. 3345–3348.
30. Hilal, M.; Berthin, C.; Martin, L.; Azami, H.; Humeau-Heurtier, A. Bidimensional multiscale fuzzy entropy and its application to pseudoxanthoma elasticum. *IEEE Trans. Biomed. Eng.* **2019**, *67*, 2015–2022. [CrossRef] [PubMed]
31. Ribeiro, H.V.; Zunino, L.; Lenzi, E.K.; Santoro, P.A.; Mendes, R.S. Complexity-entropy causality plane as a complexity measure for two-dimensional patterns. *PLoS ONE* **2012**, *7*, e40689. [CrossRef]
32. Azami, H.; da Silva, L.E.V.; Omoto, A.C.M.; Humeau-Heurtier, A. Two-dimensional dispersion entropy: An information-theoretic method for irregularity analysis of images. *Signal. Process. Image Commun.* **2019**, *75*, 178–187. [CrossRef]
33. Azami, H.; Escudero, J.; Humeau-Heurtier, A. Bidimensional Distribution Entropy to Analyze the Irregularity of Small-Sized Textures. *IEEE Signal. Proc. Lett.* **2017**, *24*, 1338–1342. [CrossRef]
34. Radostits, O.M.; Gay, C.; Hinchcliff, K.W.; Constable, P.D. (Eds.) *Veterinary Medicine E-Book: A Textbook of the Diseases of Cattle, Horses, Sheep, Pigs and Goats*; Elsevier: Amsterdam, The Netherlands, 2006.
35. Salem, S.E.; Townsend, N.B.; Refaai, W.; Gomaa, M.; Archer, D.C. Prevalence of oro-dental pathology in a working horse population in Egypt and its relation to equine health. *Equine Vet. J.* **2017**, *49*, 26–33. [CrossRef]
36. Hüls, I.; Bienert, A.; Staszyk, C. Equine odontoclastic tooth resorption and hyper-cementosis (EOTRH): Röntgenologische und makroskopisch-anatomische Befunde. In Proceedings of the 10 Jahrestagung der Internationalen Gesellschaft zur Funktionsverbesserung der Pferdezähne, Wiesbaden, Germany, 3–4 March 2012.
37. Floyd, M.R. The modified Triadan system: Nomenclature for veterinary dentistry. *J. Vet. Dent.* **1991**, *8*, 18–19. [CrossRef] [PubMed]
38. van Griethuysen, J.J.M.; Fedorov, A.; Parmar, C.; Hosny, A.; Aucoin, N.; Narayan, V.; Beets-Tan, R.G.H.; Fillon-Robin, J.C.; Pieper, S.; Aerts, H.J.W.L. Computational radiomics system to decode the radiographic phenotype. *Cancer Res.* **2017**, *77*, e104–e107. [CrossRef]
39. Lowekamp, B.C.; Chen, D.T.; Ibáñez, L.; Blezek, D. The design of SimpleITK. *Front. Neuroinform.* **2013**, *7*, 45. [CrossRef]
40. Yaniv, Z.; Lowekamp, B.C.; Johnson, H.J.; Beare, R. SimpleITK image-analysis notebooks: A collaborative environment for education and reproducible research. *J. Digit. Imaging* **2018**, *31*, 290–303. [CrossRef]
41. Lim, J.S. *Two-Dimensional Signal and Image Processing*, 1st ed.; Prentice Hall: Englewood Cliffs, NJ, USA, 1990.
42. Gonzalez, R.C.; Eddins, S.L.; Woods, R.E. *Digital Image Publishing Using MATLAB*, 1st ed.; Prentice Hall: Upper Saddle River, NJ, USA, 2004.
43. Padhye, N.; Rios, D.; Fay, V.; Hanneman, S.K. *Pressure Injury Link to Entropy of Abdominal Temperature*; Cizik School of Nursing, The University of Texas Health Science Center at Houston: Houston, TX, USA, 2022; *Preprint*.
44. Silva, L.E.V.; Senra Filho, A.C.S.; Fazan, V.P.S.; Felipe, J.C.; Murta Junior, L.O. Two-dimensional sample entropy: Assessing image texture through irregularity. *Biomed. Phys. Eng. Express* **2016**, *2*, 045002. [CrossRef]
45. Furlong, R.; Hilal, M.; O'brien, V.; Humeau-Heurtier, A. Parameter Analysis of Multiscale Two-Dimensional Fuzzy and Dispersion Entropy Measures Using Machine Learning Classification. *Entropy* **2021**, *23*, 1303. [CrossRef] [PubMed]
46. Morel, C.; Humeau-Heurtier, A. Multiscale permutation entropy for two-dimensional patterns. *Pattern Recognit. Lett.* **2021**, *150*, 139–146. [CrossRef]
47. He, J.; Shang, P.; Zhang, Y. PID: A PDF-induced distance based on permutation cross-distribution entropy. *Nonlinear Dyn.* **2019**, *97*, 1329–1342. [CrossRef]
48. Dohoo, I.; Martin, W.; Stryhn, H. *Veterinary Epidemiologic Research*, 2nd ed.; VER Inc.: Charlottetown, PE, Canada, 2009.
49. Sykora, S.; Pieber, K.; Simhofer, H.; Hackl, V.; Brodesser, D.; Brandt, S. Isolation of Treponema and Tannerella spp. from equine odontoclastic tooth resorption and hypercementosis related periodontal disease. *Equine Vet. J.* **2014**, *46*, 358–363. [CrossRef]
50. Zhang, H.; Hung, C.L.; Min, G.; Guo, J.P.; Liu, M.; Hu, X. GPU-accelerated GLRLM algorithm for feature extraction of MRI. *Sci. Rep.* **2019**, *9*, 10883. [CrossRef]

51. Smedley, R.C.; Earley, E.T.; Galloway, S.S.; Baratt, R.M.; Rawlinson, J.E. Equine odon-toclastic tooth resorption and hypercementosis: Histopathologic features. *Vet. Pathol.* **2015**, *52*, 903–909. [CrossRef]
52. Szczypiński, P.; Klepaczko, A.; Pazurek, M.; Daniel, P. Texture and color based image segmentation and pathology detection in capsule endoscopy videos. *Comput. Methods Programs Biomed.* **2014**, *113*, 396–411. [CrossRef]
53. Szczypinski, P.M.; Klepaczko, A.; Kociołek, M. QMaZda—Software tools for image analysis and pattern recognition. In Proceedings of the 2017 Signal Processing: Algorithms, Architectures, Arrangements, and Applications (SPA), Poznan, Poland, 20–22 October 2017; pp. 217–221.
54. Depeursinge, A.; Al-Kadi, O.S.; Mitchell, J.R. *Biomedical Texture Analysis: Fundamentals, Tools and Challenges*; Academic Press: Cambridge, MA, USA, 2017.
55. Al-Ameen, Z.; Sulong, G.; Gapar, M.D.; Johar, M.D. Reducing the Gaussian blur artifact from CT medical images by employing a combination of sharpening filters and iterative deblurring algorithms. *J. Theor. Appl. Inf. Technol.* **2012**, *46*, 31–36.
56. Heidari, M.; Mirniaharikandehei, S.; Khuzani, A.Z.; Danala, G.; Qiu, Y.; Zheng, B. Improving the performance of CNN to predict the likelihood of COVID-19 using chest X-ray images with preprocessing algorithms. *Int. J. Med. Inform.* **2020**, *144*, 104284. [CrossRef] [PubMed]
57. Jusman, Y.; Tamarena, R.I.; Puspita, S.; Saleh, E.; Kanafiah, S.N.A.M. Analysis of features extraction performance to differentiate of dental caries types using gray level co-occurrence matrix algorithm. In Proceedings of the 2020 10th IEEE International Conference on Control System, Computing and Engineering (ICCSCE), Penang, Malaysia, 21–22 August 2020; pp. 148–152.
58. Nagarajan, M.B.; Coan, P.; Huber, M.B.; Diemoz, P.C.; Glaser, C.; Wismüller, A. Computer-aided diagnosis for phase-contrast X-ray computed tomography: Quantitative characterization of human patellar cartilage with high-dimensional geometric features. *J. Digit. Imaging* **2014**, *27*, 98–107. [CrossRef] [PubMed]
59. Kociołek, M.; Strzelecki, M.; Obuchowicz, R. Does image normalization and intensity resolution impact texture classification? *Comput. Med. Imaging Graph.* **2020**, *81*, 101716. [CrossRef] [PubMed]

BMC Veterinary Research

RESEARCH

Open Access

An application of the density standard and scaled–pixel–counting protocol to assess the radiodensity of equine incisor teeth affected by resorption and hypercementosis: preliminary advancement in dental radiography

Kamil Górski[1], Marta Borowska[2], Bernard Turek[1], Marek Pawlikowski[3], Krzysztof Jankowski[3], Andrzej Bereznowski[4], Izabela Polkowska[5] and Małgorzata Domino[1*]

Abstract

Background Equine Odontoclastic Tooth Resorption and Hypercementosis (EOTRH) syndrome is a dental disease where the radiographic signs may be quantified using radiographic texture features. This study aimed to implement the scaled–pixel–counting protocol to quantify and compare the image structure of teeth and the density standard in order to improve the identification of the radiographic signs of tooth resorption and hypercementosis using the EOTRH syndrome model.

Methods and results A detailed examination of the oral cavity was performed in 80 horses and maxillary incisor teeth were evaluated radiographically, including an assessment of the density standard. On each of the radiographs, pixel brightness (PB) was extracted for each of the ten steps of the density standard (S1–S10). Then, each evaluated incisor tooth was assigned to one of 0–3 EOTRH grade–related groups and annotated using region of interest (ROI). For each ROI, the number of pixels (NP) from each range was calculated. The linear relation between an original X–ray beam attenuation and PB was confirmed for the density standard. The NP values increased with the number of steps of the density standard as well as with EOTRH degrees. Similar accuracy of the EOTRH grade differentiation was noted for data pairs EOTRH 0–3 and EOTRH 0–1, allowing for the differentiation of both late and early radiographic signs of EOTRH.

Conclusion The scaled–pixel–counting protocol based on the use of density standard has been successfully implemented for the differentiation of radiographic signs of EOTRH degrees.

Keywords Radiographs, Radiodensity, EOTRH, Dental care, Horse

*Correspondence:
Małgorzata Domino
malgorzata_domino@sggw.edu.pl
Full list of author information is available at the end of the article

Background

The horse's ability to chew and grind food matter correctly is an important factor in the success of every nutritional, metabolic, and gastrointestinal case [1]. In this new era, in which the detailed dental examination is becoming a standard offering in the equine veterinary practice, the potential advancement in equine dentistry drives a change from lay–dentistry to clinical veterinary dentistry [2]. Recent developments in equine dentistry consist of advances in anatomical and physiological investigations [3, 4], development of modernized equine dental equipment [5], introduction of minimally invasive surgical techniques [6], and application of diagnostic imaging techniques translated from those used in human [5, 7, 8] and canine [9] dentistry.

In human dentistry, the assessment of bone and/or tooth quality is an important part of numerous dental manipulation protocols for example implant insertion [10] and accelerated orthodontic treatment [11]. The bone quality is best assessed by combining evaluation of bone mineral density and trabecular structure, which can be achieved radiographically using high–resolution imaging modalities such as high–resolution peripheral quantitative computed tomography (hr pQCT), multi–detector computed tomography (MDCT), or high resolution–magnetic resonance imaging (hr MRI) [12]. As most of the high–resolution imaging modalities have limitations in human clinical practice [10, 12], the use of alternative systems, such as cone–beam computed tomography (CBCT), have been considered [11, 12]. Therefore, in recent years, CBCT has been used in human dentistry as a diagnostic imaging modality to assess bone quality before implant surgery [13–15]. CBCT imaging modality, even though not high–resolution, delivers Hounsfield units (HU) reflecting bone quality [14–17].

In equine dentistry, CBCT and fan–beam computed tomography (FBCT) have already been used in a diagnostic imaging of equine head. Both CBCT and FBCT modalities were used for cadaver head scanning to detect dental and sinus abnormalities [8] and anatomical advancements [4, 18], respectively. Although CBCT and FBCT have a substantial agreement in detecting dental and sinus abnormalities in equine cadaver heads [8], one may observe that in the case of the living horse's head scanning FBCT was used as the preferred modality to detect signs of dental disease [19, 20], sinonasal cysts [21, 22], osteoma, and progressive ethmoid haematomas [19]. Some authors have compared and validated the accuracy of FBCT and radiographic imaging in detecting cheek [20, 23] or incisor teeth [24] disorders again, on both cadaver [23, 24] and living horse's heads [20]. Although computed tomography (CT) modality complement and overcome the limitations of two–dimensional radiographic images [25], standard radiography is widely used in equine practice for diagnoses and treatment purposes [26–28]. In equine dentistry, CT modality remains a costly imaging technique, which is restricted to universities or large clinical centers [29, 30] and contraindicated when deep sedation or general anesthesia is not performed [31]. Therefore, from the equine practitioner's point of view, standard radiography is recommended in the equine practice as a first choice method [28] for incisor [32] or cheek [33] teeth imaging.

Both CT modality and standard radiography represent techniques based on the detection of X–ray beam attenuation [34]. As in the case of CT, the bone or tooth quality assessment is based on a linear transformation of the original linear attenuation coefficient measurement into the HU scale [11], an analogous transformation is not available for radiographs. On the HU scale, the radiodensity at standard temperature and pressure is defined as -1000 HU for air, 0 HU for distilled water, 20–100 HU for soft tissue, up to 1000 HU for bone, and 2000 HU for dense bone or tooth [35]. However, one should note that HU values obtained from CT and returned without the use of specific scaled software such as the Slice Pick module and Bone Investigational Toolkit [36] are relative and do not represent absolute HU values [11]. Therefore, we hypothesize that radiographs in equine dental practice may be more specifically analyzed using a transformation model from standard radiographs to a numerical density scale similar to HU for CT scans.

Teeth demonstrate high radiodensity and are radiographically well–defined [37], thus some dental diseases with radiographic signs of radiodensity alteration can be used to verify the hypothesis. Noteworthy are hypo– and hypercementosis, in which decrease or increase radiopacity are easily detected, respectively, in the background of the high radiodense tooth structure [37, 38]. Hypocementosis of the infundibula of cheek teeth is a common abnormality of cemental development, which is visible radiographically in the form of decrease radiopacity. This cemental defect affects most commonly the apical region of the infundibulum as a result of the reduction in the vascular supply to the mesial infundibulum [39]. Hypercementosis of incisor and canine teeth is also a common abnormality, however, appears generally in horses over 14 years of age, and is visible radiographically in the form of increase radiopacity. This cemental accumulation occurs alone or together with tooth resorption in the case of Equine Odontoclastic Tooth Resorption and Hypercementosis (EOTRH) syndrome [40], which may involve the whole tooth structure. Hypercementosis mainly appears as a result of cement accumulation forming bulbous enlargements on the reserve crown and/or apex of the tooth [41],

whereas resorption affects the enamel, cementum, dentine, and pulp cavity [40]. So far various aetiologies of EOTRH syndrome have been proposed, however, as yet none have been substantiated [2, 32]. Comparing these two diseases, EOTRH syndrome is easier to evaluate using standard radiographic technique due to the lower superimposition of soft tissue related to the favorable rostral position of the incisor than cheek teeth [42]. Infundibular hypocementosis of cheek teeth is more difficult to evaluate using standard radiographic technique due to the higher superimposition of soft tissues and the contrast reduction caused by the peripheral and infundibular enamel [43]. Therefore, standard radiographs of incisor teeth affected by EOTRH syndrome were selected as the first equine model suitable for the testing of the relative tooth quality evaluation using the scaled–pixel–counting protocol.

This study aimed to implement the scaled–pixel–counting protocol to quantify and compare the image structure of teeth and density standard in order to improve the identification of the radiographic signs of tooth resorption and hypercementosis using the EOTRH syndrome model.

Materials

Animals and study design

The study was conducted on 80 privately owned horses (age mean ± standard deviation (SD): 16.9 ± 7.0; 37 geldings, 43 mares; 30 Polish Halfbred horses, 13 Arabian horses, 10 Schlesisches Warmblood horses, 8 Wielkopolska breed horses, 7 Dutch Warmblood horses, 5 Thoroughbred horses, 4 Polish draft horses, and 3 Malopolska breed horses) between July 2021 and December 2021. The health status of the horses was inspected according to veterinary standards including a basic clinical examination [44] a detailed examination of the oral cavity [45], and an X–ray examination of the maxillary incisor teeth using the intra–oral dorso–ventral projection [32].

The X–ray images of the horses' incisor teeth and density standard were taken simultaneously, and the study was performed according to the following five–step protocol:

(i) classification of each incisor tooth of every horse to one of the four grade–related EOTRH groups (0–3); (ii) annotation of the regions of interest (ROIs) of the incisor teeth and the density standard; (iii) implementation of the scaled–pixel–counting protocol to quantify and compare the image structure of teeth and density standard; (iv) comparison of the quantification results; (v) assessment of the accuracy of identification of grade–related EOTRH groups (0–3) based on the quantification results.

Classification of horses' incisor teeth

A basic clinical examination aimed to investigate the internal temperature, heart rate, respiratory rate, mucous membranes, capillary refill time, and lymph nodes in order to qualify the horses for the sedation procedure. No clinical contraindication to the sedation procedure were found in any of the examined horses. A basic clinical examination was conducted following standard protocol [44].

The sedation procedure aimed to prepare the horses for a detailed examination of the oral cavity. Each horse received a dose of detomidine hydrochloride (0.01 mg/kg bwt i.v. of Domosedan; Orion Corporation, Espoo, Finland), or xylazine hydrochloride (0.4 mg/kg bwt i.v. of Xylapan; Vetoquinol Biowet Sp. z o.o., Gorzów Wielkopolski, Poland), or a combination of both. In some cases, horses received a dose of butorphanol tartrate (0.01 mg/kg bwt i.v. of Torbugesic; Zoetis Polska Sp. z o.o., Warsaw, Poland).

A detailed examination of the oral cavity aimed to collect the clinical signs of dental diseases, concerning the condition of teeth, interdental spaces, gums, and mucosa of the cheeks and tongue. This examination was conducted by visual examination as well as manual and using periodontal probe palpation after the mouth opening by a Haussmann's mouth speculum and the oral cavity flushing by a 400 mL syringe. Each dental tool was used in a manner that ensured the safety of the horse and veterinarian during examination. The oral cavity was flushed to remove any food which remained on, around, and between the teeth, as well as to evaluate the interdental spaces, respectively. A detailed examination of the oral cavity was conducted following standard protocol [45] and was documented using an equine dental chart [46].

An X–ray examination of the maxillary incisor teeth aimed to collect the radiographic signs of EOTRH syndrome including shape, contour, radiodensity, and delineation of the periodontal space [32]. This examination was conducted using the intra–oral dorso–ventral projection by inserting the protected radiographic cassette into the horse's oral cavity [47] as well as the guidelines of the bisecting angle technique [48]. A density standard patch was attached to the upper right corner of the radiographic cassette. Such positioning allowed to minimize the absorption of ionizing radiation, and thus false results. A density standard was positioned perpendicular to the surface of the cassette, 4 cm from the top and 4 cm from the right edge of the cassette so that the long axis of the density standard was parallel to the long axis and the thick end was caudally of the cassette (Fig. 1A). The cassette was positioned in the horse's open mouth, always the same distance from to the density standard, 15 cm from the top and 15 cm from the right edge of the cassette (Fig. 1B). The cassette was positioned so that

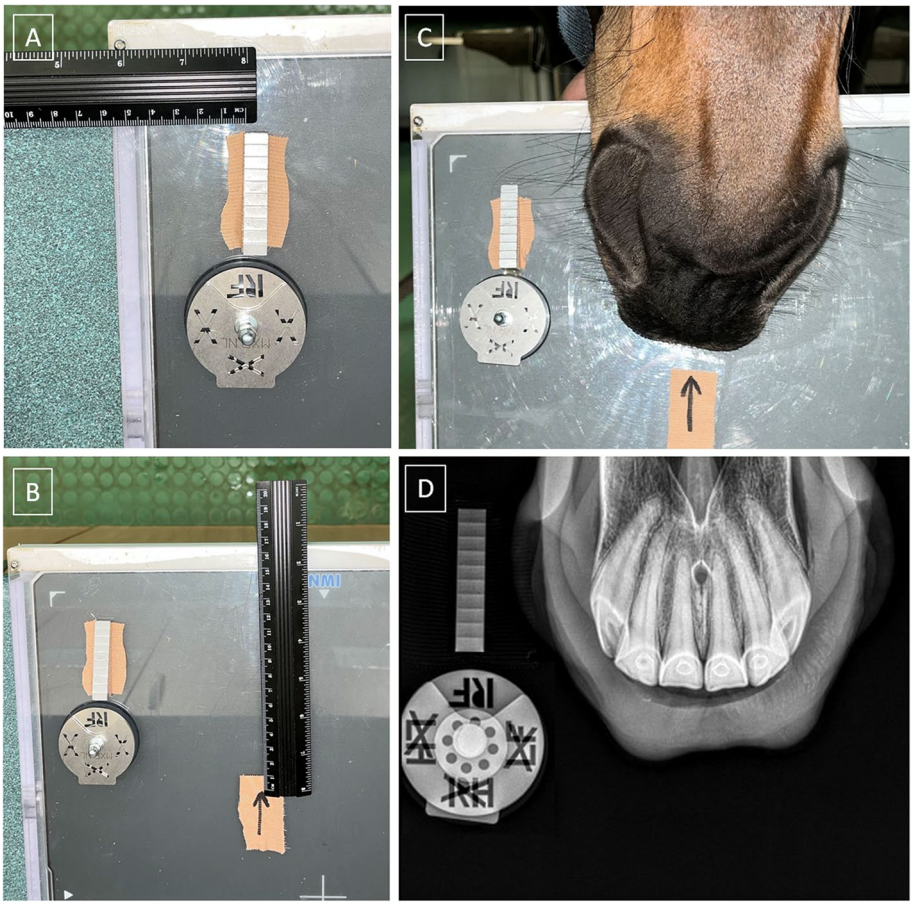

Fig. 1 The positioning of density standard (**A**), specific place of the cassette (**B**), and horse's nostrils (**C**) while obtaining the intra–oral dorso–ventral projection of the incisor teeth, density standard, and directional indicator (**D**)

the center of the horse's nostrils was in the specific place of the cassette, which was marked with a patch containing an arrow (Fig. 1C). The examination was conducted using an X–ray tube (Orange 9020HF, Ecoray Co., Seoul, Korea), a radiographic cassette (Saturn 8000, Vievorks Co., Seoul, Korea), and a portable computer (HP Inc UK Ltd, Reading, UK). The X–ray tube settings were 2.5 mAs and 65 kV, and the distance between the X–ray tube and radiographic cassette was 80 cm. The radiographs were acquired as.jpg files and processed using the DxWorks software (Vievorks Co., Ltd., Seoul, Korea). An X–ray examination was conducted following standard protocol [32], so that the incisor teeth, density standard, and directional indicator were visible on the radiograph (Fig. 1D).

The horses' incisor teeth, numbered according to the modified Triadan system [49], were classified using the radiographic classification system introduced by Hüls et al. [50] and modified by Rehl et al. [32]. Each incisor tooth, numbered as 101, 102, 103, 201, 202, or 203, was evaluated and annotated to one of the four grade–related EOTRH groups (0–3). The inclusion criterion for group 0 was no radiographic signs of EOTRH syndrome (Fig. 2A, E). The inclusion criteria for group 1 were preserved tooth shape or slightly blunted root tip as well as irregular or rough tooth surface (Fig. 2B, F). The inclusion criteria for group 2 were largely preserved tooth shape or that the intra–alveolar tooth part was not wider than the clinical crown, or obviously blunted root tip as well as irregular or rough tooth surface (Fig. 2C, G). The inclusion criteria for group 3 were loss of tooth shape or a wider intra–alveolar tooth part compared to the clinical crown, as well as obviously irregular or rough tooth surface (Fig. 2D, H). The exclusion criterion was presence of clinical and radiographic signs of diseases of the incisor teeth, including: supernumerary teeth, loose teeth, fractures, caries, and calculus [46].

Characteristic of density standard

Density standard, with a volume of 3545.93 mm^3 and dimensions: 55 mm length of the basis, 12 mm high in the highest place, 3 mm high in the lowest place, and 10 mm width, was used in this study (Fig. 3A). Density standard had the shape of an irregular cuboid with 10 steps

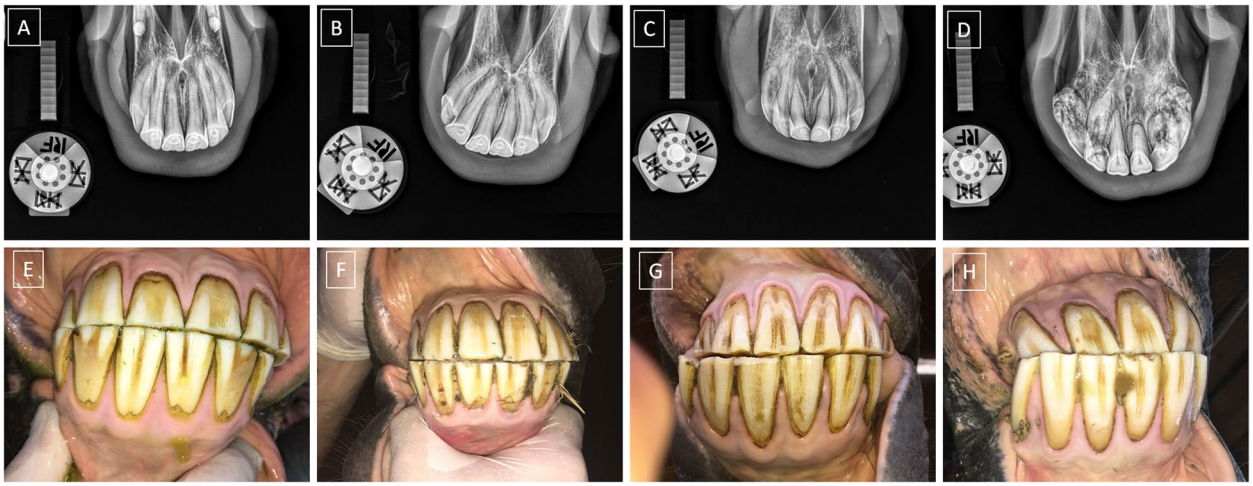

Fig. 2 Example of radiographic (**A**–**D**) and clinical (**E**–**F**) images of the incisor teeth classified to grade-related Equine Odontoclastic Tooth Resorption and Hypercementosis (EOTRH) group 0 (**A**, **E**), group 1 (**B**, **F**), group 2 (**C**, **G**) and group 3 (**D**, **H**)

(S1–S10) decreasing the height of the cuboid in the projection perpendicular to the base. Each step was 5 mm long, 1 mm high, and 10 mm wide, with the exception of the lowest step, which was 3 mm high (Fig. 3B). Density standard, with a mass of 9.39 g and a density of 2.65 g/cm^3, consisted of aluminum (Al) with a point intensity of 17 000 counts at 1.52 keV energy (Fig. 3C) and a surface intensity of 15 000 at 1.52 keV energy (Fig. 3D) measured under the scanning electron microscope (SEM) (JCM–7000 NeoScope™ Benchtop SEM, JEOL, Tokyo, Japan), which corresponded to 95.20–98,88 Mass% and 92.71–98.92 Atom% of Al (Fig. 3E–F), respectively.

The reference attenuation of the X–ray beam passing through the density standard was analysed by Materialises interactive medical image control system (MIMICS) software (Materialise HQ, Leuven, Belgium) on two referential X–ray images obtained using 2.5 mAs and 65 kV X–ray tube settings with a 80 cm distance between X–ray tube and radiographic cassette (X–ray tube, Orange 9020HF, Ecoray Co., Seoul, Korea; radiographic cassette, Saturn 8000, Vievorks Co., Seoul, Korea; portable computer, HP Inc UK Ltd, Reading, UK). The attenuation of the X–ray beam passing the density standard were presented as HU for two projections perpendicular to each other – lateral projection (Fig. 4A) and top–bottom projection (Fig. 4B). On the lateral projection, ten measuring lines corresponding to the location of the middle of S1–S10 were marked by different colors, and the HU values were displayed on the plot of HU versus distance (Fig. 4A). On the top–bottom projection, three measuring lines corresponding to the lateral, middle, and medial longitudinal sections of density standard were marked by different colors, and the HU values were displayed on the plot of HU versus distance (Fig. 4B). The values of HU measured for each of S1–S10 of density standard were summarized in Table 1 in the results section as a mean ± SD from all evaluated measuring lines.

Annotation of ROIs

On each incisor tooth, the polymorphic ROI was manually annotated using the ImageJ software (version 1.46r, Wayne Rasband, Bethesda, MD, USA). Each ROI was individually fitted to the separate tooth (101, 102, 103, 201, 202, or 203) so that the ROI covered the largest possible area of the tooth crown and root (Fig. 5A).

On each radiograph, ten rectangular regions of interest representing S1–S10 (AREAs) were manually annotated using the ImageJ software (version 1.46r, Wayne Rasband, Bethesda, MD, USA) (Fig. 5B).

Implementation of the scaled–pixel–counting protocol

The AREAs represented ten steps of density standard with various degrees of X–ray beam attenuation. Each AREAs returned the values of PB < 0; 255 > and determined the ranges of PB change in each AREAs according to the following formula:

$$< start[k], end[k] >= \langle end[k-1], \frac{1}{M \cdot N} \sum_{i=0}^{M-1} \sum_{j=0}^{N-1} AREA[k][i,j] + \left(\frac{1}{M \cdot N} \sum_{i=0}^{M-1} \sum_{j=0}^{N-1} AREA[k+1][i,j] - \frac{1}{M \cdot N} \sum_{i=0}^{M-1} \sum_{j=0}^{N-1} AREA[k][i,j] \right) /2 \rangle$$

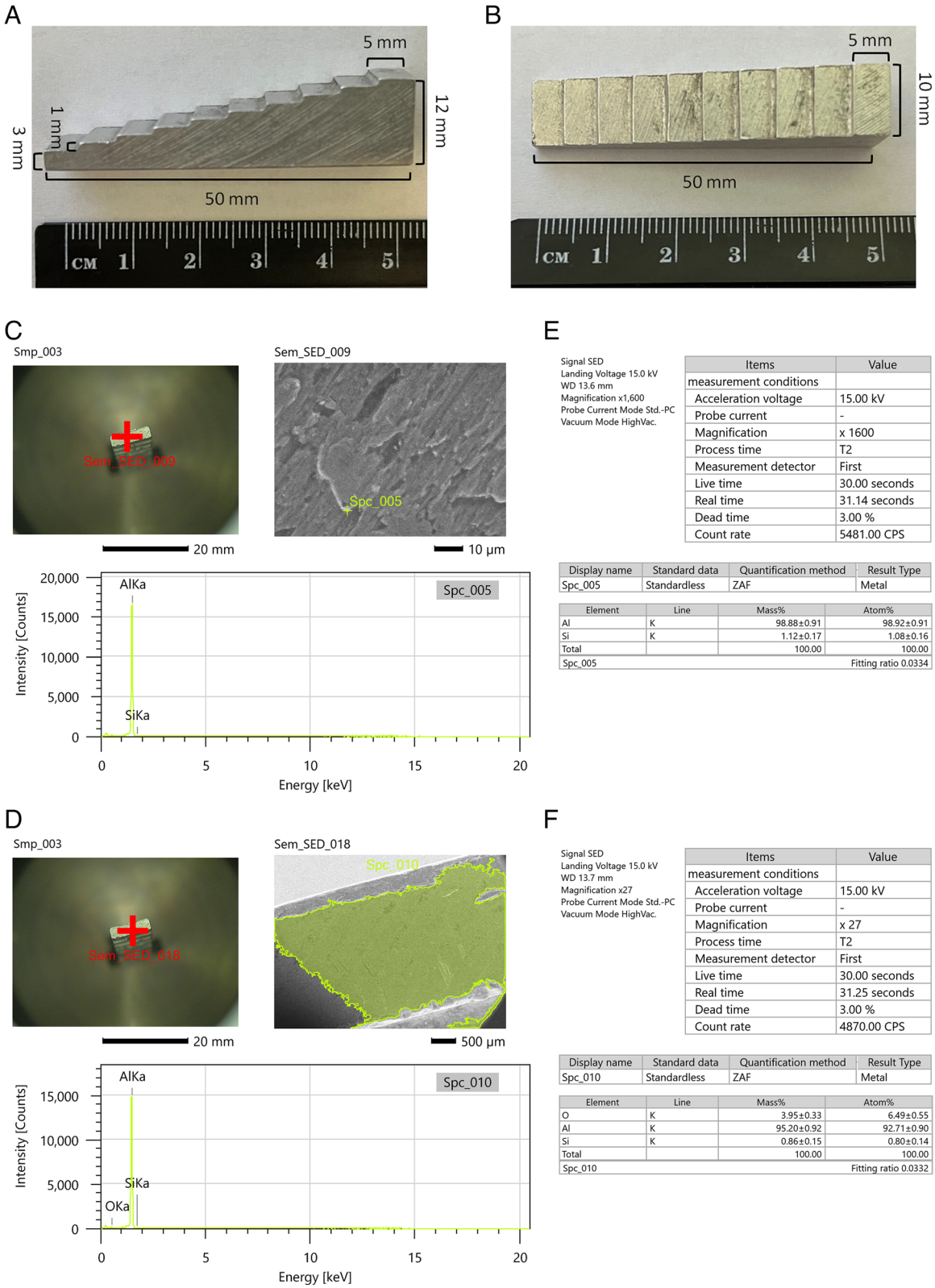

E

Signal SED
Landing Voltage 15.0 kV
WD 13.6 mm
Magnification x1,600
Probe Current Mode Std.-PC
Vacuum Mode HighVac.

Items	Value
measurement conditions	
Acceleration voltage	15.00 kV
Probe current	-
Magnification	x 1600
Process time	T2
Measurement detector	First
Live time	30.00 seconds
Real time	31.14 seconds
Dead time	3.00 %
Count rate	5481.00 CPS

Display name	Standard data	Quantification method	Result Type
Spc_005	Standardless	ZAF	Metal

Element	Line	Mass%	Atom%
Al	K	98.88±0.91	98.92±0.91
Si	K	1.12±0.17	1.08±0.16
Total		100.00	100.00
Spc_005			Fitting ratio 0.0334

F

Signal SED
Landing Voltage 15.0 kV
WD 13.7 mm
Magnification x27
Probe Current Mode Std.-PC
Vacuum Mode HighVac.

Items	Value
measurement conditions	
Acceleration voltage	15.00 kV
Probe current	-
Magnification	x 27
Process time	T2
Measurement detector	First
Live time	30.00 seconds
Real time	31.25 seconds
Dead time	3.00 %
Count rate	4870.00 CPS

Display name	Standard data	Quantification method	Result Type
Spc_010	Standardless	ZAF	Metal

Element	Line	Mass%	Atom%
O	K	3.95±0.33	6.49±0.55
Al	K	95.20±0.92	92.71±0.90
Si	K	0.86±0.15	0.80±0.14
Total		100.00	100.00
Spc_010			Fitting ratio 0.0332

Fig. 3 The lateral projection (**A**) and perpendicular to the base projection (**B**) of density standard with the marked dimensions, as well as the point (**C**) and surface (**D**) composition of density standard sample evaluated under a scanning electron microscope (SEM) and corresponding to Mass% and Atom% (E, F)

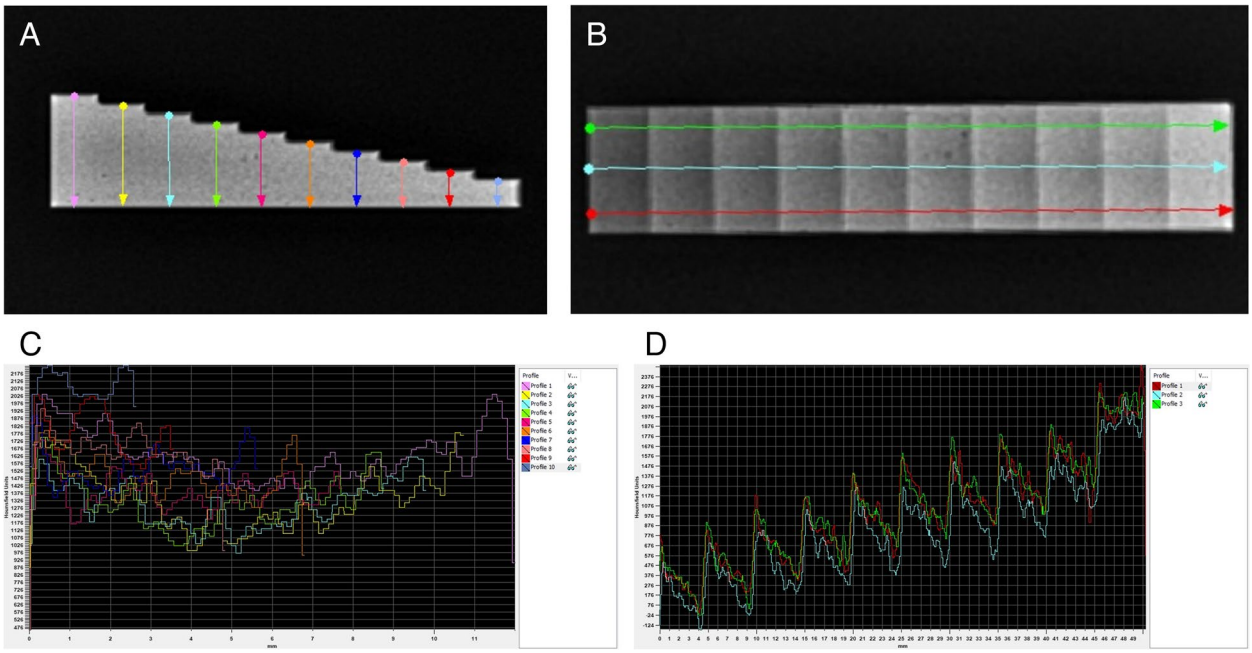

Fig. 4 The lateral projection (**A**) and top–bottom projection (**B**) of density standard with the marked measuring lines, as well as the values of ten vertical (**C**) and three horizontal (**D**) attenuations of the X–ray beam passing through the density standard evaluated by Materialises interactive medical image control system (MIMICS) and corresponding to Hounsfield unit (HU) (**E**, **F**)

Table 1 The values (mean ± standard deviation (SD)) of raw Hounsfield unit (HU) and normalized Hounsfield unit (nHU) as well as raw pixel brightness (PB) and normalized pixel brightness (nPB) measured for ten steps of density standard (S1–S10)

	S1	S2	S3	S4	S5	S6	S7	S8	S9	S10
HU mean	1009	1212	1407	1600	1804	2011	2204	2400	2607	2803
± SD	163	111	98	134	112	99	107	133	129	147
nHU	0	0.11	0.22	0.33	0.44	0.56	0.67	0.78	0.89	1.00
PB mean	83.0	93.5	101.1	108.5	115.2	121.3	127.7	133.7	143.1	168.6
± SD	10.5	10.5	11.3	12.0	12.6	12.9	13.8	14.5	16.7	17.6
nPB	0	0.07	0.17	0.21	0.26	0.29	0.35	0.42	0.53	1.00

where $start[0] = 0$ and $end[10] = 255$.

The values of PB measured for each AREAs of S1–S10 of density standard were summarized in Table 1 in the result section as a mean ± SD from all evaluated radiographs. Areas that attenuated a small amount of X–ray beam (representing soft tissue and tooth resorption) were dark, while areas that attenuated a large amount of X–ray beam (representing tooth and cement accumulation representing the areas of hypercementosis with the increased radiodensity compared to the normal lucency of the pulp canal) were bright. Thus, on the pixel brightness (PB) scale, the equivalent of radiodensity was visible in the form of different gray levels represented as 90 for soft tissue and tooth resorption, 140 for a normal tooth, and 190 for tooth cement accumulation.

These equivalents were counted for each ROI, representing each incisor tooth, as NP from each range (< PB S1; PB S10 >). In this way, the degree of X–ray beam attenuation for each incisor tooth was quantified in the form of the number of pixels (NP) data set of ten values (< NP1; NP10 >). The algorithm (Fig. 5C) was implemented in Python language.

Statistical analysis

The S1–S10 data series of mean HU and mean PB were tested independently for univariate marginal distributions using the Shapiro–Wilk normality test. Since both data series were Gaussian distributed, the Pearson correlation coefficient (r) was calculated for raw data. The value of r reflected the consistency when the $p < 0.05$. Then, the normalizing of mean HU (nHU) and normalizing of

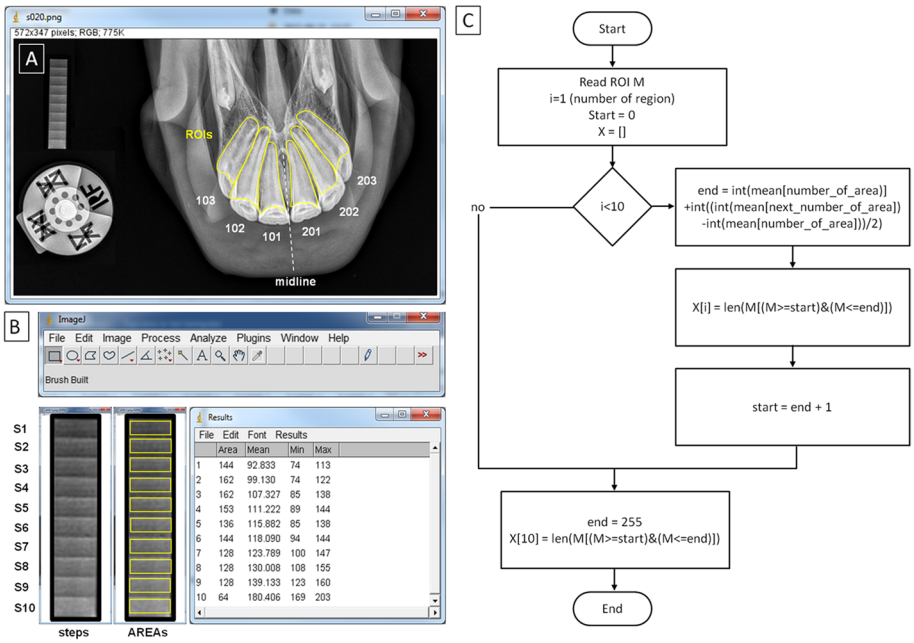

Fig. 5 Regions of interest (ROIs) annotated on incisor teeth (**A**) and regions of interest annotated on ten steps of density standard (S1-S10) (AREAs) (**B**), and the algorithm to calculate the absorption degree ranges (**C**). The algorithm counts each ROI on the incisor teeth and the number of pixels from each range (S1–S10) representing the degree of X–ray beam attenuation

mean PB (nPB) data series to the < 0,1 > range was performed. For nHU and nPB, the linear regressions were calculated. On the regression plot, regression equations for nHU and nPB were displayed and the slopes of both nHU and nPB were significantly non–zero ($p < 0.0001$). Both equations were supported with the measurement of the difference of linearity. For no significant difference between the slopes ($p > 0.05$), a single slope was calculated, and the intercepts were compared.

The whole NP data set, where each tooth of each horse represented one realization, was divided into four EOTRH grade–related groups, thus four EOTRH grade–labeled data series (EOTRH 0, EOTRH 1, EOTRH 2, EOTRH 3) were extracted. Each extracted EOTRH grade–related data series contained ten S–labeled data series (S1, S2, S3, S4, S5, S6, S7, S8, S9, S10). These forty data series were tested independently for univariate distributions using the Shapiro–Wilk normality test.

S–labelled data series were then compared between steps of density standard (S1–S10) using the Kruskal–Wallis test, followed by the Dunn's multiple comparisons test. For each data set, at least one data series was non–Gaussian distributed. The alpha value was established as $\alpha = 0.05$. Data were compared and displayed for each EOTRH group separately. The NP values were presented on plots with bars using mean + SD, where lower case letters indicated differences between steps.

EOTRH grade–labelled data series were then compared between EOTRH grades (EOTRH 0 – EOTRH 3) using the Kruskal–Wallis test, followed by the Dunn's multiple comparisons test. For each data set, at least one data series was non–Gaussian distributed. The alpha value was established as $\alpha = 0.05$. Data were compared and displayed for each step (S1–S10) separately. The NP values were presented on plots with bars using mean + SD, where lower case letters indicated differences between steps. On the respective plot, when an NP value was found to significantly increase with the EOTRH grade, the colored lines were additionally marked. An orange line was marked when the NP value increased between EOTRH 0 and 3, a red line was marked when the NP value increased between EOTRH 1 and 3, a blue line was marked when the NP value increased between EOTRH 0 and 1, and a green line was marked when the NP value increased between EOTRH 2 and 3.

Each step significantly increased with the EOTRH grades, and the accuracy of the differentiation of selected EOTRH grades was calculated using two thresholds (mean and |mean – SD|). EOTRH grade selection was marked on respective figures by the colored lines described above, thus the accuracy of differentiation of four EOTRH grade pairs, EOTRH 0 vs. 3, EOTRH 1 vs. 3, EOTRH 0 vs. 1, and EOTRH 2 vs. 3,

was estimated. The incisor tooth was annotated with a lower EOTRH grade in a pair when the individual measured value was below the threshold and annotated as higher EOTRH grade in a pair when above the threshold. The standard formulae [51] were used to calculate the sensitivity (Se), specificity (Sp), positive predictive value (PPV), and, negative predictive value (NPV) in the < 0.1, 1.0 > range.

All statistical analysis was performed using Graph Pad Prism 6 software (GraphPad Software Inc., Avenida De La Playa La Jolla, CA, USA).

Results

For density standard, mean values of HU ranged from 1009 to 2803 whereas mean values of PB ranged from 83.0 to 168.6 (Table 1). Both data series gradually increased with the thickness of the ten steps of the density standard from S1 to S10 and the Pearson correlation coefficient indicated statistically significant strong positive correlation between mean values of HU and PB (r = 0.978; $p < 0.0001$).

The similarities between nHU and nPB were tested using the linear regression model. The slope of the linear regression equations for nHU compared to the slopes of nPB were not significantly different ($p = 0.074$), and a single slope measurement was calculated (one slope = 0.098; Fig. 6). The intercept within an nHU and nPB data pair was compared and considered significant ($p = 0.001$), thus, one intercept was not calculated. Furthermore, similarity between these two X–ray beam attenuation measures can be observed.

As a result of the EOTRH group classification of the horses' incisor teeth, 105 incisor teeth passed the criteria of grade–related EOTRH group 0, 195 incisor teeth passed the criteria of grade–related EOTRH group 1, 111 incisor teeth passed the criteria of grade–related EOTRH group 2, and 61 incisor teeth passed the criteria of grade–related EOTRH group 3. On this basis the structure of maxillary incisor teeth classification was as follows: grade 0 (normal teeth) $n = 105$, grade 1 (mild EOTRH) $n = 195$, grade 2 (moderate EOTRH) $n = 111$, and grade 3 (severe EOTRH) $n = 61$. In total, eight incisor teeth were excluded from the study due to clinical and radiographic signs of the teeth encompassing the following problems: loose teeth ($n = 2$), transverse fractures ($n = 3$), sagittal fractures ($n = 2$), and infundibular caries ($n = 1$), consequently the total number of 472 incisor teeth were further investigated.

Comparing NP values between the S1–S10 for each EOTRH–related group separately, the NP values gradually increased, from the lowest values in S1 to the highest values in S10, regardless of the EOTRH grade (Fig. 3). This increase in the extracted image brightness indicator was significant from S6 in EOTRH 0 ($p < 0.0001$; Fig. 3A), from S3 in EOTRH 1 ($p < 0.0001$; Fig. 3B), from S5 in EOTRH 2 ($p < 0.0001$; Fig. 3C), and from S6 in EOTRH 3 ($p < 0.0001$; Fig. 3D). Moreover, in EOTRH group 0, one may observe the differences in NP values between S1–S4 and S8–S10, S5–S7 and S8–S10, S7–S8 and S9–S10, as well as S9 and S10. In EOTRH group 1, the most differences were noted in NP values, namely between S3–S4 and S5–S10, S5–S7 and S8–S10, S7–S8 and S9–S10, as well as S9–S10. In EOTRH group 2, the differences in NP values were observed between S4–S7 and S8–S10, S6–S8 and S9–S10, as well as S9–S10. Similarly in EOTRH group 3, the differences in NP values were noted between S4–S8 and S9–S10 as well as S8–S10.

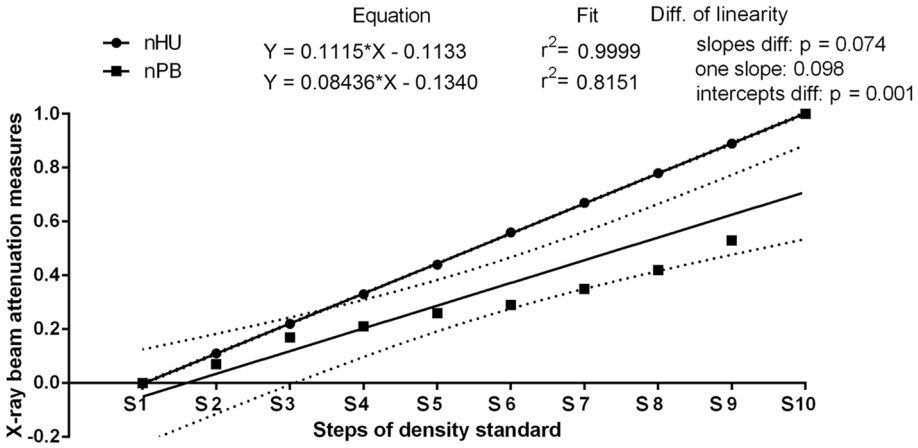

Fig. 6 Comparison of normalized Hounsfield unit (nHU) and normalized pixel brightness (nPB) throughout ten steps of density standard (S1–S10). Similarity was tested using linear regressions and considered significant for $p < 0.05$. If the difference between slopes was not significant ($p > 0.05$), a single slope measurement was calculated

Comparing NP values between the EOTRH grades for each S–labelled data series separately, NP values increased from the lowest values in EOTRH 0 to the highest in EOTRH 3 in S1–S8 (Fig. 7A–H) but not S9–S10 (Fig. 7I–J). One may observe two patterns of the increase in the extracted image brightness indicator. In the first pattern, the differences in NP values were noted between EOTRH 0 and 3 as well as EOTRH 1 and 3, and marked by orange and red lines, respectively. Whereas in the second pattern, the differences in NP values were observed between EOTRH 0 and 3, EOTRH 0 and 1, as well as EOTRH 2 and 3, and marked by orange, blue, and green lines, respectively. The first pattern was recognized for S1 ($p < 0.0001$; Fig. 7A), S2 ($p < 0.0001$; Fig. 7B), S6 ($p < 0.0001$; Fig. 7F), S7 ($p < 0.0001$; Fig. 7G), and S8 ($p < 0.0001$; Fig. 7H); whereas the second one for S3 ($p < 0.0001$; Fig. 7C), S4 ($p < 0.0001$; Fig. 7D), and S5 ($p < 0.0001$; Fig. 7E).

For the shown differences in NP values between the EOTRH grades, the accuracy of the differentiation of EOTRH 0 and 3, EOTRH 1 and 3, EOTRH 0 and 1, as well as EOTRH 2 and 3 was calculated, respectively (Table 2). For the first threshold (mean), the highest Se (0.38) was noted for EOTRH 0 and 3 in S6, EOTRH 1 and 3 in S6, EOTRH 0 and 3 in S7, as well as EOTRH 1 and 3 in S7. Se ranged from referred 0.38 to 0.17 for EOTRH 0 and 1 in S7; whereas Sp ranged from 1.00 for EOTRH 0 and 3 in S1 to 0.74 for EOTRH 1 and 3 in S7. For the second threshold (|mean – SD|), the highest Se (0.98) was observed for EOTRH 0 and 3 in S8 as well as EOTRH 1 and 3 in S8. Se ranged from referred 0.98 to 0.08 for EOTRH 0 and 1 in S3; whereas Sp ranged from 1.00 for EOTRH 0 and 3 in S1 to 0.31 for EOTRH 1 and 3 in S8. One may observe that the Se of differentiation of EOTRH 0 and 1 increased in the case of both thresholds used, from the lowest in S3, higher in S4, to the highest in S5, despite that for each of the awarded steps low Se and high Sp was noted.

Discussion

The techniques to enhance early detection of radiographic signs of dental diseases in horses is an important direction of recent research in equine dentistry [2, 38, 52–54]. Most recently, filtering algorithms and texture analysis of incisor teeth radiographs, based on the first– and second–order statistics [38] and two–dimensional entropy measures [52], have been successfully used in

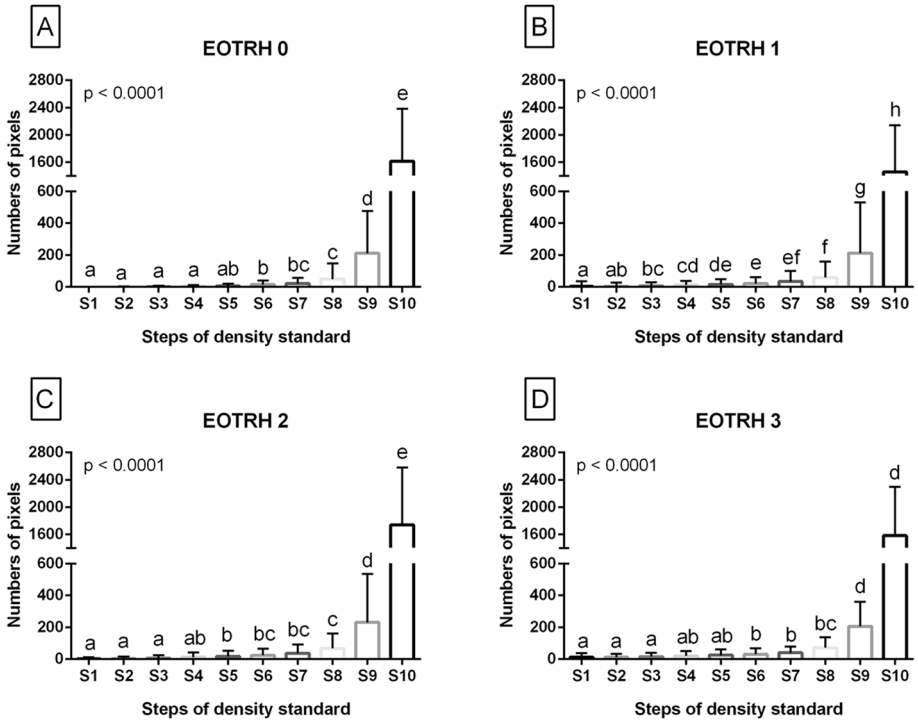

Fig. 7 The comparison of the numbers of pixels (NP) between Equine Odontoclastic Tooth Resorption and Hypercementosis (EOTRH) grades (EOTRH 0–3). Data displayed separately for consecutive steps of density standard—S1 (A), S2 (B), S3 (C), S4 (D), S5 (E), S6 (F), S7 (G), S8 (H), S9 (I) and S10 (J). Lower case letters (a–c) indicate differences between groups for $p < 0.05$. The significant increase with the EOTRH grades is marked with colored lines – orange line when the increase was noted between EOTRH 0 and 3, red line when the increase was observed between EOTRH 1 and 3, blue line when the increase was observed between EOTRH 0 and 1, and green line when the increase occurred between EOTRH 2 and 3

Table 2 The accuracy of the differentiation of radiographic signs of selected EOTRH 0 – 3 grades based on the numbers of pixels (NP) of the selected pixel brightness (PB) in consecutive steps of density standard (S1–S10). Sensitivity (Se), specificity (Sp), positive predictive value (PPV), and, negative predictive value (NPV) were calculated using two thresholds (mean and |mean – SD|)

Step	EOTRH		Se	Sp	PPV	NPV	Se	Sp	PPV	NPV
	lower	higher	mean				|mean – SD|			
S1	0	3	0.25	1.00	1.00	0.70	0.25	1.00	1.00	0.70
S2	0	3	0.30	0.99	0.95	0.71	0.30	0.96	0.82	0.70
S3	0	3	0.31	0.96	0.83	0.71	0.41	0.96	0.86	0.74
S4	0	3	0.36	0.95	0.81	0.72	0.49	0.89	0.71	0.75
S5	0	3	0.23	0.93	0.67	0.68	0.52	0.74	0.54	0.73
S6	0	3	0.38	0.82	0.55	0.69	0.67	0.68	0.55	0.78
S7	0	3	0.38	0.79	0.51	0.69	0.97	0.40	0.48	0.95
S8	0	3	0.34	0.78	0.48	0.67	0.98	0.46	0.51	0.98
S1	1	3	0.25	0.96	0.65	0.80	0.25	0.96	0.65	0.80
S2	1	3	0.30	0.94	0.60	0.81	0.30	0.91	0.51	0.81
S6	1	3	0.38	0.79	0.36	0.80	0.67	0.57	0.33	0.85
S7	1	3	0.38	0.74	0.32	0.79	0.97	0.32	0.31	0.97
S8	1	3	0.34	0.76	0.31	0.79	0.98	0.31	0.31	0.98
S3	2	3	0.30	0.90	0.65	0.67	0.39	0.83	0.59	0.68
S4	2	3	0.34	0.85	0.59	0.67	0.46	0.74	0.53	0.68
S5	2	3	0.33	0.80	0.51	0.65	0.33	0.75	0.46	0.64
S3	0	1	0.17	0.94	0.85	0.38	0.08	0.96	0.79	0.36
S4	0	1	0.21	0.91	0.82	0.38	0.16	0.94	0.84	0.38
S5	0	1	0.25	0.80	0.70	0.36	0.23	0.82	0.70	0.36

EOTRH 0 and 3 differentiation. Visually, it is less difficult to identify radiographic signs of EOTRH 3, representing severe tooth hypercementosis and resorption, and EOTRH 0, representing healthy teeth [32]. Therefore, one may conclude the use of digital processing techniques in these cases will enhance the quality of the maxillary incisor radiographs so that the radiologist can more easily identify the radiographic signs. However, no clear differentiation of radiographic signs of EOTRH 1, representing mild tooth hypercementosis and resorption [32], and EOTRH 0, were evidenced [38, 52]. In the case of visual inspection, early signs of EOTRH might be missed by merely personal evaluation of radiographs. Therefore, specific detection of early radiographic signs of EOTRH is a major component of using digital processing of radiographs to enhance automated disease detection. The first step in achieving this goal using the density standard and scaled–pixel–counting protocol was presented in the current preliminary research.

The demonstration of the strong positive correlation between mean values of HU and PB points to the relationship between a linear transformation of the original linear X–ray beam attenuation coefficient measurement into the HU scale [11] and a linear transformation of the pixel brightness degree measurement into the PB scale. This linear relationship was confirmed by linear regression equations for nHU and nPB indicating the similarity between these two X–ray beam attenuation measures, the classic direct (nHU) [11, 36] and the new indirect (nPB) one. As the X–ray beam attenuation increases with tissue thickness [55] the experimentally determined linearity was confirmed in a clinical study by an increase in the NP value with an increase in the number of steps of density standard. This increase can be seen in Fig. 8 irrespective of EOTRH grades. These observations justify the use of density standard for indirect quantification of the brightness of the radiograph, and thus the use of the proposed scaled–pixel–counting protocol for indirect quantification of the radiographic signs of tooth resorption and hypercementosis on the EOTRH syndrome model. Recent research has discussed the use of histogram–based and matrix–based texture features [38] and two–dimensional entropy measures [52] in the digital processing of EOTRH radiographs. These studies were focused only on maxillary, not maxillary and mandibular, incisor teeth. The maxillary incisor teeth were considered as the best choice for this preliminary research due to the lowest superimposition of surrounding tissues compared to other horse teeth [45]. Therefore, the implementation of the scaled–pixel–counting protocol to quantify and compare the

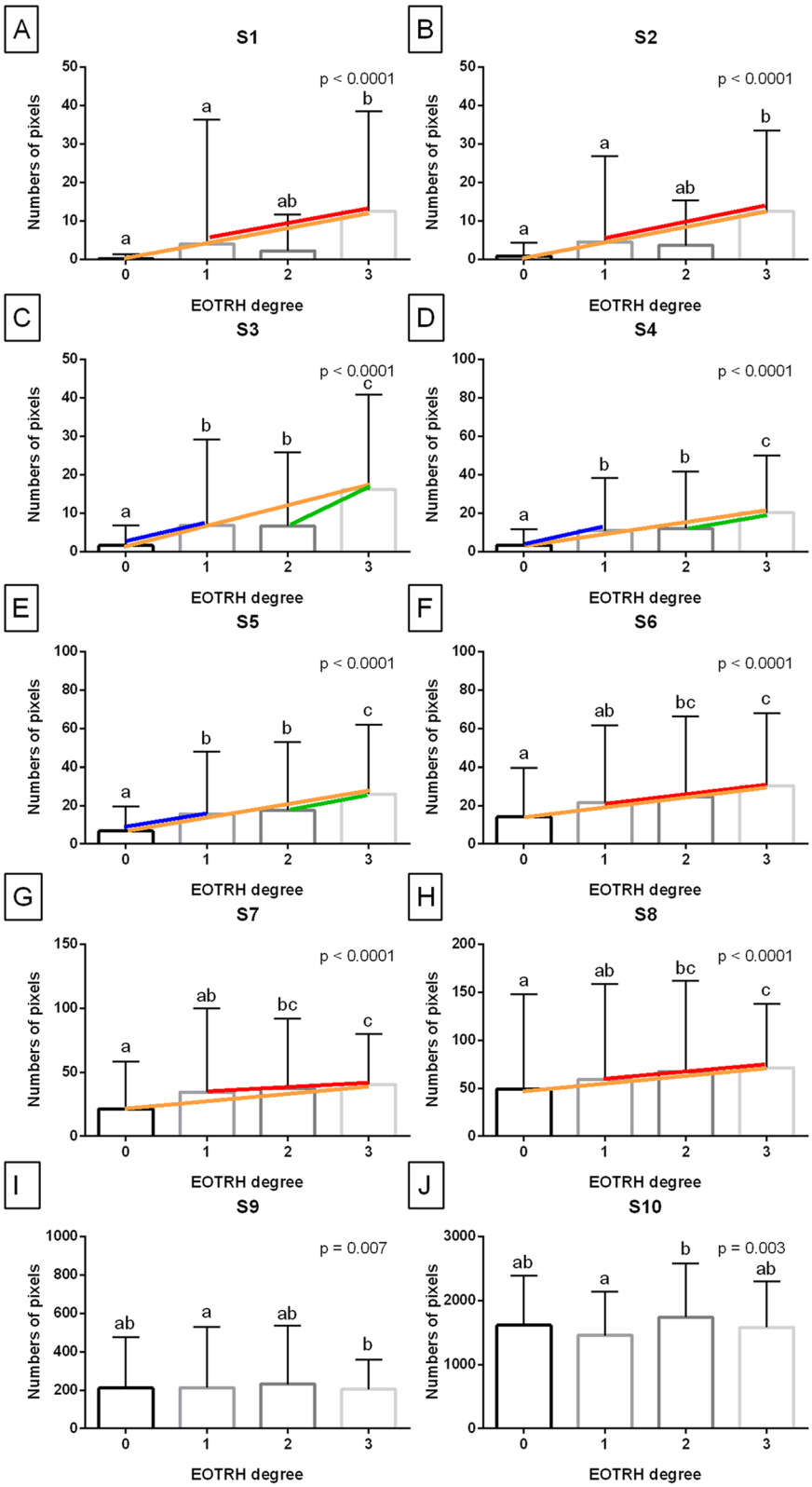

Fig. 8 The comparison of the numbers of pixels (NP) between ten steps of density standard (S1-S10). Data displayed separately for consecutive Equine Odontoclastic Tooth Resorption and Hypercementosis (EOTRH) grades – EOTRH 0 (A), EOTRH 1 (B), EOTRH 2 (C), and EOTRH 3 (D). Lower case letters (a–h) indicate differences between groups for $p < 0.05$

image structure of teeth and density standard was focused similarly, only on teeth 101, 102, 103, 201, 202, and 203. Apart from the computational part, the only modification to the standard equine dental radiographs acquisition concerned the attachment of the density standard to the radiographic cassette. Thus, use radiography according to the protocol adapted in the current study is no more contraindicated than a complete protocol of the dental examination. In many cases of equine dental diseases, a visual examination of the oral cavity allows the veterinarian to identify and manage dental problems and diagnose diseases in their early stages [45]. In some diseases, such as EOTRH [32, 56], teeth fractures [1, 57, 58], teeth infections [1, 57], or remodelling and lysis of alveolar bone [1, 57, 59], dental radiographic imaging is beneficial. This advantage can be seen in Fig. 6, where the signs of successive EOTRH grades are radiographically, rather than visually, visible.

In the current study, the differences in NP values were noted between EOTRH 0 and 3, EOTRH 0 and 2, as well as EOTRH 0 and 1. The EOTRH groups 0 and 3 are easily differentiated visually based on the radiographic signs. In the current study, most of the teeth in EOTRH group 3 showed a smooth outline despite the obvious internal changes, whereas, on recent raw [32, 37, 56, 60] and digitally processed [38, 52] radiographs, the signs of obviously irregular or rough incisor tooth surfaces were predominately. In recently published research, the accuracy of EOTRH group 0 and 3 differentiation ranged from 0.25 Sp and 0.99 Se for matrix–based texture features to 0.50 Sp and 1.00 Se for two–dimensional entropy measures [52]. In the current study, the accuracy of EOTRH 0 and 3 differentiation ranged from 0.25 Sp and 1.00 Se for S1 to 0.38 Sp and 0.82 Se for S6. In both cases, the mean threshold was used and the achieved results were at a similar level. However, the accuracy of NP–depended differentiation of referred EOTRH grades increased when |mean–SD| threshold was applied. Thus, one may conclude, an appropriate selection of threshold may improve the effectiveness of detecting radiographic signs of the disease, however further research is required. Noteworthy in the current study is that the accuracy of EOTRH 0 and 1 differentiation reached the level of 0.25 Sp and 0.80 Se, which indicates that the used indirect assessment of radiodensity of equine incisor teeth makes it possible to differentiate early radiographic signs of mild EOTRH [32] from healthy incisor teeth. Although the sensitivity to distinguish between these two is not sufficiently high, the achieved results justify the need for further research on the use of the density standard and scaled–pixel–counting protocol in digital processing of radiographs in order to provide automated disease detection. The current study was based on the raw radiographs collected directly from the X–ray scanner, which were not digitally processed, therefore the use of radiograph filtering may enhance the quality of the radiographs and thus, increase the Sp and Se of detecting early radiographic signs of EOTRH. Filtering, which enhances brightness, contrast, and/or edges of radiographs, is routinely used in human dentistry [61, 62] and has been introduced into equine dentistry [38, 52], and this direction of further research development seems to be promising.

Conclusion

The scaled–pixel–counting protocol based on the use of density standard has been successfully implemented for the differentiation of radiographic signs of EOTRH degrees. The linear relationship between an original X–ray beam attenuation coefficient measured in the HU scale and a new pixel brightness degree measured in the PB scale was confirmed, thus the NP values representing incisor teeth structure and consecutive steps of density standard were compared. The NP values increase with the number of steps of density standard as well as with EOTRH degrees, confirming the clinical usefulness of the PB–counting model in assisted differentiation of radiographic signs of EOTRH grades. Noteworthy, similar accuracy of the EOTRH grade differentiation was noted for data pairs EOTRH 0–3 and EOTRH 0–1, one may suggest the presented protocol may hereafter be applied to automated detection of both late and early radiographic signs of tooth resorption and hypercementosis.

Abbreviations

AREAs	Regions of interest representing S1–S10
CBCT	Cone–beam computed tomography
CT	Computed tomography
EOTRH	Equine Odontoclastic Tooth Resorption and Hypercementosis
FBCT	Fan–beam computed tomography
hr MRI	High resolution–magnetic resonance imaging
hr pQCT	High–resolution peripheral quantitative computed tomography
HU	Hounsfield units
MDCT	Multi–detector computed tomography
MIMICS	Materialises interactive medical image control system
nHU	Normalized Hounsfield unit
NP	Number of pixels
nPB	Normalized pixel brightness
NPV	Negative predictive value
PB	Pixel brightness
PPV	Positive predictive value
r	The Pearson correlation coefficient
ROI	Region of interest
S1–S10	Ten steps of the density standard
SD	Standard deviation
Se	Sensitivity
SEM	Scanning electron microscope
Sp	Specificity

Acknowledgements

Not applicable.

Authors' contributions
KG, MB, and MD conceived of the study and participated its design. KG, MB, BT, MP, KJ and MD collected and analyzed the data. AB and IP were involved in the clinical examination and helped edit the manuscript. All authors read, edited and approved the final manuscript.

Funding
The research was performer as a part of the project Miniatura 6 No 2022/06/X/ST6/00431 and was financed with the founds for science from the Polish Ministry of Science and Higher Education.

Availability of data and materials
All data generated or analyzed during this study are included in this published article. If any additional material used and/or analyzed during the current study is required, these are available from the corresponding author on reasonable request.

Declarations

Ethics approval and consent to participate
The study was approved by the II Local Ethical Committee on Animal Testing in Warsaw on behalf of the National Ethical Committees on Animal Testing (No WAW2/091/2020, day 29.07.2020). All methods were performed in accordance with the national (the Polish decree–law Dz. U. 2015 poz. 266) and international (the European Union (EU) law 2010–63–EU directive) guidelines and regulations.
The owners were informed of the inclusion of their horses in the study and provided written informed consent to the inclusion of their horses' data in the current study.

Consent for publication
Not applicable.

Competing interests
The authors declare no competing interests.

Author details
[1]Department of Large Animal Diseases and Clinic, Institute of Veterinary Medicine, Warsaw University of Life Sciences (WULS – SGGW), Nowoursynowska 100, 02-797 Warsaw, Poland. [2]Institute of Biomedical Engineering, Faculty of Mechanical Engineering, Białystok University of Technology, Wiejska 45C, 15-351 Bialystok, Poland. [3]Institute of Mechanics and Printing, Warsaw University of Technology, Narbutta 85, 02-524 Warsaw, Poland. [4]Division of Veterinary Epidemiology and Economics, Institute of Veterinary Medicine, Warsaw University of Life Sciences, Nowoursynowska 159C, 02-776 Warsaw, Poland. [5]Department and Clinic of Animal Surgery, Faculty of Veterinary Medicine, University of Life Sciences in Lublin, Głęboka 30, 20-950 Lublin, Poland.

Received: 7 January 2023 Accepted: 24 July 2023
Published online: 09 August 2023

References

1. Dixon PM, Dacre I. A review of equine dental disorders. Vet J. 2005;169:165–87. https://doi.org/10.1016/j.tvjl.2004.03.022.
2. Pearce CJ. Recent developments in equine dentistry. N Z Vet J. 2020;68:178–86. https://doi.org/10.1080/00480169.2020.1722971.
3. Kopke S, Angrisani N, Staszyk C. The dental cavities of equine cheek teeth: three-dimensional reconstructions based on high resolution micro-computed tomography. BMC Vet Res. 2012;8:1–16. https://doi.org/10.1186/1746-6148-8-173.
4. Englisch LM, Rott P, Lüpke M, et al. Anatomy of equine incisors: pulp horns and subocclusal dentine thickness. Equine Vet J. 2018;50:854–60. https://doi.org/10.1111/evj.12841.
5. Brounts SH, Henry T, Lund JR, et al. Use of a novel helical fan beam imaging system for computed tomography of the head and neck in sedated standing horses: 120 cases (2019–2020). J Am Vet Med Assoc. 2022;260:1361–8. https://doi.org/10.2460/javma.21.10.0439.
6. Colgate VA, Wylie CE, Barnett TP. Do Oral or Minimally Invasive Cheek Tooth Extraction Techniques Reduce the Incidence of Post-operative Complications in the Horse When Compared to Repulsion Methods? Vet Evid. 2018;3:1–27. https://doi.org/10.18849/ve.v3i3.158.
7. Lechuga L, Weidlich GA. Cone beam CT vs. fan beam CT: a comparison of image quality and dose delivered between two differing CT imaging modalities. Cureus. 2016;8:e778. https://doi.org/10.7759/cureus.778.
8. Van Zadelhoff C, Liuti T, Dixon PM, et al. Multidetector CT and cone-beam CT have substantial agreement in detecting dental and sinus abnormalities in equine cadaver heads. Vet Radiol Ultrasound. 2021;62:413–20. https://doi.org/10.1111/vru.12978.
9. Soukup JW, Drees R, Koenig LJ, et al. Comparison of the diagnostic image quality of the canine maxillary dentoalveolar structures obtained by cone beam computed tomography and 64-multidetector row computed tomography. J Vet Dent. 2015;32:80–6. https://doi.org/10.1177/0898756415031502001.
10. Ibrahim N, Parsa A, Hassan B, et al. Accuracy of trabecular bone microstructural measurement at planned dental implant sites using cone-beam CT datasets. Clin Oral Implants Res. 2014;25:941–5. https://doi.org/10.1111/clr.12163.
11. Shipley T, Farouk K, El-Bialy T. Effect of high-frequency vibration on orthodontic tooth movement and bone density. J Orthod Sci. 2019;8:15. https://doi.org/10.4103/jos.JOS_17_19.
12. Whittier DE, Boyd SK, Burghardt AJ, et al. Guidelines for the assessment of bone density and microarchitecture in vivo using high-resolution peripheral quantitative computed tomography. Osteoporos Int. 2020;31:1607–27. https://doi.org/10.1007/s00198-020-05438-5.
13. Mah P, Reeves TE, McDavid WD. Deriving Hounsfield units using grey levels in cone beam computed tomography. Dentomaxillofacial Radiol. 2010;39:323–35. https://doi.org/10.1259/dmfr/19603304.
14. Reeves TE, Mah P, McDavid WD. Deriving Hounsfield units using grey levels in cone beam CT: A clinical application. Dentomaxillofacial Radiol. 2012;41:500–8. https://doi.org/10.1259/dmfr/31640433.
15. Kim D. Can dental cone beam computed tomography assess bone mineral density? J Bone Miner Metab. 2014;21:117–26. https://doi.org/10.11005/jbm.2014.21.2.117.
16. Aranyarachkul P, Caruso J, Gantes B, et al. Bone density assessments of dental implant sites: 2. Quantitative cone-beam computerized tomography. Int J Oral Maxillofac Imp. 2015;20:416–24.
17. Yu J, Huang H, Liu C, et al. Does orthodontic treatment affect the alveolar bone density? Medicine. 2016;95:e3080.
18. Herren FL, Gerber V, Meier R, Schweizer-Gorgas D, Klopfenstein Bregger MD. Semi-Automatic Segmentation of Cone Beam Computed Tomography Datasets for Volume Measurements of Equine Cheek Teeth. J Vet Dent. 2022;39:41–8. https://doi.org/10.1177/08987564211061630.
19. Manso-Díaz G, García-López JM, Maranda L, et al. The role of head computed tomography in equine practice. Equine Vet Educ. 2015;27:136–45. https://doi.org/10.1111/eve.12275.
20. Liuti T, Smith S, Dixon PM. Radiographic, computed tomographic, gross pathological and histological findings with suspected apical infection in 32 equine maxillary cheek teeth (2012–2015). Equine Vet J. 2018;50:41–7. https://doi.org/10.1111/evj.12729.
21. Ostrowska J, Lindström L, Tóth T, et al. Computed Tomography Characteristics of Equine Paranasal Sinus Cysts. Equine Vet J. 2020;52:538–46. https://doi.org/10.1111/evj.13212.
22. Fenner MF, Verwilghen D, Townsend N, et al. Paranasal Sinus Cysts in the Horse: Complications Related to Their Presence and Surgical Treatment in 37 Cases. Equine Vet J. 2019;51:57–63. https://doi.org/10.1111/evj.12959.
23. Liuti T, Smith S, Dixon PM. A comparison of computed tomographic, radiographic, gross and histological, dental, and alveolar findings in 30 abnormal cheek teeth from equine cadavers. Front Vet Sci. 2018;4:236. https://doi.org/10.3389/fvets.2017.00236.
24. Miró F, Manso C, Diz A, et al. Maxillary Incisors of the Horse before and at the Beginning of the Teeth Shedding: Radiographic and CT Study. Animals. 2020;10:1618. https://doi.org/10.3390/ani10091618.
25. Dakin SG, Lam R, Rees E, et al. Technical Set-up and Radiation Exposure for Standing Computed Tomography of the Equine Head: Standing CT of the Equine Head. Equine Vet Educ. 2014;26:208–15. https://doi.org/10.1111/eve.12127.

26. Earley E, Rawlinson JT. A New Understanding of Oral and Dental Disorders of the Equine Incisor and Canine Teeth. Vet Clin North Am Equine Pract. 2013;29:273–300. https://doi.org/10.1016/j.cveq.2013.04.011.
27. Rawlinson JT, Earley E. Advances in the Treatment of Diseased Equine Incisor and Canine Teeth. Vet Clin North Am Equine Pract. 2013;29:411–40. https://doi.org/10.1016/j.cveq.2013.04.005.
28. Baratt RM. Dental Radiography and Radiographic Signs of Equine Dental Disease. Vet Clin North Am Equine Pract. 2020;36:445–76. https://doi.org/10.1016/j.cveq.2020.08.001.
29. Tucker RL, Farrell E. Computed Tomography and Magnetic Resonance Imaging of the Equine Head. Vet Clin North Am Equine Pract. 2001;17:131–44. https://doi.org/10.1016/s0749-0739(17)30079-2.
30. Epperly E, Whitty JA. Equine Imaging: Computed Tomography Interpretation. Vet Clin North Am Equine Pract. 2020;36:527–43. https://doi.org/10.1016/j.cveq.2020.08.007.
31. Manso-Díaz G, Taeymans O, García-López JM, et al. Application and indications of magnetic resonance imaging and computed tomography of the equine head. Equine Vet Educ. 2021;33:31–46. https://doi.org/10.1111/eve.13075.
32. Rehrl S, Schröder W, Müller C, et al. Radiological prevalence of equine odontoclastic tooth resorption and hypercementosis. Equine Vet J. 2018;50:481–7. https://doi.org/10.1111/evj.12776.
33. Townsend NB, Hawkes CS, Rex R, et al. Investigation of the sensitivity and specificity of radiological signs for diagnosis of periapical infection of equine cheek teeth. Equine Vet J. 2011;43:170–8. https://doi.org/10.1111/j.2042-3306.2010.00148.x.
34. Hathcock JT, Stickle RL. Principles and Concepts of Computed Tomography. Vet Clin North Am Small Anim Pract. 1993;23:399–415. https://doi.org/10.1016/s0195-5616(93)50034-7.
35. Hounsfield GN. Nobel Award address. Computed medical imaging Med Phys. 1980;7:283–90. https://doi.org/10.1118/1.594709.
36. Hanusch BC, Tuck SP, Mekkayil B, et al. Quantitative Computed Tomography (QCT) of the Distal Forearm in Men Using a Spiral Whole-Body CT Scanner-Description of a Method and Reliability Assessment of the QCT Pro Software. J Clin Densitom. 2020;23:418–25. https://doi.org/10.1016/j.jocd.2019.05.005.
37. Saccomanno S, Passarelli PCB, Oliva B, et al. Comparison between two radiological methods for assessment of tooth root resorption: An in vitro study. Biomed Res Int. 2018;2018:5152172. https://doi.org/10.1155/2018/5152172.
38. Górski K, Borowska M, Stefanik E, et al. Selection of Filtering and Image Texture Analysis in the Radiographic Images Processing of Horses' Incisor Teeth Affected by the EOTRH Syndrome. Sensors. 2022;22:2920. https://doi.org/10.3390/s22082920.
39. Suske A, Pöschke A, Schrock P, et al. Infundibula of equine maxillary cheek teeth. Part 1: Development, blood supply and infundibular cementogenesis. Vet J. 2016;209:57–65. https://doi.org/10.1016/j.tvjl.2015.07.029.
40. Staszyk C, Bienert A, Kreutzer R, et al. Equine odontoclastic tooth resorption and hypercementosis. Vet J. 2008;178:372–9. https://doi.org/10.1016/j.tvjl.2008.09.017.
41. Smedley RC, Earley ET, Galloway SS, et al. Equine odon-toclastic tooth resorption and hypercementosis: Histopathologic features. Vet Pathol. 2015;52:903–9. https://doi.org/10.1177/0300985815588608.
42. Dixon PM, Tremaine WH, Pickles K, et al. Equine dental disease Part 3: A long term study of 400 case: Disorders of wear, traumatic and idiopathic fractures, tumours and mis-cellaneous disorders of the cheek teeth. Equine Vet J. 1999;32:9–18. https://doi.org/10.2746/042516400777612099.
43. Pearce CJ. Treatment of maxillary cheek teeth apical infection caused by patent infundibula in six horses (2007–2013). Equine Vet Educ. 2016;28:600–8.
44. Costa LR. History and Physical Examination of the Horse. In: Manual of clinical procedures in the horse. Hoboken, New Jersey, USA, Wiley-Blackwell; 2017 pp. 27–58.
45. Limone L. General clinical, oral and dental examination. In: Equine Dentistry and Maxillofacial Surgery. Newcastle upon Tyne: UK, Cambridge Scholars Publishing; 2022. p. 302.
46. Górski K, Stefanik E, Turek B, et al. Malocclusions and Dental Diseases in Privately Owned Horses in the Mazovia Region of Poland. Animals. 2022;12:3120. https://doi.org/10.3390/ani12223120.
47. Górski K, Tremaine H, Obrochta B, et al. EOTRH Syndrome in Polish Half-Bred Horses-Two Clinical Cases. J Equine Vet Sci. 2021;101:103428.
48. Barrett MF, Easley JT. Acquisition and interpretation of radiographs of the equine skull. Equine Vet Educ. 2013;25:643–52. https://doi.org/10.1111/eve.12086.
49. Floyd MR. The modified Triadan system: Nomenclature for veterinary dentistry. J Vet Dent. 1991;8:18–9. https://doi.org/10.1177/089875649100800402.
50. Hüls I, Bienert A, Staszyk C. Equine odontoclastic tooth resorption and hyper-cementosis (EOTRH): Röntgenologische und makroskopisch-anatomische Befunde. In Proceedings of the 10 Jahrestagung der Internationalen Gesellschaft zur Funktionsverbesserung der Pferdezähne,Wiesbaden, Germany, 3–4 March 2012.
51. Dohoo I, Martin W, Stryhn H. Veterinary Epidemiologic Research. 2nd ed. Charlottetown: PE, Canada, VER Inc; 2009. p. 112–31.
52. Górski K, Borowska M, Stefanik E, et al. Application of Two-Dimensional Entropy Measures to Detect the Radiographic Signs of Tooth Resorption and Hypercementosis in an Equine Model. Biomedicines. 2022;10:2914. https://doi.org/10.3390/biomedicines10112914.
53. Weller R, Livesey L, Maierl J, et al. Comparison of radiography and scintigraphy in the diagnosis of dental disorders in the horse. Equine Vet J. 2001;33:49–58. https://doi.org/10.2746/042516401776767458.
54. Henninger W, Mairi Frame E, Willmann M, et al. CT features of alveolitis and sinusitis in horses. Vet Radiol Ultrasound. 2003;44:269–76. https://doi.org/10.1111/j.1740-8261.2003.tb00454.x.
55. Laskey MA. Dual-energy X-ray absorptiometry and body composition. Nutrition. 1996;12:45–51. https://doi.org/10.1016/0899-9007(95)00017-8.
56. Henry TJ, Puchalski SM, Arzi B, et al. Radiographic evaluation in clinical practice of the types and stage of incisor tooth resorption and hypercementosis in horses. Equine Vet J. 2016;49:486–92. https://doi.org/10.1111/evj.12650.
57. Greet TRC. Oral and dental trauma. In: Baker GJ, Easley J, editors. Equine Dentistry. 1st ed. London: UK; W.B. Saunders; 1999. p. 60–9.
58. Dacre I, Kempson S, Dixon PM. Equine idiopathic cheek teeth fractures. Part 1: Pathological studies on 35 fractured cheek teeth. Equine Vet J. 2007;39:310–8. https://doi.org/10.2746/042516407x182721.
59. Easley J. A new look at dental radiography. In Proceedings of the 48th Annual Convention of the American Association of Equine Practitioners, Orlando, FL, USA, 4–8 December 2002; 48: pp. 412–420.
60. Rahmani VH, Häyinen L, Kareinen I, et al. History, clinical findings and outcome of horses with radiographical signs of equine odontoclastic tooth resorption and hypercementosis. Vet Rec. 2019;185:730. https://doi.org/10.1136/vr.105253.
61. Belém MDF, Ambrosano GMB, Tabchoury CPM, et al. Performance of digital radiography with enhancement filters for the diagnosis of proximal caries. Braz Oral Res. 2013;27:245–51. https://doi.org/10.1590/S1806-83242013000300004.
62. Geetha V, Aprameya KS. Textural analysis based classification of digital X-ray images for dental caries diagnosis. Int J Manuf Eng. 2019;9:44–5. https://doi.org/10.5815/ijem.2019.03.04.

Publisher's Note

9.2. Oświadczenia współautorów

Dr hab. Bernard Turek

bernard_turek@sggw.edu.pl

Warszawa, 10.04.2024 r.

Rada Dyscypliny Weterynaria

Szkoły Głównej Gospodarstwa Wiejskiego w Warszawie

Oświadczenie o współautorstwie

Niniejszym oświadczam, że w pracy:

Górski, K.; Tremaine, H.; Obrochta, B.; Buczkowska, R.; Turek, B.; Bereznowski, A.; Rakowska, A.; Polkowska, I. EOTRH syndrome in polish half-bred horses-two clinical cases. J. Equine Vet. Sci. **2021**, 101, 103428. 2920 mój indywidualny udział w jej powstaniu wynosił 5% i polegał na udziale w pisaniu manuskryptu;

Górski, K.; Borowska, M.; Stefanik, E.; Polkowska, I.; Turek, B.; Bereznowski, A.; Domino, M. Selection of Filtering and Image Texture Analysis in the Radiographic Images Processing of Horses' Incisor Teeth Affected by the EOTRH Syndrome. Sensors **2022**, 22, 2920 mój indywidualny udział w jej powstaniu wynosił 5% i polegał na udziale w opracowaniu koncepcji badań, opracowaniu metodologii badań;

Górski, K.; Stefanik, E.; Turek, B.; Bereznowski, A.; Czopowicz, M.; Polkowska, I.; Domino, M. Malocclusions and Dental Diseases in Privately Owned Horses in the Mazovia Region of Poland. Animals **2022**, 12, 3120 mój indywidualny udział w jej powstaniu wynosił 5% i polegał na udziale w opracowaniu koncepcji badań, opracowaniu metodologii badań;

Górski, K.; Borowska, M.; Stefanik, E.; Polkowska, I.; Turek, B.; Bereznowski, A.; Domino, M. Application of Two-Dimensional Entropy Measures to Detect the Radiographic Signs of Tooth Resorption and Hypercementosis in an Equine Model. Biomedicines **2022**, 10, 2914, mój indywidualny udział w jej powstaniu wynosił 5% i polegał na udziale w opracowaniu koncepcji badań, opracowaniu metodologii badań;

Górski, K.; Borowska, M.; Turek, B.; Pawlikowki, M.; Jankowski, K.; Bereznowski, A.; Polkowska, I.; Domino, M. An application of the density standard and scaled-pixel-counting protocol to assess the radiodensity of equine incisor teeth affected by resorption and hypercementosis: preliminary advancement in standard in field dental radiography. BMC Veterinary Research **2023**, 19, 116, , mój indywidualny udział w jej powstaniu wynosił 5% i polegał na udziale w opracowaniu koncepcji badań, opracowaniu metodologii badań.

Podpis

Dr hab. Małgorzata Domino

malgorzata_domino@sggw.edu.pl

Warszawa, 12.04.2024 r.

Rada Dyscypliny Weterynaria

Szkoły Głównej Gospodarstwa Wiejskiego w Warszawie

Oświadczenie o współautorstwie

Niniejszym oświadczam, że w pracy:

Górski, K.; Borowska, M.; Stefanik, E.; Polkowska, I.; Turek, B.; Bereznowski, A.; Domino, M. Selection of Filtering and Image Texture Analysis in the Radiographic Images Processing of Horses' Incisor Teeth Affected by the EOTRH Syndrome. Sensors **2022**, 22, 2920, mój indywidualny udział w jej powstaniu wynosił 10% i polegał na udziale w pisaniu oryginalnego szkicu manuskryptu, udziale w opracowaniu koncepcji badań, opracowaniu metodologii badań, udziale w analizie danych;

Górski, K.; Stefanik, E.; Turek, B.; Bereznowski, A.; Czopowicz, M.; Polkowska, I.; Domino, M. Malocclusions and Dental Diseases in Privately Owned Horses in the Mazovia Region of Poland. Animals **2022**, 12, 3120, mój indywidualny udział w jej powstaniu wynosił 10% i polegał na udziale w pisaniu oryginalnego szkicu manuskryptu, udziale w opracowaniu koncepcji badań, opracowaniu metodologii badań, udziale w analizie danych;

Górski, K.; Borowska, M.; Stefanik, E.; Polkowska, I.; Turek, B.; Bereznowski, A.; Domino, M. Application of Two-Dimensional Entropy Measures to Detect the Radiographic Signs of Tooth Resorption and Hypercementosis in an Equine Model. Biomedicines **2022**, 10, 2914, mój indywidualny udział w jej powstaniu wynosił 10% i polegał na udziale w pisaniu oryginalnego szkicu manuskryptu, udziale w opracowaniu koncepcji badań, opracowaniu metodologii badań, udziale w analizie danych;

Górski, K.; Borowska, M.; Turek, B.; Pawlikowki, M.; Jankowski, K.; Bereznowski, A.; Polkowska, I.; Domino, M. An application of the density standard and scaled-pixel-counting protocol to assess the radiodensity of equine incisor teeth affected by resorption and hypercementosis: preliminary advancement in standard in field dental radiography. BMC Veterinary Research **2023**, 19, 116, mój indywidualny udział w jej powstaniu wynosił 10% i polegał na udziale w pisaniu oryginalnego szkicu manuskryptu, udziale w opracowaniu koncepcji badań, opracowaniu metodologii badań, udziale w analizie danych;

Podpis

Lek. wet. Alicja Rakowska

alicja_rakowska@sggw.edu.pl

Warszawa, 12.04.2024 r.

Rada Dyscypliny Weterynaria

Szkoły Głównej Gospodarstwa Wiejskiego w Warszawie

Oświadczenie o współautorstwie

Niniejszym oświadczam, że w pracy:

Górski, K.; Tremaine, H.; Obrochta, B.; Buczkowska, R.; Turek, B.; Bereznowski, A.; Rakowska, A.; Polkowska, I. EOTRH syndrome in polish half-bred horses-two clinical cases. J. Equine Vet. Sci. **2021**, 101, 103428. 2920 mój indywidualny udział w jej powstaniu wynosił 10% i polegał na udziale w pisaniu oryginalnego szkicu manuskryptu, udziale w nadzorze nad powstawaniem manuskryptu.

Podpis

Lek. wet. Elżbieta Stefanik

elzbieta_stefanik@sggw.edu.pl

Warszawa, 12.04.2024 r.

Rada Dyscypliny Weterynaria

Szkoły Głównej Gospodarstwa Wiejskiego w Warszawie

Oświadczenie o współautorstwie

Niniejszym oświadczam, że w pracy:

Górski, K.; Borowska, M.; Stefanik, E.; Polkowska, I.; Turek, B.; Bereznowski, A.; Domino, M. Selection of Filtering and Image Texture Analysis in the Radiographic Images Processing of Horses' Incisor Teeth Affected by the EOTRH Syndrome. Sensors **2022**, 22, mój indywidualny udział w jej powstaniu wynosił 5% i polegał na udziale w opracowaniu koncepcji badań, udziale w przeprowadzeniu doświadczenia;

Górski, K.; Stefanik, E.; Turek, B.; Bereznowski, A.; Czopowicz, M.; Polkowska, I.; Domino, M. Malocclusions and Dental Diseases in Privately Owned Horses in the Mazovia Region of Poland. Animals **2022**, 12, 3120 mój indywidualny udział w jej powstaniu wynosił 5% i polegał na udziale w opracowaniu koncepcji badań, udziale w przeprowadzeniu doświadczenia;

Górski, K.; Borowska, M.; Stefanik, E.; Polkowska, I.; Turek, B.; Bereznowski, A.; Domino, M. Application of Two-Dimensional Entropy Measures to Detect the Radiographic Signs of Tooth Resorption and Hypercementosis in an Equine Model. Biomedicines **2022**, 10, 2914, mój indywidualny udział w jej powstaniu wynosił 5% i polegał na udziale w opracowaniu koncepcji badań, udziale w przeprowadzeniu doświadczenia;

Stefanik Elżbieta

Podpis

Prof. dr hab. Izabela Polkowska

izabela.polkowska@up.lublin.pl

Lublin, 12.04.2024 r.

Rada Dyscypliny Weterynaria

Szkoły Głównej Gospodarstwa Wiejskiego w Warszawie

Oświadczenie o współautorstwie

Niniejszym oświadczam, że w pracy:

Górski, K.; Tremaine, H.; Obrochta, B.; Buczkowska, R.; Turek, B.; Bereznowski, A.; Rakowska, A.; Polkowska, I. EOTRH syndrome in polish half-bred horses-two clinical cases. J. Equine Vet. Sci. **2021**, 101, 103428. 2920 mój indywidualny udział w jej powstaniu wynosił 5% i polegał na udziale w opracowaniu koncepcji badań, opracowaniu metodologii badań, udziale w nadzorze nad powstawaniem manuskryptu;

Górski, K.; Borowska, M.; Stefanik, E.; Polkowska, I.; Turek, B.; Bereznowski, A.; Domino, M. Selection of Filtering and Image Texture Analysis in the Radiographic Images Processing of Horses' Incisor Teeth Affected by the EOTRH Syndrome. Sensors **2022**, 22, 2920 mój indywidualny udział w jej powstaniu wynosił 5% i polegał na udziale w opracowaniu koncepcji badań, opracowaniu metodologii badań, udziale w nadzorze nad powstawaniem manuskryptu;

Górski, K.; Stefanik, E.; Turek, B.; Bereznowski, A.; Czopowicz, M.; Polkowska, I.; Domino, M. Malocclusions and Dental Diseases in Privately Owned Horses in the Mazovia Region of Poland. Animals **2022**, 12, 3120 mój indywidualny udział w jej powstaniu wynosił 5% i polegał na udziale w opracowaniu koncepcji badań, opracowaniu metodologii badań, udziale w nadzorze nad powstawaniem manuskryptu;

Górski, K.; Borowska, M.; Stefanik, E.; Polkowska, I.; Turek, B.; Bereznowski, A.; Domino, M. Application of Two-Dimensional Entropy Measures to Detect the Radiographic Signs of Tooth Resorption and Hypercementosis in an Equine Model. Biomedicines **2022**, 10, 2914. mój indywidualny udział w jej powstaniu wynosił 5% i polegał na udziale w opracowaniu koncepcji badań, opracowaniu metodologii badań, udziale w nadzorze nad powstawaniem manuskryptu;

Górski, K.; Borowska, M.; Turek, B.; Pawlikowki, M.; Jankowski, K.; Bereznowski, A.; Polkowska, I.; Domino, M. An application of the density standard and scaled-pixel-counting protocol to assess the radiodensity of equine incisor teeth affected by resorption and hypercementosis: preliminary advancement in standard in field dental radiography. BMC Veterinary Research **2023**, 19, 116, mój indywidualny udział w jej powstaniu wynosił 5% i polegał na udziale w opracowaniu koncepcji badań, opracowaniu metodologii badań, udziale w nadzorze nad powstawaniem manuskryptu;

Podpis Izabela Polkowska

Dr Andrzej Bereznowski

andrzej_bereznowski@sggw.edu.pl

Warszawa, 12.04.2024 r.

Rada Dyscypliny Weterynaria

Szkoły Głównej Gospodarstwa Wiejskiego w Warszawie

Oświadczenie o współautorstwie

Niniejszym oświadczam, że w pracy:

Górski, K.; Tremaine, H.; Obrochta, B.; Buczkowska, R.; Turek, B.; Bereznowski, A.; Rakowska, A.; Polkowska, I. EOTRH syndrome in polish half-bred horses-two clinical cases. J. Equine Vet. Sci. **2021**, 101, 103428. 2920 mój indywidualny udział w jej powstaniu wynosił 5% i polegał na udziale w opracowaniu koncepcji badań, opracowaniu metodologii badań;

Górski, K.; Borowska, M.; Stefanik, E.; Polkowska, I.; Turek, B.; Bereznowski, A.; Domino, M. Selection of Filtering and Image Texture Analysis in the Radiographic Images Processing of Horses' Incisor Teeth Affected by the EOTRH Syndrome. Sensors **2022**, 22, 2920 mój indywidualny udział w jej powstaniu wynosił 5% i polegał na udziale w opracowaniu koncepcji badań, opracowaniu metodologii badań;

Górski, K.; Stefanik, E.; Turek, B.; Bereznowski, A.; Czopowicz, M.; Polkowska, I.; Domino, M. Malocclusions and Dental Diseases in Privately Owned Horses in the Mazovia Region of Poland. Animals **2022**, 12, 3120 mój indywidualny udział w jej powstaniu wynosił 5% i polegał na udziale w opracowaniu koncepcji badań, opracowaniu metodologii badań;

Górski, K.; Borowska, M.; Stefanik, E.; Polkowska, I.; Turek, B.; Bereznowski, A.; Domino, M. Application of Two-Dimensional Entropy Measures to Detect the Radiographic Signs of Tooth Resorption and Hypercementosis in an Equine Model. Biomedicines **2022**, 10, 2914. mój indywidualny udział w jej powstaniu wynosił 5% i polegał na udziale w opracowaniu koncepcji badań, opracowaniu metodologii badań;

Górski, K.; Borowska, M.; Turek, B.; Pawlikowki, M.; Jankowski, K.; Bereznowski, A.; Polkowska, I.; Domino, M. An application of the density standard and scaled–pixel–counting protocol to assess the radiodensity of equine incisor teeth affected by resorption and hypercementosis: preliminary advancement in standard in field dental radiography. BMC Veterinary Research **2023**, 19, 116 mój indywidualny udział w jej powstaniu wynosił 5% i polegał na udziale w opracowaniu koncepcji badań, opracowaniu metodologii badań.

Podpis

Dr hab. Michał Czopowicz

michal_czopowicz@sggw.edu.pl

Warszawa, 17.04.2024 r.

Rada Dyscypliny Weterynaria

Szkoły Głównej Gospodarstwa Wiejskiego w Warszawie

Oświadczenie o współautorstwie

Niniejszym oświadczam, że w pracy:

Górski, K.; Stefanik, E.; Turek, B.; Bereznowski, A.; Czopowicz, M.; Polkowska, I.; Domino, M. Malocclusions and Dental Diseases in Privately Owned Horses in the Mazovia Region of Poland. Animals **2022**, 12, 3120 mój indywidualny udział w jej powstaniu wynosił 10% i polegał na udziale w pisaniu oryginalnego szkicu manuskryptu, udziale w analizie danych.

Podpis

Dr hab. Marta Borowska

m.borowska@pb.edu.pl

Warszawa, 17.04.2024 r.

Rada Dyscypliny Weterynaria

Szkoły Głównej Gospodarstwa Wiejskiego w Warszawie

Oświadczenie o współautorstwie

Niniejszym oświadczam, że w pracy:

Górski, K.; Borowska, M.; Stefanik, E.; Polkowska, I.; Turek, B.; Bereznowski, A.; Domino, M. Selection of Filtering and Image Texture Analysis in the Radiographic Images Processing of Horses' Incisor Teeth Affected by the EOTRH Syndrome. Sensors **2022**, 22, 2920, mój indywidualny udział w jej powstaniu wynosił 10% i polegał na udziale w pisaniu oryginalnego szkicu manuskryptu, udziale w opracowaniu koncepcji badań, opracowaniu metodologii badań, udziale w analizie danych;

Górski, K.; Borowska, M.; Stefanik, E.; Polkowska, I.; Turek, B.; Bereznowski, A.; Domino, M. Application of Two-Dimensional Entropy Measures to Detect the Radiographic Signs of Tooth Resorption and Hypercementosis in an Equine Model. Biomedicines **2022**, 10, 2914, mój indywidualny udział w jej powstaniu wynosił 10% i polegał na udziale w pisaniu oryginalnego szkicu manuskryptu, udziale w opracowaniu koncepcji badań, opracowaniu metodologii badań, udziale w analizie danych;

Górski, K.; Borowska, M.; Turek, B.; Pawlikowki, M.; Jankowski, K.; Bereznowski, A.; Polkowska, I.; Domino, M. An application of the density standard and scaled-pixel-counting protocol to assess the radiodensity of equine incisor teeth affected by resorption and hypercementosis: preliminary advancement in standard in field dental radiography. BMC Veterinary Research **2023**, 19, 116, mój indywidualny udział w jej powstaniu wynosił 5% i polegał na udziale w pisaniu oryginalnego szkicu manuskryptu, udziale w opracowaniu koncepcji badań, opracowaniu metodologii badań, udziale w analizie danych.

Podpis

Marta Borowska

Wyrażam zgodę na udostępnienie mojej pracy w czytelniach Biblioteki SGGW

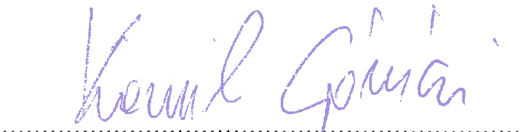

.....

(czytelny podpis autora)